CR-120878
D6-54351

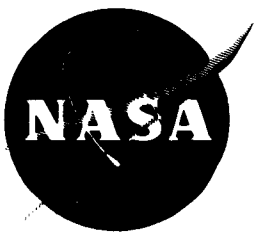

APPLICATION OF POLYIMIDE ACTUATOR ROD SEALS

by

A. W. Waterman, B. F. Gay, E. D. Robinson, S. K. Srinath, W. G. Nelson

THE BOEING COMPANY

prepared for

NATIONAL AERONAUTICS AND SPACE ADMINISTRATION

NASA Lewis Research Center
Contract NAS3-14317
William F. Hady, Project Manager

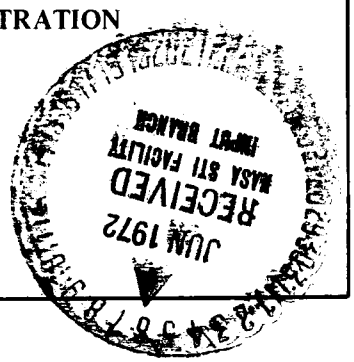

1. Report No.	2. Government Accession No.	3. Recipient's Catalog No.
CR-120878		

4. Title and Subtitle	5. Report Date
APPLICATION OF POLYIMIDE ACTUATOR ROD SEALS	January 30, 1972
	6. Performing Organization Code

7. Author(s)	8. Performing Organization Report No.
A. W. Waterman, B. F. Gay, E. D. Robinson, S. K. Srinath, and W. G. Nelson	D6-54351

9. Performing Organization Name and Address	10. Work Unit No.
The Boeing Company, Commercial Airplane Group P.O. Box 3707, Seattle, Washington 98124	YON 1347
	11. Contract or Grant No. NAS3-14317

12. Sponsoring Agency Name and Address	13. Type of Report and Period Covered
National Aeronautics and Space Administration Washington, D.C. 20546	CONTRACTOR REPORT 7/1/70–1/30/72
	14. Sponsoring Agency Code

15. Supplementary Notes

Project Manager: W. F. Hady, Fluid System Component Division, NASA Lewis Research Center, Cleveland, Ohio

16. Abstract

Development of polyimide two-stage hydraulic actuator rod seals for application in high-performance aircraft was accomplished. The significant portion of the effort was concentrated on optimization of the chevron and K-section second-stage seal geometries to satisfy the requirements for operation at 450° K (350° F) with dynamic pressure loads varying between 1.379 x 10^6 N/m^2 (200 psig) steady-state and 1.043 x 10^7 N/m^2 (1500 psig) impulse cycling. Particular significance was placed on reducing seal gland dimensions by efficiently utilizing the fatigue allowables of polyimide materials. Other objectives included investigation of pressure balancing techniques for first-stage polyimide rod seals for a 2.758 x 10^7 N/m^2 (4000 psig), 450° K (350° F) environment and fabrication of a modular retainer for the two-stage combination. Seals were fabricated in 0.0254 m (1.0 in.) and 0.0635 m (2.5 in.) sizes and tested for structural integrity, frictional resistance, and endurance life. Test results showed that carefully designed second stages using polyimides could be made to satisfy the dynamic return pressure requirements of applications in high-performance aircraft. High wear under full system pressure indicated that further research is necessary to obtain an acceptable first-stage design. The modular retainer was successfully tested and showed potential for new actuator applications.

17. Key Words		18. Distribution Statement
Polyimides	Seal friction	Unclassified–unlimited
Rod seals	Stress design	
Endurance life	Modular seal	
Impulse life		

19. Security Classif. (of this report)	20. Security Classif. (of this page)	21. No. of Pages	22. Price*
Unclassified	Unclassified	179	$11.00

*For sale by the National Technical Information Service, Springfield, Virginia 22151

CONTENTS

CONTENTS–Concluded

TABLES

FIGURES

FIGURES (Concluded)

I. SUMMARY

The primary objective of the program conducted under NASA contract NAS3-14317 was to develop the basic B-1 and HB-1 second-stage hydraulic acutator rod seals of a two-stage configuration from NASA contract NAS3-11170 into seals acceptable for application in high-performance aircraft. This objective was accomplished by analytically determining the optimum geometry of the chevron and K-section seal cross sections that would satisfy the gland dimensions and stress allowables for Boeing/DOT SST flight control applications using polyimide materials. A polyimide first-stage rod seal was also developed as an adjunct to the second-stage development with the major objective of determining the degree of pressure balancing most conducive to reducing friction and wear, without compromising fluid containment. A seal modular retainer was designed and tested to demonstrate feasibility of a two-stage seal unitized assembly.

Seals designed to the above objectives were fabricated in 0.0254 m (1.0 in.) and 0.0635 m (2.5 in.) sizes. The fabricated seals were tested to evaluate their structural integrity during a 200 000-cycle impulse life requirement and frictional resistance over the temperature and pressure range of the application. Endurance tests were conducted with an operational goal of 3 850 000 cycles at 450°K (350°F) when installed in an actuator as part of a 2.758×10^7 N/m^2 (4000 psig) hydraulic system.

Screening test results indicated that 70% maximum pressure balanced polyimide first-stage seals were subject to intermittent periods of erratic and excessive leakage due to seal lifting. As a result 50% balance polyimide seals were initially installed in the endurance tests and replaced with cast iron seals after high wear rates showed polyimides unacceptable. The second-stage seals maintained fluid containment in all tests, although impulsing between 0 and 1.043×10^7 N/m^2 (0 and 1500 psig) produced cracks in some redundant elements of the seals. These seals completed 3 210 026 cycles of endurance satisfactorily at the conclusion of testing.

It was concluded from the design analysis and testing completed during this program that the advantage of polyimide seals is satisfactory-operational-capability over a wide temperature range where seals in present usage cannot compete. The disadvantages are the low material allowables and high coefficient of thermal expansion. The test results demonstrated that by carefully designing polyimide second-stage rod seals they can be made to satisfy the dynamic hydraulic actuator requirements of applications in high-performance aircraft. Further effort will be needed to determine whether the same conclusion can be reached for the application of polyimide first-stage seals.

Tests should be continued to evaluate the chevron and K-section second-stage seal configurations at higher temperatures and with other fluids and environments to further expand the field of knowledge regarding the application of these seals to satisfy the ever-expanding demands for reliable methods of fluid containment.

II. INTRODUCTION

The traditional objective in new aircraft design has been to improve the operational performance and systems reliability/maintainability record in the new airplane above its predecessors. The performance considerations now include supersonic flight where long operational life at high temperatures precludes the use of many heretofore conventional design practices. One such practice, the use of elastomeric rod seals in flight control hydraulic actuators, can no longer be considered satisfactory standard practice. Similarly, polytetrafluoroethylene (PTFE) used in combination with elastomers to form two-piece seals offers only some improvement in life at elevated temperatures. Typically, seals that are presently selected for Type II applications (219° K to 480° K) (-65° F to 275° F) are limited in life at high temperature while seals selected for Type III applications (219° K to 505° K) (-65° F to 450° F) have low-temperature fluid containment deficiencies.

The material properties of polyimides are acceptable for the entire range of Type III hydraulic system temperatures and considerably higher temperatures, making these materials prime candidates for experimental seal research for advanced aircraft applications. Experimental investigations with polyimides to date have emphasized these materials' stable strength properties at high temperatures over long durations. NASA-initiated research was instrumental in the early development of new seal concepts using polyimides in exploratory tests to determine sealing characteristics under various operating environments. These efforts were conducted under the NAS3-7264 and NAS3-11170 contracts, references 1 and 2, respectively.

The program reported herein is a follow-on effort of the above-mentioned NASA contracts. It was intended to extend the seal development from the category of exploratory testing to that of seal performance verification testing simulating an actual high-performance airplane's requirements. The seals were required to meet the stresses of the application temperature range with cyclic impulse and the temperature range with fatigure life loadings. The evaluation was particularly significant with polyimide seals because the material fatigue allowables were in the same range as the imposed stresses for the aircraft application, based on a required mean-time-between-overhaul life. Performance measurement under such dynamic stress conditions, simulating requirements for aircraft presently on the drawing boards, is the first step leading to seal development for advanced applications having more severe environments uniquely suitable for polyimide materials. The program included analyses of the basic seal sections and modifying these sections based on recommended stress distributions. Seals were fabricated and tested to the fatigue environments of cyclic impulse and fatigue life typical of a supersonic transport or a high-performance military aircraft.

III. SEAL DESIGN ANALYSIS

DESIGN REQUIREMENTS

Seal design criteria were selected and test objectives established to reflect a high degree of compatibility with the requirements of the general category of flight control actuators to be used on high-performance aircraft similar to the Boeing/DOT SST. These requirements were generally consistent with those that would be expected for any high-performance aircraft except they may have been somewhat severe for seal life when compared with military aircraft requirements.

Flight control actuator requirements were investigated because such actuation equipment receives the highest degree of time utilization in flight and is subject to the most severe environmental conditions. The general criteria, applicable to the most representative candidate primary flight control actuators, having rod sizes nearest those available for the test evaluation, were used to establish the design and test parameters for the rod seals studied.

General Requirements

Seal configuration.—The seal configuration acceptable for the application was a continuously pressurized high-pressure two-stage linear actuator rod seal with bleedoff between stages to return. The design goal for the seal was that there should be no external leakage other than a slight wetting of the rod downstream of the second stage. Some leakage was allowed to pass by the first stage to return during system operation. Endurance requirements for the static and dynamic seals were to provide a component overhaul life of 4.5×10^7 sec (12 500 hr). (Refer to par. 5.2.10, ref. 3.)

Hydraulic fluid.—The hydraulic fluid used for design and during testing was the fluid specified in the requirements of reference 4, Humble Oil WS-8228. The fluid was designed for use in a closed aircraft hydraulic system, operating normally over the temperature range of 244° to 450° K (-20° to 350° F), and at a nominal working pressure of 2.758×10^7 N/m^2 (4000 psig). The fluid had the capability of operating over the extreme range of 228° to 506°K (-50° to 450°F) at 2.758×10^7 N/m^2 (4000 psig), and was required to perform satisfactorily in an overheat condition at 506°K for 3600 sec in flight. The fluid basic chemistry was that of the polyolester family. (Refer to par. 5.2.4, ref. 3.)

Fluid pressure.—The hydraulic systems used as a pattern for establishing test requirements operated with a nominal pressure of 2.861×10^7 N/m^2 (4150 psig) at 408° K (275° F) for supply and 1.034×10^6 N/m^2 (150 psig) at 408° K (275° F) for return. The most demanding design conditions were 2.758×10^7 N/m^2 (4000 psig) at 506°K (450° F)

for supply and 1.431×10^7 N/m^2 (2075 psig) at 244° K (-20° F) for return. The main system pressure relief valves were designed to have a full flow setting of 3.448×10^7 N/m^2 (5000 psig) maximum. Cracking pressure was $3.206 \times 10^7 \pm 3.447 \times 10^5$ N/m^2 (4650 ±50 psig) and reseat pressure was 2.930×10^7 N/m^2 (4250 psig) maximum. (Refer to par. 5.1.3, ref. 3 and par. 3.2.2.1, ref. 5.)

External leakage.—The external leakage allowable, based on the selected application, was 10^{-7}m^3 (2 drops) per 25 cycles passed by the second-stage seal, for each rod end of an actuator at any temperature and pressure. A goal of zero leakage was established but was not justification for rejection of the seal if the goal could not be obtained. (Example requirements: par. 3.3.14, ref. 6 and par. 3.3.11, ref. 7.)

Friction.—Seal friction requirements that were stated in flight control actuator specifications provided data related to the complete actuator assembly, i.e., the combined sum of friction for the piston and for the two-stage rod seal of a single-ended actuator. These requirements were not usable for the seal evaluations to be performed in the reported contract. Specific criteria for testing of each seal separately were, therefore, based on the mean friction forces obtained during seal friction tests which were the basis for SST requirements. These criteria were:

- 245 N (55 lbf) maximum friction force at the first-stage seal on a 0.0254 m (1.0 in.) diameter rod with a 2.758×10^7 N/m^2 (4000 psig) chamber pressure.

- 1334 N (300 lbf) maximum friction force at the first-stage seal on a 0.0635 m (2.5 in.) diameter rod with a 2.758×10^7 N/m^2 (4000 psig) chamber pressure.

- 36 N (8 lbf) maximum friction force at the second-stage seal on a 0.0254 m (1.0 in.) diameter rod with a 1.379×10^6 (200 psig) chamber pressure.

- 133N (30 lbf) maximum friction force at the second-stage seal on a 0.0635 m (2.5 in.) diameter rod with a 1.379×10^6 N/m^2 (200 psig) chamber pressure.

Temperature.—The fluid and component operating temperatures stated in flight control actuator specifications varied with flight duration and environmental temperatures associated with the application. Figure 1 shows a composite of the SST hydraulic system temperature limits. The criterion of the normal maximum operation temperature of the heat exchanger fluid at flight completion from this figure was 450° K (350° F) and was used as the steady-state test temperature for design and testing. This temperature magnitude was extreme for a steady-state value for an entire flight. It was justified as a realistic test condition only on the basis that it was applied over a nominal endurance life. Such a combined temperature-life testing condition provided a maximum test exposure at high-temperature conditions. (Refer to par. 5.1.4, ref. 3.)

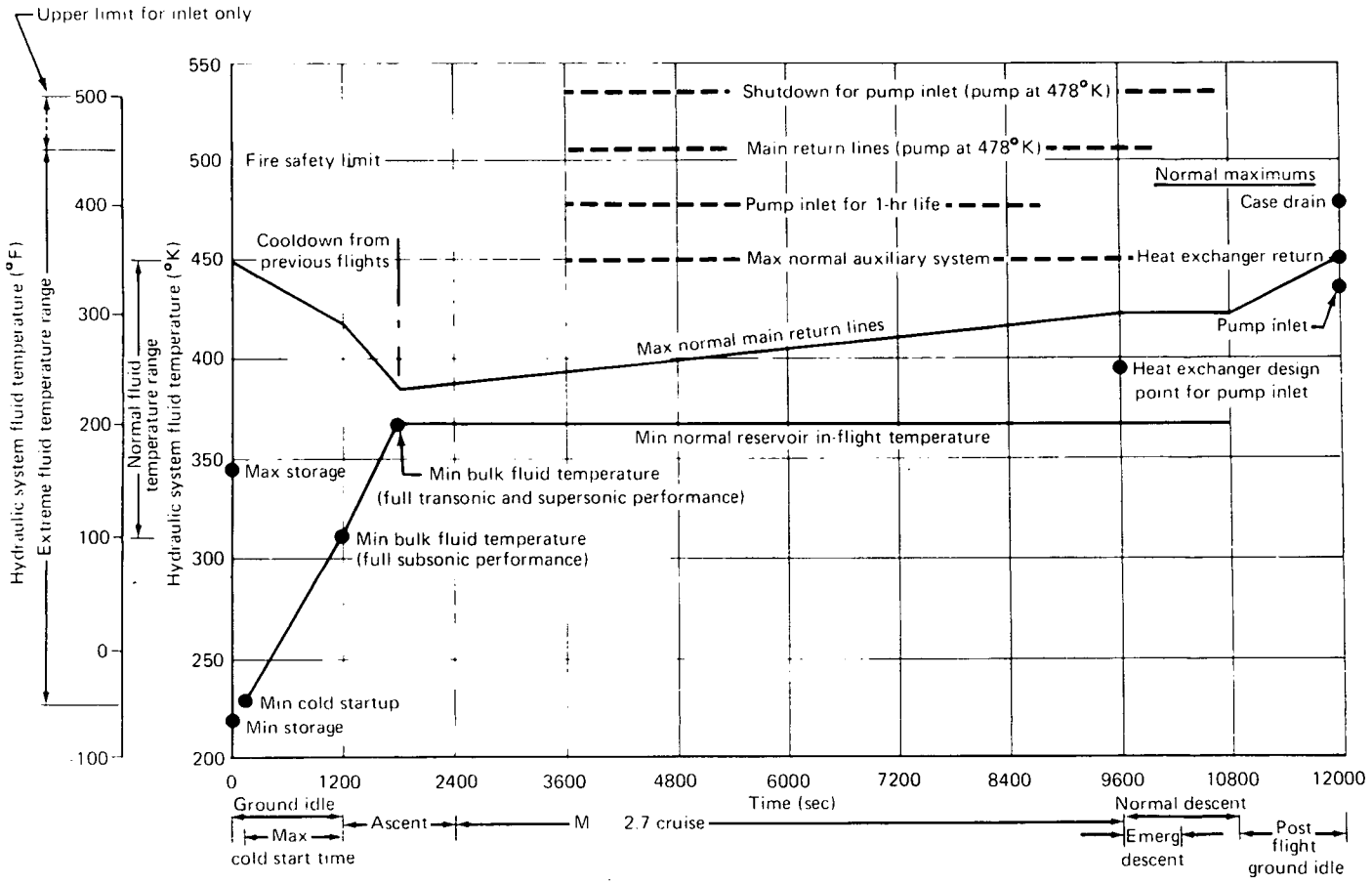

Figure 1 – Hydraulic system criteria–bulk fluid temperature

Endurance.—The required flight life of the SST hydraulic components was established at 1.8×10^8 sec (50 000 hr) with flight control actuator overhaul periods at a minimum of 4.5×10^7 sec (12 500 hr) intervals. Seals were to be replaced during each overhaul; thus overhaul life was established as the endurance life for actuator seals. The mean or nominal cycle life for rod seals in flight control actuators during one period between overhauls was established at approximately 8×10^6 cycles, this being nearly equivalent to the cycle life for the SST rudder actuators as shown in table I. (Refer to par. 3.3.9, refs. 8, 9, and 10 and par. 5.2.10, ref. 3.)

Pressure impulse at first stage.—The pressure impulse requirements established for flight control actuators were 200 000 cycles of 1.448×10^7 to 3.861×10^7 to 1.448×10^7 N/m^2 (2100-5600-2100 psig) at the supply port with a rate of pressure rise between 6.206×10^8 and 7.585×10^8 N/m^2/sec (90 000-110 000 psig/sec) applicable to the first-stage seal. The total number of cycles were accumulated by testing at the environmental temperature shown in table II. (Refer to par. 3.3.15, ref. 6 and par. 3.3.10, ref. 7.)

Specific Requirements for Second-Stage Seal

An analysis was performed to establish the minimum pressure impulse requirement for second-stage rod seal design. A relationship was determined for the pressure fluctuations between the first and second stages (interstage gallery) of a typical linear actuator during a maximum pressure surge created in an operational maneuver. This effort was performed to determine whether lesser requirements than those adopted for the SST were practical where applications of low-strength polyimide materials were practical.

Impulse pressure with maximum allowable first-stage clearance.—The first step in determining the magnitudes of surge pressures was to simulate the no-load, maximum rate, ground operation of the combined rudder and stabilizer activities for the SST airplane. This was the worst case for pressure surge in the fluid return lines and provided the limiting pressure condition of exposure for the second-stage seal. The analytical simulation was performed using the HYTRAN (ref. 11) computer program and the mathematical model of the SST "A" hydraulic system, figure 2. Pressure conditions observed at the inlet and return to an actuator representative of the size available for testing are shown in figure 3. The second step of the analysis was to determine how these pressures were translated through the internal passages in the typical actuator, and how these pressure interactions combined to establish the pressure profile to which the second-stage seal would be exposed.

Figure 4 shows the dimensions of the seal gallery for the typical actuator used in the analysis. This actuator design was selected because it had a 0.0635 m (2.5 in.) rod diameter, which was the largest size rod evaluated in the test program. The configuration of the interstage gallery contained a poppet-type check valve to prevent loss of system fluid in case of a failure at the second-stage seal. The free-flow direction of the valve allowed leakage that passed the first stage to be returned to the system downstream of the poppet.

Table I.—Endurance test sequence

Sequence number	Cycles	% Load and stroke	Maximum cycle rate, Hz	Actuator temperature	
				°K	°F
1	7.5×10^5	2	5	450	350
2	5 000	25	0.67	450	350
3	10 000	50	0.50	450	350
4	5 000	100	0.40	450	350

Notes:

1) All cycles are to be run around actuator midstroke position.

2) A portion of the cycles from sequences 2, 3, and 4 are to be randomly interspersed during performance of sequence 1.

3) Testing spectrum is to consist of ten consecutive runs in the sequence shown, i.e., 1, 2, 3, 4, 1, 2, 3, 4, 1, 2 .... with the sum of sequences 1 + 2 + 3 + 4 equalling one run.

Table II.—Impulse spectrum

Temperature		Impulse cycles
°K	°F	
311	100	40 000
408	275	115 000
450	350	40 000
478	400	5 000

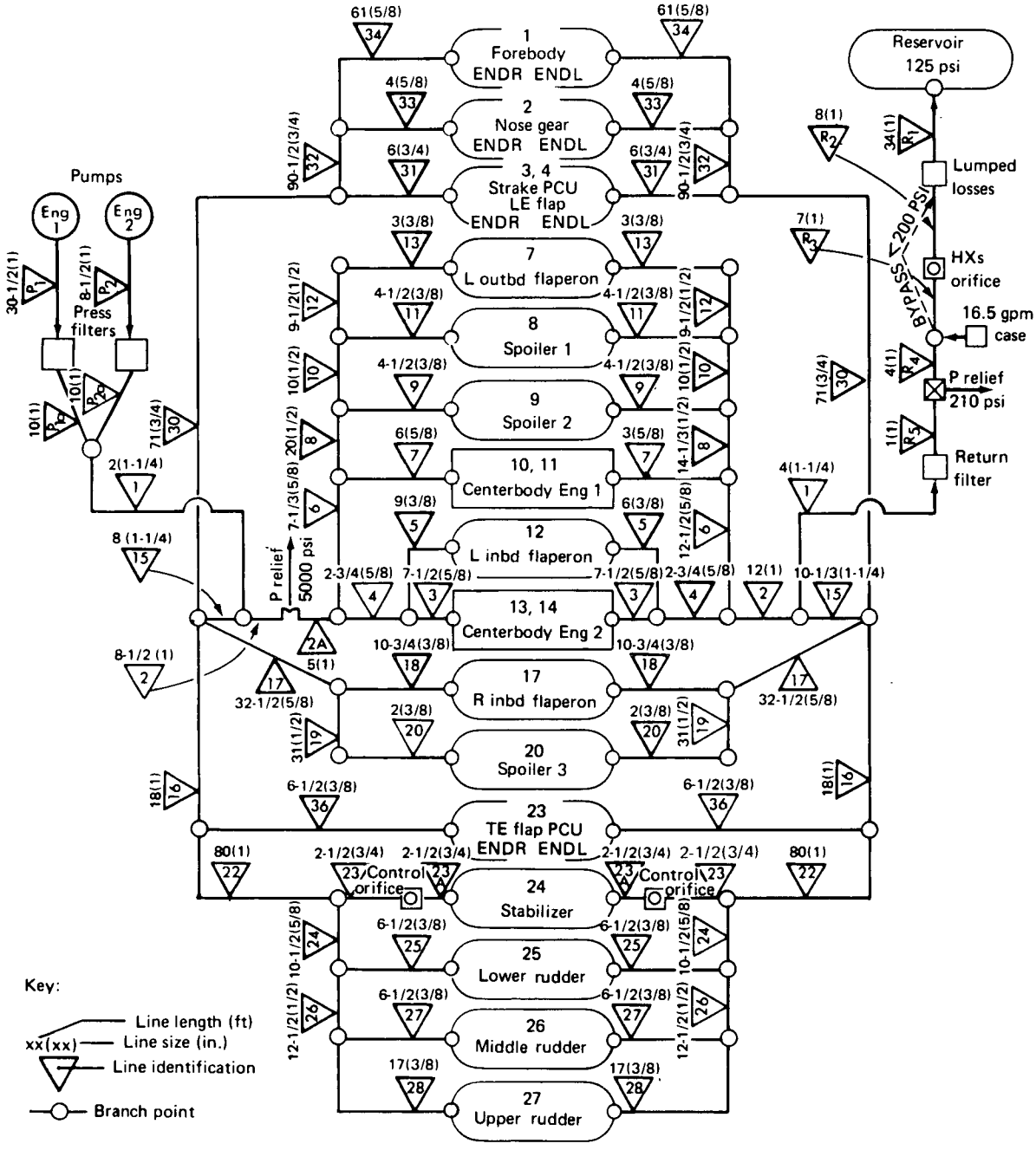

Note: No SI conversion was made on dimensioned parts (see appendix 9)

Figure 2 – HYTRAN model hydraulic system "A"–SST

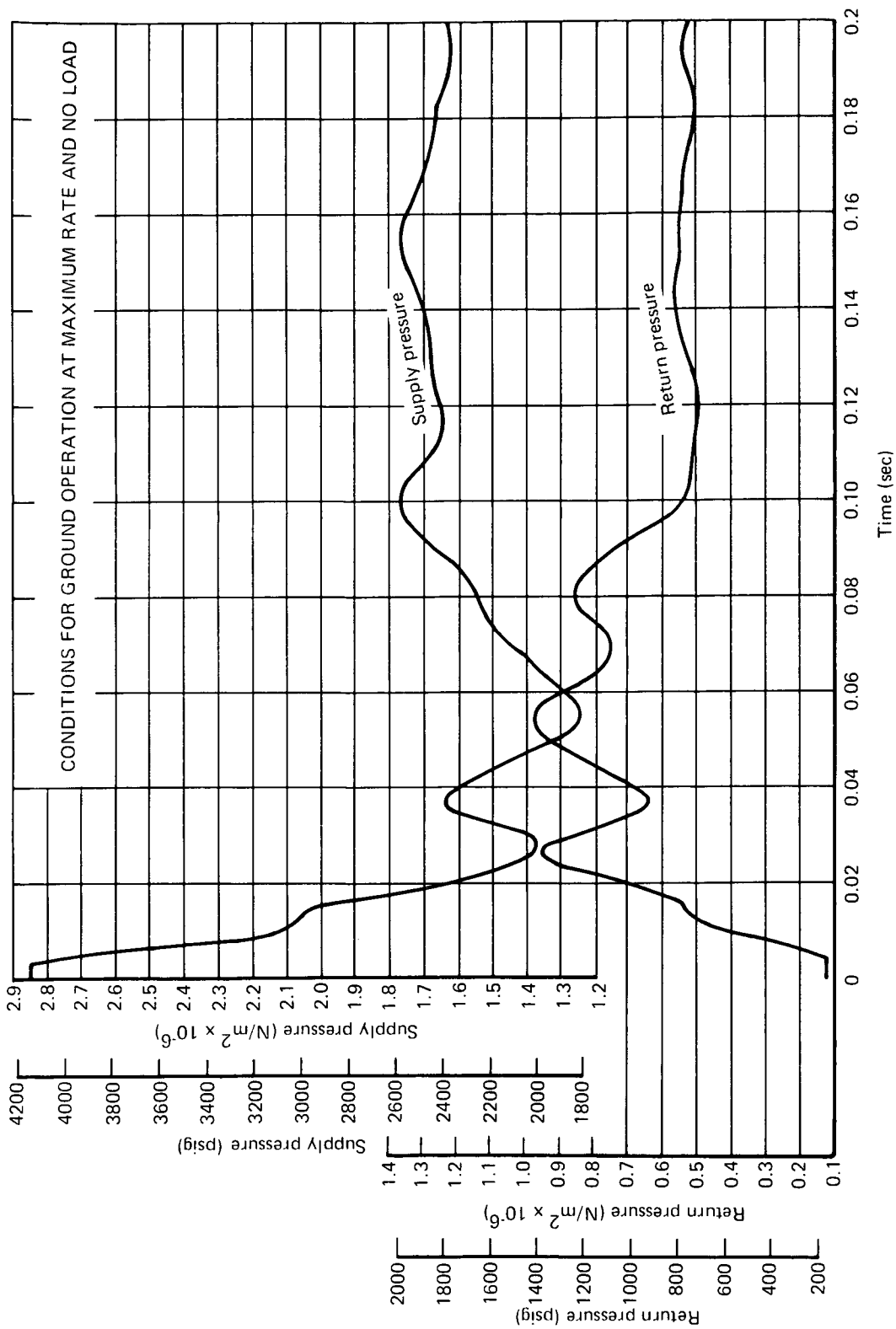

Figure 3 – Computer simulation: Upper rudder pressure surge

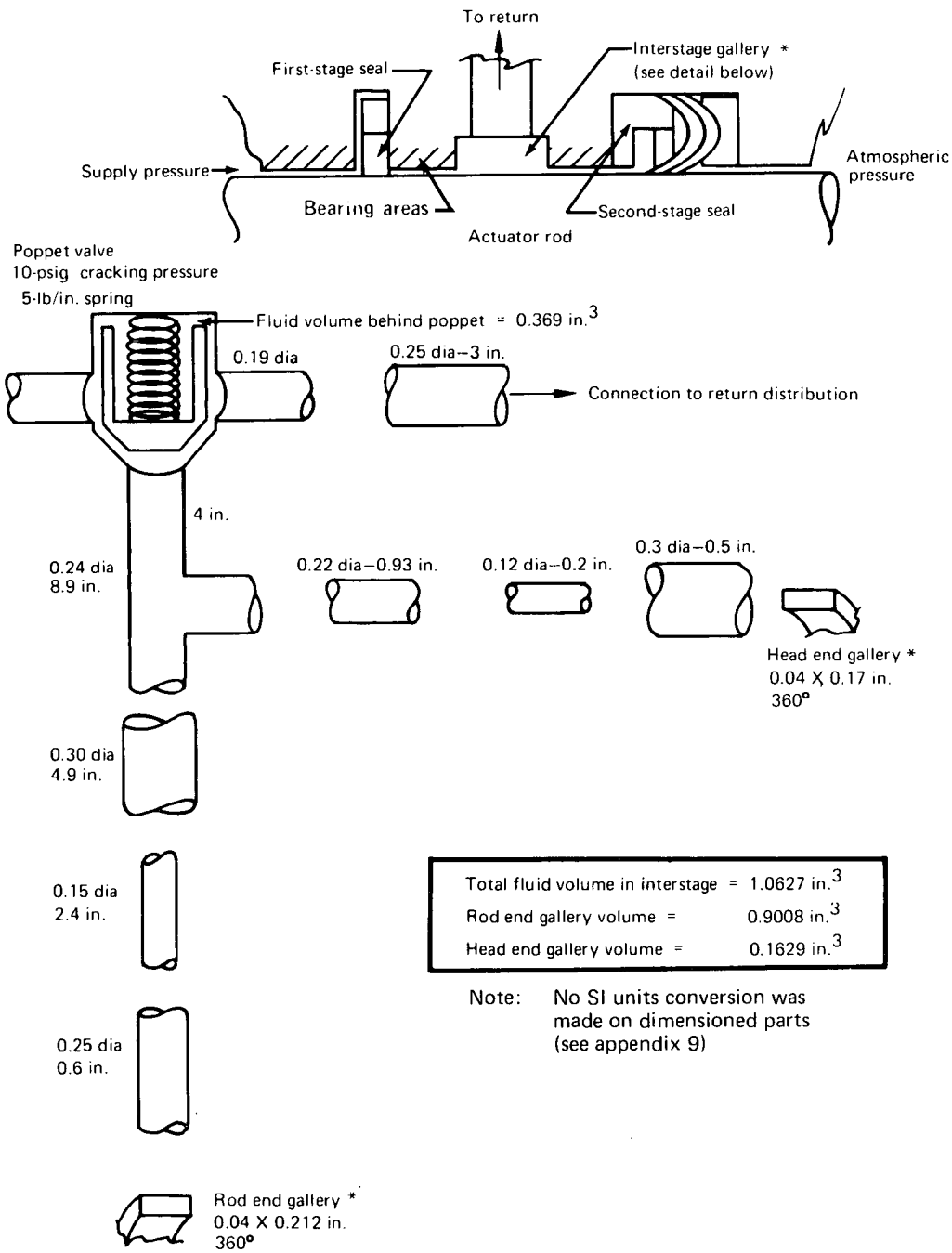

Figure 4 — Rod seal interstage gallery configuration—typical flight control actuator

The first dynamic analysis trial used the HYTRAN program to evaluate the downstream pressure at the poppet valve simulating the condition that this valve were to close at the time of initiation of a return line surge. A branch was added to the upper rudder servo in the model to idealize the seal gallery and the passages between it and the servo return port. The data resulting from this analysis are shown in figure 5. The results indicate that the poppet downstream pressure builds to a stabilized pressure, equivalent to the magnitude of the damped surge. This would be a realistic case if there were no, or nearly no, leakage flowing by the first-stage seal.

The first-stage rod seals were not designed to maintain a no-leak condition because such a design would also impose high friction penalties against actuation power and available response. Thus, when there was first-stage leakage, the interstage gallery pressures (between the first and second stages) were a function of the supply pressure and leakage flow dynamics of that first-stage seal and the pressure-flow dynamics of the poppet valve and the return line pressure fluctuations.

The leakage allowed to pass by the first-stage seal was 1.67×10^{-7} m^3/sec (10 cc/min) for a new seal and a maximum of 8.33×10^{-7} m^3/sec (50 cc/min) under any service conditions thereafter. For the purpose of analysis the radial clearance between the first-stage seal and the rod under static conditions preceding initiation of the dynamic surge was established as 2.245×10^{-6} m (0.884×10^{-4} in.) to allow passage of the maximum leakage allowed. This uniform radial clearance was assumed constant for all calculations of dynamic pressure-flow evaluation. The dynamic leakage curve on figure 5 was determined using the equation

$$Q = \pi D b^3 [1 + 1.5(\epsilon/b)^2](Pu - Pd)/12\nu L$$

describing the flow through the annular clearance, the pressure data from the SST upper rudder response to surge on figure 5, and a mean pressure drop of 4.137×10^4 N/m^2 (6 psig) through the gallery passages. The mean pressure drop through the gallery was used to simplify calculations since error by substituting this constant value rather than a flow-related variable pressure was determined to be less than 6.895×10^3 N/m^2 (1 psig). The leakage flows thus determined were combined with the upper rudder return pressure profile to determine the fluctuations in movement of the poppet in the poppet valve and evaluate how those movements reflected changes in seal interstage gallery pressure.

The analysis of the poppet valve was simplified by selecting two constant leakage flow conditions at the first-stage seal. This simplification was adopted because the problem complexity resulting by retaining leakage as the variable shown in figure 5 was much more detailed than necessary to determine maximum pressure conditions in the seal-interstage gallery. The constant flow conditions selected were 1.67×10^{-7} m^3/sec (10 cc/min), the maximum new seal allowable, and 8.33×10^{-7} m^3/sec (50 cc/min), the maximum allowable.

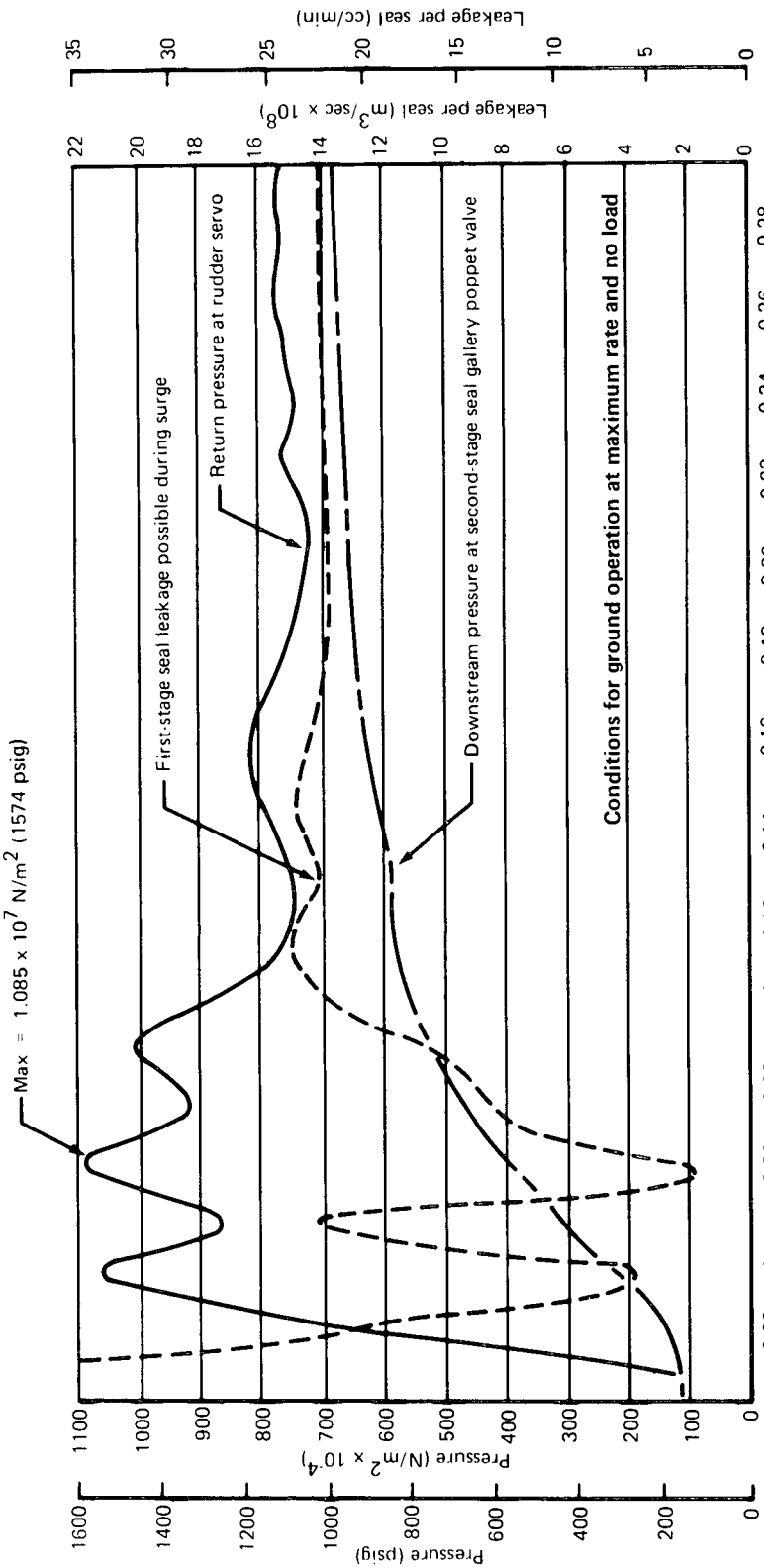

Figure 5.—Computer simulation: Leakage variation during return pressure surge

Figure 6 shows the results of the determination of pressure in the seal interstage gallery during these conditions. The following describe the meanings of the data:

Analysis with maximum new seal leakage– 1.67×10^{-7} m^3/sec (10 cc/min): The differential pressure across the first-stage seal supported a maximum new seal leakage until return pressure reached 8.667×10^6 N/m^2 (1257 psig) at 0.023 sec elapsed time. The poppet then closed and gallery pressure rose at the rate of 2.068×10^7 N/m^2/sec (3000 psig/sec) as shown by the dotted line on figure 6. The resulting gallery pressure rise lagged the return pressure downstream of the poppet until 0.039 sec elapsed time. The poppet opened when gallery pressure reached 6.895×10^4 N/m^2 (10 psig) greater than the dynamic return pressure and closed as the gallery pressure reduced toward return pressure, causing a differential less than necessary to support the maximum new seal leakage. This occurred along the dotted line on figure 6 in the manner shown by the lower inset, except where the line was lower than the return surge pressure. The maximum gallery pressure reached during a constant maximum new seal leakage was 8.915×10^6 N/m^2 (1293 psig).

Analysis with maximum allowable leakage–8.33×10^{-7} m^3/sec (50 cc/min): The initial effects of the surge cause pressure fluctuations to begin at 0.005 sec. At that time the poppet closed because the initial condition for first-stage seal dimensional clearance was based on passing maximum leakage at static conditions, i.e., maximum pressure drop. This meant that any pressure drop would produce a condition where the configuration would not support the maximum leakage flow rate. With the poppet closed the continued leakage caused fluid compressibility in the seal gallery at the rate of 1.076×10^8 N/m^2/sec (15 600 psig/sec) based on maintaining a constant fluid bulk modulus of 1.124×10^9 N/m^2 (163 000 psi). The poppet thus opened at a differential pressure of 6.895×10^4 N/m^2 (10 psig), which occurred prior to 0.006 sec of elapsed time. As soon as the poppet opened the gallery pressure adjusted to return pressure, the resulting differential pressure across the first stage would not support maximum leakage flow, and the poppet closed. This situation did not repeat because by 0.0065 sec elapsed time the return pressure was rising more rapidly than the pressure rise due to compressibility in the gallery. At 0.086 sec elapsed time the gallery pressure due to compressibility from maximum first-stage leakage flow increased to 6.895×10^4 N/m^2 (10 psig) above the return surge pressure and the poppet opened. Subsequent to that point in time the gallery pressure oscillated between the return pressure and 6.895×10^4 N/m^2 (10 psig) greater than return pressure as shown in the upper inset on figure 6. Those pressure reversals occurred as the poppet opened at the higher pressure, causing the gallery pressure to reduce to return pressure. This reduction resulted in a lower differential pressure that could no longer support first-stage leakage and the poppet closed. This sequence was repeated at intervals of 0.00064 sec throughout the remainder of the surge, assuming the poppet had immediate response to the dynamic pressure conditions that formed its environment. The maximum pressure in the interstage gallery during this sequence reached 9.998×10^7 N/m^2 (1450 psig).

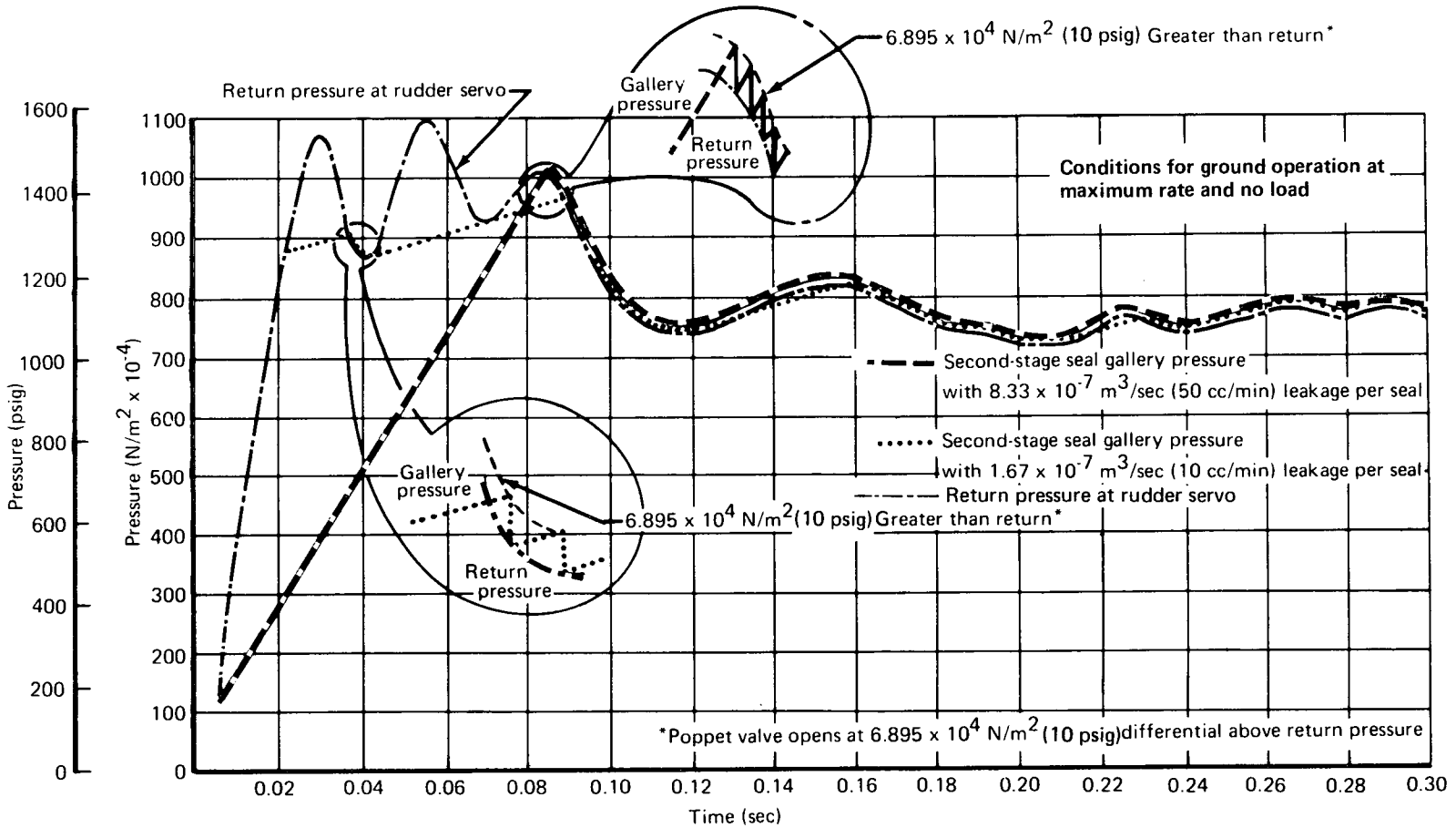

Figure 6.—Computer simulation: Return pressure surge dynamics

Impulse pressure with new first-stage seals.—The above discussion considered examples where the clearance between the first-stage seal and the rod would allow the maximum tolerable installed leakage of 8.33×10^{-7} m^3/sec (50 cc/min) and resulted in the maximum gallery pressure under any operable condition. This condition was not expected to exist except with very worn first-stage seals. When the first-stage seal was new only 1.67×10^{-7} m^3/sec (10 cc/min) leakage would be allowed.

The resulting fluctuations in interstage gallery pressure with a new first-stage seal were determined as follows. The first poppet valve closure occurred at 0.005 sec with a return pressure of 1.158×10^6 N/m^2 (168 psig) and remained closed until 0.366 sec elapsed time when gallery pressure rose to 6.895×10^4 N/m^2 (10 psig) due to compressibility. At that time the poppet opened and dynamic response followed the fluctuations described above in the "Analysis with maximum new seal leakage." The maximum pressure resulting in the interstage gallery under that condition was 7.584×10^6 N/m^2 (1100 psig), which was less than the maximum pressure condition which would exist during operation with maximum wear on the first-stage seal.

Discussion of analysis results.—It was concluded from the analyses described above that there was no practical way to substantially reduce the interstage gallery pressure requirements below the maximum dynamic return pressure during a surge. The excitation of the poppet showed that any ability to assist in producing a low-pressure sensation in the gallery was dependent on having continuous low first-stage leakage during seal life. Such a requirement was unrealistic because, if it was practical to provide a minimum leakage first stage, there would be no need for a low-pressure second-stage seal.

Present actuator design philosophy does not allow that the design encumber the actuator performance to allow adaptation to other than the most efficient seal concept. Under this philosophy, it was necessary to develop a polyimide seal to satisfy the 9.998×10^6 N/m^2 (1450 psig) dynamic requirement described above.

The second-stage pressure impulse requirement was thus established as 200 000 cycles of 0 to 1.043×10^7 to 0 N/m^2 (0 to 1500 to 0 psig) at the return port with a rise rate between 1.724×10^8 to 2.413×10^8 N/m^2/sec (25 000 to 35 000 psig/sec) based on the HYTRAN simulator runs. The total number of cycles were accumulated by testing at the same environmental temperatures as imposed for the first-stage seals per table II.

In future years this philosophy may of necessity change where temperature environments require the use of polyimides. In such applications the polyimide may become the most efficient, or the only usable, seal and special design considerations may be necessary to utilize the polyimide material properties to their best advantage.

FIRST-STAGE ROD SEAL

A typical first-stage rod seal in aircraft linear actuator applications is a seal of rectangular cross section having controlled leakage characteristics to facilitate lubrication of the bearing located downstream of the seal, refer to figure 4. The sealing ring is usually divided, or split, to preclude use of a split gland installation. The split sealing ring is loaded by a spring compression ring around the outside circumference of the sealing ring. Various materials have been evaluated in development of such seals including cast iron, unfilled polyimide, and polyimides with fillers such as graphite, molybdenum disulfide, and Teflon. A Boeing standard for a cast iron first-stage rod seal of this configuration is included as appendix 1.

The objective of the development effort on first-stage seals reported herein was to expand the base of information on the existing seal configuration described above, not to develop a new or unique seal design. Research involving testing was concentrated on the various aspects of using polyimides as the material for the inner sealing ring and on evaluations of the potential for pressure balancing of this ring. Additional analytic research, which Boeing provided to supplement the contract, was performed to develop a theoretical tool for relating displacements and stresses in a rectangular seal section. This effort is reported in reference 12 and is offered as valuable design data, applicable to the development of new rectangular cross-section seals.

Basic Seal Design

The first-stage seal cross section was defined as an inner rectangular section seal ring with a step cut and an outer spring compression ring similar in design to the Boeing BACS11AM standard (appendix 1) for metallic rod seals. The step cut of the sealing ring was the critical design section. The necessary section thickness for a seal made of polyimide rather than cast iron was determined by the following analyses.

- A seal section was evaluated using fracture mechanics techniques with the result that it was not possible to produce the cantilever deflections necessary to develop a fracture stress in the material at the step cut.

- A seal section was evaluated as a rectangular section compression spring that was axially loaded with the same result as above.

- Neither of the above analyses considered fatigue failure because equations for fatigue required use of empirical constants that had to be established by test data. Material testing was excluded from the scope of the contract reported; thus the Koppers Company was informally contacted about their related experience. Koppers was consulted because they were the only approved source for the above-mentioned Boeing seal standard. Koppers' reply indicated that a 3.175×10^{-3} m (0.125 in.) wide seal with radial thickness of 2.286×10^{-3} m (0.090

in.) would provide the proper strength in a polyimide ring, based on tests relating fatigue failures to step fillet radius.

Pressure Balancing

A pressure balancing technique was developed for a first-stage seal model as shown in figure 7. A digital program for the high-speed digital computer was written to optimize pressure balancing with the prime objectives of:

- Determining the minimum sealing forces needed in both the axial and radial directions to control leakage within allowable limits when using polyimide material properties

- Balancing the axial and radial sealing forces to minimize the distortion of the seal cross section

An example seal was used to establish the computer program validity. The analysis considered a series of radial balancing grooves between D_2 and D_4 on the model (D_3 is one example) with each of a series of axial grooves between O and A (A_1 being an example). Considerations determined within the analysis included radial and axial friction on the sealing faces, radial and axial mechanical loading of the seal, and pressure distribution across the leakage paths. The example analysis results indicated that the most effective groove dimensions for force balancing radial and axial loads were 25% cuts on both seal faces. This condition did not provide the minimum forces for the control of leakage, thus indicating the need for design compromise and iteration to optimize the design.

The analytical optimum of both axial and radial balancing had drawbacks in applications where dynamic pressure surges were expected. Under delicately balanced conditions, rapid fluctuations in localized pressures cause seal lifting and increase leakage more readily than under conditions of less optimum balancing. This tradeoff between balancing and friction had to be placed in a realistic perspective for the application under consideration. Experience in testing revealed that side balancing did not contribute significantly toward reducing overall seal friction but it did detrimentally affect sealing in dynamic conditions. This practical viewpoint was considered to have greater value in the contract application than would provision of optimum balancing.

The above considerations were incorporated in a proposal to seal manufacturers for the procurement of test seals. The discussion of the design features of the procured hardware is provided under "Seal Procurement and Manufacture."

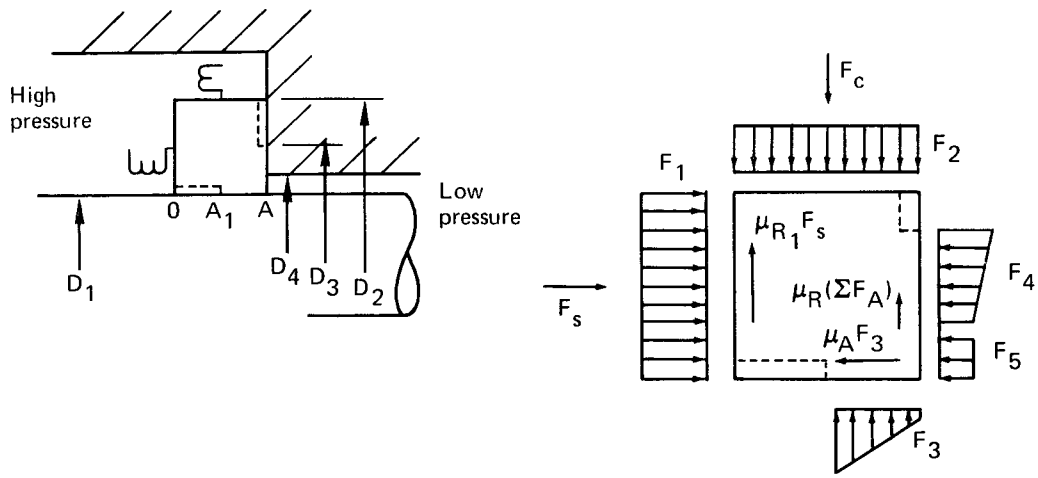

Terminology:

F_s	=	mechanically applied axial spring force
F_c	=	mechanically applied radial compression force
F_1	=	axial hydraulic high-pressure force in direction of system pressure
F_2	=	radial hydraulic high-pressure force toward rod
F_3	=	radial hydraulic pressure force along axial sealing face (assumed to reduce in a linear manner through oil film between rod and seal)
F_4	=	axial hydraulic pressure force along radial sealing face (reducing linearly through oil film)
F_5	=	axial hydraulic low-pressure force opposing system pressure
$\mu_{R_1}F_s$	=	friction between mechanical axial spring and seal in radial direction
$\mu_R(\Sigma F_A)$	=	friction force on radial sealing face
$\mu_A F_3$	=	friction force on axial sealing face

Figure 7—First-stage seal pressure balancing

SECOND-STAGE ROD SEALS

The primary design objective of the evaluation was to optimize the cross-sectional areas of the NASA Contract NAS3-11170 (ref. 2) B-1 and HB-1 second-stage seal designs and test the revised designs to realistic and existing requirements for actuators used in high-performance aircraft.

Seal and Gland Descriptions

Figures 8 and 9 show drawings of the B-1 and HB-1 seal assemblies, as configured in the reference 2 contract. Dimensions given on these drawings show percentage of seal gland depth. These proportions were maintained, in the initial design iteration, for the stress analysis to determine the ability of the B-1 and HB-1 configurations to satisfy alternating load cycling consistent with aircraft applications.

Figure 10 shows the second-stage seal cavity dimensions within the two actuators available for test evaluation. These dimensions could be used to establish the design outside diameters where seal modules are not to be incorporated. However, these outside diameters needed to be reduced in this study, where the seal module was considered, to ensure adequate thicknesses in the cylinder and module parts for the stresses imposed. The desirable goal was to have the final seal fit MIL-G-5514F envelopes. Dimensions for these glands are referenced in figure 10.

The use of three chevrons in the NAS3-11170 (ref. 2) B-1 configuration provided two redundant sealing surfaces. The first seal size reduction was to consider only two chevrons, thus providing one redundant seal. The design for the NAS3-11170 HB-1 seal assembly included only one redundant sealing surface, and it was not considered desirable to eliminate one of the K-sections in that configuration.

The design for the mechanical spring loading of the B-1 and HB-1 seals provided a static force on the inside lip of the sealing legs. This spring loading was designed to compensate for differential expansion during temperature rise. Initial seal deformation compensated the differential contraction during cooling. It was considered a very desirable goal in terms of simplifying seal design, to eliminate the need for the differential mechanical spring load on the seal lips.

Materials Considerations in Stress Analysis

An important aspect of design optimization was selecting the polyimide material with the properties best suited to the application under consideration. Comparison of candidate material properties for seal design applications was based on manufacturers' published information and test data obtained during evaluations reported in reference 2. The

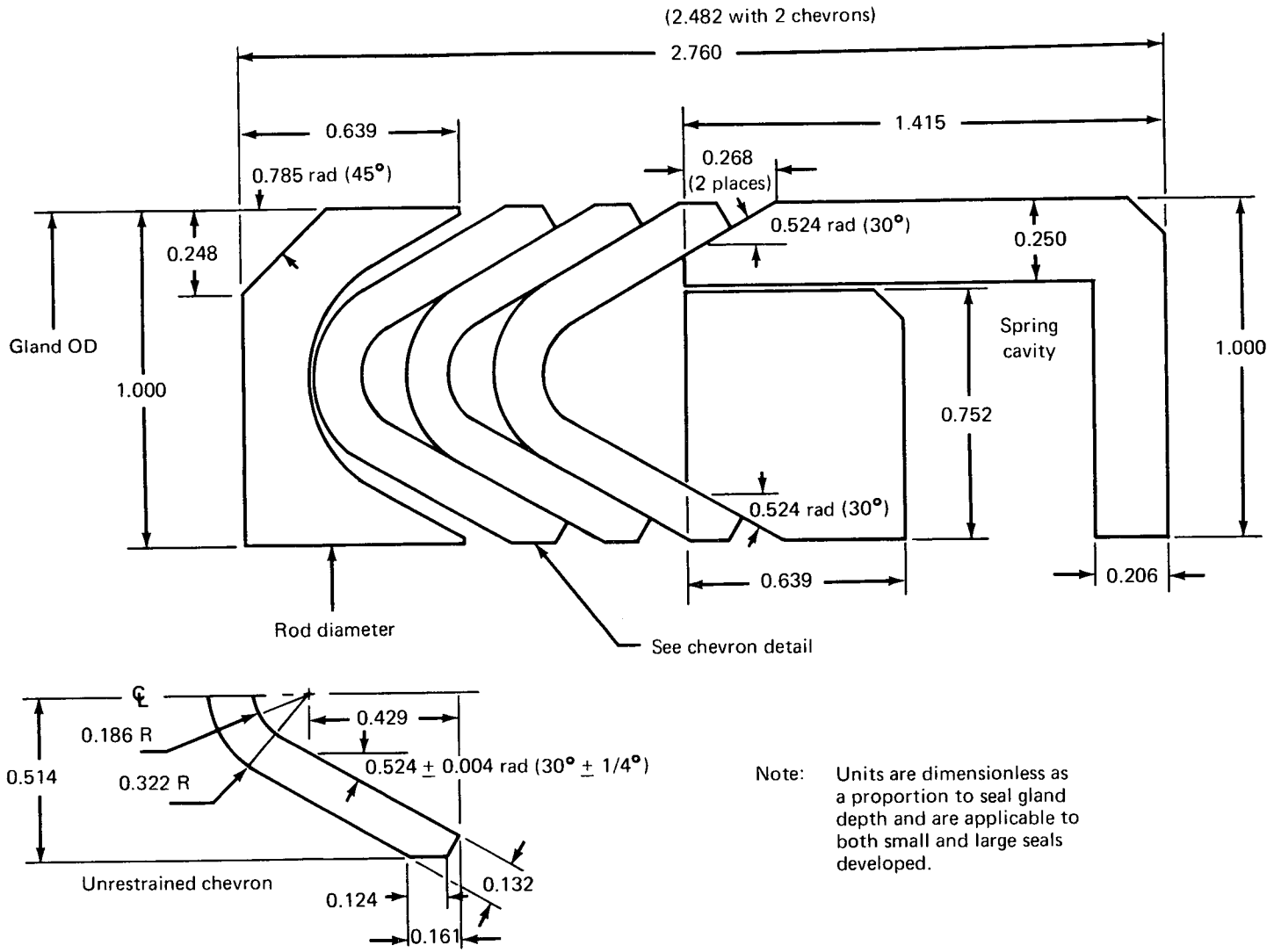

Note: Units are dimensionless as a proportion to seal gland depth and are applicable to both small and large seals developed.

Figure 8 – 0.524 Radian (30°) V-seal assembly (NAS3-11170 B-1 configuration)

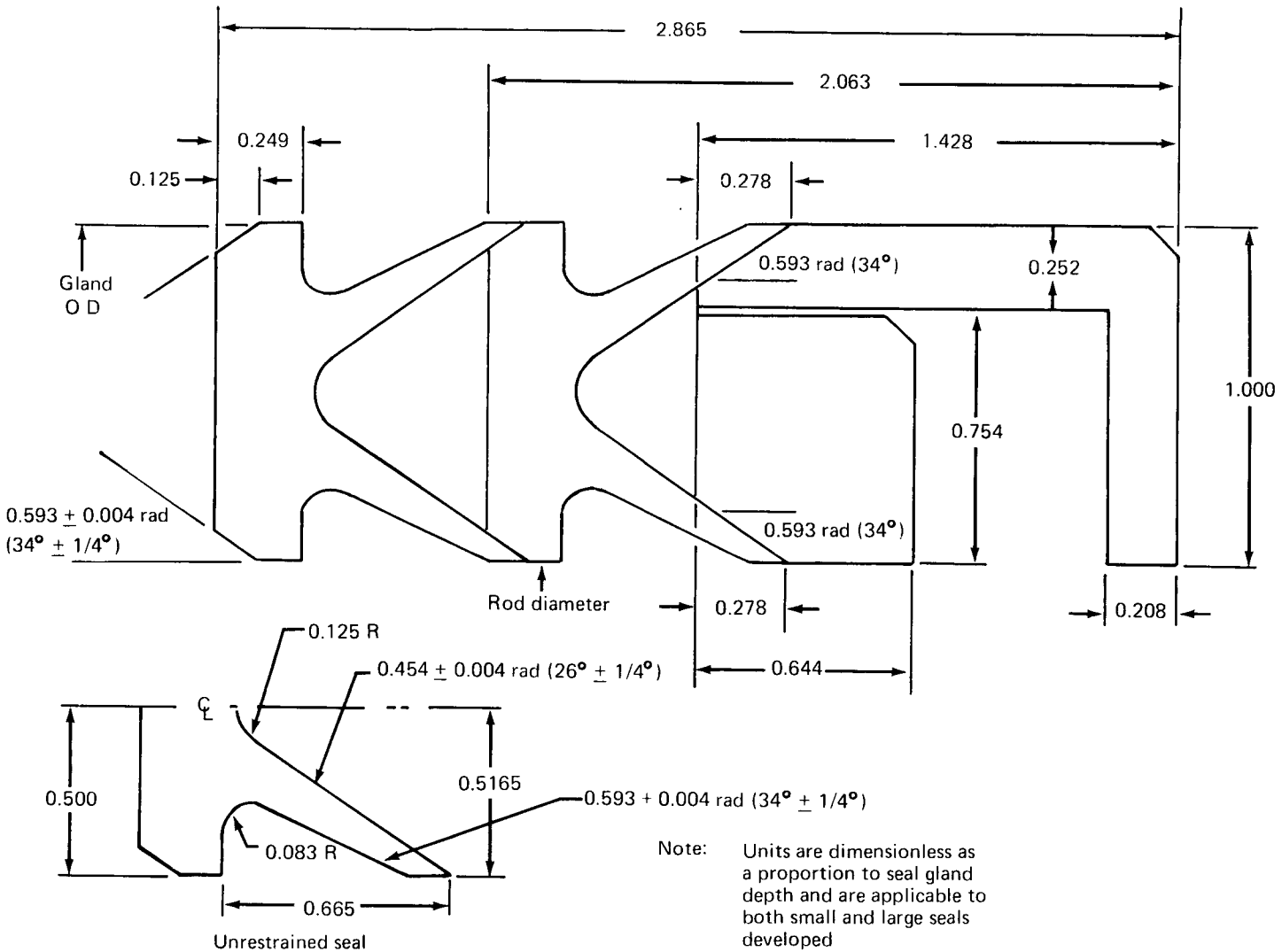

Figure 9 — Tapered leg seal NAS3-11170 HB-1 configuration

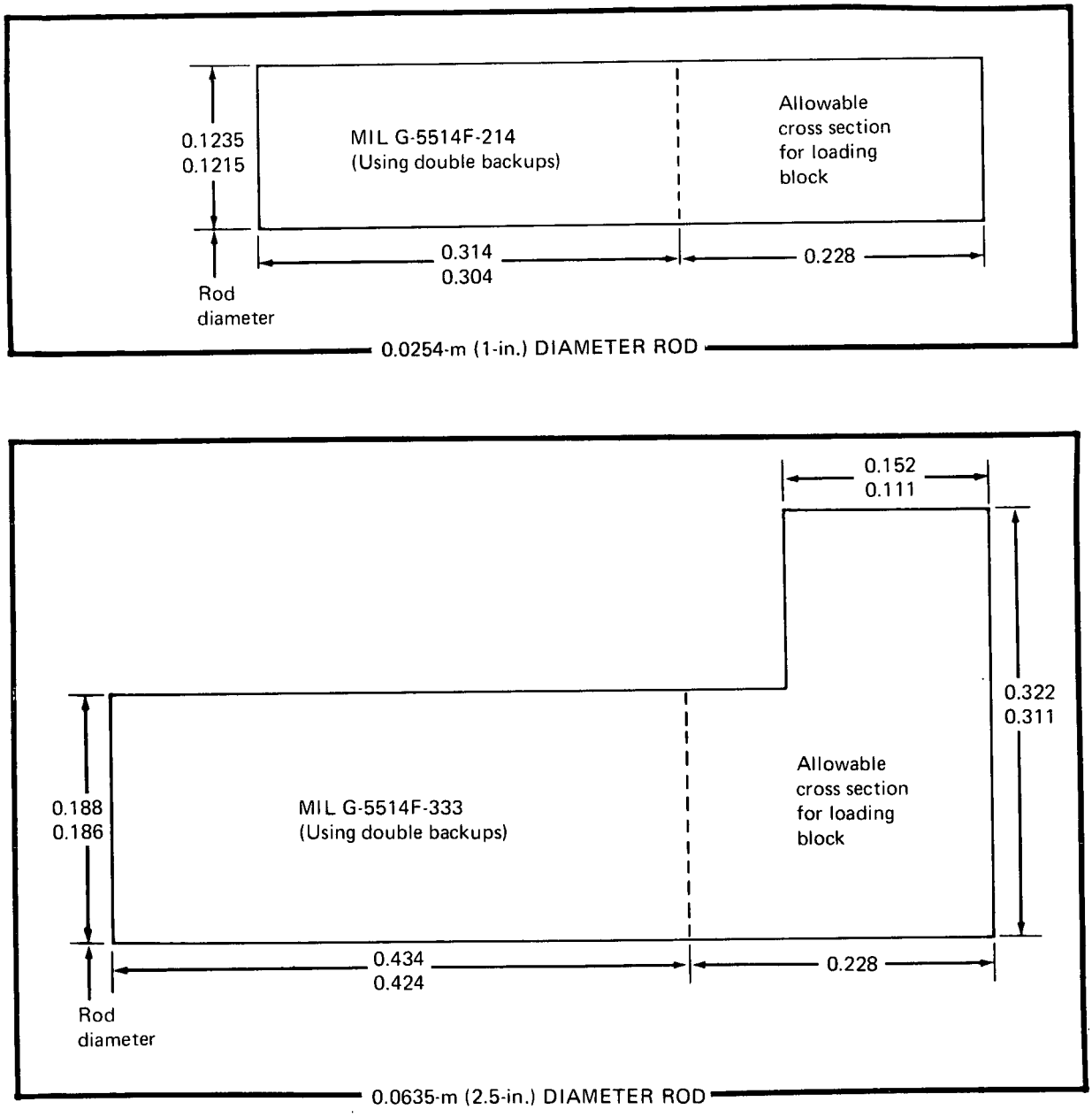

(all dimensions in inches)

Note: No SI conversion was made on dimensioned parts (See Appendix 9)

Figure 10.– Test Actuators Seal Gland Dimensions

properties of Gemon, Meldin, and Vespel polyimides were reviewed to determine whether material advancements since the reference 2 contract would provide an advantage to the seal designs under consideration. Table III shows the characteristic properties of candidate materials from each of these families best suited for seal design. The following are analyses of those properties.

- Gemon 2010, General Electric (Graphite filled—exact percentage proprietary)

  This material possesses the best combination of material ultimate strength properties and fabrication cost. It is relatively inexpensive and could be compression molded, and it appeared to yield superior wear resistance characteristics. Somewhat lower mechanical properties and the need to perform seal designs without complete knowledge of how the material behaves are disadvantages. The low elongations for Gemon 2010 and 2012 shown in table III were verified by the manufacturer and therefore disqualified these materials from further application because the strain introduced by preset interference would fail the material in elongation.

- Gemon 2012, General Electric (Tetrafluoroethylene filled—exact percentage proprietary)

  Comments for Gemon 2010 also apply to 2012, except that the latter had lower mechanical properties and was subject to lower wear rates.

- Meldin PI-15Y, Dixon (15% Graphite filled)

  This material is available in the form of molded flat sheet stock. Detail parts have to be machined. It does have very good mechanical and thermal properties. This material was not given further consideration after determining that stresses due to a 2.286×10^{-4} m (0.009 in.) required preset interference fit would cause excessive permanent set, an effect of the low elongation property of the material.

- Meldin PI-30X, Dixon (30% PTFE filled)
  The load capacity of less than 6.895×10^{6} N/m^2 (1000 psig) eliminates this material from consideration in dynamic load applications.

- Vespel SP-21 DuPont (15% Graphite filled)

  This material is available from DuPont as formed blocks or as machined parts. Supplied materials have been shown to have uniform properties, and considerable research data on properties have been published in reference 13. Because machining is the only method of fabrication, parts are more expensive than if they could be molded.

As a result of the material investigation discussed above, the DuPont Vespel SP-21 polyimide was determined to be the optimum material of the candidates considered.

Table III.—Candidate seal material properties (S.I. units—see next page for English units)

Property	Data source	Temp, °K	Time, sec x 10^3	Measured values for material candidates					
				Vespel SP-1	Vespel SP-21	Meldin PI-15Y	Meldin PI-30X	Gemon 2010	Gemon 2012
Compressive strength, N/m^2	Boeing	294	–	1.234×10^8	1.069×10^8	2.455×10^8	1.131×10^8		–
ASTM D-695	Supplier	294	–	1.655×10^8	1.241×10^8	2.179×10^8	8.964×10^7	1.889×10^8	1.269×10^8
	Supplier	478	1.8			–	–	1.103×10^8	7.240×10^7
	Boeing	533	1.8	6.281×10^7	4.958×10^7	9.653×10^7	3.999×10^7	–	–
	Supplier	533	1.8		–	1.124×10^8	4.827×10^7	8.688×10^7	5.576×10^7
	Boeing	533	1800	5.826×10^7	5.840×10^7	1.076×10^8	3.896×10^7	–	–
Tensile strength, N/m^2	Boeing	294	–	8.826×10^7	7.240×10^7	5.557×10^7	2.730×10^7	–	–
ASTM D-638	Supplier	294	–	7.240×10^7	4.482×10^7	4.964×10^7	2.289×10^7	5.171×10^7	3.448×10^7
	Supplier	478	1.8	5.033×10^7	2.689×10^7	–	–	3.310×10^7	2.758×10^7
	Boeing	533	1.8	4.061×10^7	3.965×10^7	3.599×10^7	9.832×10^6	–	–
	Supplier	533	1.8	4.137×10^7	2.413×10^7	2.303×10^7	9.446×10^6	2.413×10^7	2.344×10^7
	Boeing	533	1800	3.275×10^7	2.861×10^7	3.110×10^7	6.219×10^6	–	–
	Supplier	533	1800	2.813×10^7	–	–		–	–
Elongation, %	Supplier	294	–	5 to 6	3 to 4	2	1.7	< 1	< 1
ASTM D-1708	Supplier	524	1.8	5 to 6	3 to 4	–	–	–	–
Deformation under load, %	Supplier	323	1.8	0.14	0.10	–	–	–	–
1. Measured % at $1.379 \times 10^7 N/m^2$ ASTM D-621	Supplier	294	–		–	0.5	1.2	–	–
	Supplier	533	1.8	–	–	0.7	1.5	–	–
2. Measured % at 2.758×10^7 N/m^2	Supplier	294	–		–	–	–	0.0	0.14
Coefficient of friction measured by supplier methods	Supplier	294	–	0.15 to 0.26	0.11 to 0.20	0.30 to 0.35	0.20 to 0.25	0.13 to 0.25	0.10 to 0.25
Wear rate									
1. m/sec in air at 1.379×10^6 N/m^2	Supplier	294	–	1.764×10^{-9} to 8.467×10^{-9}	6.350×10^{-8}	–	–	5.545×10^{-8}	2.822×10^{-7}
2. m/m on ~~6~~Al-4V titanium	Boeing	456	–			2.75×10^{-8}	2.5×10^{-8}		
at 1.379×10^6 N/m^2	Boeing	506	–	2.67×10^{-8} (with 5% PTFE added)	1.33×10^{-8}	1.83×10^{-8}	2.33×10^{-8}		
Thermal coefficient of	Supplier	256 to 533	–		–	–	–	3.78×10^{-5}	5.4×10^{-5}
expansion, m/m/°K, ASTM D-696	Supplier	294 to 478	–	5.04×10^{-5}	4.32×10^{-5}	–	3.96×10^{-5}	–	–
Mold shrinkage, m/m	Supplier		–	–	–	–	–	0.008	0.008

Table III.—Candidate seal material properties (English units)

Property	Data source	Temp, °F	Time, hr	Measured values for material candidates					
				Vespel SP-1	Vespel SP-21	Meldin PI-15Y	Meldin PI-30X	Gemon 2010	Gemon 2012
Compressive strength, ksi ASTM D-695	Boeing	70	–	17,900	15,500	35,600	16,400	–	–
	Supplier	70	–	24,000	18,000	31,600	13,000	27,400	18,400
	Supplier	400	0.5	–	–	–	–	16,000	10,500
	Boeing	500	0.5	9,110	7,190	14,000	5,800	–	–
	Supplier	500	0.5	–	–	16,300	7,000	12,600	8,000
	Boeing	500	500	8,450	8,470	15,600	5,650	–	–
Tensile strength, ksi ASTM D-638	Boeing	70	–	12,800	10,500	8,060	3,960	–	–
	Supplier	70	–	10,500	6,500	7,200	3,320	7,500	5,000
	Supplier	400	0.5	7,300	3,900	–	–	4,800	4,000
	Boeing	500	0.5	5,890	5,750	5,220	1,428	–	–
	Supplier	500	0.5	6,000	3,500	3,340	1,370	3,500	3,400
	Boeing	500	500	4,750	4,150	4,510	0,902	–	–
	Supplier	500	500	4,080	–	–	–	–	–
Elongation, % ASTM D-1708	Supplier	70	–	5 to 6	3 to 4	2	1.7	< 1	< 1
	Supplier	483	0.5	5 to 6	3 to 4	–	–	–	–
Deformation under load, %	Supplier	122	0.5	0.14	0.10	–	–	–	–
	Supplier	70	–	–	–	0.5	1.2	–	–
1. measured % at 2000 psig ASTM D-621	Supplier	500	0.5	-	–	0.7	1.5	–	–
2. measured % at 4000 psig	Supplier	70	–	–	–	–	–	0.0	0.14
Coefficient of friction measured by supplier methods	Supplier	70	–	0.15 to 0.26	0.11 to 0.20	0.30 to 0.35	0.20 to 0.25	0.13 to 0.25	0.10 to 0.25
Wear rate 1. in./1000 hr in 200 psig air	Supplier	70	–	0.25 to 1.2	0.09	–	–	0.08	0.004
2. in./ft on 6Al-4V titanium	Boeing	360	–			3.3×10^{-7}	3.0×10^{-7}		
at 200 psig	Boeing	450		3.2×10^{-7} (with 5% PTFE added)	1.6×10^{-7}	2.2×10^{-7}	2.8×10^{-7}		
Thermal coefficient of expansion, in./in./°F, ASTM D696	Supplier	0-500						2.1×10^{-5}	3.0×10^{-5}
	Supplier	70-400		2.8×10^{-5}	2.4×10^{-5}		2.2×10^{-5}		
Mold shrinkage, in./in.	Supplier							0.008	0.008

Isotropic property data were investigated. There were no direct test data available; however, the opinion of DuPont was that SP-21 isotropic fatigue curves would have the same slope as those for the parallel and perpendicular grain dimensions and would be half way between these curves. Due to lack of data, further consideration was not given to designing for use of isotropic properties.

The Boeing proposal for the reported research contract, reference 14, suggested use of DuPont Vespel SP-1 for the second-stage seal material to provide correlative results between reference 2 and the evaluation being reported. This course of action would have precluded use of advanced polyimides which might show improved seal characteristics. On the basis of the investigation of the material developments described above, Vespel SP-21 was allowed for initial second-stage seal design to take advantage of DuPont technology advancements.

Because there was insufficient manufacturers' information on polyimide fatigue properties, an attempt was made to more accurately predict these properties for other than zero mean stresses by using the DuPont zero-mean data and formulas applicable to metallic materials. The Stuessi method was used to shape the S-N curves in figure 11 (perpendicular and parallel grains for SP-21 material) for different constant mean stress levels. The crossplot of the S-N curves in figure 11 for perpendicular and parallel material grains, respectively, indicate the maximum stress levels as a function of the shape of the stress cycle. These curves were considered applicable for plastics in the region where there was no plastic flow. There was no attempt to verify the data by testing, this being outside the scope of the study.

Correlative test data were needed to substantiate the validity of the curves developed above. Tests reported in reference 2 and those performed at NASA-Lewis during evaluations concurrent to this study were reviewed for applicable fatigue data that would assist in this correlation. A compilation was made of such data and is included as table IV. These data indicate that in tests 3A and 4B the DuPont fatigue allowables have been exceeded successfully, providing the correlation desired. Because the number of tests were few, and the test conditions varied, this type of correlation did not provide sufficient data to describe the values to which the fatigue allowables could be adjusted. The data did indicate conservatism in the manufacturers' allowables sufficient to indicate that SP-21 material could be used with the chevron design parameter optimizations.

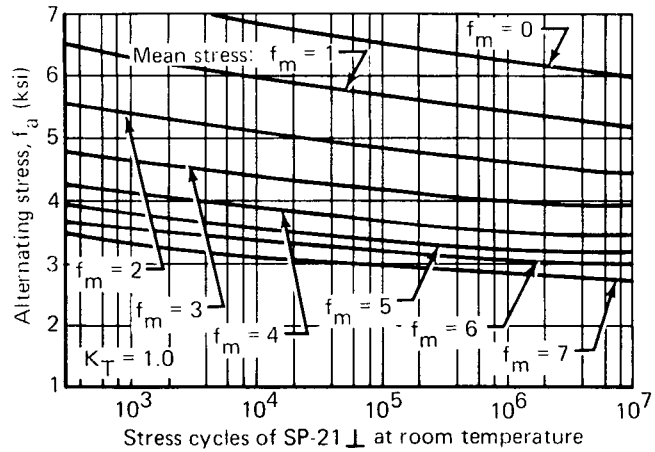

Mean stress data

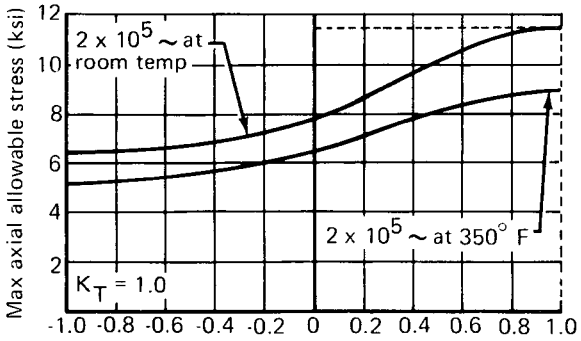

SP-21 ⊥ corrected stress

REFERENCE DATA ONLY
do not use for design

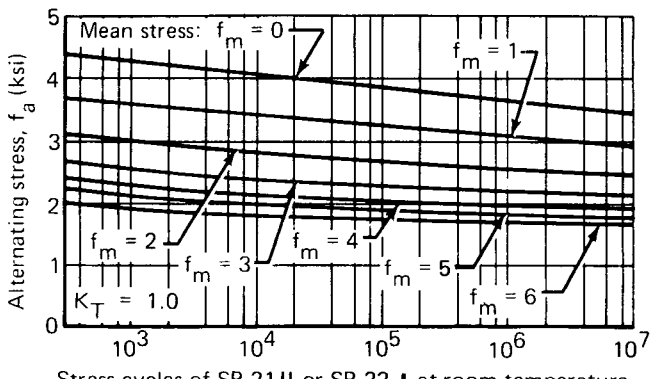

Mean stress data

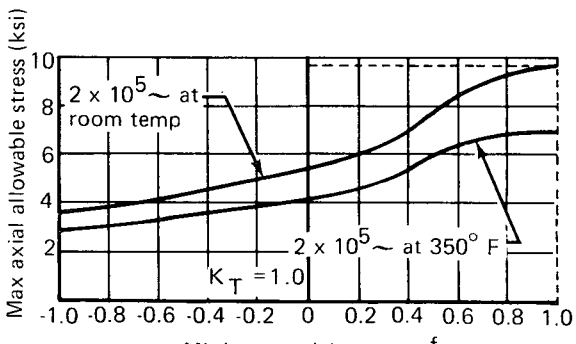

SP-21 ∥ or SP-22 ⊥ corrected stress

Figure 11.—Steussi corrections for mean stresses

Table IV.—Fatigue Test Data

Test no	By	Seal configuration	Preset		Load cycle*	Stress Cycle				Cycles applied x 10^3	Failure type	Predicted life in cycles	Comments
						Minimum		Maximum					
			m x 10^5	in. x10^3		N/m^2 x 10^6	ksi	N/m^2 x 10^6	ksi				
1A	NASA	Single NAS3-11170 HB-1 seal without backup	3.810	1.5	(c) at room temp					0	Circumferential		Progressive leak with applied pressure
1B	NASA	Single NAS3-11170 HB-1 with outer leg backup	3.810	1.5	(a) at room temp					201			No failure
1C	Contractor	Double NAS3-11170 HB 1 seal	11.43	4.5	(b) at room temp (b) at 533°K (500°F)					3 480 17 870			No failure
2A	NASA	Single NAS3-11170 0.5236 rad V-seal without backup	3.175	1.25	(a) at room temp	4 137	0.6	>137.9	>20	0	Circumferential at apex		Instantaneous failure
2B	NASA	Single NAS3-11170 0.5236 rad V-seal with outer leg backup	3.810	1.5	(a) at room temp	5 516	0.8	>137.9	>20	0	Circumferential at apex		Instantaneous failure
2C	NASA	Single NAS3-11170 0 5236 rad V-seal with 2.094 rad backup	3.810	1.5	(a) at room temp	5 516	0.8	113.1	16.4**	258			No failure
2D	Contractor	Triple NAS3-11170 0.5236 rad V-seal	11.43	4.5	(b) at room temp (b) at 533°K (500°F)					3 480 17 870			No failure
3A	NASA	Single 0.5236 rad V-seal with Mil spec depth–no backup	5.080	2.0	(a) at room temp	51.02	7 4	75 16	10.9	192		$< 10^3$	No failure
4A	NASA	Single 0.3491 rad V-seal with Mil spec depth–no backup	5.080	2.0	(a) at room temp	26.20	3.8	43.44	6.3	218		$\approx 10^8$	No failure
4B	NASA	Single 0.3491 rad V-seal with Mil spec depth–no backup	5.080	2.0	(a) at room temp (a) at 450°K (350°F)	22.06	3.2	47.58	6.9	50 104	Circumferential at apex	$\approx 10^4$	Failed at 154 000 cycles
4C	NASA	Single 0.3491 rad V-seal with Mil spec depth–2.44 rad backup	5.080	2.0	(a) at room temp (a) at 408°K (275°F) (a) at 450°K (350°F) (a) at 478°K (400°F)	22.06	3.2	3.448	0.5	5 126 10 14		$>10^8$	No failure at 215 000 cycles Leakage at cooldown probably due to aging
5A	Contractor	Triple NAS3-11170 0.7854 rad V-seal	11.43	4.5	(b) at room temp (b) at 533°K (500°F)					11300	Circumferential		Failed at 11 300 000 cycles
6A	Contractor	Triple NAS-11170-1.1519 rad V-seal	11.43	4.5	(b) at room temp (b) at 533°K (500°F)					18820	Circumferential		Failed at 18 820 000 cycles

*(a) 0 to 1.034 x 10^6 N/m^2 (0-1500 psig hydraulic pressure)
(b) 0 to 1.034 x 10^5 N/m^2 (0-150 psig hydraulic pressure)
(c) unknown load cycle

**Stress exceeds reasonable allowables data indicate full backup contact

Stress Analysis Modeling

The chevron seal geometry was extremely sensitive to the relationship between material stresses and the imposed hydraulic pressure loading. The object of the stress analysis was to determine the specific chevron geometry, adaptable within available test actuators, that would tolerate the highest hydraulic pressure reversals occurring during dynamic operation of the design service application. The analysis was necessary because the geometry of the reference 2 B-1 and HB-1 seals, without a modification, would not sustain the stresses in an actual airplane application. There were a number of design iterations leading to the final configuration of a tapered-leg, thickened-apex chevron design. Those that received major consideration are discussed in chronological order of evaluation.

Initial program definition.—There were a number of differences between the requirements applied to the reference 2 test seal designs and the design needed for an airplane service application. These differences all reflected increases in stress loads. The following had a significant relationship to determining the conditions of stress in the seal as it would be used in a high-performance aircraft service application such as the SST or Air Force B-1.

- Polyimides are plastics having no definite yield point, this being shown on the stress-strain curve in figure 12. Yield points that were used in calculations were selected using 0.002 m/m (in./in.) strain parallel offsets to the slope of the tension-compression curve at 0 strain. The modulus of elasticity used in calculations was the slope of the 2% offset lines.

- The large differential between coefficients of thermal expansion for the steel actuator 1.26×10^{-5} m/m/°K (7×10^{-6} in./in./°F), and the polyimide seal, 4.14×10^{-5} m/m/°K (23×10^{-6} in./in./°F), needed to be considered in the seal design so that leakage paths at the seal ID at high temperature and at the seal OD at low temperature would not be introduced. The magnitudes of these effects are illustrated in figure 13, showing the free dimension relationships between the seal and cavity if the full effects of aging and differential expansion are allowed without compensation.

- The most important of the properties affecting the subject analysis of stress was fatigue strength. Very little data were found in a literature search and by discussions with DuPont to describe polyimide fatigue allowables. The DuPont Vespel design handbook, reference 13, indicated the following allowables for SP-21 material in the perpendicular grain.

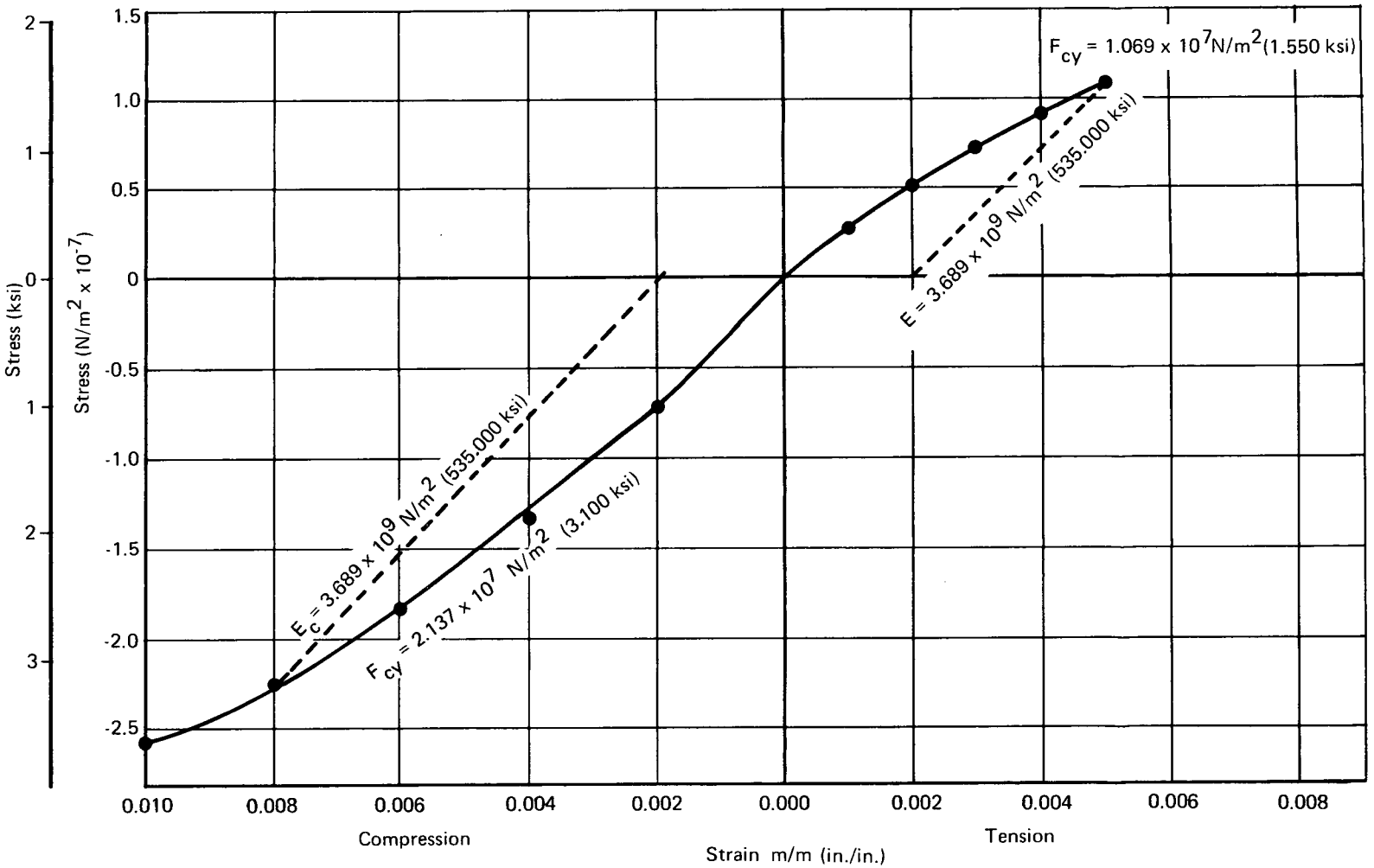

Figure 12.— Stress-strain curve, Vespel SP-21 at 533°K (after 1.8 x 10^6 sec @ 533°K)

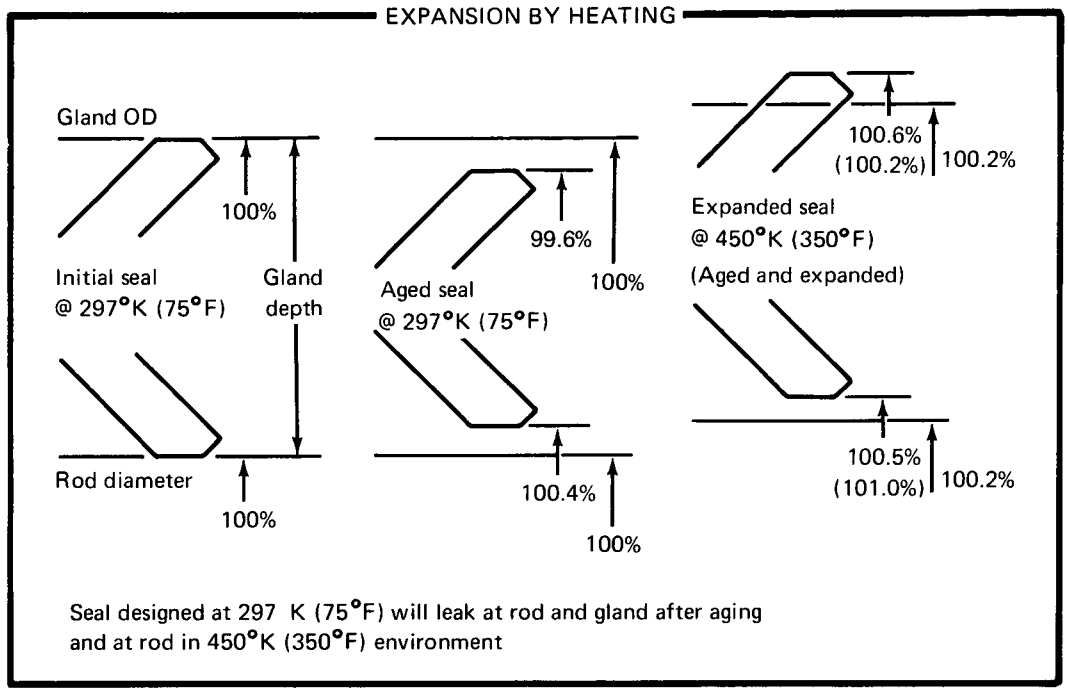

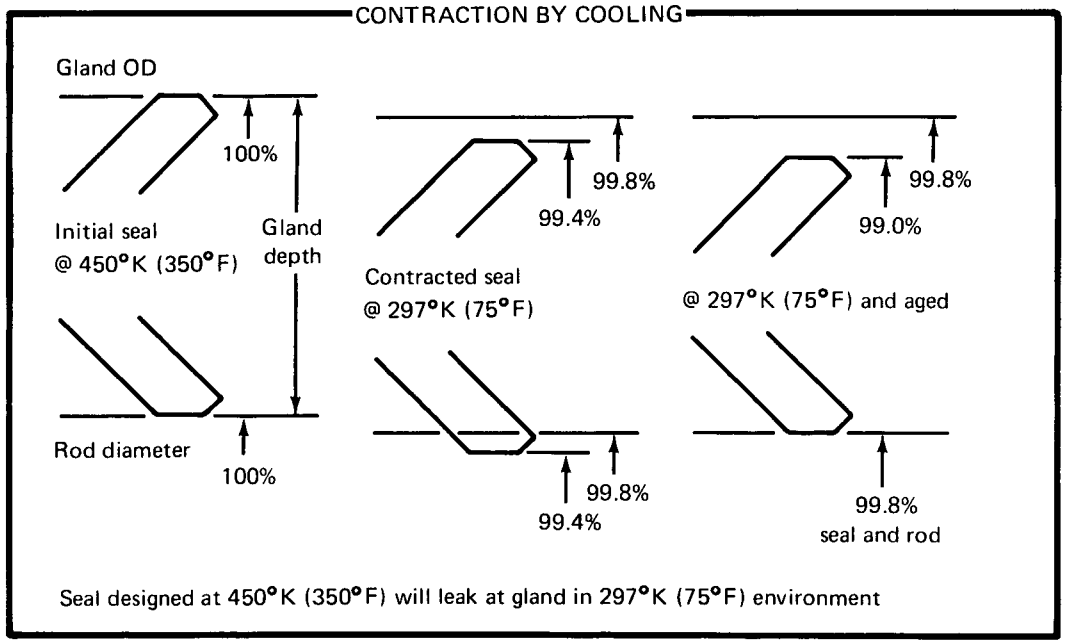

Note: Percentages are final dimensions of unrestrained parts

Figure 13.—NAS3-11170 B-1 seal vs steel actuator: thermal effects

For SP-21, allowable fatigue stress

$= 4.620 \times 10^7$ N/m^2 (6.700 ksi) @ 2×10^5 cycles, room temperature (for 1.043×10^7 N/m^2 (1500 psig) impulse during ground servicing)	Impulse
$= 2.965 \times 10^7$ N/m^2 (4.300 ksi) @ 2×10^5 cycles, 450° K (350° F) (for 6.895×10^6 N/m^2 (1000 psig) impulse during flight service)	Life
$= 4.137 \times 10^7$ N/m^2 (6.000 ksi) @ 8×10^6 cycles, room temperature (for 1.379×10^6 N/m^2 (200 psig) steady state ground service)	Fatigue
$= 2.620 \times 10^7$ N/m^2 (3.800 ksi) @ 8×10^6 cycles, 450° K (350° F) (for 2.758×10^6 N/m^2 (400 psig) steady state flight service)	Life

These allowables were established at a specific stress cycle with a zero mean. (A zero-mean stress was defined as equal magnitude tension and compression loading about a zero stress.) This requirement is illustrated as the allowable material stress cycle in figure 14.

The difference between the maximum and minimum values in the applied stress cycle from figure 14 for the application being investigated were significantly less than the allowable stress limits, although the maximum tension stress for the applied cycle at 450° K (350° F) exceeded the allowable for this temperature. Because the applied stress amplitude was only 28% of the allowable and the maximum stress exceeded the tension allowable by only 9%, it was concluded that the seal could meet the high-temperature cyclic stress requirements.

The stress analysis of the chevron seal was initially treated as the combination of internal and external cones interacting with a circular plate, which approximates the apex action of the cross section. The best seal from the above analysis was mathematically modeled for a finite-element solution using a high-speed digital computer.

The method of interacting cones was abandoned in favor of the finite-element plate analysis, which was considered to better represent the elemental interactions of the chevron seal. The initial rough design analyses, using the plate analysis method, are described in appendix 2. Figure 15 shows a simplified diagram of the finite-element mathematical model using plate theory. The advantages of the improved model were integrally tied to its use in the stress analyses to formulate an optimum seal configuration. The advantages include the following.

- The increase in the number of nodes at the apex of the downstream chevron improved accuracy in analysis of effects of leg angle change and support block stress relief. In analyzing the effects of variation in support block contact a backup block was simulated for a large angle of contact about the seal apex. This was in contrast to the apex point loading used in the unit cases analyzed in the preliminary evaluations (see appendix 2).

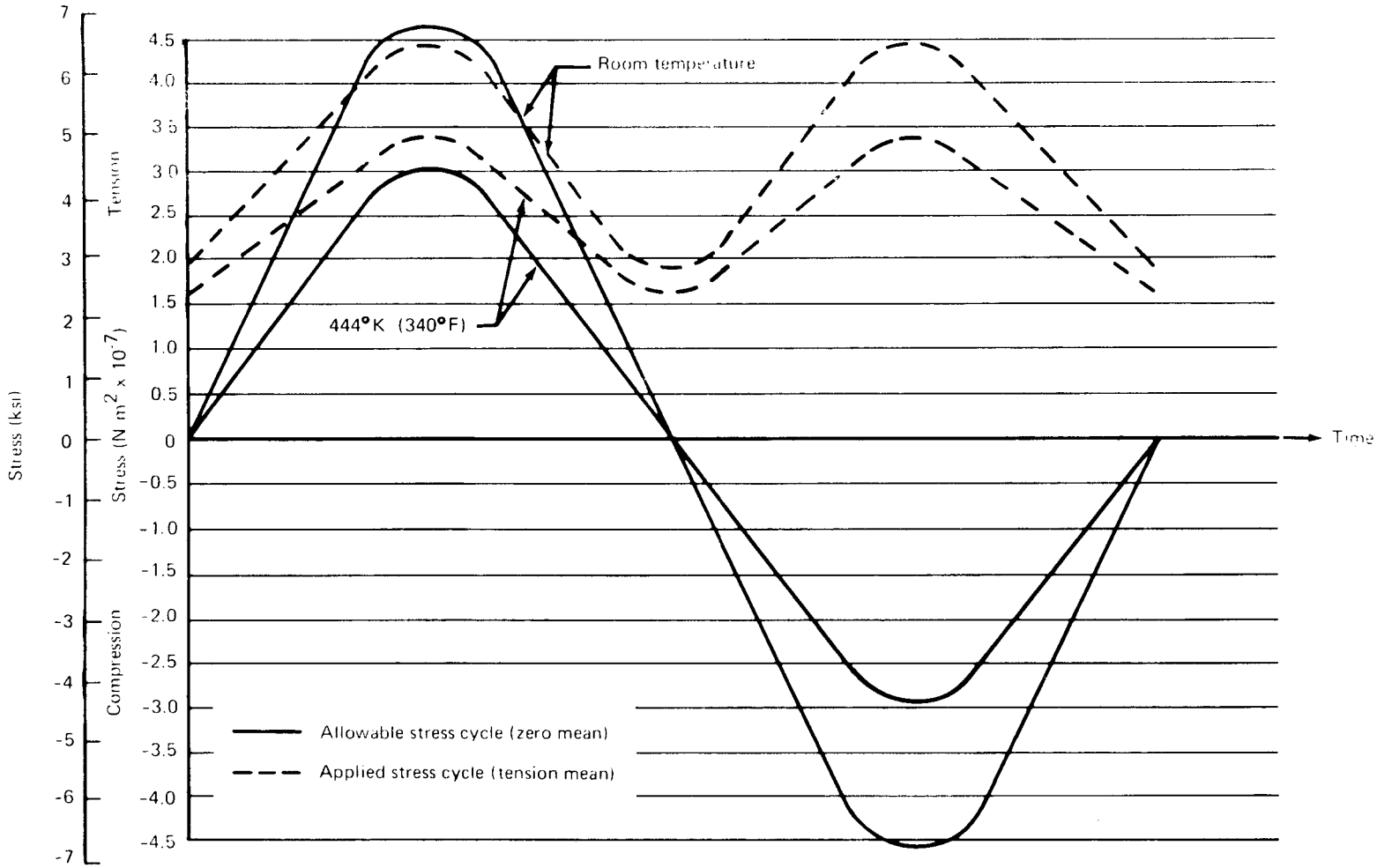

Figure 14.—Upstream chevron stress cycle

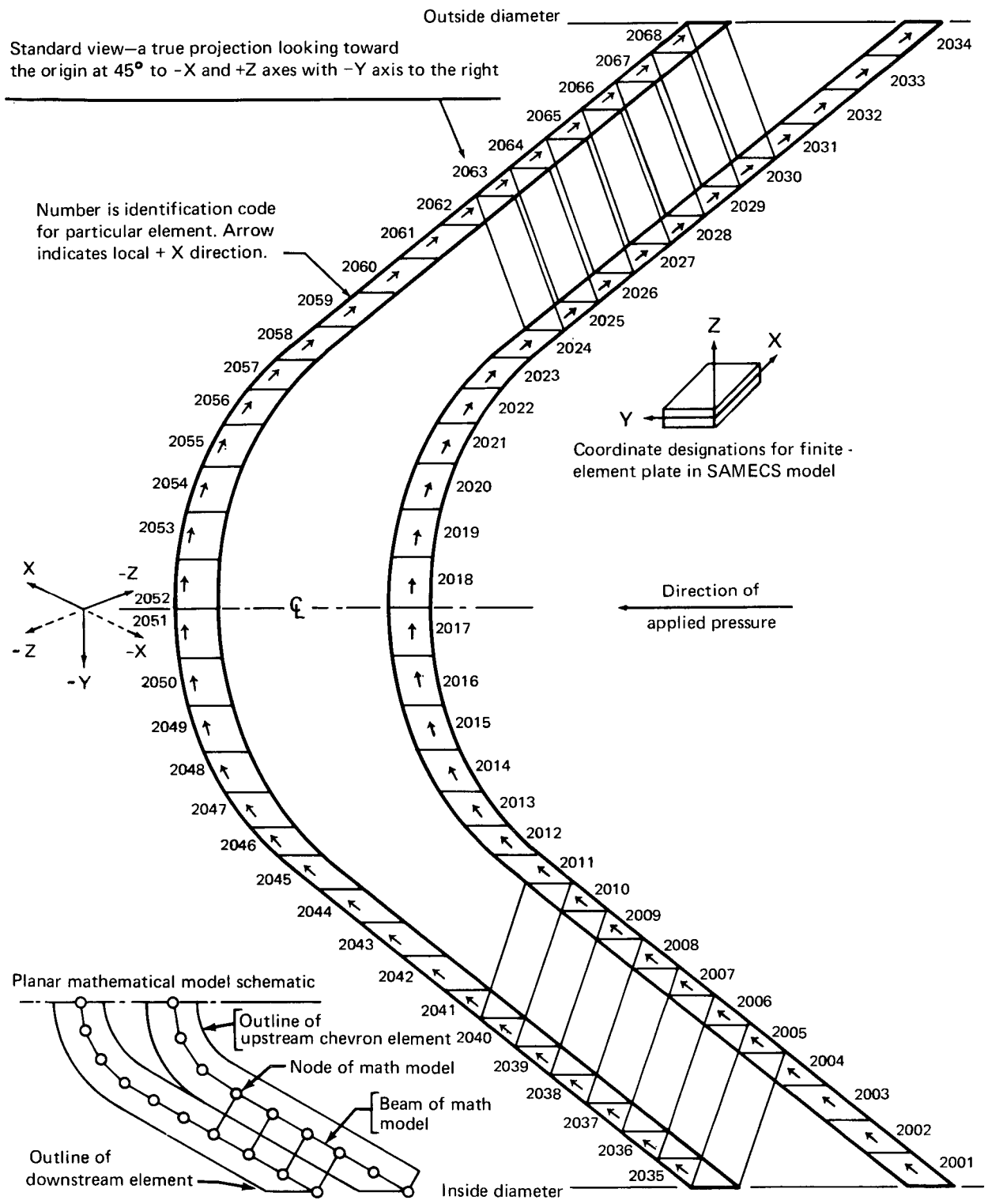

Figure 15 — SAMECS stress model: two chevron, 0.524-rad (30°) seal

- The addition of nodes and interconnecting beams across the area of contact between the upstream and downstream seal elements facilitated more accurate definition of the interactions between seal elements when exposed to ranges of hydraulic pressures, element thicknesses, and leg angles.

The definition used for each of the finite elements of the chevron seal is the plate as described in figure 15, a reproduction of the computer printout of the idealized seal model. The method of analysis used evaluated the response of individual plates, or elements, and subsequently combined those responses to produce compatibility within the structure.

The Boeing SAMECS computer program, reference 15, used the direct stiffness (displacement) method to perform the required analyses. Unknown rotations and displacements of the seal were determined using the matrix form of the following equation:

$$[\rho] = [K]^{-1} [F]$$

where [K] was the stiffness matrix, [F] was the force matrix, and $[\rho]$ was the matrix of unknown displacements.

Specified pressure and preset interference loads were introduced into this equation to yield a seal displacement vector in global coordinates. The computer program then transformed this displacement vector into elemental displacements which, when multiplied by the element stiffness matrix, produced the element loads.

The chevron seal finite-element model had 68 plates. In order to economically analyze the large number of plates, a thin-slice approach was used. The thin slice, 0.01745 rad (1°), of seal circumference, was restrained between a coordinate system plane and a plane slightly skewed to the coordinate system. The chevron seal model was particularly suitable to a thin-slice analysis because the structure and applied loads were axisymmetric. In such cases a very thin slice of the structure may be analyzed in place of a quarter shell.

Symmetric boundary conditions dictated that the shell could not translate perpendicular to the boundary or rotate at the boundary. Since one boundary was in a coordinate plane, translation and rotation were deleted from the problem by removing the entire row and column, corresponding to zero deformation, from the stiffness matrix. On the thin-slice boundary, mechanisms were used which employed artificially stiff elements (torque tubes and axial rods) to restrain the structure in the required directions. These elements were assigned stiffnesses 1000 times greater than the hoop stiffness of the actual structure at the boundary, assuring zero deflection.

The predominant stresses encountered in the finite-element analysis of the chevron seal were meridional bending stresses. The hoop stresses were approximately 30% to 40% of the meridional stresses in most cases and therefore were not critical to design. The meridional bending stresses were caused by interaction forces between the chevron legs and boundary reactions at the gland OD and ID.

Figure 16 shows the results of the finite-element analysis of a two-chevron seal on a 0.0254 m (1 in.) diameter rod with varying groove depths. All seal dimensions were retained in the same proportions as configured in the B-1 chevron design, the model being shown on figure 8.

The stresses plotted are the most critical meridional stresses, which occur at plate 2017, figure 15, for different pressure levels and a constant 2.286×10^{-4} m (0.009 in.) interference fit.

These results indicated that gland depth did not greatly affect the stress in a chevron seal. The curves also showed the sensitivity of the chevron seal to pressure loading by the relationship of internal stresses to the 4.137×10^{7} N/m^2 (6.00 ksi) nominal stress level allowable for SP-21 polyimide material in the seal configuration.

The freebodies in figure 17 are presented to illustrate the predominate forces and reactions to which a two-chevron configuration was subjected. Hoop stiffness (K_{hoop}) and beam bending stiffness were interrelated such that, as rod diameter became larger, the load reacted by increased beam bending. For rod diameters of 0.0254 m (1.0 in.) and larger, that were of interest for the applications under consideration, the dominant influence was beam bending. A plot of beam bending stress versus rod diameter is shown in figure 18 for the conditions of 1.034×10^{7} N/m^2 (1500 psi) pressure loading with a seal having a 0.5236 rad (30°) leg angle and various leg thicknesses. These results show a near flat characteristic of applied bending stress and rod diameter.

For rod diameters less than 0.0254 m (1.0 in.) the hoop stiffness may become dominant due to the lower allowables in the parallel grain of the polyimide material. This relationship was not evaluated in the stress analysis for the reported evaluation, but it will be a factor for consideration in the future to prepare seal dimension standards for a range of seal sizes for industry use.

Another parameter important to stress analysis was the curved-beam correction factor for bending stresses. Because there was a nonlinear distribution of stresses due to curved-beam bending, correction factors had to be applied as indicated in figure 19. The R/c value for the reference 2 seals was 4.0. This value was accepted as a minimum objective for design to keep the inside fiber stresses from exceeding practical allowable limits. Control of R/c was thus maintained by the proper selection of R with respect to optimum t such that $R > 2t_{opt}$.

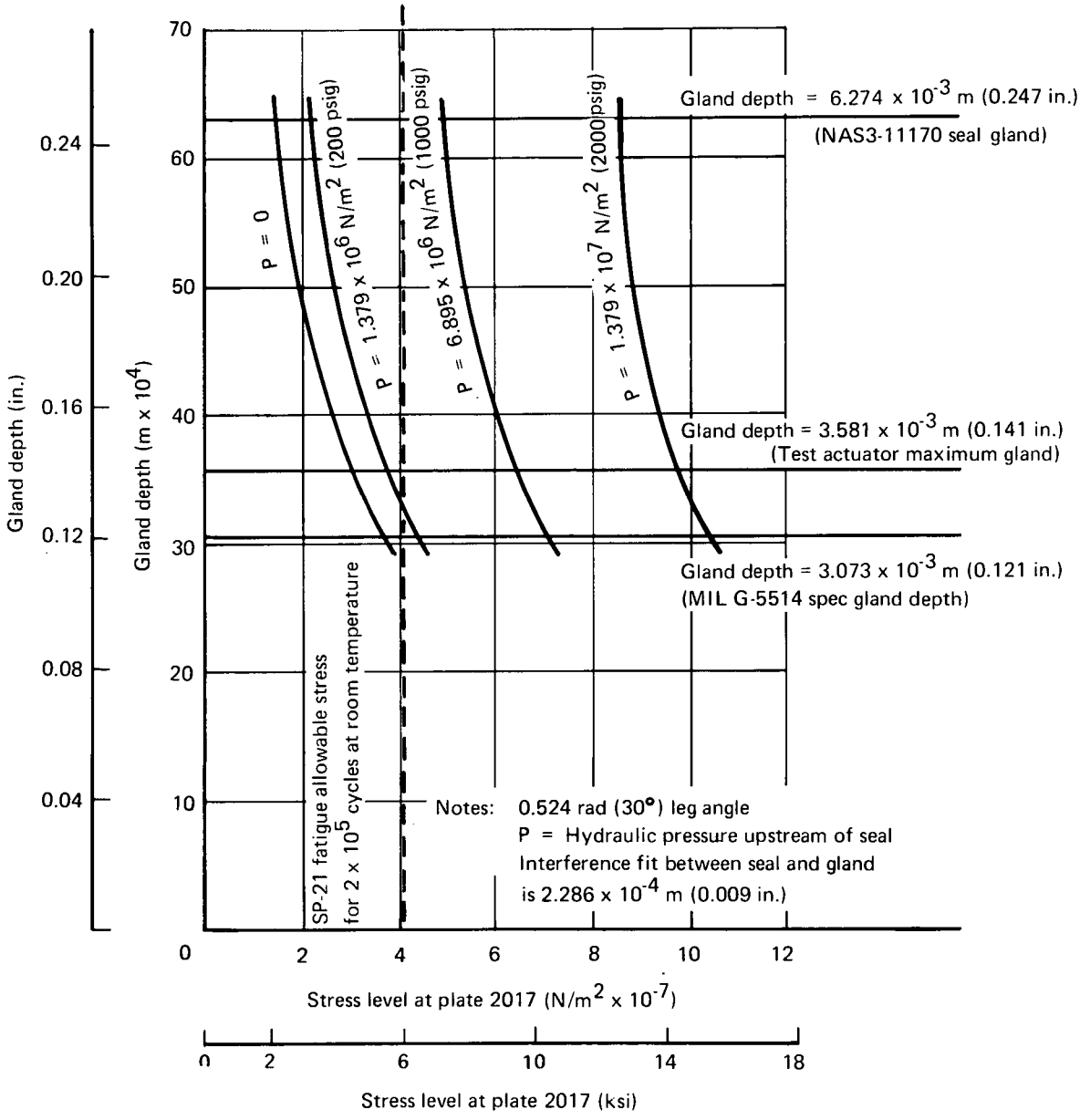

Figure 16.– SAMECS model stress vs gland depth

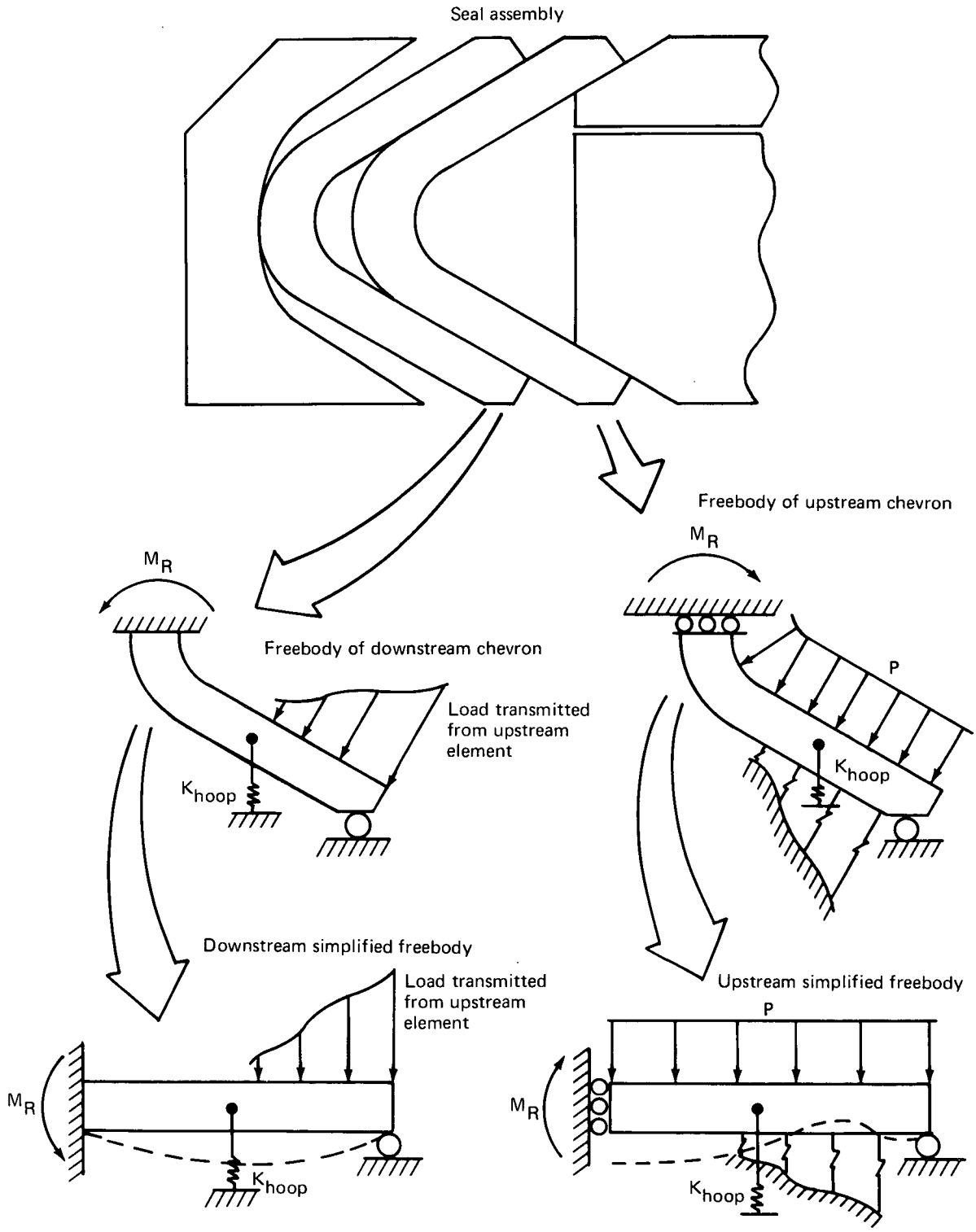

Figure 17.– Freebody diagrams for chevron seal

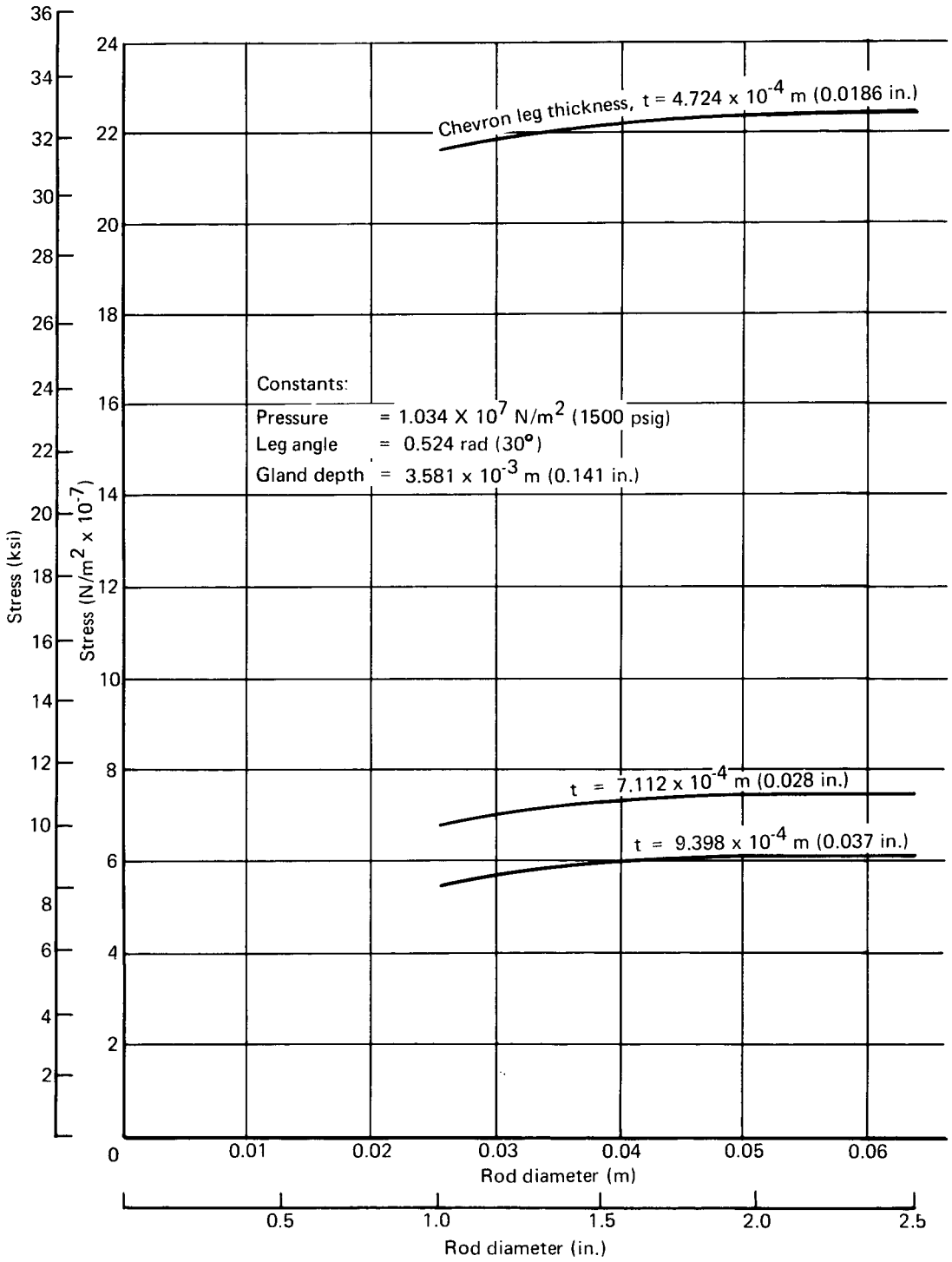

Figure 18.-- Stress variation with diameter

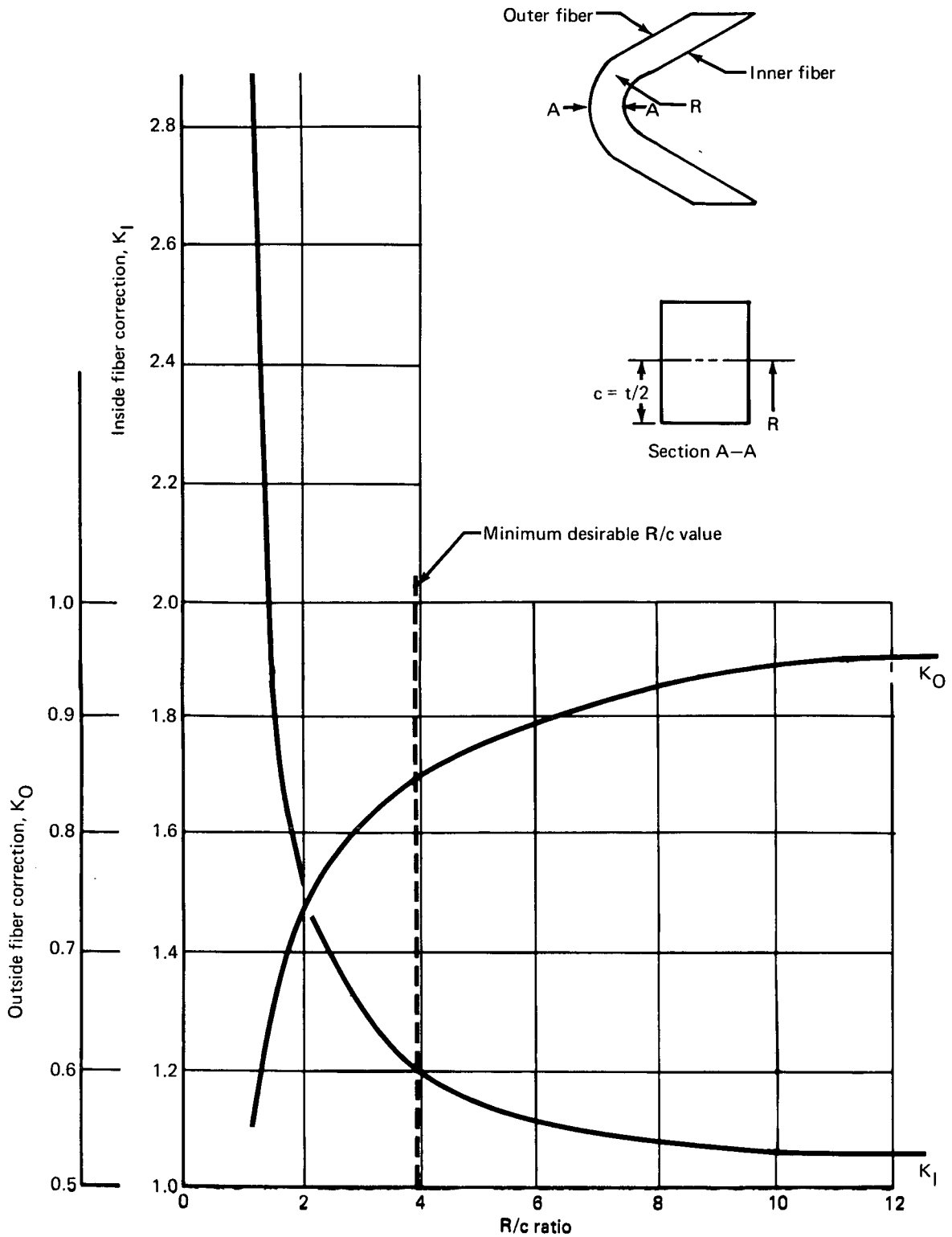

Figure 19.– Curved beam correction factors

- The airplane application seal designs were developed for a reduced-size seal when compared to the reference 2 test seal. The size reduction created higher material stresses due to a higher percentage squeeze on the seal cross section, this being necessary to prevent leakage at temperature extremes and being independent of seal dimensions.

- The service temperature range for the SST seal application was 450° K to 228° K (+350° F to -50° F). Seal prestresses were required to account for the differential expansion of materials at both temperature extremes. This created higher material stresses than encountered in the reference 2 program that evaluated only high-temperature performance.

- The dynamic pressures encountered by a seal in an aircraft application are primarily those bearing a direct relation to the alternating differential pressure fluctuations in the fluid supply that powers the actuator. Those alternating stresses are a fatigue problem. The reference 2 seal test program did not impose alternating stresses on the seal because internal actuator pressure was not used to drive the actuator rod. This pressure regime accounted for the major difference between the requirements of the reported study and previous NASA programs.

Figures 20 and 21 illustrate, in summary form, the iterations of the initial stress optimization studies performed for the 0.0254 m (1.0 in.) rod application and discussed in detail in appendix 2. Analysis was initiated with a gland depth assignment, curve 1. Optimizations were then conducted for tension loading with each step, 2 and 3 producing a favorable addition to the stress allowable. This pattern was not reflected in the compression load analysis. Leg angle evaluation, curve 3, showed a severely reduced stress allowable in compression. This effect was unavoidable and important to the analyst to ensure that proper optimizations for both tension and compression were evaluated.

Analysis validity.—The DuPont Vespel Design Handbook (ref. 13) shows that there are insignificant differences between the axial and flexural fatigue allowables for 10^7 life cycles. The near-linear relation indicated that a Hooke's law approximation used in the analytical treatment had good accuracy in reproducing realistic conditions. At 10^3 life cycles there were larger differences between quoted axial and flexural stress allowables, and nonlinearities were in evidence. The application being evaluated was concerned with an impulse life of 2×10^5 cycles and an endurance life of 8×10^6 cycles. Errors from a linear approximation at these cycle magnitudes were within the accuracy that other material properties could be determined, and no correction was considered necessary.

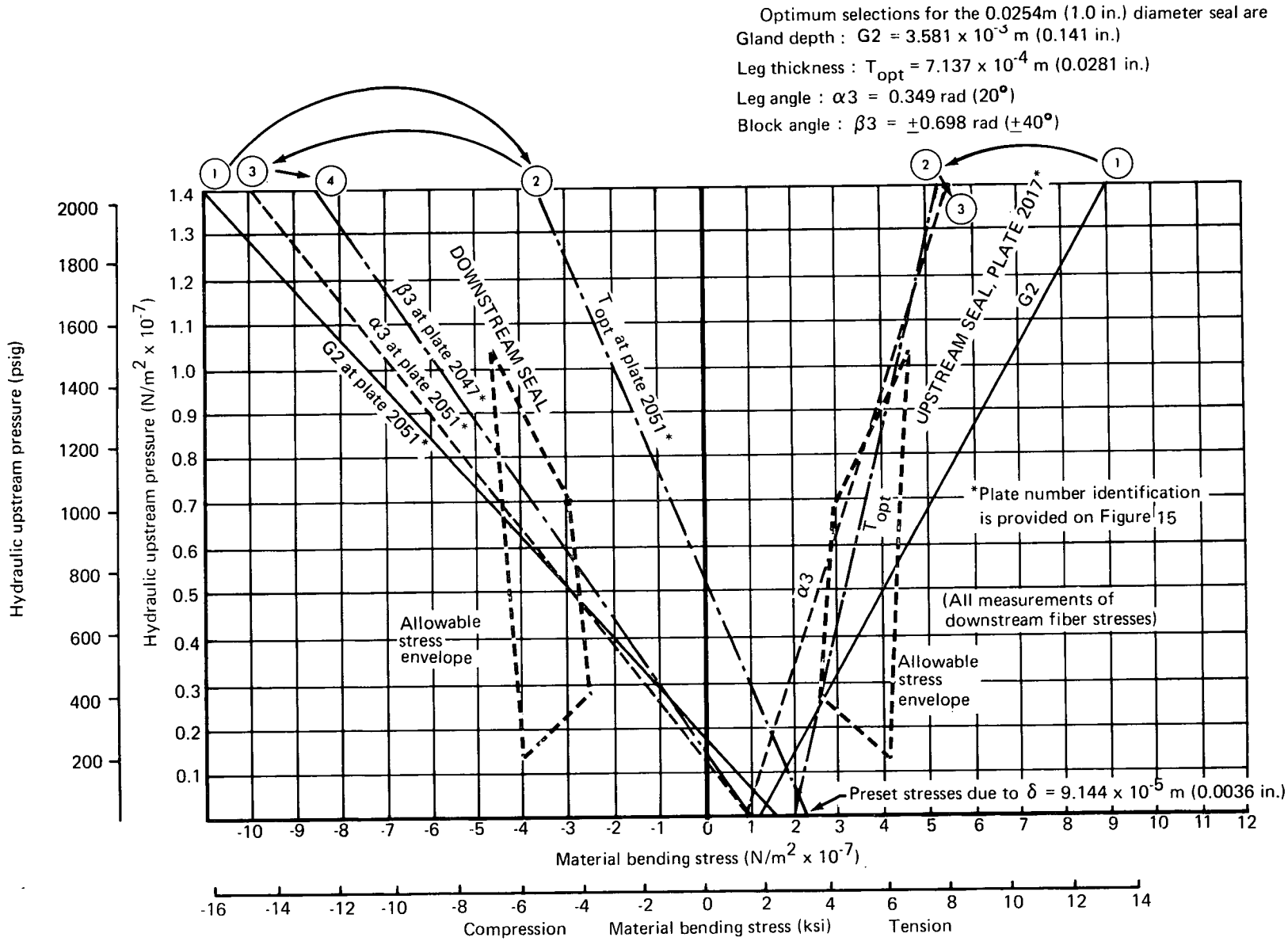

Figure 20.— Summary: SP-21 material seal design

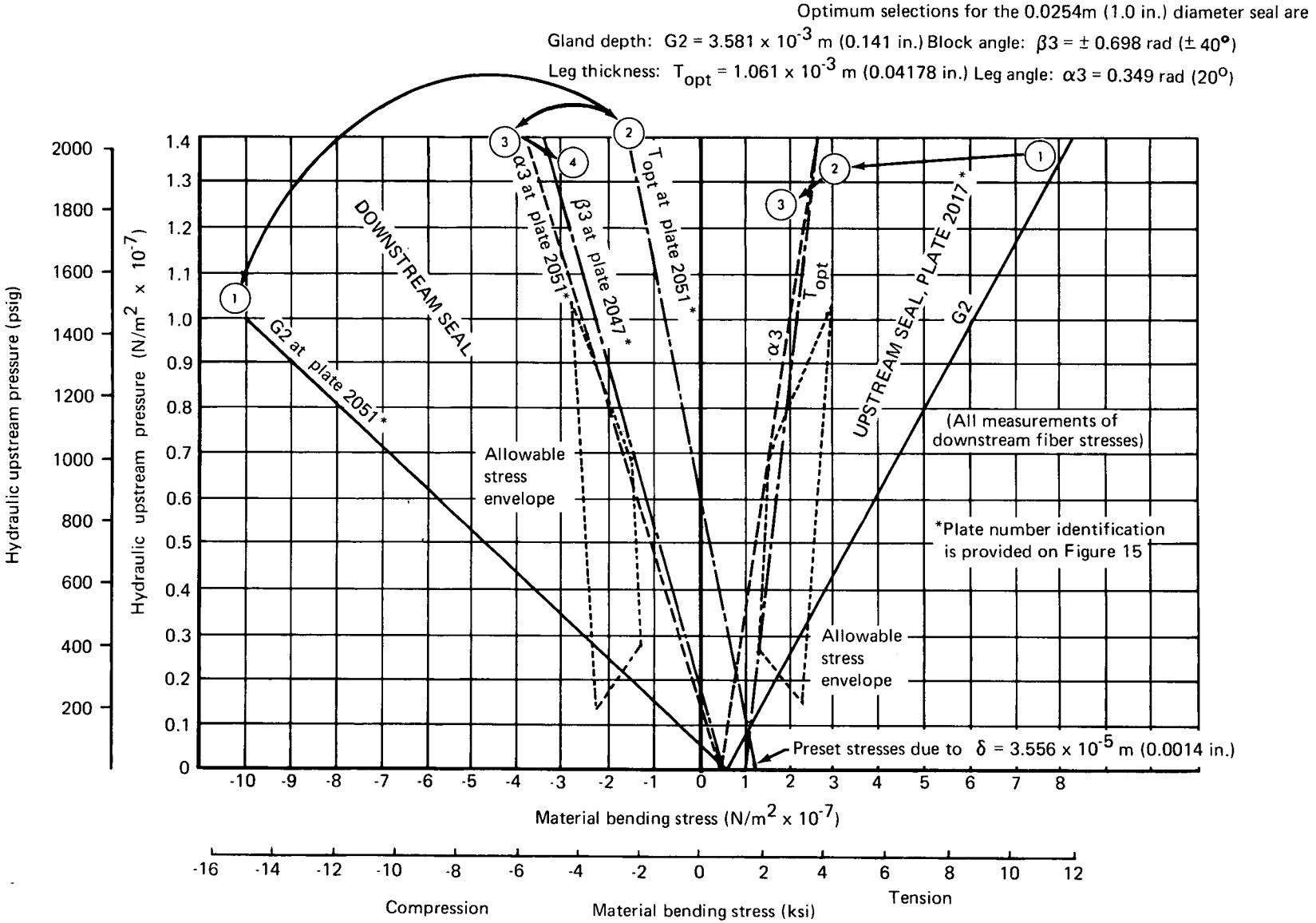

Figure 21.—Summary: SP-22 material seal design

Practical Constraints

An evaluation was conducted to define the geometry options for the total chevron seal configuration in the 0.0254 m (1.0 in.) ID size. The considerations were: (1) how many chevrons offered the best seal efficiency, (2) what material offered the best combination of allowables, (3) what cross sections were most favorable for fatigue environments, and (4) what tolerance difficulties were encountered that affected design options.

Configuration options.—Figure 22 shows diagrammatically the option potentials considered to be the most effective for proceeding to design, preparatory for chevron seal fabrication. These options were determined to have the best combinations of characteristics out of the matrix of possible combinations of section geometry, materials, and gland depths listed below.

Section Geometry	Materials	Gland Depth
1. Uniform thickness	1. Unfilled polyimide (SP-1)	1. NAS3-11170 seal 6.274×10^{-3} m (0.247 in.)
2. Tapered thickness		
3. Single element	2. 15% graphite fill (SP-21)	2. Maximum Boeing actuator 3.581×10^{-3} m (0.141 in.)
4. Dual element		
5. Triple element	3. 40% graphite fill (SP-22)	3. Military Specification 3.073×10^{-3} m (0.121 in.)
6. Strongback for each sealing element		
7. Flexible back for upstream sealing element		

Section geometry: The consideration of geometry relates to the number of sealing elements, element thicknesses, and configurations of supporting elements that are part of the total seal.

- Uniform thickness was optimum for the downstream chevron because maximum stresses occurred at the point of separation of the chevron from the backup support. This separation point shifted during loading and temperature variations.

- Tapered thickness was optimum for the upstream chevron because maximum stress occurred at the chevron apex with reduced stresses toward the leg tips. The

Configuration	Material	Advantages	Disadvantages
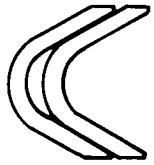	SP-22 SP-21	● Element redundancy ● Seal and gland thermal expansion difference is least using SP-22 ● Higher ultimate stress with SP-21 ● Interchangeability	● Insufficient SP-22 data ● Both tension and compression loads influence design of cross section ● May exceed fatigue allowable using SP-21
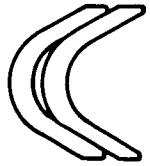	SP-21	● Interchangeability of elements	● One element overdesigned ● Must exercise design to determine whether elements will stack properly
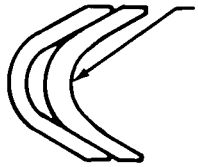	SP-21	● Strengthened critical stress section	● Different geometries of sections increase installation problems and fabrication costs
	SP-21 or SP-22	● Strengthened upstream apex without change to chevron geometry	● Three elements make seal cavity longer
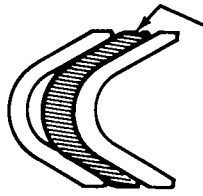	SP-21 or SP-22	● Teflon midelement will deform under load to support upstream element	● Growth for applications limited by Teflon sublimation temperature
	SP-21	● Section designed for only compression loading if second element need not be considered	● No redundancy ● Apex is either underdesigned or legs are overdesigned
	SP-21	● Cross section designed for local stress giving greatest flexibility	● No redundancy

Figure 22.—Seal configuration options

apex could not be completely supported in a dual-element configuration, and a thickened apex section was mandatory.

- A single-element seal had the advantage of a configuration that could provide optimum backup support to the sealing element at the expense of redundancy.

- A dual element provided sealing redundancy at the expense of allowing stress optimization by manufacturing the upstream and downstream elements to different geometric shapes, or at the expense of a nonoptimum design of one element.

- Triple-element seals had an advantage of allowing either a flexible or strongback element to be used between redundant sealing elements, at the expense of a longer seal gland.

Materials: The consideration of materials relates to the percentage of graphite filler in the polyimide and the variations in material properties resulting from introduction of the filler.

- SP-1 had the highest ultimate allowables but also the highest coefficient of thermal expansion and the poorest friction properties. Designs with SP-1 material could not meet the requirements for the allowable stress envelope.

- SP-21 had moderate ultimate allowables with a moderate thermal expansion coefficient and good friction properties. Stresses in designs with SP-21 material were within the calculation error tolerance using the minimal fatigue data supplied by DuPont.

- SP-22 had low ultimate allowables for polyimides, good friction properties, and the lowest coefficient of thermal expansion of the materials investigated. Stresses for designs with SP-22 material were acceptable to the allowable fatigue design envelope but were based on judgmental fatigue information that has not been validated.

Gland depth: The reduction of gland depth was a primary objective of the design study.

- The reference 2 gland depth of 6.274×10^{-3} m (0.247 in.) was too large for practical usage and reduction of this dimension was one objective of the study effort.

- The maximum gland depth of 3.581×10^{-3} m (0.141 in.), using a modular installation in the 0.0635 m (2.5 in.) rod diameter Boeing actuator, was used as a standard for stress calculations under the assumption that problems would be compounded with a greater than necessary reduction in depth.

- The MIL-G-5514 (ref. 16) gland depth of 3.073×10^{-3} m (0.121 in.) in the 0.0254 m (1.0 in.) rod diameter actuator was the objective for eventual design and in addition had the advantage of minimizing differential expansion between chevron ID and OD more than the larger glands. This occurred at the expense of manufacturing problems with the smaller size.

Optimum seal: The optimum seal was determined to be the two-element configuration to fit a MIL-G-5514 (ref. 16) gland with a uniform-thickness downstream chevron and a thickened apex in the upstream chevron. This selection provided a redundancy of sealing elements, optimum geometry for a backed downstream element and an unbacked upstream element, and a gland depth meeting the established objective. The major disadvantages of the selected seal were the noninterchangeability of the seal elements and the added cost of manufacturing two different element geometries.

Material selection.—The use of DuPont Vespel SP-22 as the optimum polyimide material for the chevron seal concept was based on accepting judgmental estimations of appropriate property allowables for fatigue data that did not have testing validation. This risk was considered to be beyond the scope of the study objectives and therefore Vespel SP-21 was selected as the best practical choice of materials for the second-stage seals. The risk taken in using SP-21 was that of not knowing quantitatively the degree of conservatism in the analytical stress analysis. This analysis employed zero-mean stress data to a set of operational conditions where complete reversals were not experienced. The resulting design data indicated that fatigue allowables were exceeded, based on the zero-mean stresses. In a more precise analysis, using the applications means cyclic stress envelope, the results would be within the allowables acceptance region. Such allowables, if available, would have relationships to zero-mean allowables similar to those discussed earlier. As a result of this conservatism, SP-21 was judged to be the practical optimum material for seal fabrication.

Seal dimensions.—The optimum dimensions for a chevron seal in a Military Specification (ref. 16) gland depth, applied to a 0.0254 m (1.0 in.) diameter rod application, were determined as being an optimum thickness of 6.096×10^{-4} m (0.024 in.) and an optimum leg angle of 0.471 rad (27°) using SP-21 material. At this angle compression stresses were not exceeded for the fatigue cycle envelope and the effect of exceeding allowable tension stresses could be eliminated by using a thickened section at the apex of the upstream seal. These relationships are shown in figure 23. The radius at the apex was determined using a minimum R/c of 4 from figure 19 for curved-beam correction. This ratio was not compatible with the other dimensions as stated above and an R/c of 3 was of

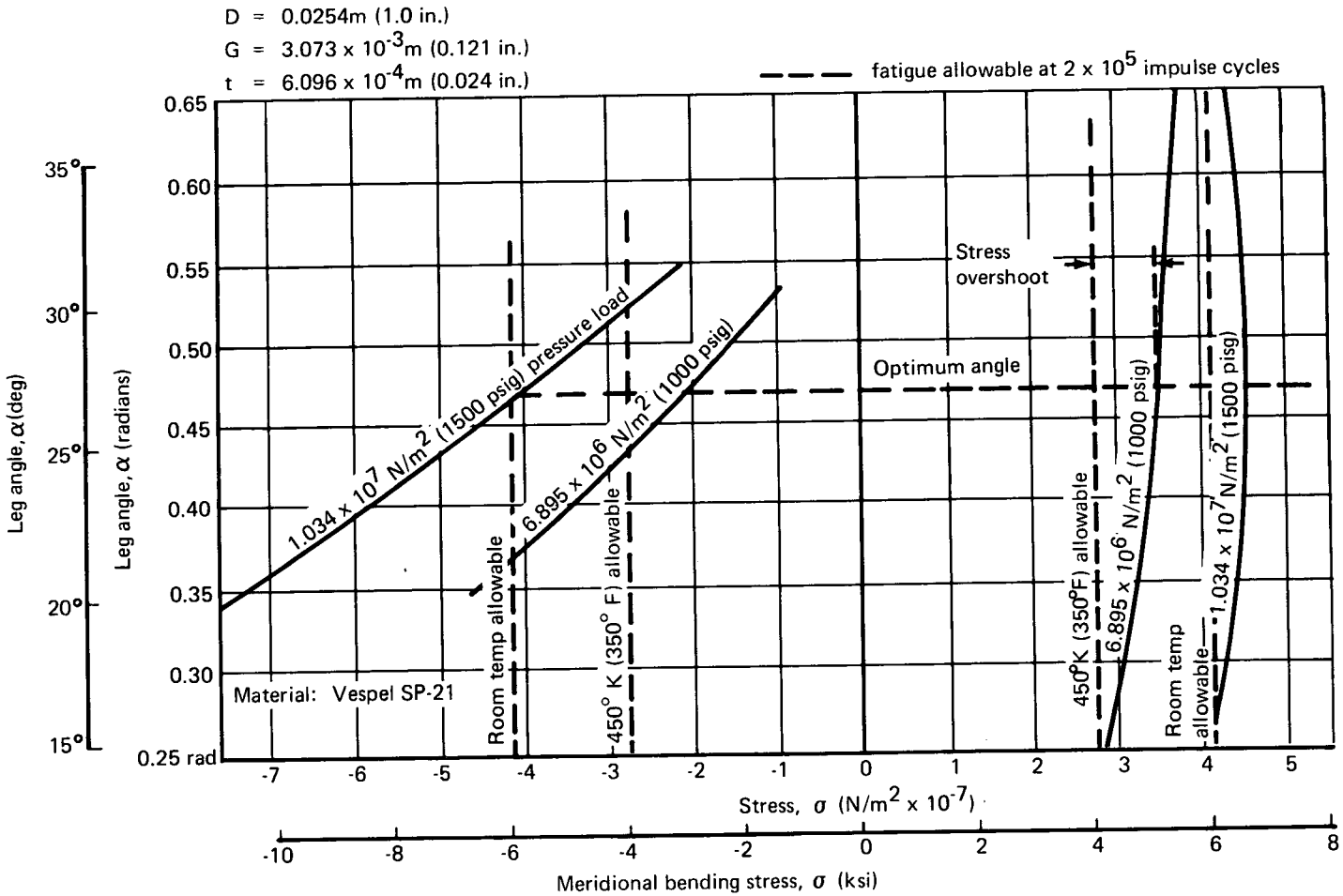

Figure 23.—Stress vs leg angle for optimum chevron shape

necessity adopted. The ratio value of 3 was less than the minimum suggested value and thus increased the curved-beam correction factor more than optimally desired. The resulting radius for the center of a uniform chevron cross section was 9.144×10^{-4} m (0.036 in.). The downstream and upstream radii became 1.219×10^{-3} m (0.048 in.) and 6.096×10^{-4} m (0.024 in.), respectively. The upstream radius for the nonuniform section of the upstream chevron was 7.620×10^{-4} m (0.030 in.) and was fitted to accommodate the thickened apex section needed to keep tension stresses within the fatigue limit allowables. An illustration of this configuration is shown in figure 24.

The optimum chevron configuration was established as the one where the total preset interferences and gaps between the chevron and its gland were minimized to reduce preset stresses. This was accomplished at the rod contact surface by making the free shape interference at 228° K (-50° F) equal 4.064×10^{-5} m (0.0016 in.) and the gap at 450° K (350° F) equal the same value. The same procedure was used at the chevron OD, or contact surface with the gland. On this surface, at 228° K (-50° F), there would be a 4.826×10^{-5} m (0.0019 in.) gap and an equal value interference at 450° K (350° F) between the chevron free shape and the gland.

Under temperature conditions, where the free shape produced a gap, an added loading system was necessary to force contact between the chevron and the rod or gland surfaces. The magnitudes of these forces were determined by computer stress analysis. The forces varied between 66.7 and 111.2 N (15 and 25 lbf), depending on whether they were applied in a radial or tangential direction to the rod centerline. The distances over which loading forces were required to act were established by evaluating the dimensional variations due to thermal expansion of the chevrons in the seal assembly. The variations determined are described in tables V and VI.

Either of the analyses in tables V and VI reflect movement due to thermal expansion of the chevron assembly within the seal cavity constraints. The two analyses were not additive. To maintain sealing contact at 450° K (350° F) at the rod surface and at 228° K (-50° F) at the gland OD surface, the upstream chevron needed to be forced downstream from the positions indicated in the above analyses by the amounts indicated in table VII.

At 228° K (-50° F) on the rod surface, and at 450° K (350° F) on the gland OD, the seal cavity surfaces kept the chevron in contact by interference fit. These fits required the legs in contact with the cavity to move upstream by the total amounts indicated in the tangential variations presented in table V. At low temperature on the rod, and at high temperature on the gland OD, the upstream faces of the assembly were farther upstream than at high temperature on the rod or at low temperature on the gland OD. This condition made it necessary to use a spring loading system to provide the forces to close the clearances resulting from thermal expansion. The spring loading for the inner and outer legs of the assembly needed to be independent since the clearance conditions occurred at opposite ends of the temperature spectrum for the two legs.

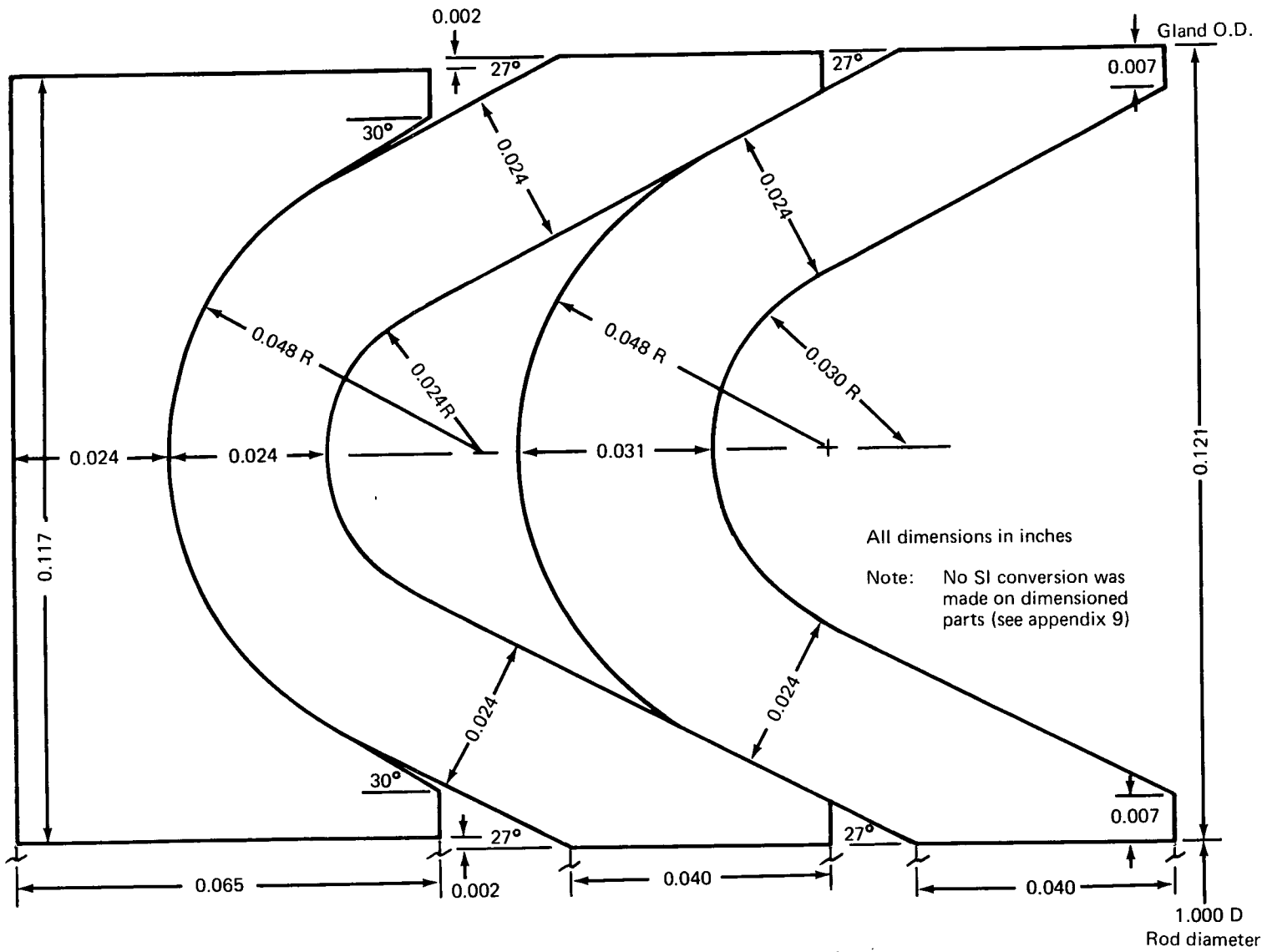

Figure 24 – Chevron seal–theoretical optimum dimensions

Table V.— Tangential variations

	At rod surface		At gland OD surface	
	min temp 228°K (-50°F)	max temp 450°K (350°F)	min temp 228°K (-50°F)	max temp 450°K (350°F)
Backup block effect	C = 4.318×10^{-5}m (0.00017 in.)	E = 9.144×10^{-5}m (0.00036 in.	C = 4.138×10^{-5}m (0.00017 in.)	E = 9.144×10^{-5}m (0.00036 in.)
Identical chevron pair effect	E = 2.339×10^{-3}m (0.00921 in.)	E = 5.994×10^{-4}m (0.00236 in.)	C = 1.184×10^{-3}m (0.00466 in.)	E = 4.280×10^{-3}m (0.01685 in.)
Total	E = 2.296×10^{-3}m (0.00904 in.)	E = 6.909×10^{-4}m (0.00272 in.)	C = 1.227×10^{-3}m (0.00483 in.)	E = 4.371×10^{-3}m (0.01721 in.)

C = compression of seal assembly along rod centerline

E = expansion of seal assembly along rod centerline

Table VI.— Radial variations

	At rod surface		At gland OD surface	
	min temp 228°K (-50°F)	max temp 450°K (350°F)	min temp 228°K (-50°F)	max temp 450°K (350°F)
Backup block effect	–	–	–	–
Identical chevron pair effect	I = 1.204×10^{-3}m (0.00474 in.)	I = 3.048×10^{-3}m (0.00120 in.)	O = 6.020×10^{-4}m (0.00237 in.)	I = 2.182×10^{-3}m (0.00859 in.)
Total	I = 1.204×10^{-3}m (0.00474 in.)	I = 3.048×10^{-3}m (0.00120 in.)	O = 6.020×10^{-4}m (0.00237 in.)	I = 2.182×10^{-3}m (0.00859 in.)

I = inward movement of surface diameter to rod centerline

O = outward movement of surface diameter to rod centerline

Table VII.—Compression distances to close clearances resulting from thermal expansion

Location	Temperature °K	Temperature °F	Direction of motion	Movement required m	Movement required in.
Inner leg at rod surface	450	350	Horizontal compression	1.778×10^{-3}	0.0070
			or vertical outward	9.652×10^{-4}	0.0038
Outer leg at gland OD	228	-50	Horizontal compression	3.912×10^{-3}	0.0154
			or vertical outward	1.778×10^{-3}	0.0077

Spring loading considerations.—The Belleville spring was considered optimum for use to provide the required compressive loading because it could be designed in a region of deflection vs load with a negative slope. With such a design, loading was provided with an extended spring to close the clearance resulting from thermal expansion, while the same spring induced lesser stresses in the chevron, at lower spring deflections, where the chevron interference fit in the gland forced unwanted spring compression. As attractive as this concept was in theory, it could not be fabricated to the dimensions of the seal gland for the applications under consideration because the ratio of OD to ID for the spring approached unity.

The alternate spring considered was the "garter" spring because it provided a soft action characteristic. This spring would act in the radial direction on the inner leg but would not be applicable for outer leg loading. The small size of the seal gland precluded use of this spring because wire diameter would have to be greater than one-half the allowable coil diameter for the spring.

Calculations for a simple compression spring showed that the allowable torsional stiffness of the spring material was exceeded when spring dimensions were limited to the cavity size for the application.

Conclusions.—The preceding results all supported difficult aspects of fabricating the chevron seal design where the theoretical optimum preset for the pair of chevrons was the minimum preset equally divided between the ID and OD legs of the seal. The alternative was to design the seal configuration for the optimum downstream element and configure the assembly to incorporate two such elements. A strongback between the elements, see figure 22, was necessary to allow the upstream element to be designed so that the pressure and interference bending stresses were opposite rather than additive. These stresses were additive when this element was not supported. The preset was applied so that maximum interference would occur at 228° K (-50° F), with decreasing interference as temperature was elevated. In this way the stresses always remained opposite and spring loading was not required to keep the chevrons seated.

Chevron Seal Design

Chevron design drawings were prepared to utilize the advantages of opposing pressure and preset loads to offset the disadvantages of large presets and provide seal concepts that required no loading springs.

The downstream chevron element was rigidly supported by a rounded backup block through contact at the chevron apex. This support produced a less severe stress condition in the downstream chevron element than was present in the upstream element, which was not similarly supported. By placing a "strongback" or rigid body between the downstream and upstream chevron elements of a two-element assembly the stress distribution in both elements was made similar. Designs for the small 0.0254 m (1.0 in.) and large 0.0635 m (2.5 in.) diameter rod assemblies using this rigid supporting technique for both elements were developed as follows.

Small-size chevron design.—The 0.254 m (1.0 in.) chevron preset was assigned to provide a minimum of 2.54×10^{-5} m (0.001 in.) interference fit at both the inside and outside legs of the chevrons at any temperature condition. Maximum preset at the extremes of the temperature range was 1.27×10^{-4} m (0.005 in.) in a 3.073×10^{-3} m (0.121 in.) gland. With such an interference fit, loading springs were unnecessary but the stress in unsupported upstream chevrons was excessive. To avoid such overstressing, two design criteria needed to be satisfied. These were:

- The chevron leg section between the tip and the tangent point to the apex curvature needed to be sufficiently flexible, under conditions of maximum preset and no pressure loading, that fiber bending stresses remained within the allowable stress envelope.

- The chevron leg, including the curved-beam section at the apex, needed to be strong enough to ensure that the maximum pressure-induced bending stresses, in addition to stresses due to preset, remained within the allowable stress envelope.

The critical stresses in the two-chevron configuration, using a 0.349 rad (20°) to 0.698 rad (40°) leg angle range with the apex of the upstream seal unrestrained, did not remain within the allowable stress envelope for presets greater than approximately 5.08×10^{-5} m (0.002 in.) per leg. This is indicated by the data in figure 20, where the preset equals 9.144×10^{-5} m (0.0036 in.) total for two legs. This limitation occurred because the pressure-induced load, and preset load, produced bending moments that were additive, i.e., both tension or both compression at the same extreme fiber. By placing a strongback between the upstream and downstream chevrons the critical pressure-induced moment opposed the moment produced by preset loading, and the resultant stresses were minimized. This result only partially satisfied the two criteria mentioned above.

In order to arrive at a complete solution for a chevron design, an approximate hand analysis was performed treating the chevron leg as a simple beam with an equivalent length and thickness. The freebodies used were as follows:

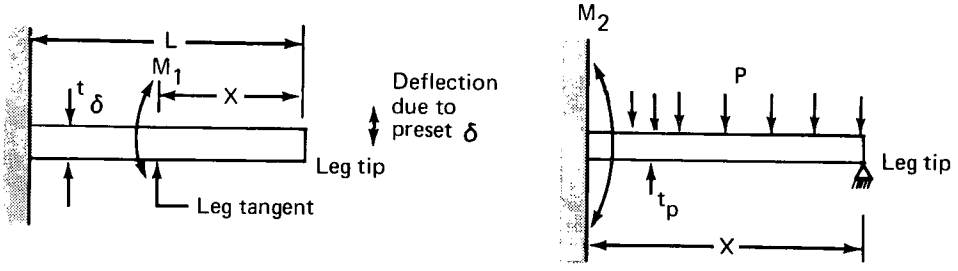

It was found that no realistic solution existed for a chevron with a leg thickness that was capable of resisting 1.270×10^{-4} m (0.005 in.) preset and 6.895×10^{6} N/m^2 (1.00 ksi) pressure loading without drastically exceeding the $\pm 2.964 \times 10^{7}$ N/m^2 ($\pm$4.30 ksi) allowable stress envelope at 450° K (350° F). Acceptable solutions had different equivalent leg thickness for the deflection and pressure conditions, indicating that a tapered leg chevron was required. Hand calculations were not used for further calculations because approximations for curved-beam stiffness and the taper ratio for the leg were too gross, requiring calculations by the finite-element analysis to provide acceptable data correlation.

Computer solutions using the finite-element analysis were obtained to evaluate the model shown in the figure below for the region of acceptable configuration design.

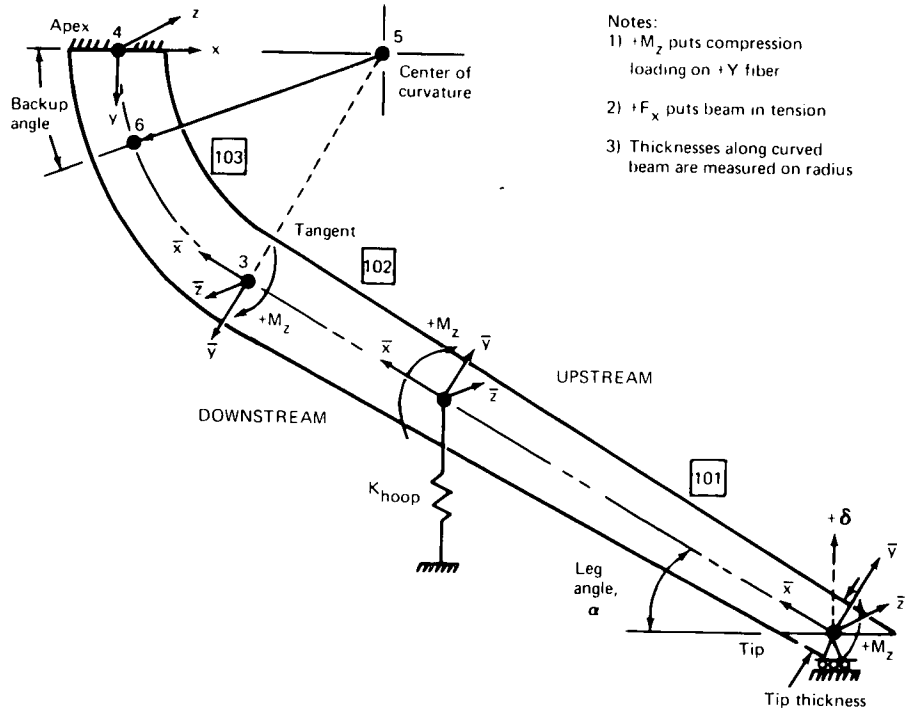

C.2

Limitations were imposed on certain dimensions for the computer analysis. The minimum practical thickness for the leg tip was limited to 3.810×10^{-4} m (0.015 in.) so that there would be sufficient thickness to support shear forces imposed by the cutting tools during fabrication. The thickness at the apex was required to be 1.2 times the leg thickness at the tangent, based on prior analysis that this ratio would not overstress the apex at maximum preset when the stresses at the tangent were acceptable. In addition, the allowable critical stress was limited to $\pm 2.964 \times 10^7$ N/m^2 ($\pm$4.300 ksi). This value was based on the most current DuPont data, which was believed to be conservative; however, the degree of conservatism could not be determined without additional property data. Such property evaluation was outside the scope of the study effort.

The results of the computer analysis are shown in figure 25 for the region of solutions acceptable for the envelope of stress allowables. An evaluation of the results was made to reach a practical solution for the 0.0254 m (1.0 in.) rod application. A minimum of 0.349 rad (20°) for the leg angle was established as a compromise to keep the leg length within practical limits. Lower angles required high taper ratios, which increased the contact foot area of the chevron. A limiting value occurred at 0.262 rad (15°) where the entire leg was in contact with the gland.

At a 0.349 rad (20°) leg angle there was no theoretical solution within the $\pm 2.964 \times 10^7$ N/m^2 ($\pm$4.300 ksi) stress envelope. The best practical solution provided stresses within -3.310×10^7 to 2.551×10^7 N/m^2 (-4.800 to 3.700 ksi) using a tangent point thickness of 6.350×10^{-4} m (0.025 in.). This solution was practical from two standpoints: (1) the deviation from either the preset or pressure curve was small and judged to be within the conservatism of the allowable, and (2) the accuracy of dimensional control in fabrication could not guarantee the tolerance applied to the angle of crossover between the theoretical preset and pressure curves shown.

Large-size chevron design.—An analysis similar to that described above was performed to determine the region of acceptable design for the 0.0635 m (2.50 in.) rod application using a two-element chevron assembly with a midelement strongback. The criterion for a 2.54×10^{-5} m (0.001 in.) minimum preset was also applied for the large-size rod application, resulting in a maximum preset, at temperature extremes, of 2.286×10^{-4} m (0.009 in.). The 3.581×10^{-3} m (0.141 in.) gland depth acceptable for use with a modular seal was used in the finite-element computer analysis to produce the results shown in figure 25.

The results show no area of common solution for the preset and pressure curves. Because the 3.581×10^{-3} m (0.141 in.) gland depth was the maximum considered practical for the test actuator under consideration, an engineering judgment was made to determine the most practical design to satisfy the constraints of 3.810×10^{-4} m (0.015 in.) tip thickness, apex thickness equal to 1.2 times tangent thickness, and leg angle equal to 0.349

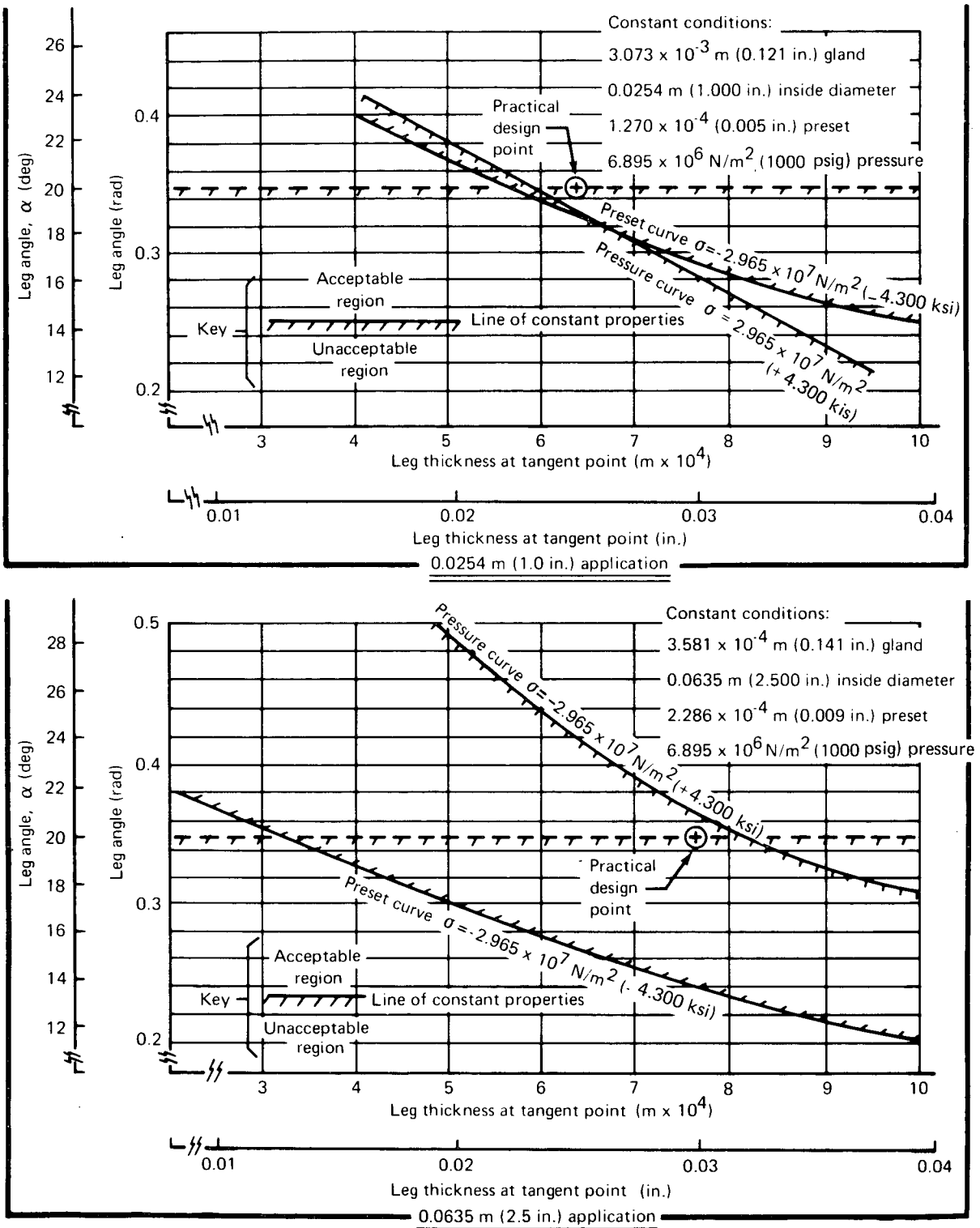

Figure 25. Finite-element stress envelope

rad (20°). The choice was between exceeding either the tension or compression allowable in the stress envelope. A tangent point thickness of 7.620×10^{-4} m (0.03 in.) was selected as the best solution by exceeding the compression allowable because a shift in stress cycle in the compression direction gave a better fatigue life. The above tangent point thickness was considered a maximum allowable so that the compressive loading of the extreme fiber at the tangent point due to preset would not cause permanent set. The resulting stress cycle was -5.171×10^7 to 3.930×10^7 N/m^2 (-7.500 to 5.700 ksi).

Chevron seal design summary.—The chevron seal design drawings that were produced using the results of the above analyses are shown in figures 26 and 27. These seal drawings are also produced in references 17 and 18, which include machining tolerances and finishes for all parts.

In summary, there were a number of design iterations leading to the final configuration of a tapered-leg, thickened-apex chevron design. Those that received major consideration are described briefly in table VIII in chronological order of evaluation, and their advantages and disadvantages cited. Concept 5 appeared to be most satisfactory on the basis of both theoretical stress analysis and practical fabrication constraints, and was therefore recommended for fabrication and test.

K-Section Seal Design

The design evaluation of the K-section seal, similar in concept to the reference 2 HB-1 configuration, was initiated independent of the chevron analysis. Stress considerations were based on the K-section being comprised of a stiff vertical member of constant cross section and two independent, tapered legs. As such, each leg was a flexible cantilever beam having a specific taper ratio. The loading condition on each leg was composed of a pressure component and a preset component in similar fashion to the chevron leg loads. The pressure-induced load was the same as the load induced in a chevron leg having the same dimensional parameters; however, the K-section leg reacted with greater rigidity to preset loading because there was no interaction between legs of the K-section.

The reduced flexibility in the K-section legs due to preset loading was indicated in computer printouts for the optimum taper ratio analysis. Stresses were extremely sensitive to the distribution of thicknesses along the tapered leg to the extent that the sensitivity was within the manufacturing tolerances needed in fabrication. A choice was presented to accept the best design out of that analysis, requiring a leg thickness distribution having a shape as shown in exaggerated fashion below:

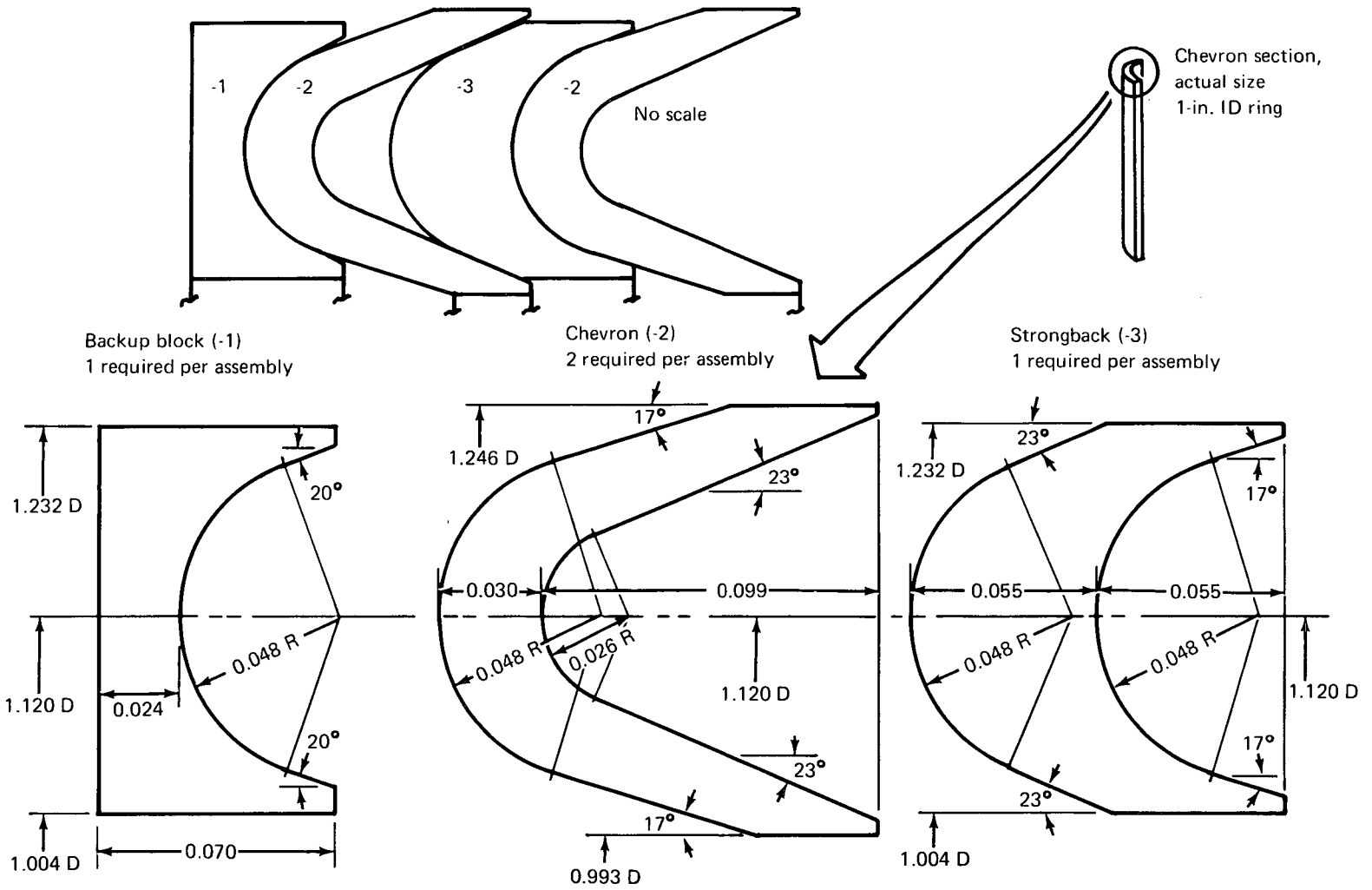

All dimensions in inches: No SI conversion was made on dimensioned parts (see appendix 9)

Figure 26.—Second-stage rod seal assembly—1-in. 1D chevron application

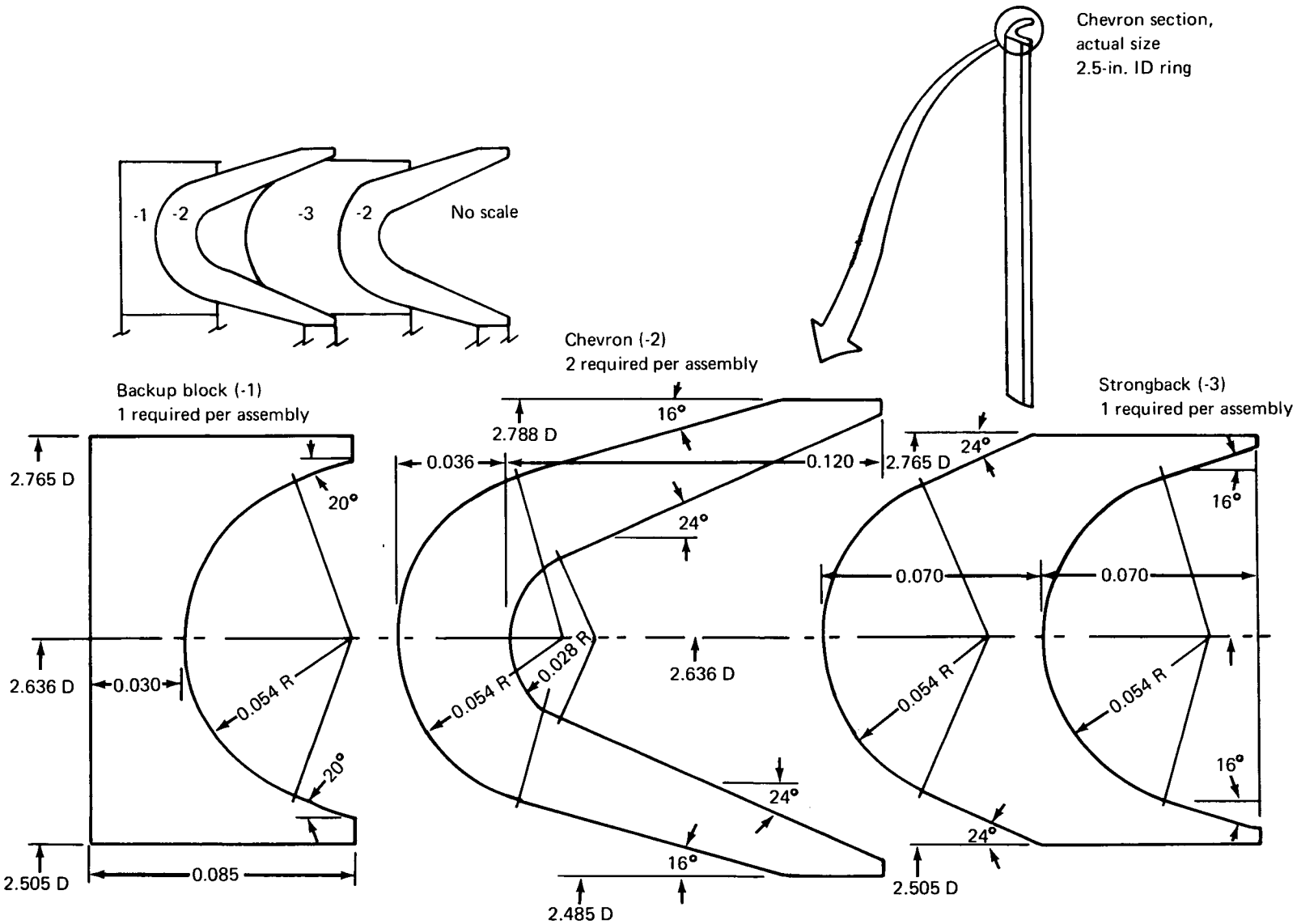

All dimensions in inches: No SI conversion was made on dimensioned parts (see appendix 9)

Figure 27.— Second-stage rod seal assembly—2.5-in. ID chevron application

Table VIII.– Chevron design summary

Concept	Description	Advantages	Disadvantages	Conclusion
1	SP-21, two chevrons back to back Apex of upstream element unrestrained No spring loading	Pressure load sharing between two seals Minimum assembly complexity Redundant seal Interchangeable elements	Overstress of upstream fiber of upstream element due to 1.143×10^{-4} m (0.0045 in.) preset per leg Additive pressure-induced bending moments	Reduce preset
2	SP-21, two chevrons back to back Apex of upstream element unrestrained Minimum preset using spring loading	Same as for concept 1 but with reduced critical stresses	Continued overstress of upstream fiber of upstream element	Consider SP-22 material
3	SP-22, two chevrons back to back Apex of upstream element unrestrained Minimum preset using spring loading	Same as for concept 1 with stresses within allowable envelope	Lower material allowables of SP-22 Fatigue data used in calculations unsupported by property tests	Risk of depending on unconfirmed SP-22 properties considered unwarranted
4	SP-21, two chevrons back to back Thickened apex of upstream element, which remained unrestrained Minimum preset using spring loading	Pressure load sharing between two elements Seal element redundancy Stresses remain within allowable envelope	Seal elements not interchangeable Springs could not be designed to provide necessary loading within dimensional restraints of gland	Change design configuration to restrained apex for both sealing elements and sufficient preset to preclude use of loading springs
5	SP-21, two chevrons with midelement strongback and tapered leg No spring loading	Redundant seal surfaces Bending moments due to pressure and preset-induced loads oppose each other Minimum assembly complexity Interchangeable elements	High preset values Design complexity with tapered leg	Reasonably acceptable on basis of both theoretical stress analysis and practical fabrication constraints. Recommended for fabrication and test

or to use the final chevron design with a rigid vertical beam as an integral part of the apex geometry. The latter choice was selected for the following reasons:

- The average taper ratio of approximately 1 to 2 from tip to root, recommended from the computer analysis for taper ratio, was the same as the ratio of 3.810×10^{-4} m (0.015 in.) at the chevron tip to 7.620×10^{-4} m (0.030 in.) at the chevron apex.

- There was no guarantee that the tolerances of the shape determined by taper ratio analysis could be maintained sufficiently accurate in fabrication.

- A uniform taper was preferable to a contoured shape for seal simplicity.

- Tooling was minimized by generating the inside shape of the chevron and K-section with the same forming cutter if the chevron geometry was accepted for K-section design.

K-section seal design drawings were produced using the results of the above analyses. These designs are shown in figures 28 and 29. These seal drawings are also produced in references 19 and 20, which include machining tolerances and finishes for all parts.

MODULAR RETAINER

The development objective for a modular retainer was to design a mechanism that would permanently hold both the first- and second-stage rod seals in their proper orientation, independent of other actuator parts, and could be installed in an actuator as a single unit with the seals encapsulated.

Test Actuator Applications

Designs were prepared for the inclusion of modular seal retainers in both the 0.0254 m (1.0 in.) and 0.0635 m (2.5 in.) actuators to be used during endurance testing. These modular designs are shown on figure 30 and with the complete actuator designs in references 21 and 22. The modular assembly, -2 part, is assembled by spiraling the first-stage, split-ring seal into place. The second-stage seal is installed in the module gland, -3 part, by sequentially introducing parts from the downstream end of the gland. The retainer, -4 part, is then added to provide capture of the seal in the gland. The 0-80 screw is used to hold the retainer in place prior to actuator installation. The module gland also acts as the rod bearing and a retainer for the static seals on both sides of the interstage bleed. The module retention nut, -5 part, is used to hold the module in the actuator and to react static thrust loads. The module designs were configured to best complement the existing actuators. This was satisfied by consolidating the rod gland bearings with the rod seals

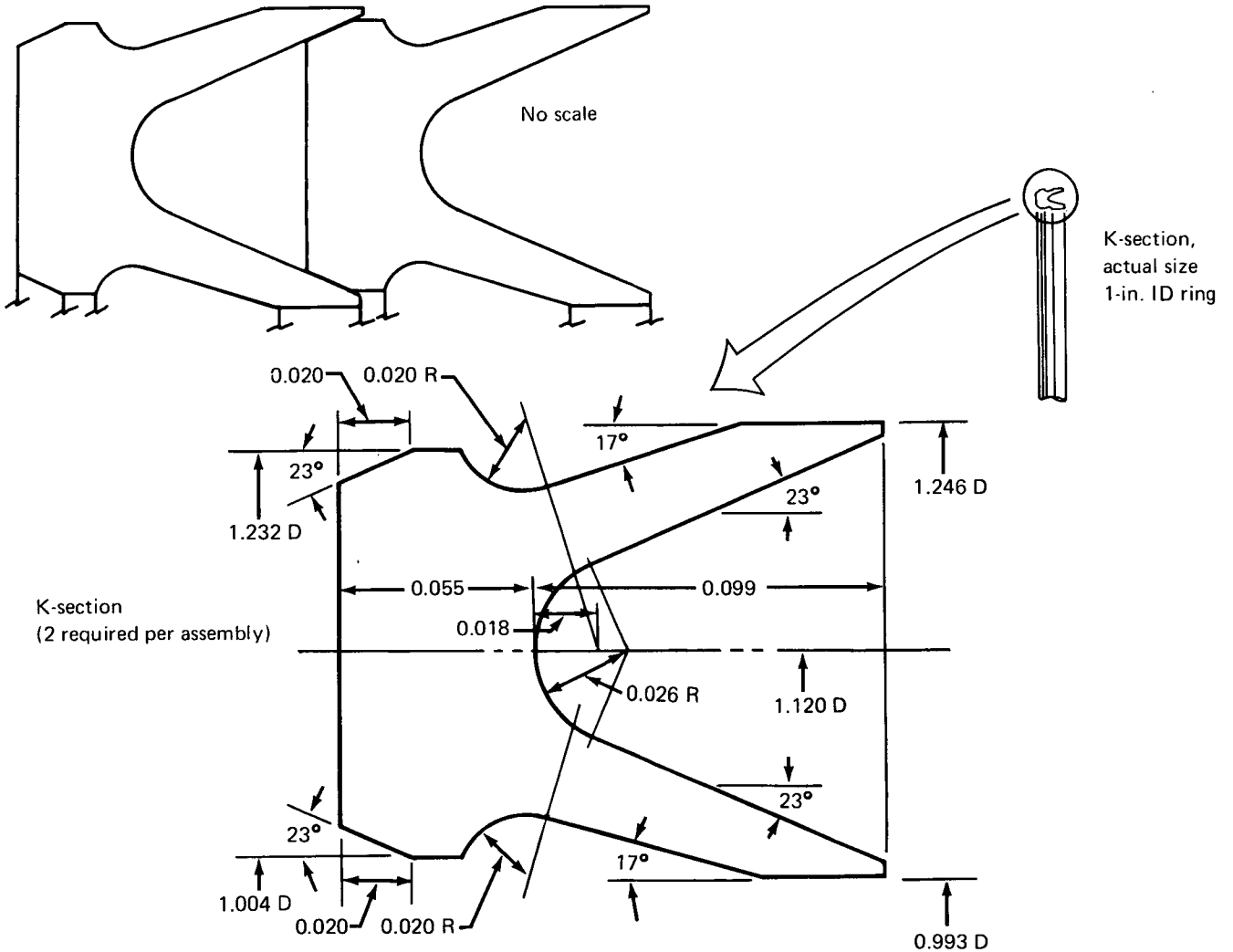

All dimensions in inches: No SI conversion was made on dimensioned parts (see appendix 9)

Figure 28 — Second-stage rod seal assembly—1-in. ID K-section application

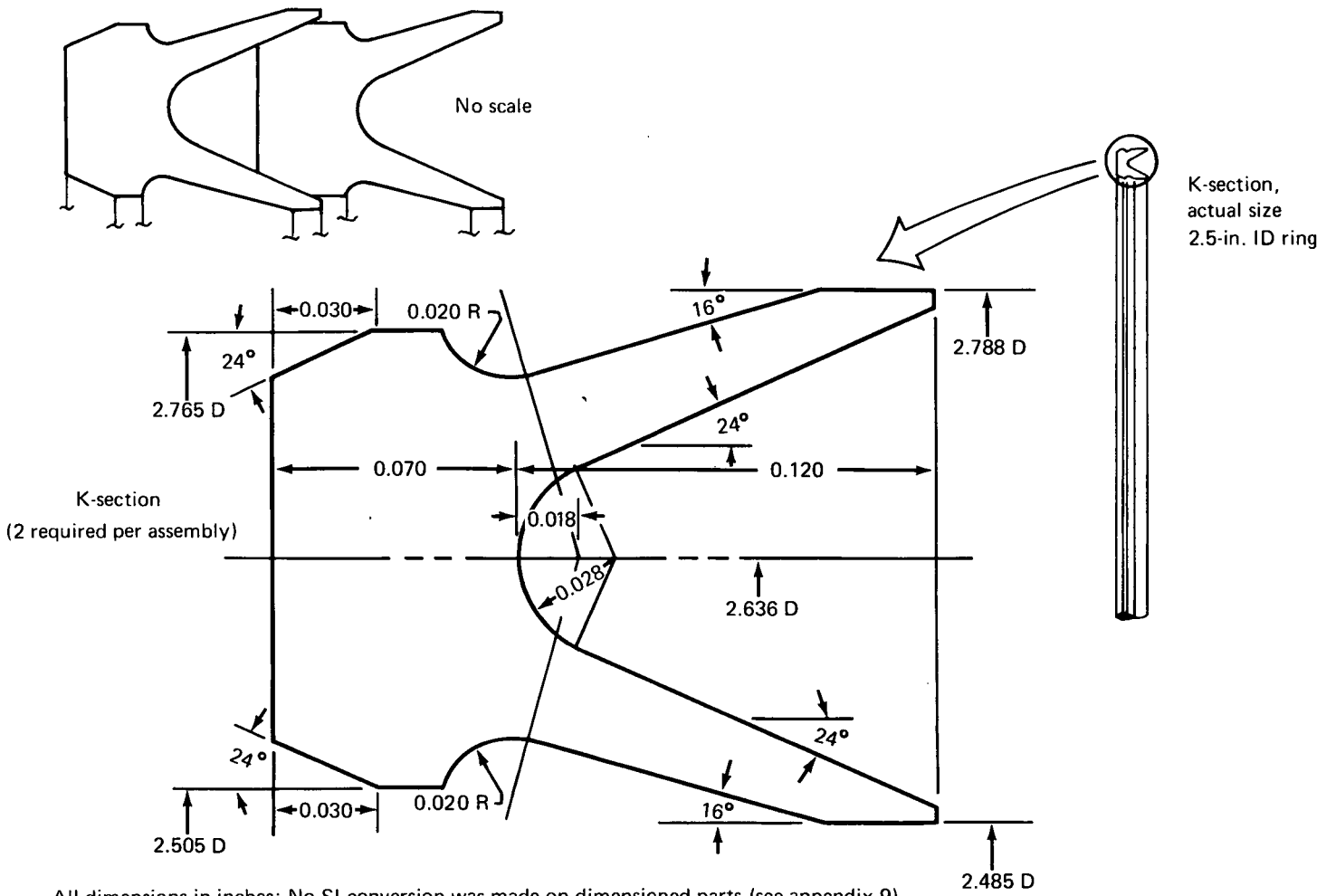

All dimensions in inches: No SI conversion was made on dimensioned parts (see appendix 9)

Figure 29—Second-stage rod seal assembly—2.5-in. ID K-section application

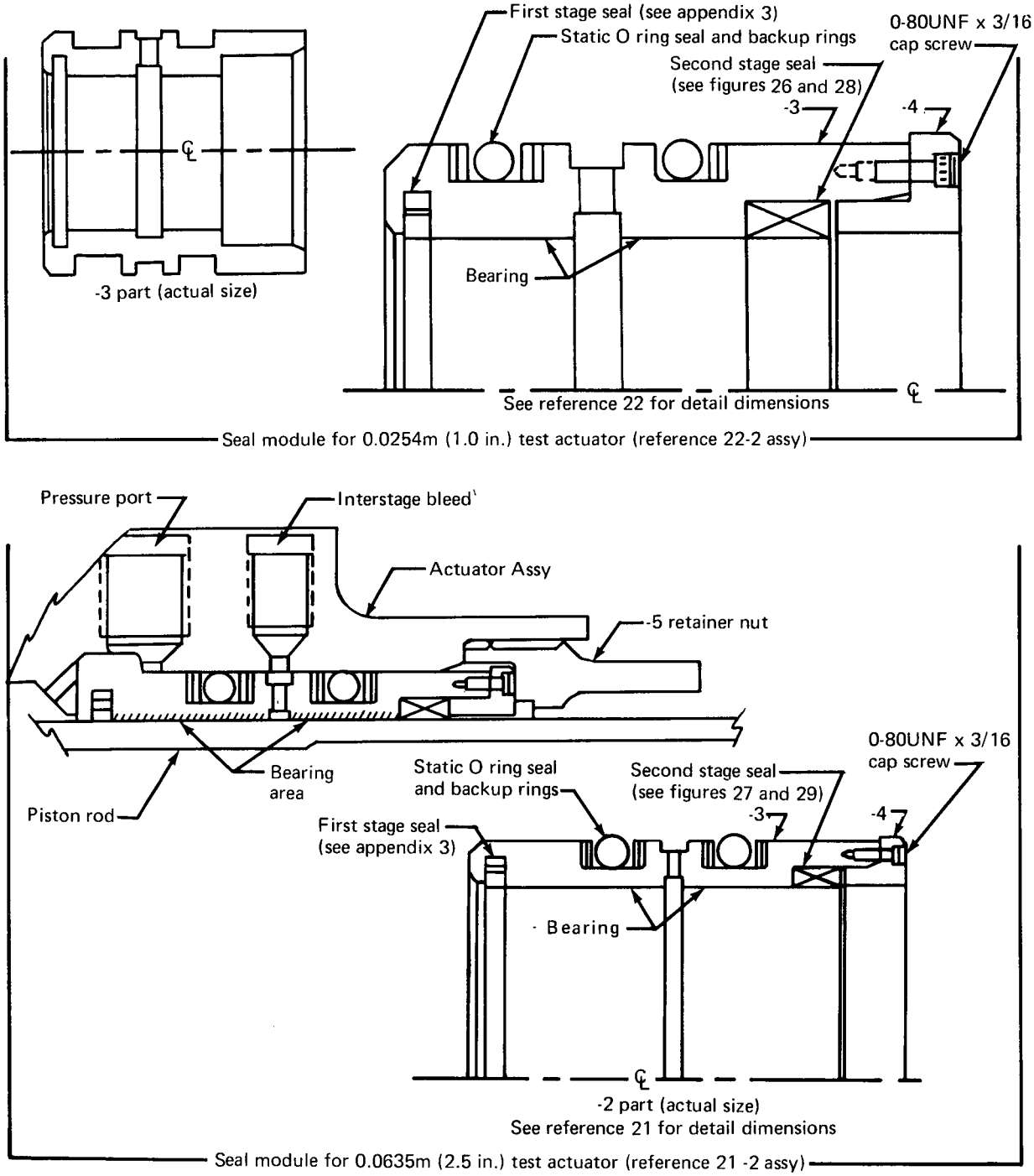

Figure 30 – Seal modules for test actuators

in the modular units, resulting in a seal module that was longer than if the bearing and seal modules were separately constructed.

Whether or not the seals are installed in modular retainers does not affect the results of testing either the first- or second-stage seals. Thus, the use of the modular retainer during endurance testing was considered only to determine whether installation procedures facilitated maintainability, and precluded improper installation. Because this objective could be accomplished successfully during tests of only one size of retainer, the 0.0635 m (2.5 in.) actuator size was selected. This choice was based on considerations of minimum modification to existing hardware.

New Actuator Applications

When the seal module is considered for new actuator designs, there are alternate approaches available. Two factors determining the practicality of these possibilities are as follows:

- The ratio of piston diameter to rod gland diameter determines the rod gland material thickness available for machining of seal glands, bosses, and leakage ports. The larger this ratio, the more freedom is available in design.

- The optimum placement of each rod bearing is at the maximum distance from the neutral piston position so as to minimize rod side motion and piston cocking.

If a separate bearing is placed upstream of the seal module, it will reduce the distance between the bearing and the neutral piston position below the possible maximum and require tighter seal module dimensional tolerances to allow the seal retainer to act as a secondary bearing against side loads. Placement of the bearings downstream of a separate seal module imposes the requirement for nonlubricated bearings and results in problems with the selection of materials for the interfacing bearings, rod, and housing. Such placements as those discussed above are unconventional for aircraft design; however, incorporating the seal module and bearing into a single unit makes the unit larger and more costly than if the two were considered separately.

The sketches in figure 31 show: (a) the integrated unit of a bearing and seal module recommended for a new actuator, and (b) a separate seal module for a new actuator. Either of these configurations could be fabricated for use as a unit installation for actuators to be developed for future programs. Selection of one or the other, or modifications of either, would depend on the application and the design options available to satisfy the operational requirements.

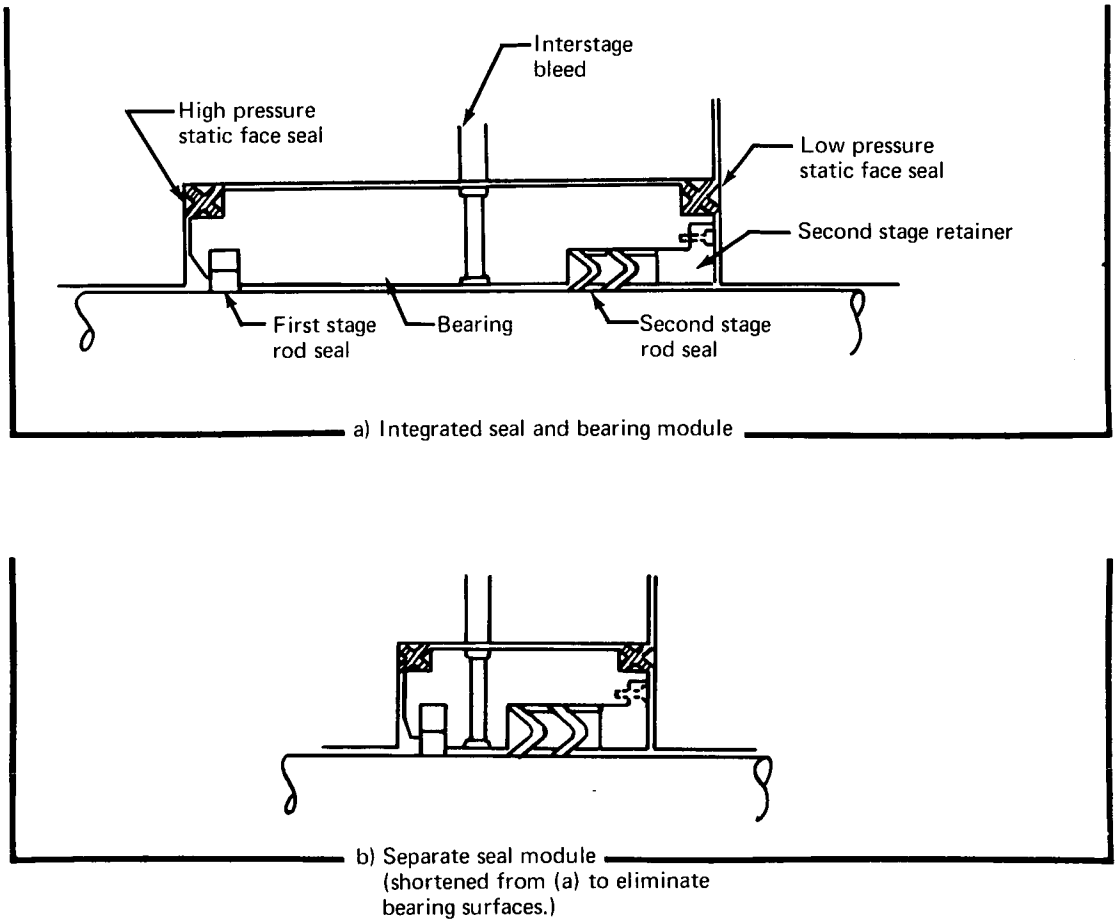

Figure 31. New actuator modular retainer concepts

IV. SEAL PROCUREMENT AND MANUFACTURE

FIRST-STAGE PROCUREMENT

Requests to the Dover Corporation–Cook Airtomic Division, Koppers Company–Metal Products Division, and Royal Industries–Tetraflour Division, were made to establish their design experience applicable to polyimide step-cut rings. As a result of the responses received, Koppers was engaged to design and fabricate 36 first-stage seals; six each in two diameters with three percentages of diametral balancing for each diameter seal. The seal internal diameters were to match a 0.0254 m (1.0 in.) rod and a 0.0635 m (2.5 in.) rod. Pressure balancing percentages were 30%, 50%, and 70%. The seal geometries were patterned to the appendix 1 configuration and were designed to be capable of a life that would satisfy the impulse and endurance requirements, as stated earlier. The final design configurations are reproduced in appendix 3.

SECOND-STAGE MANUFACTURE

Boeing fabricated the second-stage seals at its precision instrument machine shops to have close logistic contact between design engineering and the manufacturing personnel. This allowed near-constant feedback regarding the procedures and processes employed and the effect of these on quality of the final machined parts.

The first step in manufacture was to configure a method of holding the SP-21 polyimide material during the various operations required to form the seal geometries. This was accomplished by rough machining the polyimide into washer shapes which had extra material on both the ID and OD of the finished part dimensions. The washers were machined with the material perpendicular grain along the washer diameters and the parallel grain through the washer centerline to utilize the stress properties as indicated in the design analysis. The rough machined washers were heat treated at 533° K (500° F) for 7200 sec (2 hr) to drive out moisture that, if allowed to remain during final machining, would be released during high-temperature testing and result in shrinkage of the final part. Holding fixtures were fabricated to retain the polyimide washers during machining of the seals. These fixtures, diagrammatically illustrated in figure 32, were employed in the sequence shown during chevron fabrication. Similar fixture pieces were used for fabrication of the K-section. Seals were fabricated in the following sequence: 0.0254 m (1.0 in.) chevron, reference 17; 0.0635 m (2.5 in.) K-section, reference 19; 0.0635 m (2.5 in.) chevron, reference 18; and 0.0254 m (1.0 in.) K-section, reference 20. This sequence was used to allow the machine operator to proceed through the learning curve with a less critical configuration. It also allowed fabrication of the seals most desired for endurance testing (0.0254 m, 1.0 in., chevron and 0.0635 m, 2.5 in., K-section) prior to others, such that screening tests of these seals could be started as early in the program as possible.

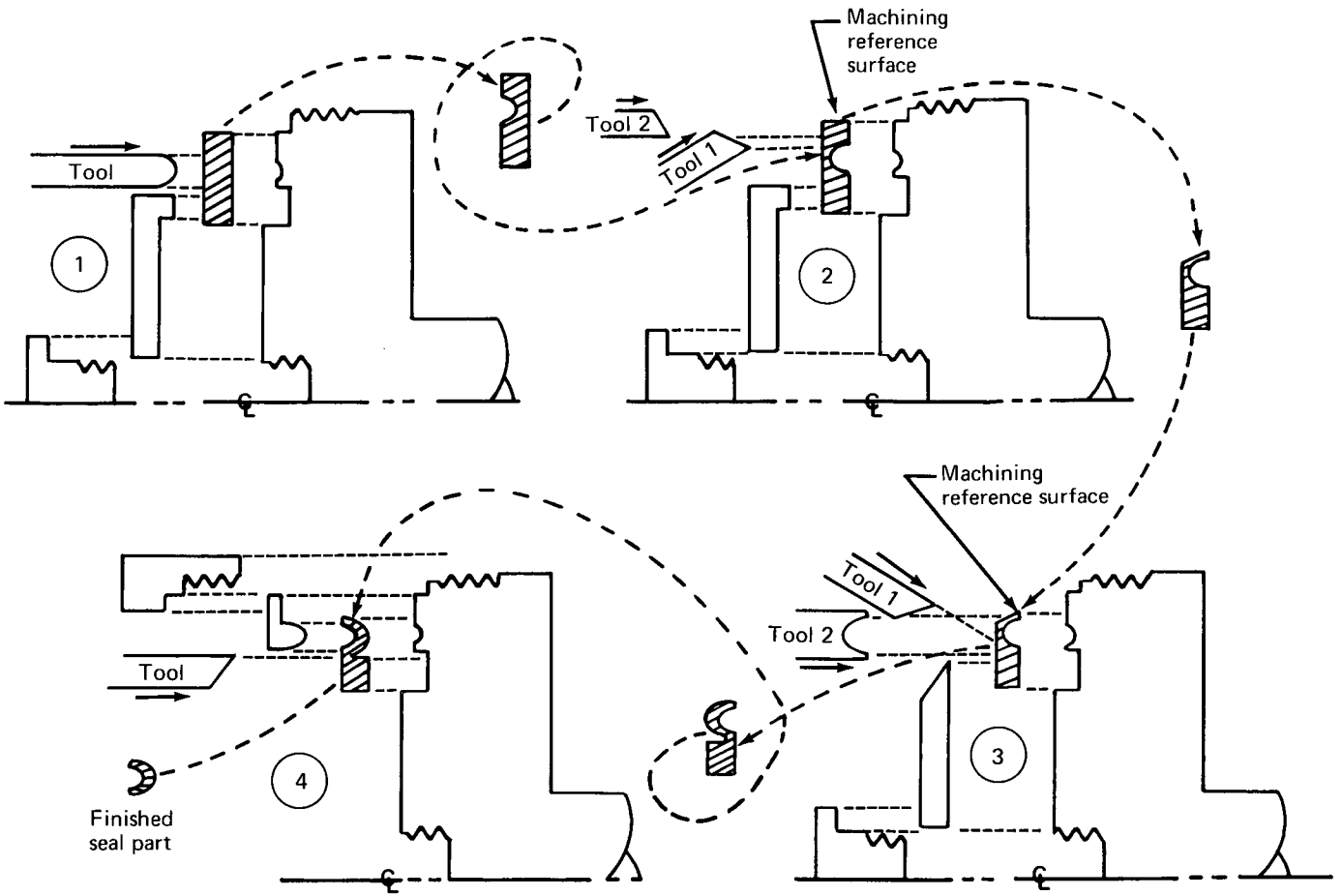

Figure 32.– Chevron seal fabrication sequence

Cutting tools were ground to the shapes conforming to the finished geometry of each section of a given part. A single tool was used to generate the concave surface in step 1 in figure 32. Similarly, a single tool was made to generate the finished convex surface in step 3. It was necessary, however, to rough cut the convex side of the part prior to final machining in order to limit the final cut with the finishing tool to 2.54×10^{-5} m (0.001 in.). This limitation was needed to prevent the resilience of the thin leg section of the part being machined from distorting the final shape due to loading produced by the machining tool. It was determined that, without the rough cuts, the 0.0254 m (1.0 in.) chevron inside leg could be distorted as much as 7.62×10^{-5} m (0.003 in.)on its finished diameter and the 0.0635 m (2.5 in.) chevron as much as 1.778×10^{-4} m (0.007 in.) on its finished inside diameter.

The finish cutters were inspected for proper shape against a 100X template of the finished part on a comparator. The machined part was inspected for conformance to its cutting tool after machining was completed to ensure that the resilience of the part under tool load did not affect the finished shape. It was necessary to periodically reinspect the tool against the template on the comparator to determine tool wear and plan when tool regrinding would be necessary. The process of fabricating the SP-21 into the concave surface produced a flaky finish that was apparently a function of the graphite in the material. Attempts at polishing the surface did not improve the appearance. Because machine inspections of the concave surface roughness were not possible, a more complete analysis of the flakiness could not be made. The condition did not lead to rejection of finished parts, but was watched for any evidence of flake removal that would become a source of contamination. Photographs of the completed seals are shown in figure 33. These photographs show that a polyimide part, identified as an upstream radius block, was fabricated in addition to the parts detailed on figures 26 through 29. This radius block was used in the seal gland as a practical means of preventing leg tip damage on the upstream sealing element for either the chevron or K-section seals during installation. Another method to accomplish the same objective would have been to fabricate a more complex geometry in the seal gland.

V. TEST PERFORMANCE

Testing was performed with the objective of determining whether the design methodology used to develop the rod seals as described in previous sections of this report could be validated by testing to critical design requirements. An additional objective was to demonstrate the advantages of the use of polyimides in satisfying the requirements of long life at elevated temperatures. The tests selected to meet these objectives were divided into the categories of screening and endurance testing. Screening tests were used to evaluate the

Scale 1.0 = 1.08

0.0254 m (1.0 in.) chevron

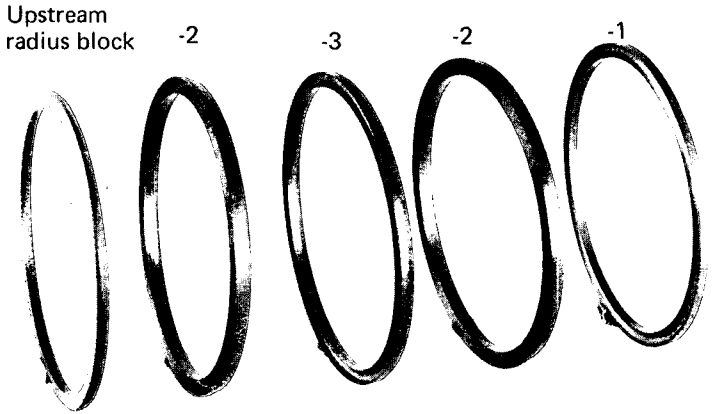

Scale 1.0 = 1.7

0.0635 m (2.5 in.) chevron

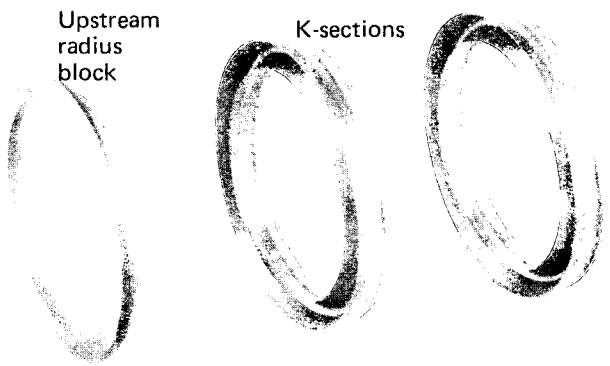

Scale 1.0 = 1.08

0.0254 m (1.0 in.) k-section

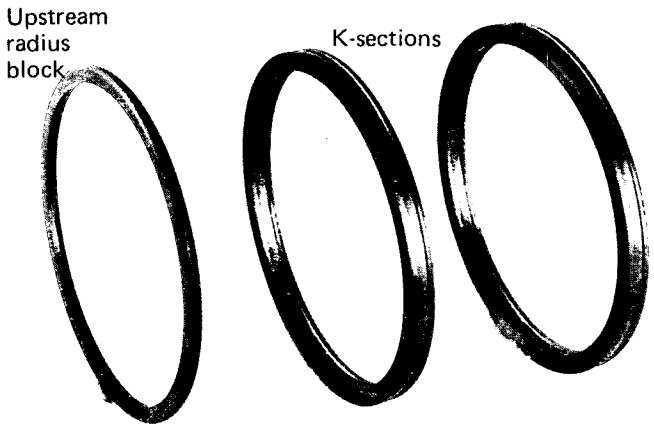

Scale 1.0 = 1.7

0.0635 m (2.5 in.) k-section

Figure 33.— Second-stage test seal assemblies

various configurations for both the first- and second-stage applications and from these select the configurations to be used during endurance testing. The endurance test was conducted to evaluate the selected seals to the accelerated life cycle requirement representative of the 4.5×10^7 sec (12 500 hr) overhaul life for rod seals to be used on the Boeing/DOT supersonic transport airplane.

SCREENING TESTS

Screening tests were developed for the purpose of providing data that would show the differences between the alternate seal candidates as well as data that would show a quantitative measure of the potential for the seals under stress environments typical of an advanced airplane application. The screening tests selected were: (1) an impulse test to evaluate the structural integrity of the seal cross section, and (2) a friction test to evaluate the friction forces that contribute to inefficiency of the hydraulic actuator.

Impulse Testing

Pressure impulse tests were conducted to evaluate the integrity of both the first- and second-stage seals under the environment described in figure 34. The existing test facility, shown in figure 35, was utilized and the hydraulic setup modified as required to provide the specific test environment. Impulse tests were perfomred on both the small (0.0254 m, 1.0 in.) and large (0.0635 m, 2.5 in.) first-stage seals with two of the three balancing conditions, and on both the small and large sizes of chevron and K-section second-stage seals. Descriptions of the test sequences and instrumentation are provided in appendix 4.

First-stage impulse results.—The 0.0254 m (1.0 in.) ID first-stage seals, in both conditions of 30% and 50% pressure balancing, and the 0.0635 m (2.5 in.)ID first-stage seals, in both 30% and 70% balancing configurations, were impulse tested. There was no evidence that impulse testing had any effect on the structural integrity of these seals. The 0.0635 m (2.5 in.) 30% seal showed damage in the area of the step cut subsequent to impulse testing. This damage was judged to be due to material contamination or notch sensitivity at machine marks and not attributable to stress failure under load. Figure 36 is a photograph of this seal and the area of damage. Leakage measurements during testing indicated that fluid containment was not dependent on pressure balancing. Leakage averages at the test temperatures evaluated showed variations as indicated in table IX. These are compared against a 8.3×10^{-7} m^3/sec (50 cc/min) allowable.

Two values are shown where low and high leakages were sufficiently separated that a statistical mean would be misleading. One value is shown where measurements were clustered and averaging was meaningful.

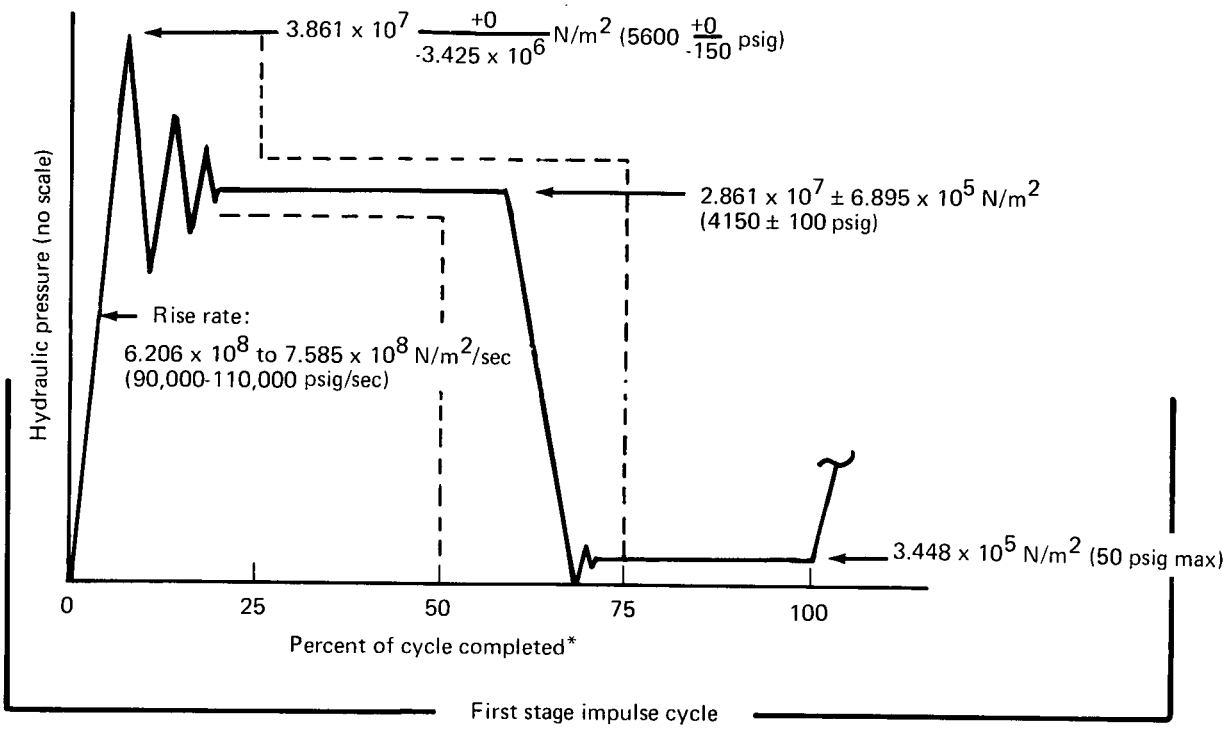

*Cycle rate = 1.167 $^{+0}_{-0.0833}$ Hz (70 cycles per min.)

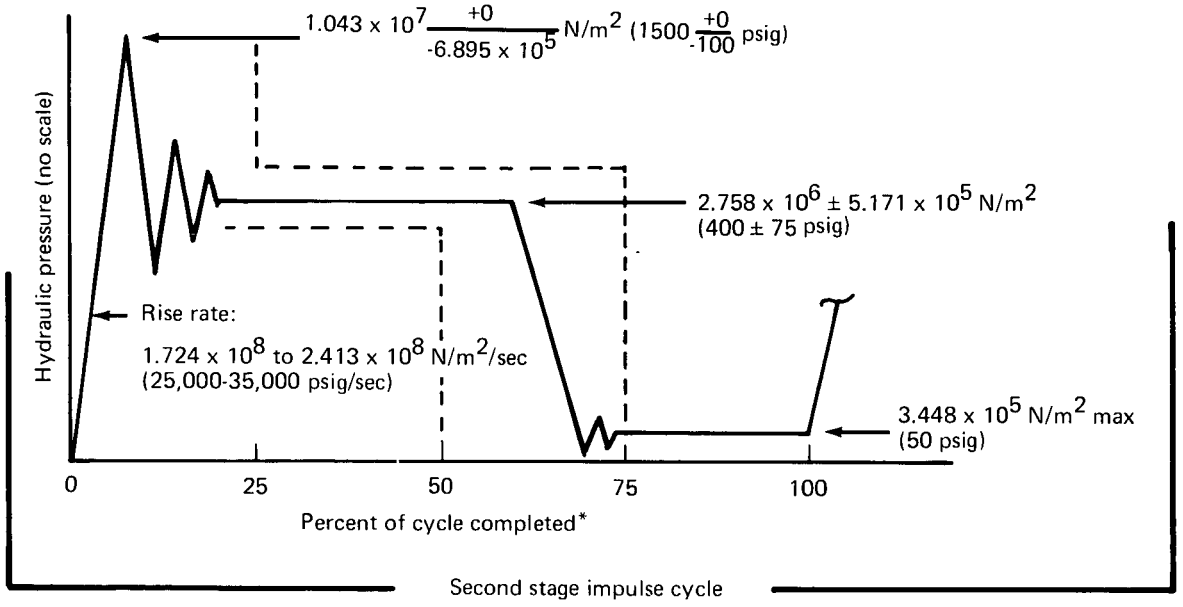

Figure 34.—Impulse cycle

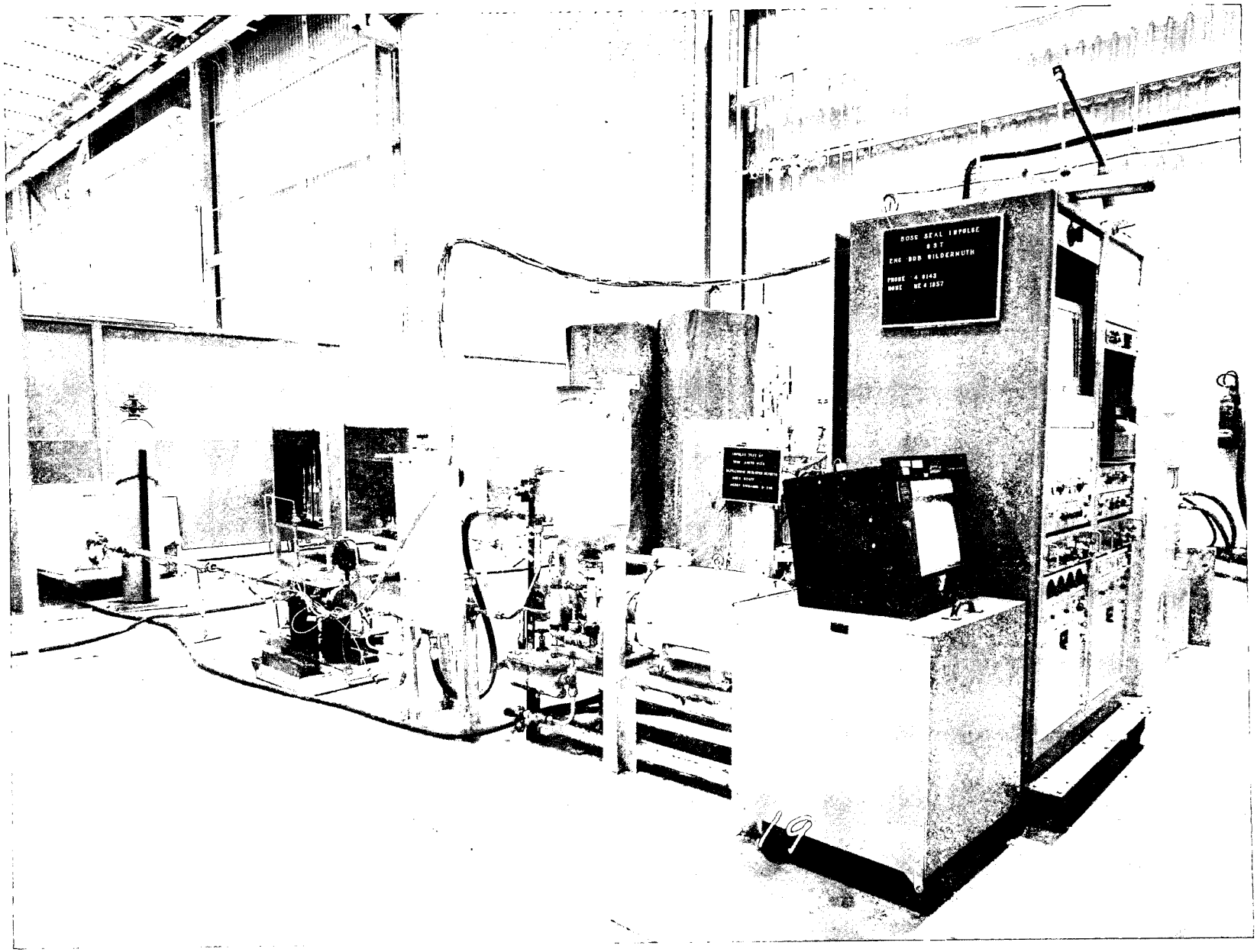

Figure 35.—Impulse test facility

Figure 36.—Post impulse 30% balanced first stage

Table IX.—Leakage data—first-stage impulse test

		Leakage variation with temperature			
Seal	Units	311°K(100°F)	408°K(275°F)	450°K(350°F)	478°K(400°F)
0.0254 m ID (1.0 in.)	$m^3 \times 10^{-8}$/sec (cc/min)	4.17 (2.5)	16.7 to 48.3 (10 to 29)	23.3 to 35.8 (14 to 21.5)	25.0 to 45.0 (15 to 27)
0.0635 m ID (2.5 in.)	$m^3 \times 10^{-8}$ sec (cc/min)	2.83 (1.7)	4.17 to 20.0 (2.5 to 12)	6.67 to 18.3 (4 to 11)	6.67 (4)
Allowable leakage was 8.33×10^{-7} m^3/sec (50cc/min)					

None of the first-stage seals were received with the antirotation pin installed to lock the inner sealing ring to the outer compression ring. The impulse tests were initiated with the seals as received, with the intention of returning them for pin installation only if test results showed that the pins were essential.

During testing, differential rotation of 3.141 rad (180°) between the sealing and compression rings produced lineup of the step cut in the sealing ring with the gap in the compression ring resulting in extreme external leakage. This occurred three times with the 0.0254 m (1.0 in.) 30% balanced seal, three times with the 0.0254 m (1.0 in.) 50% balanced seal, and once with the 0.0635 m (2.5 in.) 30% balanced seal. As a consequence, two sets of seals were returned to Koppers to have the antirotation pins installed in preparation for other tests.

The 0.0254 m (1.0 in.) 70% balanced and 0.0635 m (2.5 in.) 50% balanced seals were accepted as satisfactory under the impulse requirement by similarity to the seals that were tested. This was justifiable since the impulse test was performed for structural integrity of the sealing element cross section at the step cut. Since the 0.0254 m (1.0 in.) 30% and 50% balanced seals passed impulse with the same step cut section as the 70% balanced seal, it was statistically safe to assume that the 0.0254 m (1.0 in.) 70% section would also pass. Since the 0.0635 m (2.5 in.) 30% and 70% balanced seals passed the impulse test and bracket the 50% balanced section, it was also safe to assume that the 50% section would pass the same test.

Second-stage impulse results.—Tests were conducted to evaluate the second-stage chevron and K-section cross sections in both the 0.0254 m (1.0 in.) and 0.0635 m (2.5 in.) sizes. The seal leakage obtained during testing is shown in table X and is comparable to an allowable leakage of 5×10^{-8} m^3 (1 drop) per 900 sec (15 min) or an equivalent 1050 cycles. The completion of these tests, with no more than the above leakage, verified the acceptability of the seals tested for the application requirements.

Examinations were made of the tested seals subsequent to completion of 200 000 cycles of impulse. The examinations revealed some structural cracks in the legs of the sealing

Table X.– Leakage data–second-stage impulse test

Test condition	Seal configuration – leakage measured			
	0.0254 m (1.0 in.) chevron	0.0254 m(1.0 in.) k-section	0.0635 m(2.5 in.) chevron	0.0635 m(2.5 in.) K-section
450°K(350°F) proof pressure $3.425 \times 10^7 N/m^2$ (1500 psig) for 300 sec (5 min)	None	None	None	None
228°K(-50°F) proof pressure $3.425 \times 10^7 N/m^2$ (1500 psig for 300 sec (5 min)	None	None	None	None
40 000 cycles at 311°K (100°F) of figure 34 profile	None	$5 \times 10^{-8} m^3$(1 drop) /6712 cycles	$5 \times 10^{-8} m^3$(1 drop) /6712 cycles	None
115 000 cycles at 408°K (275°F) of figure 34 profile	None	$5 \times 10^{-8} m^3$(1 drop) /6077 cycles	$5 \times 10^{-8} m^3$(1 drop) /6077 cycles	None
40 000 cycles at 450°K 350°F) of figure 34 profile	$5 \times 10^{-8} m^3$(1 drop) /7583 cycles	$5 \times 10^{-8} m^3$(1 drop) /4368 cycles	$5 \times 10^{-8} m^3$(1 drop) /4368 cycles	None
5 000 cycles at 478°K (400° F) of figure 34 profile	None	Less than $5 \times 10^{-8} m^3$ (1 drop)/5 000 cycles	$5 \times 10^{-8} m^3$(1 drop) /5 000 cycles	$5 \times 10^{-8} m^3$(1 drop) at 5 000 cycles

Allowable leakage was 5×10^{-8} m^3 (1 drop) per 900 sec (15 min) or an equivalent 1050 cycles.

elements. Details of the locations of these cracks and interpretations of their significance are described in figures 37 through 42. Despite the cracking, the seals retained the ability to provide fluid containment during a test more severe than expected in normal service. There was no evidence of chips or broken pieces from the seal parts.

An attempt was made to determine when the cracks developed during the impulse sequence. This was accomplished by testing single sealing elements from the 0.0635 m (2.5 in.) K-section assembly and the 0.0254 m (1.0 in.) chevron assembly. It was anticipated that, under these conditions, cracking would be accompanied by a measurable increase in external leakage because the second or redundant element in both configurations was not used. Results with the K-section test were that 3.33×10^{-9} m^3/sec (4 drops/min) leakage was evidenced during startup cycles following a weekend shutdown. This occurred after 40 000 cycles at 311° K (100° F) plus 28 206 cycles at 408° K (275° F) were completed. A disassembly inspection was conducted showing cracks on the outer leg of the seal very similar to those described in note 3 in figure 39.

Cracking with only the indicated number of cycles accumulated could be attributed to a number of causes, all equally plausible separately or in combination. Those causes judged most significant are listed below.

- A near-constant stress level existed throughout the tapered leg under any given set of operating conditions due to similarly proportional changes in both the bending moment and area moment of inertia from tip to apex of the leg. As a result there was no particular reason why cracks should have occurred at one location or another, except where material notch sensitivity caused increased local stress at machine marks.

- A comparison of seal design data against flexural fatigue data from DuPont and mean stress data approximations from figure 11 showed that it was remotely possible that flexural failure could occur at a life as low as 20 000 cycles with the 0.0635 m (2.5 in.) K-section seal. The validity of quantifying failure in this manner is questionable due to the origin of the curves in figure 11, but the inference of low cycle life has qualitative value as an explanation.

- Progressively accumulated fatigue cycles reduce seal leg cross-section strength. When this effect of reducing the allowable stress matches the stress produced by preset, failure will occur. The stress allowable due to preset was less than optimum with the 0.0635 m (2.5 in.) seal because preset and pressure load requirements could not be equally satisfied with a single seal configuration, as shown in figure 25.

- The evidence of wear on the outer leg tips of some 0.0635 m (2.5 in.) seals showed that contact with the gland extended downstream of the machined contact surface. Under this condition localized loading was developed in excess of normal, possibly exceeding the fracture strength of the material.

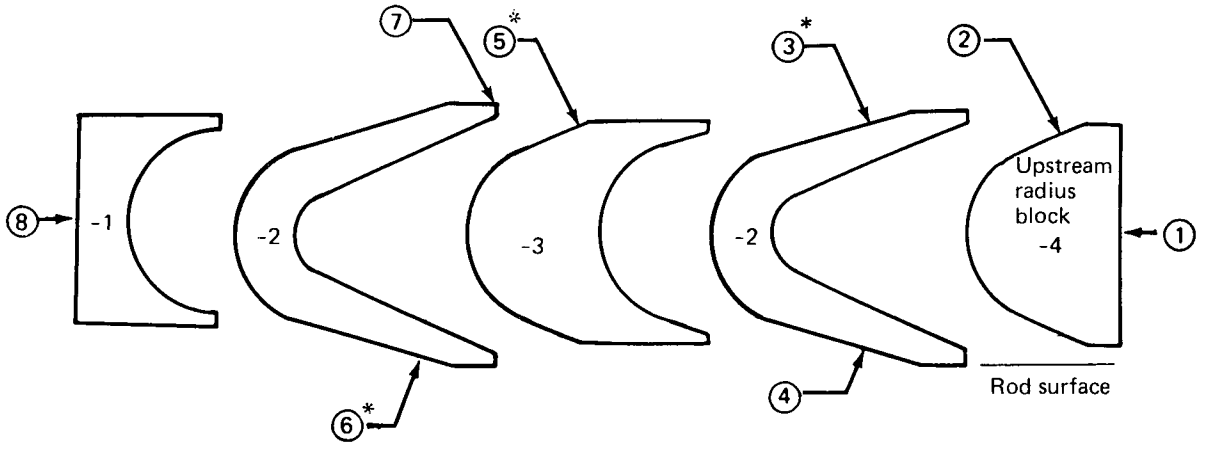

① No contact was noted, indicating that the gland was long enough so that the thermally expanding seal did not completely fill the cavity.

② The contact surface appeared different than ⑤. Since this was the last chevron component fabricated, tool wear may have been contributor to roughness.

③ A crack on the outside of the outer leg, 6.283 rad (360°) in circumference, was at the extreme downstream edge of the polished area due to contact. The contact surface was between the crack and the downstream end of the machined flat on the OD indicating wear was farther downstream than expected and the leg pivot point was not at the place anticipated in design.

④ The wear surface was only one-half as wide as on the outer leg and occurred at the extreme downstream edge of the machined flat, indicating that the leg pivot point for flexing was different than anticipated in design.

⑤ A crack, 6.283 rad (360°) in circumference, on the inside surface was cracked through to the outside along 6.109 rad (350°) at the downstream edge of the machined flat. The crack was attributed to loading transferred through the -4 and -2 parts. The polished area of contact was just downstream of the machined flat and the crack, as was anticipated in the design.

⑥ A crack, 6.283 rad (360°) in circumference, was about midway between the downstream edge of the machined flat and the tangent point of the tapered leg and apex curvature. The polished contact area was only on the machined flat. The crack was attributed to load being transferred thorugh the -4, -2 and -3 parts.

⑦ Edge cracks appeared at four random locations within a 0.438 rad (30°) section of the seal circumference. Contact area was on the machined flat only, as evidenced by polishing.

⑧ Contact was noted by polishing as expected on the downstream surface.

*See figure 41 for photograph of this area.

Figure 37.—0.0635m(2.5in.) chevron inspection following impulse

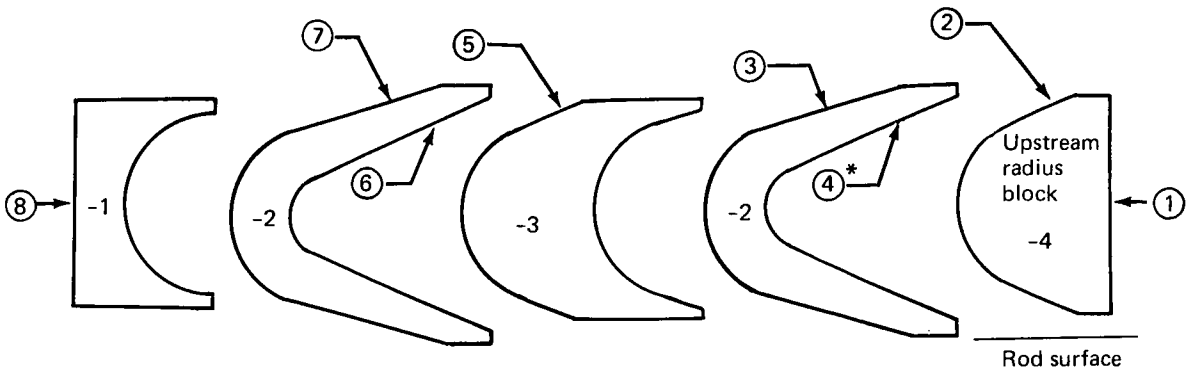

① No contact was noted, indicating that the gland was long enough so that the thermally expanding seal did not completely fill the cavity.

② This contact surface appeared different than ⑤. Since this was the last chevron component fabricated, tool wear may have been the contributor to roughness.

③ Very small random cracks were evidenced, possibly due to notch sensitivity. These may have been due to original material imperfections since the cracks had random direction orientation with the average direction progressing around the circumference.

④ This surface had a very minutely cracked inner edge, possibly attributable to notch sensitivity, or loading from pressure on part -4, or both.

⑤ This contact surface was smooth, indicating contact between parts to have occurred between the downstream edge of the face and approximately 2/3 of the depth from the upstream edge.

⑥ Small 0.146 rad (10°) cracks occurred in four places, approximately 90 degrees apart on the circumference, and appeared to start in machine grooves, indicating a notch sensitivity effect.

⑦ Small cracks describable as in ③ above occurred on this surface.

⑧ Contact was noted in the form of polishing as expected on this downstream surface.

* See figure 41 for photograph of this area

Figure 38.—0.0254m (1.0 in.) chevron inspection following impulse

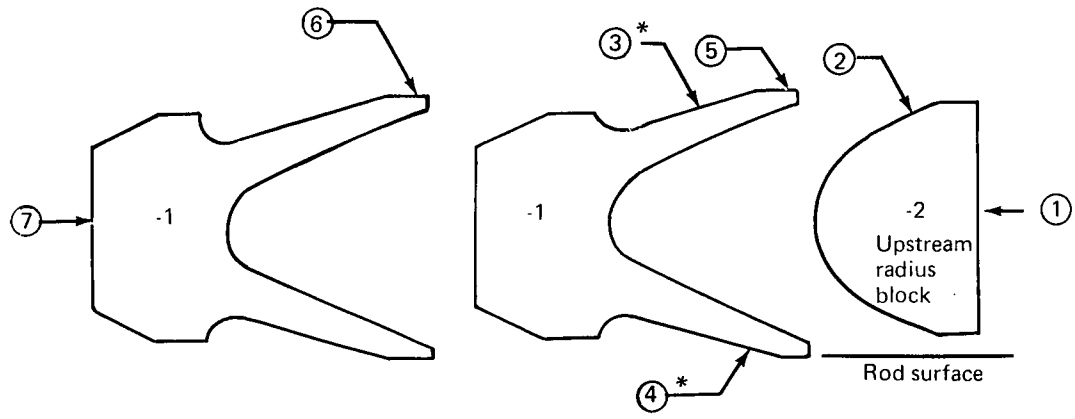

(1) The contact area noted on this surface may be attributable to the gland length being too short to account for full thermal expansion of the seal.

(2) Roughness on the surface may be attributable to this being the last fabricated part of the seal and tool wear could cause a rougher surfacing.

(3) Surface cracks on the inside and outside of the outer leg, approximately 6.283 rad (360°) in circumference, were at the downstream edge of the polished wear surface. The wear surface was between the crack and the downstream end of the machined flat on the OD, indicating wear had produced an extension of this flat due to high loading.

(4) Small random cracks were evidenced approximately 0.524 rad (30°) in arc around the circumference and 1.57 rad (90°) apart. This appeared to be similar to (3) above, but of lesser magnitude, since thermal expansion of the seal tends to load the outside leg and unload the inside leg.

(5) This seal surface was not polished as expected, indicating the contact wear as described in (3) was occuring.

(6) This seal surface was polished as expected on the machined flat.

(7) A contact area was noted as expected for the downstream contact with the seal gland.

* See figure 42 for photograph of this area

Figure 39.—0.0635m (2.5in.) K-section inspection following impulse

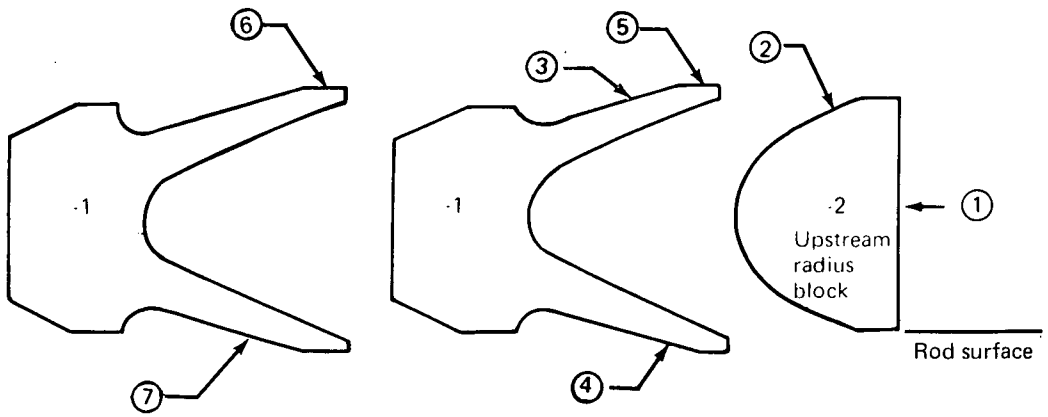

① No contact was noted, indicating that the gland was long enough so that the thermally expanding seal did not completely fill the cavity.

② Roughness of this surface may be attributable to this being the last fabricated part of the seal and tool wear could have caused the rougher surfacing.

③ The polished contact surface was at the downstream edge of the machined flat indicating wear had produced an extension of the flat due to high loading.

④ This leg was damaged in installation due to pressure against the key slot in the end of the actuator rod. The damage was a crack the full depth of the leg. Contact with the rod was maintained on the machined flat of the leg.

⑤ This seal surface was not polsihed as expected indicating the contact areas was as described in ③ above.

⑥ This seal surface was not as highly polished as expected on a machined flat in contact with the gland.

⑦ This seal surface was polished as expected on a machined flat in contact with the rod.

Figure 40.– 0.0254m(1.0 in.)K-section inspection following impulse

Large chevron—ID leg (see fig. 37 ⑥)

Large chevron—OD leg (see fig 37 ③)

Small chevron—OD leg (see fig 38 ④)

Large strongback (see fig 37 ⑤)

Figure 41.– Typical material cracks from chevron seal impulse testing

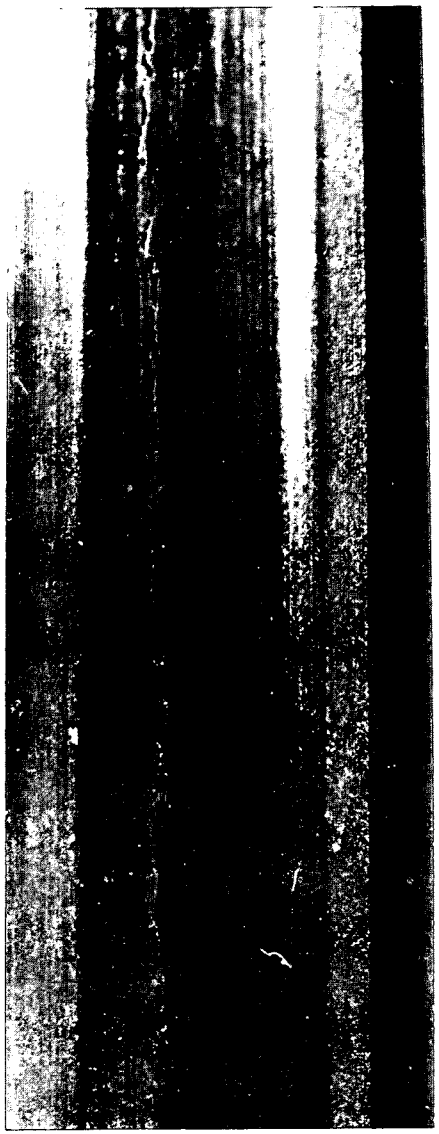

Large K—(see fig 39 ③)

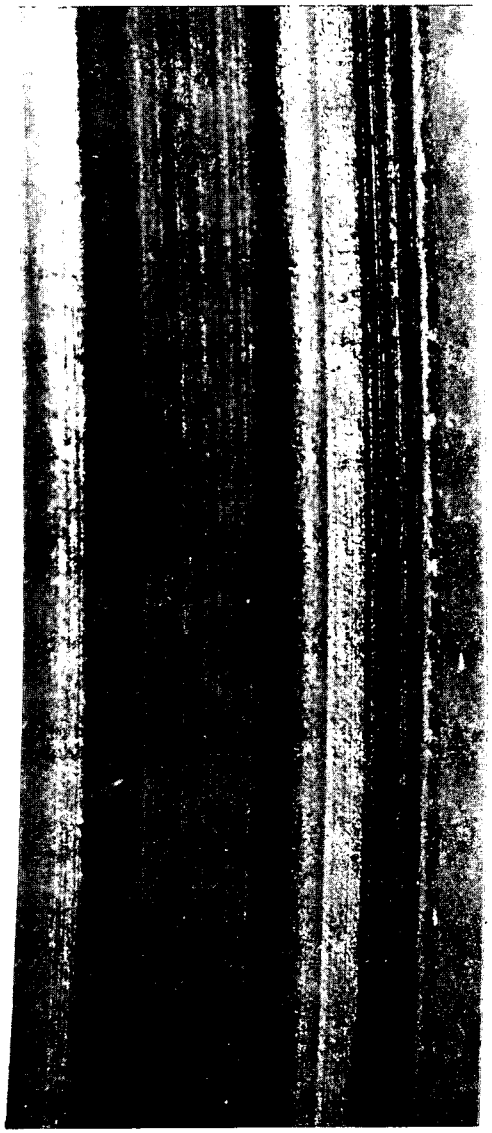

Large K—(see fig 39 ④)

Figure 42.—Typical material cracks from K-section seal impulse testing

Results with the 0.0254 m (1.0 in.) chevron test were that 40 000 cycles at 311° K (100° F) plus 87 998 cycles at 408° K (275° F) were completed with leakage not in excess of the 5×10^{-11} m^3/sec (1 drop/15 min) allowable. The test was terminated with this number of cycles to release the test fixture for use in endurance testing. There was no evidence of cracking.

Friction Testing

Static friction is the measure of force necessary to produce rod breakaway from a stationary position. Dynamic friction is the measure of force necessary to overcome running friction at specific rod velocity. Tests of both static and dynamic friction were conducted to determine the quantitative relationship between the friction forces developed by all three pressure balancing conditions, for both sizes of first-stage seals and for both sizes of chevron and K-section configurations of second-stage seals. The test facility, shown in figure 43, was utilized to perform the friction testing. Descriptions of the test sequences and instrumentation are provided in appendix 5.

First-stage friction test results.—Figure 44 provides the results of the friction testing of the 0.0635 m (2.5 in.) ID first-stage rod seals. The results of the dynamic friction tests show that higher temperatures and pressures are associated with higher friction, as expected. Higher pressure balancing is associated with reducing friction. The maximum dynamic friction, at the highest temperature and pressure, with the lowest pressure balancing, did not exceed the 1.335×10^3 N (300 lbf) friction level established as a criterion earlier in the report. With the highest pressure balancing the friction was less than one-half the criterion goal.

The static breakout friction data for the 0.0635 m (2.5 in.) seals did not show friction as a uniform linear function with pressure as was evidenced with dynamic friction. This was caused by a number of phenomena, presumed to be primarily associated with stick-slip friction (or chatter) and differences between breakout in the extend and retract directions. Because the extend and retract data were averaged to provide the overall trend, the curves in figure 44 break, and crossovers are evidenced. By obtaining more data to provide a larger statistic base, these phenomena would not be as significant. The data obtained were, however, sufficient to show that the pressure balancing was reciprocally proportional with friction.

Figure 45 provides the results of the friction testing of the 0.0254 m (1.0 in.) ID first-stage rod seals. The static breakout data show the same nonlinearities that were experienced in testing the larger size seals. These results are also attributed to chatter and data averaging in the same manner as indicated above. The dynamic friction for the small seals was higher than the criterion of 2.447×10^2 N (55 lbf) established as an objective under design requirements. This may be attributed to a larger seal axial dimension than that necessary to

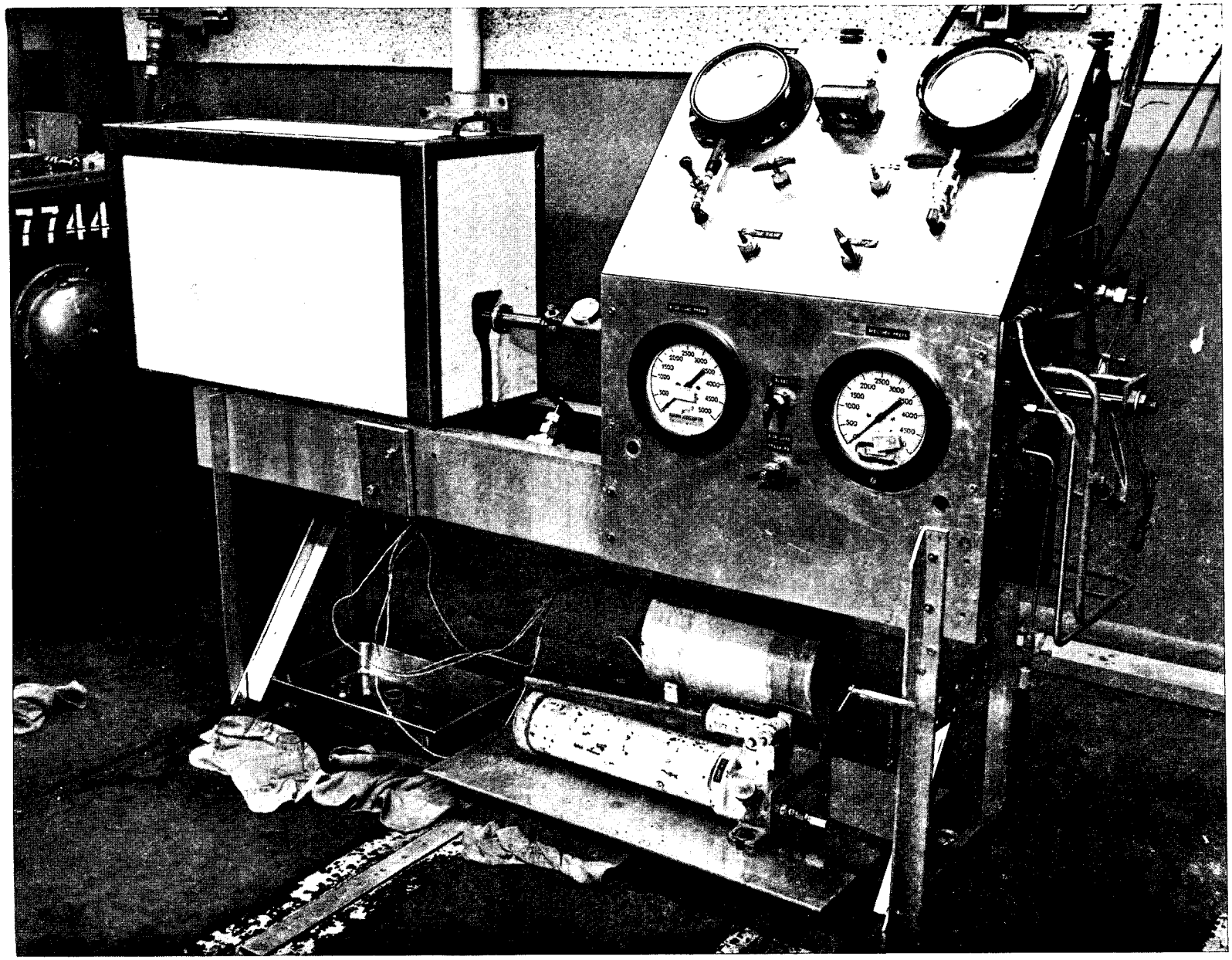

Figure 43.—Friction test facility

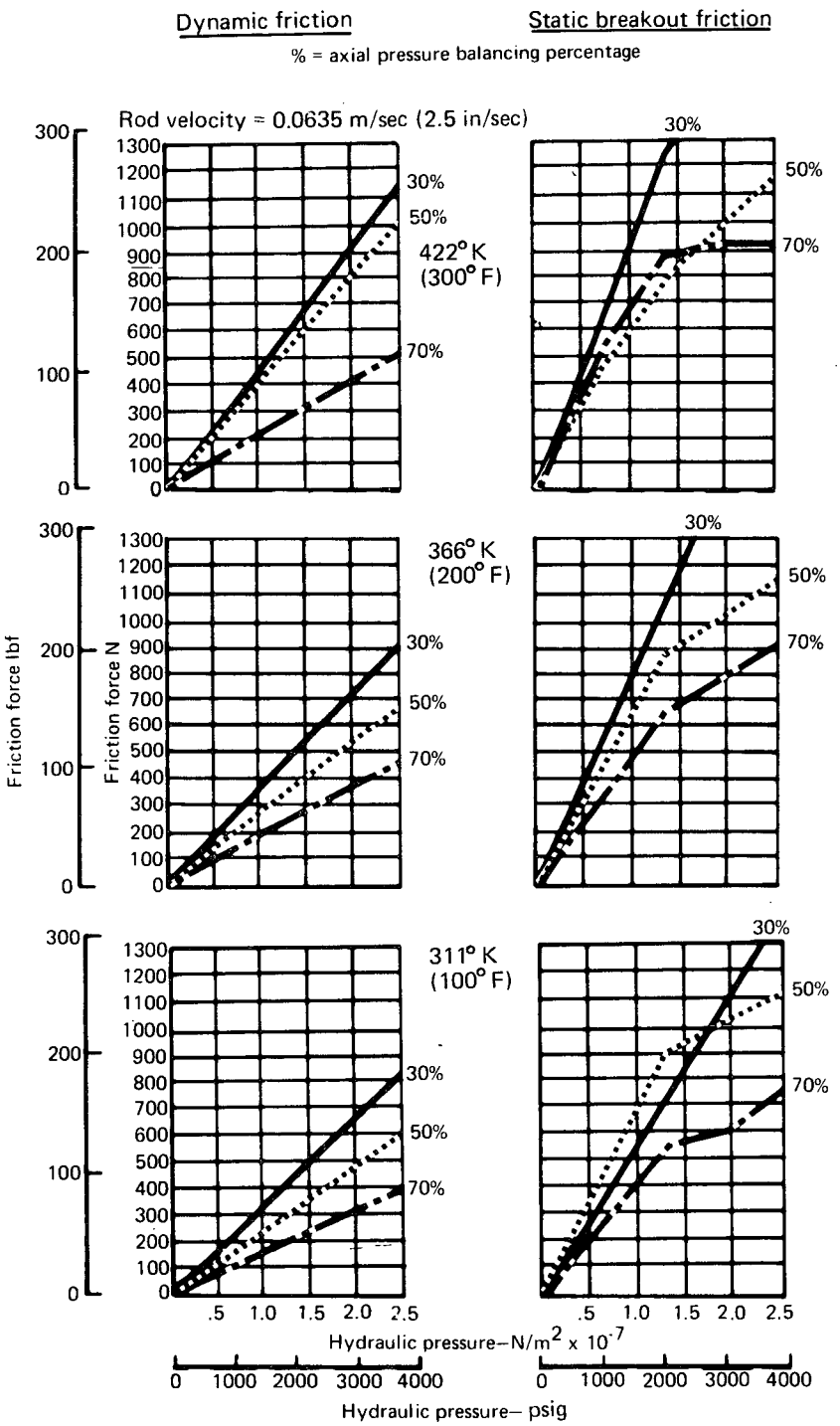

Figure 44.– 0.0635m (2.5 in) first-stage rod seal friction

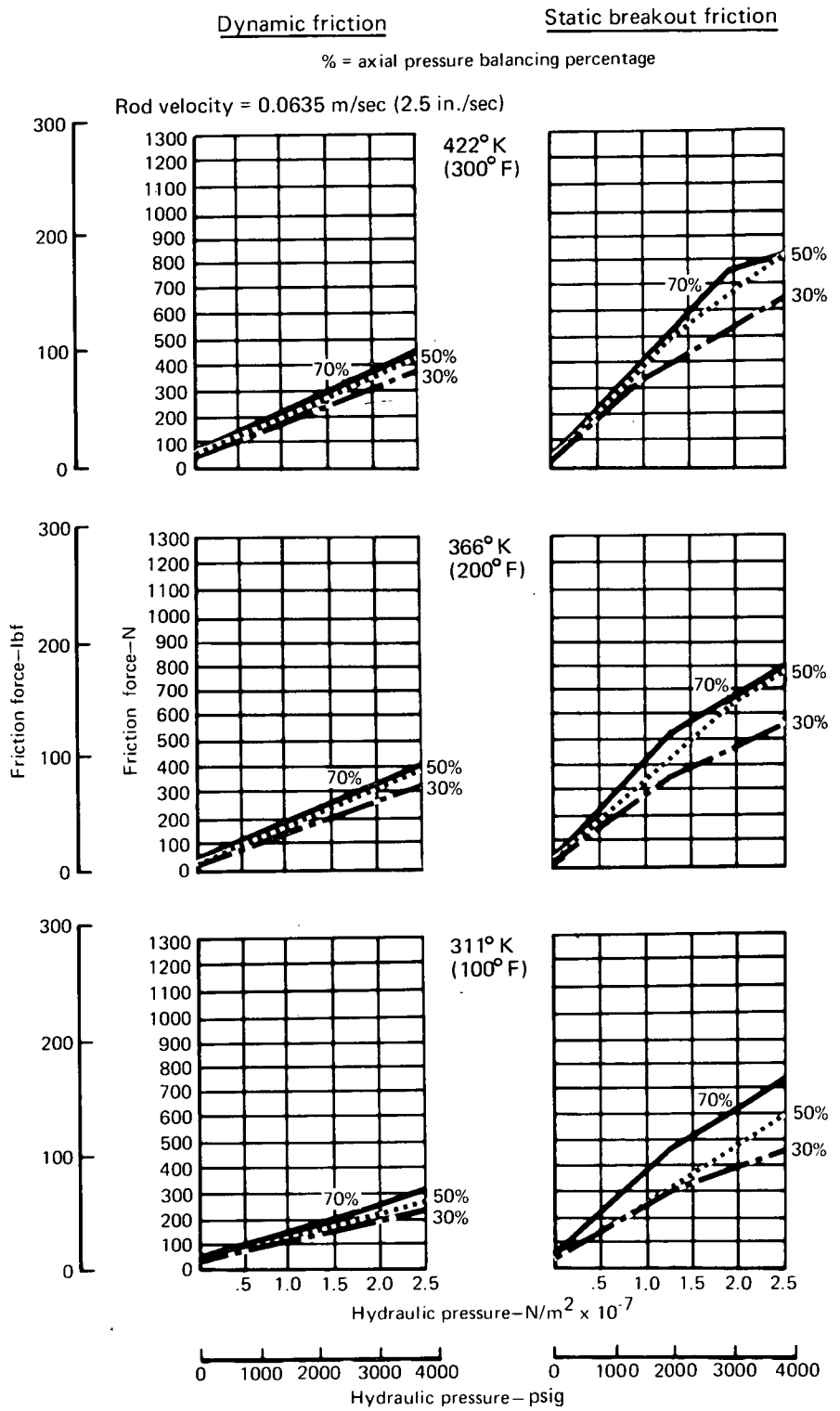

Figure 45.—0.0254 m (1.0 in.) first-stage rod seal friction

ensure only the friction level stated above. The larger dimension was required to properly design a step cut that was structurally capable of the application impulse life requirement.

The results of both static breakaway and dynamic friction tests with the 0.0254 m (1.0 in.) seals show a different trend than that obtained with the 0.0635 m (2.5 in.) seals. This trend was that increased balancing with the smaller seals was directly related to increased friction rather than the expected inverse relationship as shown with the larger seals. A lack of separation of data at higher percent balancing and higher temperatures indicated a relationship between seal contact area and friction. Contact area for the 30% seal was less than that for the 50% and 70% seals, which were about equal in a given size.

The nature of the small-size-seal friction test results, with data contradictory to the design objective, was examined using the seal dimensions from appendix 3 and the first-stage pressure balancing computer program described in section III. This analysis is described in detail in appendix 6. The analysis showed that seal dimensional variations influence contact pressure, which in turn significantly affects seal friction. The manner that friction is influenced is also affected by an inverse relation between contact pressure and coefficient of friction as well as by the distribution of contact pressure, which depends on surface characteristics and seal distortion under load. Because a definition of these characteristics was not quantifiable in the design stage for these seals, there could be no guarantee that increased balancing would result in reduced friction.

Friction testing with the 70% balanced first-stage seals was randomly interrupted by instances of extreme external leakage resulting from the seal becoming unseated. Reseating could be accomplished by a sudden application of high pressure. This condition was attributed to exceeding the practical limit of axial balancing for a linear rod seal application. By adding radial balancing, using the design approach described in section III, it may be possible to provide a 70% balanced seal that will not encounter lifting under static, and near-static, loads. There is reservation that such a seal would be effective under dynamic pressure surge environments.

Second-stage friction test results.—The friction screening test results for the evaluation of all second-stage seals are contained in figures 46 and 47. Dynamic data were as expected, with friction increasing with temperature. This was particularly evident with 0.0635 m (2.5 in) seals.

The dynamic friction levels recorded were about double the goals established in the requirements stated earlier in the report. This is consistent with the evolving design method, which in final form required use of high preset interferences after it was determined that loading springs could not be used successfully. The dynamic friction also showed the trend that friction with the K-section seal was higher than with the chevron.

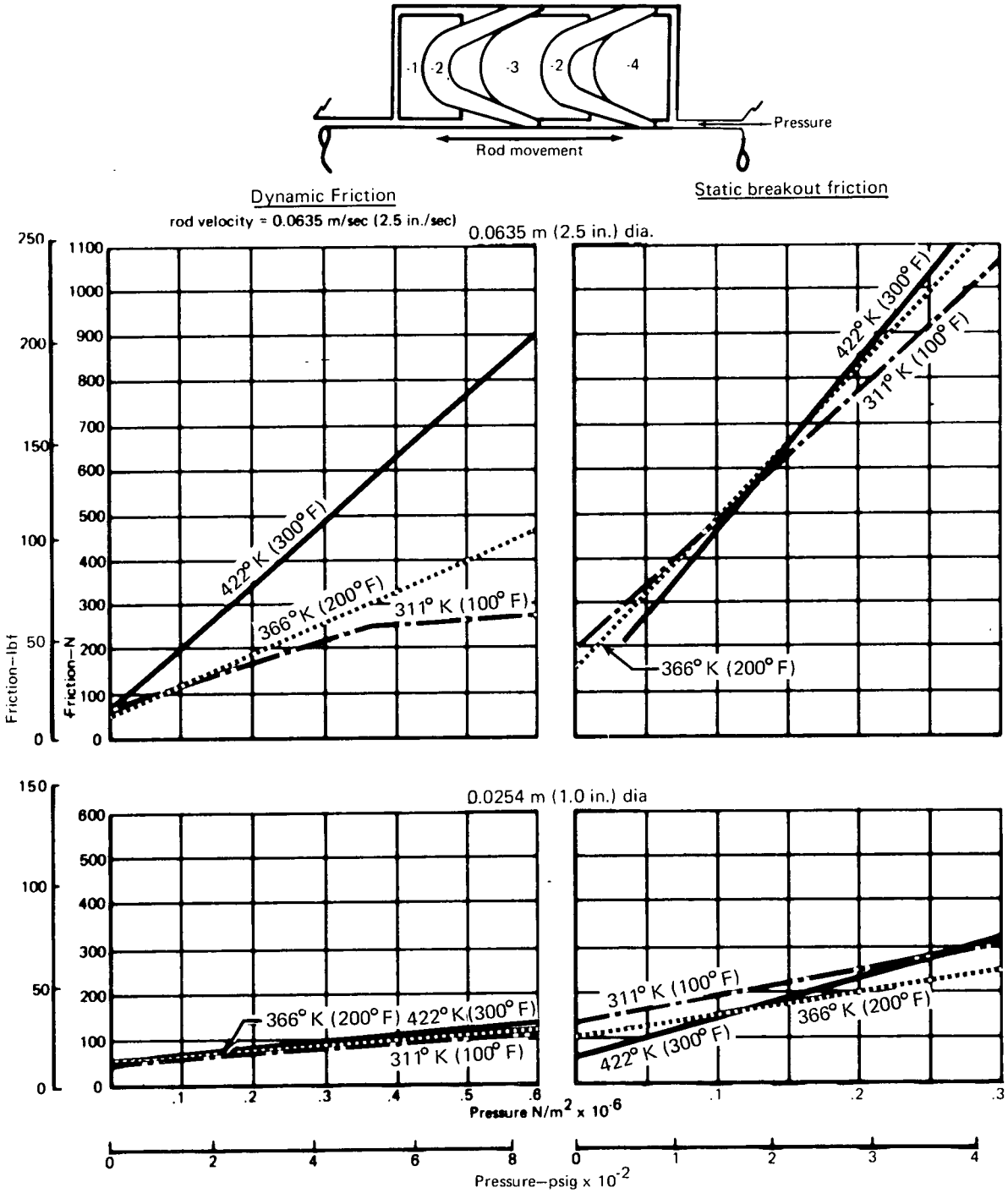

Figure 46.-- Chevron seal friction data

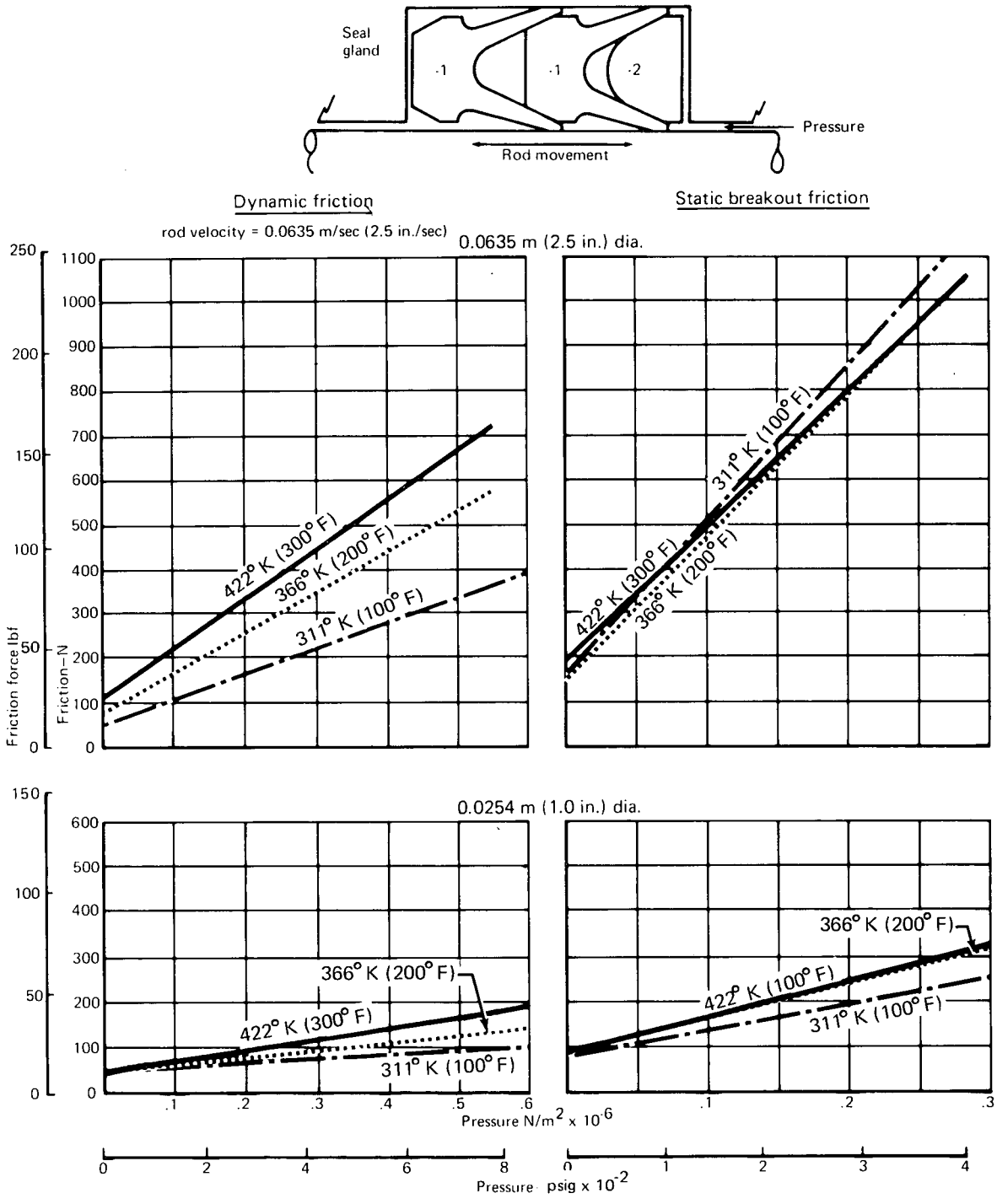

Figure 47.—K-section seal friction data

Breakout data for the 0.0254 m (1.0 in.) seals showed no difference between the friction of the chevron and K-section configurations when instrument accuracies are considered. There was an indication that this size K-section seal friction varied slightly more with temperature than did the chevron in the same size. This may be attributed to the K-section being a stiffer section than the chevron. Breakaway data for the 0.0635 m (2.5 in.) size seals were equivalent for both geometries within the accuracies of repeatability.

Recommended Seals for Endurance Testing

The selection of seals for installation in the endurance test actuators was based on the results of the screening tests. The significance of the impulse test in this selection was that it was the only test measure available that allowed fatigue evaluation per the exact requirement used in design. As a result, structural integrity of all seals was proven to be satisfactory by completing the 200 000 impulse cycles without leakage exceeding the allowable. Because material cracking in seal parts did not result in any condition where fluid containment was jeopardized, the evidence of cracks was not considered a negating effect on the success of impulse testing.

The 0.0635 m (2.5 in.) K-section second-stage seal configuration was considered the least conservative design of the seals being developed. Because this seal successfully completed impulse testing it was recommended for use in the endurance tests. The alternate chevron configuration was recommended for endurance testing in the 0.0254 m (1.0 in.) actuator to provide test data for this, the second, configuration of second-stage seals.

The function of friction testing was to determine a performance distinction between seals that could not be provided through impulse testing. Results from these tests were the basis for recommending that a 50% balanced first-stage seal with the antirotation pin installed should be used during endurance testing. The 0.0635 m (2.5 in.) 30% balanced seal was less attractive due to higher than desirable friction, and the 70% balanced seals in both sizes were considered calculated risks due to the intermittent erratic leakage conditions observed at low pressures. The 50% balanced condition was also advocated for the 0.0254 m (1.0 in.) ID seal to have a uniform test condition during the endurance tests, because data scatter between the 30%, 50%, and 70% friction tests with the 0.0254 m (1.0 in.) seal was not large, and because it was not within the scope of work to establish the seal size where the friction data pattern inverts.

ENDURANCE TESTS

The objective of the endurance test was to provide data on the life of polyimide seals in a typical fatigue environment for flight control actuators of a high-performance aircraft. Testing was accomplished using the test facility shown in figure 48. This facility was used to simultaneously operate actuators with 0.0254 m (1.0 in.) and 0.0635 m (2.5 in.) rod

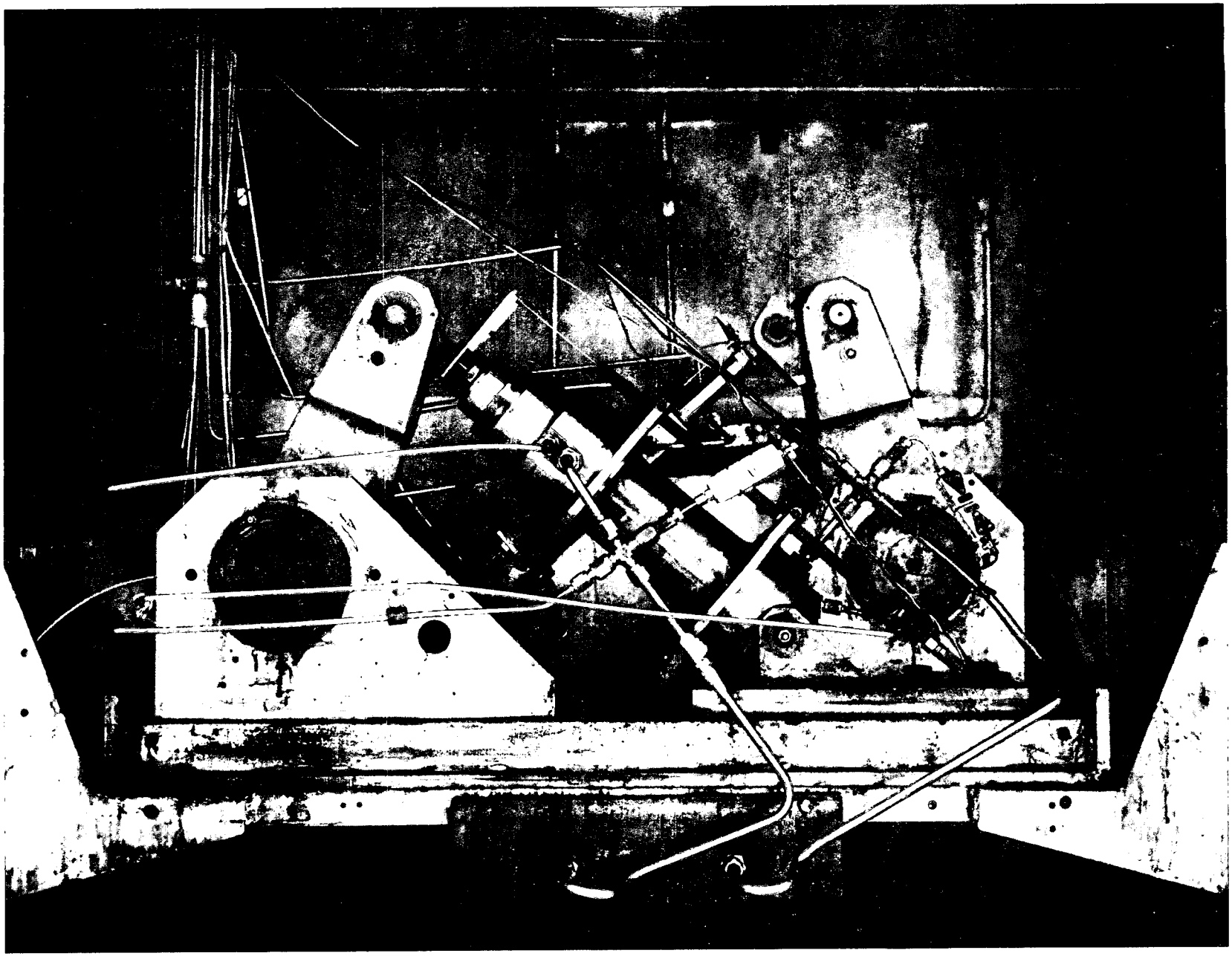

Figure 48.—Seal endurance test, actuator assemblies

diameters against torque loads of aircraft magnitude. Seals tested in the larger actuator were the 50% balanced first stage and the K-section second stage; these were installed in a modular retainer. Seals tested in the smaller actuator were a separately installed 50% balanced first stage and a chevron second stage. Descriptions of the test sequences and instrumentation are provided in appendix 7.

The test actuator rods contacting the seals were fabricated from 4340 steel with a minimum of 5.08×10^{-5} m (0.002 in.) chrome plate ground to a 4.06×10^{-7} m (16 microinch) surface finish. The condition of these surfaces prior to and following the endurance test is shown in figure 49. Longitudinal marks accumulated during testing were primarily due to cycling the first-stage polyimide seal. These wear marks passed beneath the second-stage seal during long stroke cycling but did not appear to adversely affect second-stage wear characteristics.

First-Stage Results

After completing 436 758 cycles of a scheduled 3 850 000, the first-stage seals were removed from both actuators to determine the cause of excessive interstage leakage. Disassembly inspection revealed that wear on the polyimide sealing surfaces was sufficient to allow the contraction of the inner sealing ring to the position where no further gap remained at the step cut. Because further contraction could not occur as wear progressed from the above condition, a clearance between the polyimide ring and the rod resulted, accompanied by increasing leakage. Wear was measured as the change in polyimide ring cross section depth and is shown in figure 50 compared with new ring dimensions. This wear was accumulated under conditions averaging 2.0684×10^{7} N/m^2 (3000 psig) and 450° K (350° F) at the first-stage seal, with the rod traversing 3328 m (131 027 in.) across the seal. This wear resulted in a maximum material wear rate of 1.832×10^{-7} m/m (in./in.) travelled, which was 7.26 times the rate stated for the material in table III. A photograph comparing the new and worn seals in the 0.0635 m (2.5 in.) size ring is shown in figure 51.

A new second set of 50% balanced first-stage seals was installed in each actuator to continue cycle testing. After completing 158 000 additional cycles (572 892 total cycles) excessive leakage was evidenced at the interstage of the 0.0635 m (2.5 in.) actuator. Similarly, after 455 923 cycles with the new set (892 681 total cycles) excessive leakage was evidenced at the interstage of the 0.0254 m (1.0 in.) actuator. Disassembly inspection showed that the seals from both actuators had excessive wear at localized spots on the inner circumference that contacted the rod. These wear positions are shown in the photographs in figure 52.

The wear evidenced with the second set of seals did not duplicate the results with the first set. A possible explanation is that wear occurred in both cases at localized positions but was not evidenced with the first set because the wear at a single location was not to a sufficient depth to produce excessive leakage before wear progressed at other locations.

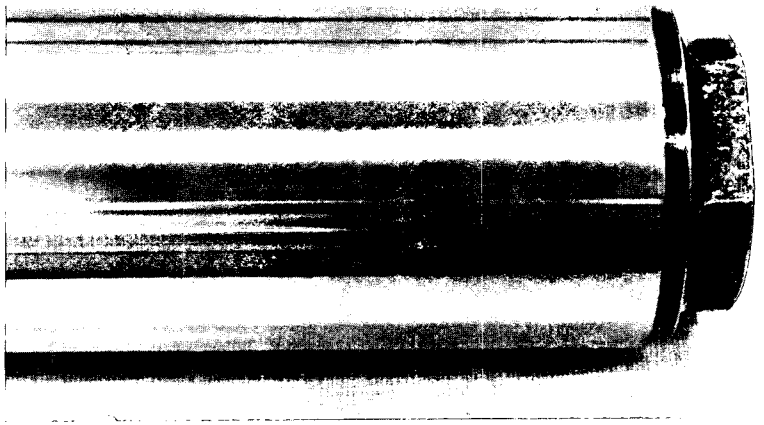

Initial condition

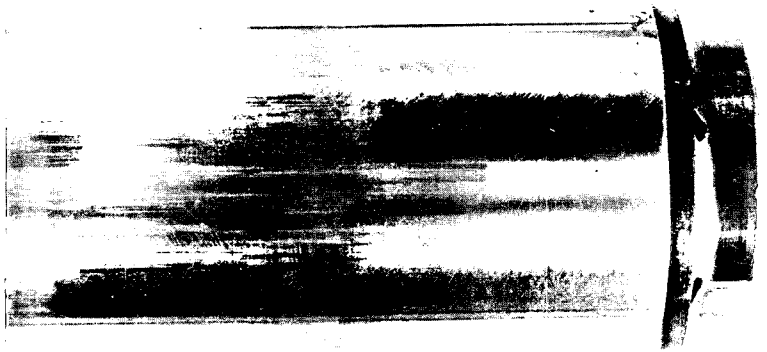

Condition at test completion

0.0254m (1.0 in.) endurance actuator rod wear

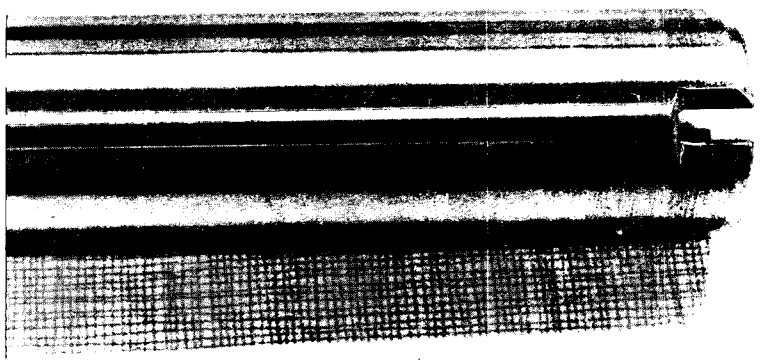

Initial condition

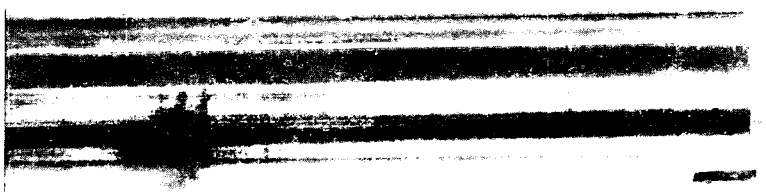

Condition at test completion

0.0635 m (2.5 in.) endurance actuator rod wear

Figure 49.—Endurance test, actuator rod wear

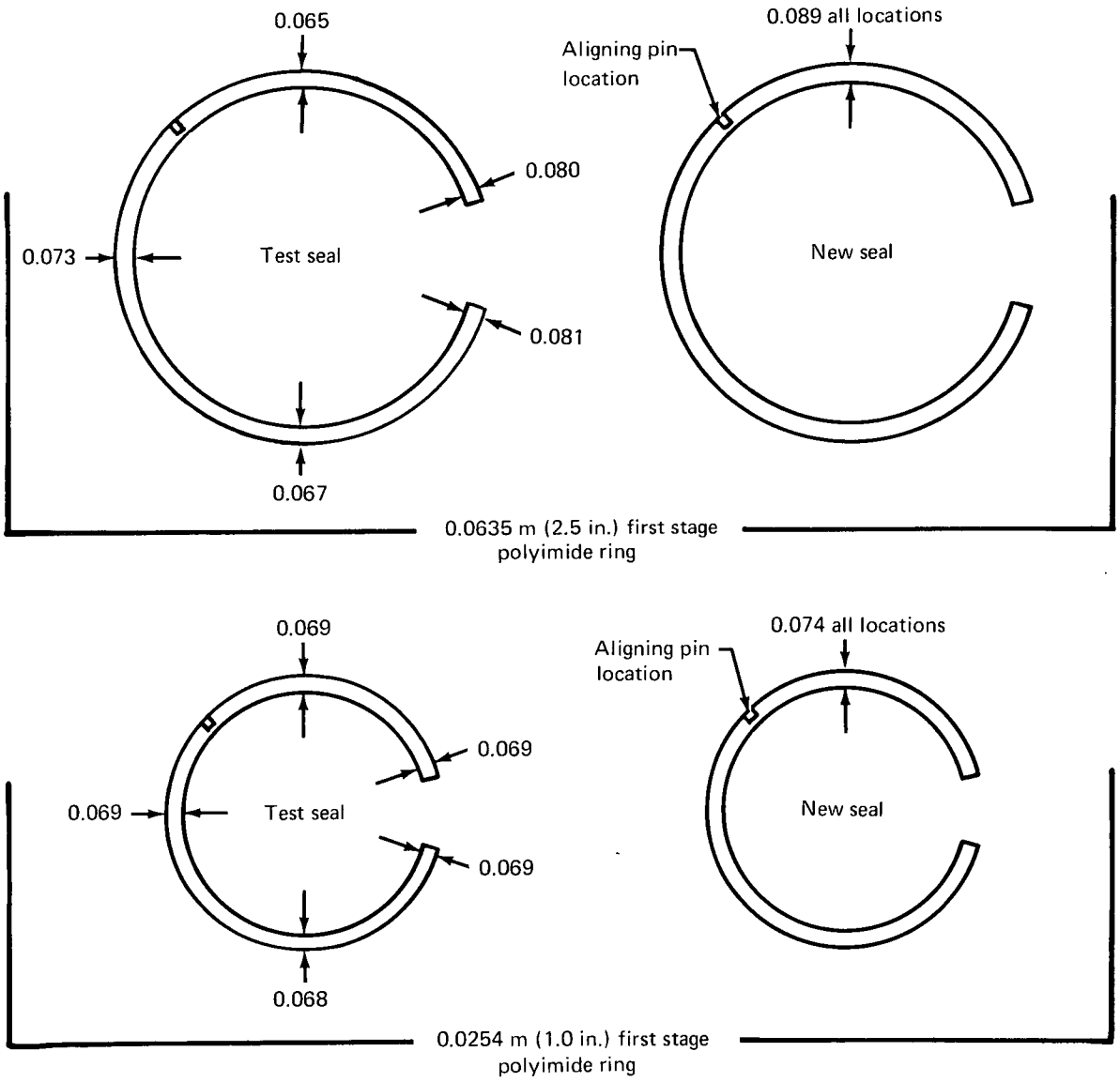

Note: All thickness dimensions are given in inches: No SI conversion was made on dimensioned parts (see appendix 9)

Figure 50.—Wear: First set of first-stage endurance seals

Figure 51.—0.0635m (2.5 in.) first-stage seal wear

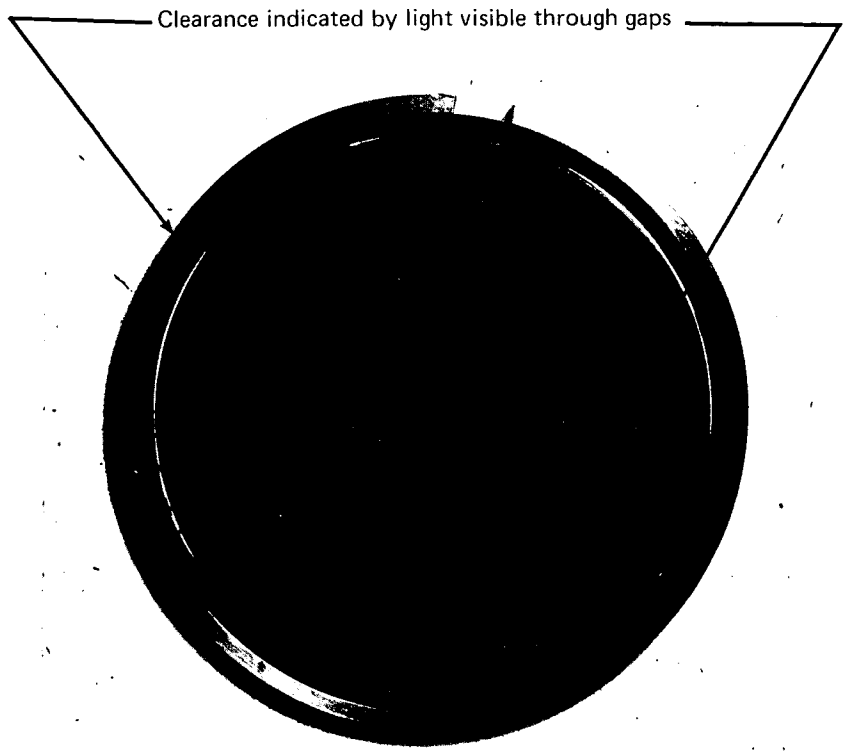

0.0635 m (2.5 in) first stage

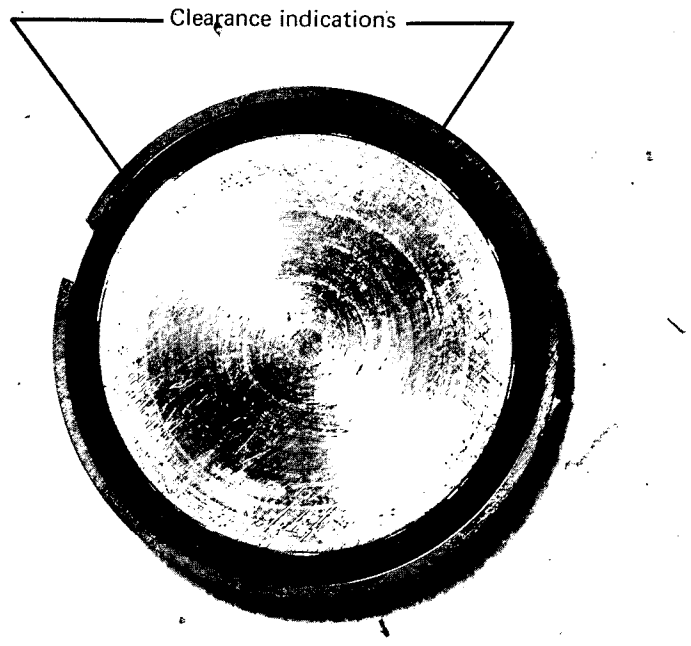

0.0254 m (1.0 in) first stage

Figure 52.—Wear: Second set of first stage endurance seals

Because of such action the first seal removed appeared to exhibit more even wear. It is suggested that wear developing in this manner is a random instance and that a conservative design approach would be to expect wear as was evidenced with the second set of seals.

Second-Stage Results

Cyclic testing, in the endurance rig, subsequent to first-stage failures, was continued to the extent allowable by contract schedule and funding. Cast iron first-stage rod seals, of the configuration shown in appendix 1, were used to perform the sealing function of the first stage but were not considered to be under test. The second-stage seals originally installed for endurance testing were retained and monitored for performance. At the completion of testing the second-stage seals had completed the cycling indicated in table XI.

The results shown indicate that a 42% life test was completed for the K-section 0.0635 m (2.5 in.) seal and a 38% life test for the chevron 0.0254 m (1.0 in.) seal. The average leakages obtained during testing were all within the allowable of 10^{-7} m^3 per 25 cycles (2 drops/25 cycles) except during 100% stroking with the smaller actuator. The leakage during this 100% stroking condition should not, however, be considered by itself since a typical flight profile contains only a small portion of 100% strokes. The overall mean for leakage during the entire endurance test approaches the short-stroke leakage with very little error. Posttest inspection of the second-stage seals from both actuators showed no abnormal wear patterns, no evidence of cracking, and polished contact areas as expected on the inside and outside diameter faces.

SUMMARY DISCUSSION OF TEST RESULTS

First-Stage Seals

The satisfactory completion of impulse testing of the first-stage seals showed that the step-cut cross-section was not overstressed in the dynamic impulse environment. The friction testing of the first-stage seals indicated that, within qualified restriction, balancing effectively reduced friction. The qualification for the use of 70% axial balancing was the concern that, though friction level was reduced, seal lifting occurred unpredictably, resulting in excessive and uncontrollable leakage. Further evaluation of a correction for these occurrences was not within the scope of the contracted work. It was believed, however, that a 70% axially balanced seal with a proper percentage of radial balancing might provide a more acceptable seal configuration.

A second qualification in the relationship between balancing and friction level was related to seal size. The larger (0.0635 m) seal showed that increased balancing percentage resulted in lower friction levels while the smaller (0.0254 m) seal showed the reverse. Analyses performed to evaluate these results indicated a possibility of seal distortions

Table XI. Endurance test results, external leakage

Seal Configuration	Cycles completed		Cycles accumulated per $5 \times 10^{-8} m^3$ (1 drop) of seal leakage (Acceptable operation was a minimum of 12.5 cycles/drop)							
			2% stroke		25% stroke		50% stroke		100% stroke	
	Short stroke (2%)	Long stroke (≥25%)	Avg	Min	Avg	Min	Avg	Min	Avg	Min
0.0635m (2.5 in.) K-section	3,149,871	60,155	75	17.5	37.5	30	22.5	10	20	15
0.0254m (1.0 in.) Chevron	2,844,071	60,000	300	33	94	19	90	18	8.5	6.7

Nominal differential pressure across second-stage seal was 1.379×10^6 N/m^2 (200 psig)

causing a redistribution of pressure areas. These analyses indicated that it is desirable to perform an analysis of a first-stage balancing design prior to fabricating the seal. Such an analysis would assess the conditions of optimum balancing, since it is not necessarily true that higher balancing percentage provides a preferable design for reduced leakage and friction. An analysis tool with these features is described in appendix 6.

The excessive wear of the polyimide first-stage rings during endurance testing was unexpected. A second test to verify the high wear rate confirmed that SP-1 polyimide material wear accelerates at pressures above 2.0864×10^7 N/m^2 (3000 psig) when at elevated temperatures. Tests performed under the NAS 3-11170 contract (ref. 2), indicate acceptable performance at 2.0864×10^7 N/m^2 (3000 psig). These results would indicate a need for further evaluation by the material manufacturer of the wear characteristics of the material as a function of both higher pressures and temperatures. With such data, the design of polyimide seals could be based on less risky property information and would undoubtedly show better performance.

Second-Stage Results

The impulse testing of second-stage seals was completed successfully, as evidenced by leakage rates being well within the requirement allowables. Cracking of the polyimide material during impulsing was attributed primarily to material notch sensitivity, as illustrated in microphotos taken during posttest inspections (see figs. 41 and 42). There was some evidence that the modes of flexing of the sealing legs for both the chevron and K-section seals were not as anticipated. The unnatural flexing could have contributed to additional stresses.

The design of the seal leg provided stress distribution in proportion to the variation in cross-sectional area of the tapered legs, assuming that local stresses were neglected. These distributed stresses were at the upper margin of the fatigue allowable for the SP-21 material, as nearly as could be determined. Thus, the addition of local stresses due to machining scratches (notch sensitivity), or stresses resulting from inaccurate prediction of leg bending, would possibly result in cracking of the material. The cracking only occurred because there was a small tolerance margin between the design distribution stress and the fracture allowable under fatigue impulse cycling. This condition was further complicated due to a lack of material data on polyimide fatigue, making it difficult to establish a safe level for maximum allowable stress.

The fact that cracks occurred during impulse did not negate the successful completion of the test because the structural integrity of the total seal was not weakened. The impulse test accumulated 200 000 cycles of the most severe environment expected in the life of the seal. As such, this was a much more severe test than the seal would experience in actual service, where maximum impulse cycles would be accumulated in random sequence and

only during environmental conditions involving a few aircraft in a total fleet. The fact that the seals continued to provide fluid containment in this severe environment is sufficient proof of their structural integrity.

The second-stage seal friction test results indicated friction levels near twice those projected as an objective for design. These friction values obtained in test were not predictable based on manufacturers' information. The test data show that the friction coefficient for SP-21 changes substantially with temperature and load and could also indicate that the friction coefficient for a polyimide-on-chrome combination varies significantly with temperature. A further consideration for higher-than-anticipated friction is the fact that under increasing pressure, more complete contact between the uneven seal and rod surfaces is obtained, resulting in higher friction.

The endurance test operation was not conducted to second-stage failure. Thus, the fatigue limitation in cycling, or quantitative data relating wear to leakage, could not be provided. Posttest inspection showed no evidence of material cracking or unusual wear patterns, indicating that fatigue life had not been reached. The polished areas on the inside and outside diameters were as expected for these seal designs, indicating that under normal second-stage pressure loading there was no distorted flexing of the seal legs as experienced during the impulse tests. The average leakages measured during testing were well within the allowables set as seal requirements but did not approach zero. Though the zero leakage was mentioned as a theoretical goal it was not considered a practical objective. To attempt reduction of the external leakage obtained in test it will be necessary to use smoother finishes on both the rods and seals, which will increase cost. The practical limit of the improvement that might be expected by this modification has not been determined.

VI. CONCLUSIONS AND RECOMMENDATIONS

The three primary objectives of the reported effort were to:

- Determine second-stage chevron and K-section polyimide seal optimum geometry with a goal of not exceeding MIL G-5514F (ref. 16) gland dimensions and high-performance aircraft requirements
- Evaluate pressure balancing of polyimide first-stage seals
- Develop a modular retainer for a two-stage seal to allow unit installation in a linear actuator

These objectives were all satisfactorily completed, with the following conclusions.

CONCLUSIONS

–On Second-Stage Seals

- Seal size reduction to MIL G-5514F gland depths precluded the use of springs to provide seal leg expansion to fill the gland at design temperature extremes, necessitating design to higher stress conditions.

- The seal dimension having the highest impact on stress optimization was the leg cross-section thickness.

- Chevron seal geometry was optimized for severe fatigue requirements by compromise design between pressure stresses and preset interference stresses.

- The K-section seal design was more critical than the chevron due to less flexibility in the sealing element legs.

- A polyimide material with a balanced combination of high ultimate stress allowables and low coefficient of thermal expansion was preferred rather than one with superior characteristics in one or the other of the above properties.

- The life capabilities of the second-stage seals were not fully evaluated because fatigue failures were not encountered and testing was limited to less than the fatigue design life of the seals.

–On First-Stage Seals

- Axial balancing of 70% was shown to be in near proximity to the condition of a neutrally balanced seal in the radial direction. Without the addition of radial balancing, erratic leakage as experienced in test will be encountered.

- The critical stressed step-cut section in the polyimide sealing ring of the two-piece contracting seal was proven adequate by satisfying impulse requirements during test.

- An antirotation pin was proven mandatory between the concentric sealing ring and compression ring of the two-piece contracting seal. This pin prevents co-rotation which, if allowed to occur, can result in uncontrolled leakage, as evidenced during test.

- A design analysis is needed, prior to seal fabrication, which includes the effects of coefficient of friction and contact pressure variations and distribution. These quantifications have not been accomplished and present practice in analysis only considers the force variation as a function of area.

- The excessive wear data collected during testing was not considered sufficient to conclude that polyimides are not useable at 2.758×10^7 N/m^2(4000 psig). These data should be used to update manufacturers' design data for polyimide applications at high pressure and applied to future seal designs.

—On the Modular Retainer

- A modular retainer was satisfactorily designed, fabricated, and tested to demonstrate unit installation of a complete two-stage seal in a linear actuator. For new aircraft design the modular approach incorporating the gland bearing, two-stage rod seals, and required static seals has definite advantages in both reliability and maintainability. In specific cases a module excluding the gland bearing may also have aircraft application.

RECOMMENDATIONS

Continued research is recommended to complete the assessment of the practical use of polyimide seals in aircraft actuator applications. Efforts toward the following recommendations are specifically encouraged.

- Complete the endurance validation of the chevron and K-section second-stage seals to their design requirements, by testing these seals to failure. This testing will provide results quantifying the design analysis tool and provide data to update the tool for any design conservatism, making it dependable for future use.

- Develop polyimide material property data for fatigue allowables at other than zero-mean stress, for wear at pressures of 2.758×10^7 N/m^2 (4000 psig) and greater, and for the relationship between friction coefficient and contact pressure for a family of temperature and lubrication conditions. This information is needed for any design work with polyimides. It is directly applicable to rod seal design of both first and second stages using the tools developed in this program.

- Extend the development testing of polyimide first-stage seals designed to incorporate updated material property information. These tests will determine whether seals, designed for a known wear characteristic at high pressure, actually perform in the manner designed. This testing contrasts the program being reported where the wear characteristic of SP-1 material at 2.758×10^7N/m^2 (4000 psig) was not known.

- Determine limitations for the practical use of polyimide rod seals at higher temperatures. The advantages of polyimides as rod seals are realized at high temperature where other less costly seals are not adequate. The fatigue limits for these seals in a type III hydraulic system (219° K, -65° F to 505° K, 450° F) are currently important since there is immediate potential for application in this environment.

- Complete and document the design tools for both first- and second-stage rod seals for which initial development was conducted in the reported program. The completion of these tools would relieve the costly design development and validation testing required to date to establish the primary parameters and dimensions for each individual seal with merit for an application.

APPENDIX 1

BOEING STANDARD, SEAL ASSEMBLY, ROD, METALLIC

Figure 53 shows the specification data for the Boeing seal used as a pattern for the contract first-stage seals.

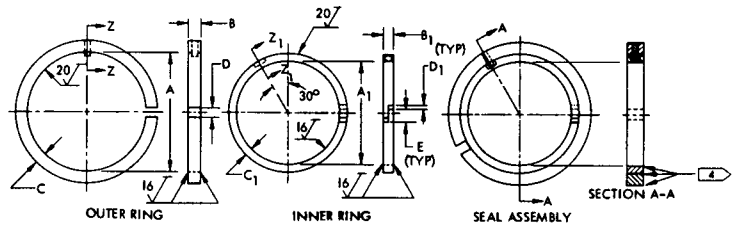

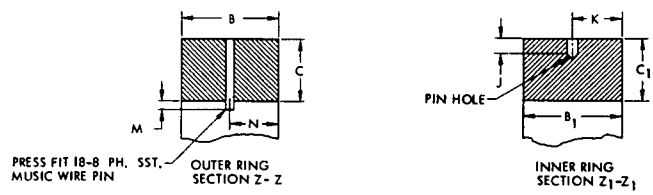

TOLERANCES: ±.005 UNLESS OTHERWISE SPECIFIED

BOEING STD. NO. BACS11AM	KOPPERS PART NUMBER	OUTER RING A	OUTER RING B ±.0005	OUTER RING C	OUTER RING D TOL	INNER RING A_1	INNER RING B_1 ±.0005	INNER RING C_1	INNER RING D_1 TOL	E +.030 -.000	J +.005 -.000	K	M	N ±.001	PIN DIA	PIN HOLE	D
112	56695	.538		.023-.027	.115	.496		.019-.023									.047-.077
113	56698	.600		.023-.027	.115	.558		.019-.023									.047-.077
114	56701	.667		.025-.029	.115 -.000	.621		.021-.025	.020 +.005 -.000	.074							.047-.077
115	56704	.729		.025-.029	.115 +.020	.683		.021-.025					NO PIN				.047-.077
116	56707	.792		.027-.031	.125	.746		.021-.025									.052-.082
211	56710	.854		.027-.031	.125	.808		.021-.025									.052-.082
212	56713	.917		.028-.032	.135	.871	.0610	.028-.033									.060-.090
213	56716	.979	.0620	.028-.032	.135	.933		.028-.033									.060-.090
214	56719	1.041		.030-.035	.135	.996		.028-.033									.060-.090
216	56722	1.172		.035-.040	.150	1.121		.028-.033		.105	.013		.009 .012				.062-.102
218	56725	1.303		.040-.045	.170	1.246		.028-.033	.035			.0295 .0325		.031	.015	.025	.072-.112
220	56728	1.434		.045-.050	.185	1.371		.029-.034									.080-.120
222	56731	1.565		.048-.053	.200	1.496		.032-.037									.087-.127
326	56734	1.698		.053-.058	.220	1.621		.036-.041									.092-.142
327	56737	1.829		.057-.062	.240	1.746		.039-.044	.040	.136							.102-.152
328	56740	1.955		.057-.067	.255	1.871		.041-.047	+.015 .000				.012				.110-.160
329	56743	2.080		.057-.067	.255	1.996		.041-.047			.018		.017				.110-.160
330	56746	2.217		.067-.077	.295	2.121		.043-.053				.0445 .0475		.046	.020	.035	.130-.180
331	56749	2.342	.0920	.067-.077	.295	2.246	.0910	.043-.053	.050								.130-.180
332	56752	2.479		.074-.084	.320	2.371		.049-.059									.142-.192
333	56755	2.614		.078-.088	.320 -.000	2.496		.054-.064		.167							.142-.192
334	56758	2.741		.084-.094	.360 +.030	2.621		.055-.065									.157-.217
335	56761	2.874		.088-.098	.375	2.746		.059-.069	.055								.165-.225
336	56764	2.999		.088-.098	.375	2.871		.059-.069									.165-.225
337	56767	3.135		.097-.107	.415	2.995		.065-.075									.185-.245
338	56770	3.260		.097-.107	.415	3.120		.065-.075					.015				.180-.250
339	56773	3.397		.106-.116	.450	3.245		.071-.081			.022		.020		.025	.040	.197-.267
340	56776	3.522		.106-.116	.450	3.370		.071-.081									.197-.267
341	56779	3.659		.115-.125	.485	3.495		.077-.087									.215-.285
342	56782	3.784	.1235	.115-.125	.485	3.620	.1225	.077-.087									.215-.285
343	56785	3.923		.123-.133	.520	3.745		.084-.094				.0600 .0630		.0615			.232-.302
344	56788	4.048		.123-.133	.520	3.870		.084-.094									.232-.302
345	56791	4.185		.133-.143	.560	3.995		.090-.100									.242-.332
347	56794	4.447		.141-.151	.590	4.245		.096-.106									.257-.347
349	56797	4.709		.150-.160	.625	4.495		.102-.112	.060								.275-.365
427	56800	4.972		.159-.169	.660	4.744		.109-.119			.037		.030 .035				.277-.397
429	56803	5.234		.168-.178	.710	4.994		.115-.125	+.030 -.000	.220					.030	.052	.302-.422
431	56806	5.484		.168-.178	.710	5.244		.115-.125									.302-.422
433	56809	5.748		.181-.191	.765 -.000	5.494		.122-.132									.332-.452
435	56812	5.998		.181-.191	.765 +.040	5.744		.122-.132									.332-.452

DATE 18 MAR 70 REV.

1 -- 2 --
LIST OF ACTIVE SHEETS

CODE IDENT NO. 81205

BAC S11AM SH 1 OF 2

SEAL ASSEMBLY, ROD, METALLIC

BAC S11AM SH 1 OF 2

BOEING STANDARD

PAGE 60.15.6.8.1

PAGE 60.15.6.8.1

Figure 53.—(continued on page 106)

(1) END CLEARANCE OF EACH RING TO BE MEASURED IN A GUAGE OF "A_1" ±.0005 DIAMETER.

(2) END CLEARANCE OF EACH RING TO BE MEASURED IN A GUAGE OF "A" ±.0005 DIAMETER.

(3) TENSION CONTROLLED BY OUTER RING GAP, RING IN FREE STATE.

(4) I.D. EDGES OF INNER RING MAY HAVE A RADIUS OF .003 MAX FOR SIZES THROUGH BACS11AM345. SIZES LARGER THAN 345 MAY HAVE A RADIUS OF .005 MAX. O.D. EDGES OF OUTER RING MAY HAVE A RADIUS OF .015 MAX. INNER RING O.D. AND OUTER RING I.D. EDGES SHALL BE SHARP. ALL EDGES SHALL BE FREE OF BURRS.

MATERIAL: INNER: KOPPERS K-6E, ALLOY GREY IRON PER AMS 7310 EXCEPT CHROMIUM AND MOLYBDENUM ALLOYING ELEMENTS ADDED.
OUTER: 17-4PH CRES PER AMS 5643 OR AMS 5398, HARDNESS - R_c30-40.
PIN: 18-8 CRES PER AMS 5688.

FINISH: INNER RING ONLY. PARCO LUBRITE NUMBER 2 PER BAC5810, CLASS 1. THE RING SHALL THEN BE IMMEDIATELY IMMERSED IN HYDRAULIC FLUID WHICH MEETS THE REQUIREMENTS OF BMS3-10 AND PACKAGED WHILE DRIPPING WET WITH FLUID.

SURFACE ROUGHNESS: 63 RHR PER USAS B46.1 UNLESS OTHERWISE SPECIFIED. ROUGHNESS TO BE MEASURED PRIOR TO PARCO LUBRITE TREATMENT.

MARKING: EACH PACKAGE SHALL BE MARKED WITH THE SUPPLIER'S NAME, TRADEMARK OR CODE NUMBER, THE SUPPLIER'S PART NUMBER, AND THE BOEING STANDARD NUMBER.

CLEANING: PER KOPPERS COMPANY SPECIFICATION E-3803 TITLED "CLEANING AND PACKAGING PARTS TO BE USED IN PRECISION SEAL APPLICATIONS." CHLORINATED SOLVENT SHALL NOT BE USED IN THE CLEANING PROCESS.

PACKAGING: RING SETS CONSISTING OF AN OUTER AND INNER RING IN MATCHED SETS SHALL BE INDIVIDUALLY PACKAGED IN A HEAT SEALED POLYETHYLENE BAG. THE BAG SHALL THEN BE PLACED IN RIGID OR SEMI-RIGID BOXES.

INSPECTION: 100% INSPECTION BY THE MANUFACTURER. ASSEMBLY TO BE 100% LIGHT TIGHT BETWEEN INNER RING AND GAGE IN A GAGE OF "A_1" ±.0005 DIAMETER, AND 100% LIGHT TIGHT BETWEEN INNER AND OUTER RINGS FOR A DISTANCE EXTENDING 20° EITHER SIDE OF INNER RING STEP JOINT. LIGHT WHICH CAN BE PRESSED OUT WITH A RADIAL FORCE NOT EXCEEDING 5 LBS/INCH OF RING DIAMETER SHALL NOT BE CAUSE FOR REJECTION. EACH ASSEMBLY SHALL BE INSTALLED IN A TEST FIXTURE WITH A ROD FINISH OF 8 RHR AND A DIAMETER EQUAL TO THE MINIMUM ALLOWABLE PER MIL-G-5514, TABLE I, COLUMN "B". THE FOLLOWING TESTS SHALL BE CONDUCTED: MAXIMUM STATIC LEAKAGE USING MIL-F-7024, TYPE II AT ROOM TEMPERATURE AT 750 AND 4000 PSI SHALL NOT EXCEED 10 CC/MIN UP TO 2.500 INCH ROD DIAMETER, 25 CC/MINUTE FOR RODS 2.501 TO 5.000 INCH AND 50 CC/MINUTE FOR RODS OVER 5.000 INCH DIAMETER.

PROCUREMENT: KOPPERS COMPANY INCORPORATED, METAL PRODUCTS DIVISION, BUSH AND HAMBURG, BALTIMORE, MARYLAND 21203 (CODE IDENT NO. 75370)

THE SUPPLIERS LISTED AND THEIR AUTHORIZED DISTRIBUTORS ARE THE ONLY APPROVED SOURCES FOR THE ABOVE QUALIFIED PRODUCTS. CHANGES IN PRODUCT DESIGN OR QUALITY WITHOUT PRIOR BOEING APPROVAL MAY RESULT IN SUPPLIER DISQUALIFICATION. SUPPLIERS OF COMPETITIVE PRODUCTS MAY APPLY TO A MATERIEL DEPARTMENT OF THE BOEING COMPANY FOR QUALIFICATION.

USAGE AND APPLICATION INFORMATION

THESE SEAL RINGS ARE INTENDED AS ROD SEAL RINGS IN HYDRAULIC ACTUATORS WITH FLUID PER BMS 3-10 AT OPERATING TEMPERATURES OF 350° WITH EXCURSIONS TO 500°F. THESE SEALS TO BE USED WITH GROOVES PER BACD2040. THESE SEALS ARE NOT INTENDED FOR ZERO LEAKAGE APPLICATIONS.

DATE 18 MAR 70 REV.

SEE PREFACE FOR GENERAL USAGE NOTES.

CODE IDENT NO. 81205

BAC S11AM SH 2

SEAL ASSEMBLY, ROD, METALLIC

BAC S11AM SH 2

BOEING STANDARD

PAGE 60.15.6.8.2

Figure 53.—(continued)

APPENDIX 2

PRELIMINARY SECOND-STAGE STRESS ANALYSES

Seal dimension optimization was accomplished using stress analysis computer techniques embodied in the Boeing SAMECS program, reference 15. The problem was initially coded to evaluate the following conditions.

- Use of DuPont Vespel SP-21 material.
- Seal ID = 0.0254 m (1.0 in.)
- Seal section thickness (t) = 4.064×10^{-4} and 5.080×10^{-4} m (0.016 and 0.020 in.).
- Radial interference at the ID (δ) = 1.524×10^{-4} and 3.048×10^{-4} m (0.006 and 0.012 in.).
- Both one- and two-piece mechanical load blocks.

ROUGH DESIGN ANALYSIS

Figure 54 shows the seal idealization for SAMECS computer simulation. The cross section of each of the 0.5236 rad (30°) V chevrons were divided into nodes designated by X—. Beams were used to connect nodes between chevrons at positions where two chevrons were in contact with each other. These beams allowed limited sliding motion of one seal on the other, but not seal separation.

The initial computer program evaluation used the variations in the force and compression interference parameters as listed in table XII to solve the following design cases:

- Cases 1 to 8: A condition where there was no leakage by the first-stage seal. The normal force of the seal on the rod was determined for each case and compared with the hand calculation result of 1.891×10^3 N/m (10.8 lb/in.).
- Cases 9 to 16: Simulate a seal where leakage under 1.379×10^6 N/m^2 (200 psig) pressure passed the primary seal. The maximum stresses were determined for these cases and compared against 1.034×10^7 N/m^2 (1.500 ksi) tension and 2.137×10^7 N/m^2 (3.100 ksi) static compression allowables with the use of Vespel SP-21 material.
- Validation: Simulate the most satisfactory seal design using the minimum normal force determined above the 1.891×10^3 N/m (10.8 lb/in.) requirement and within the maximum stress level allowables.

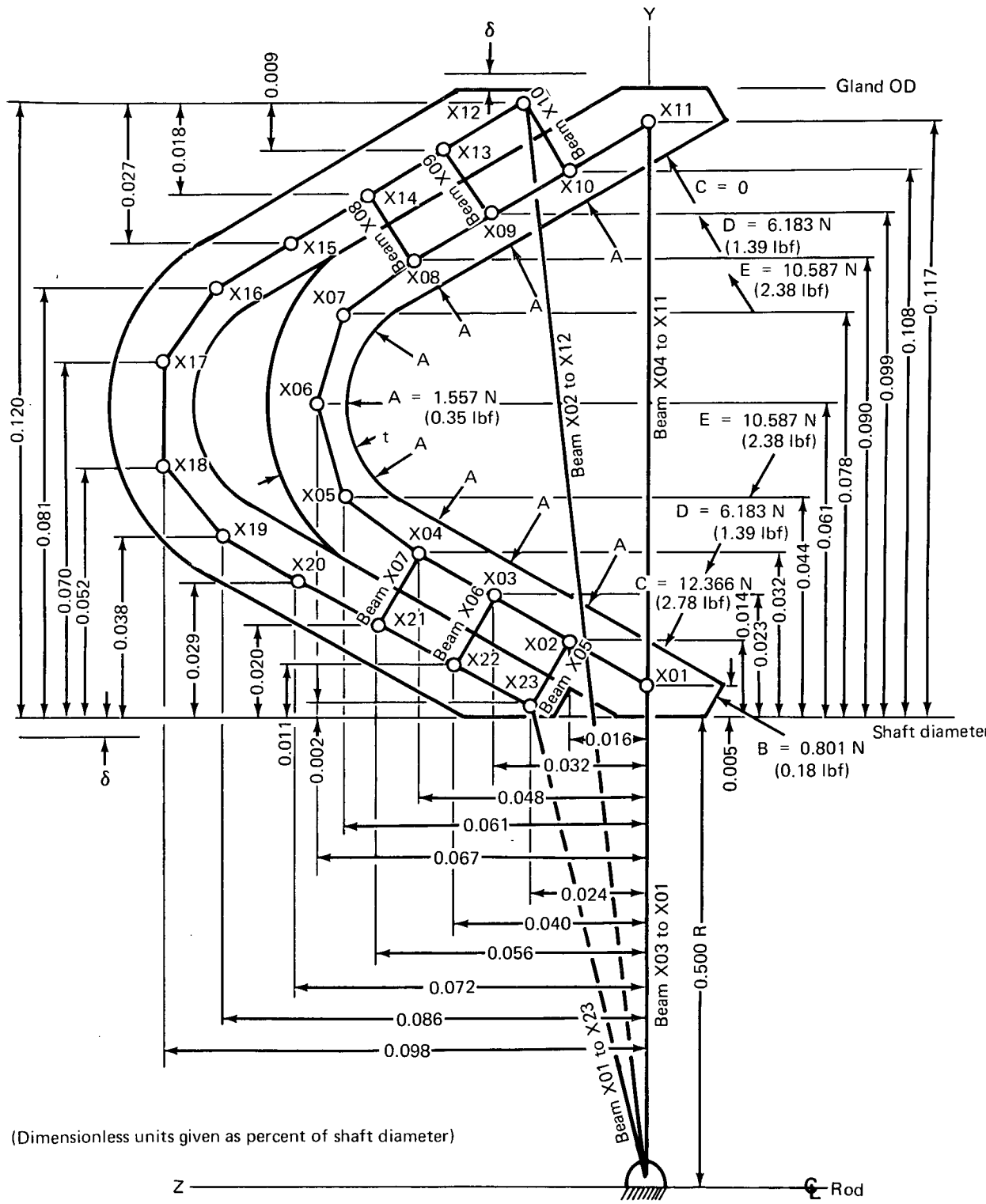

Figure 54.—Seal idealization

Table XII.—Computer evaluation parameters

		δ		t		
Case no.	Loading	m x 10^{-4}	in.	m x 10^{-4}	in.	Forces applicable
1	Split-block	1.524	0.006	4.064	0.016	C
2				5.080	0.020	C
3	Single-block			4.064	0.016	D
4				5.080	0.020	D
5	Split block	3.048	0.012	4.064	0.016	C
6				5.080	0.020	C
7	Single-block			4.064	0.016	D
8				5.080	0.020	D
9	Split-block	1.524	0.006	4.064	0.016	A B C E
10				5.080	0.020	A B C E
11	Single-block			4.064	0.016	A B D E
12				5.080	0.020	A B D E
13	Split block	2.048	0.012	4.064	0.016	A B C E
14				5.080	0.020	A B C E
15	Single-block			4.064	0.016	A B D E
16				5.080	0.020	A B D E

δ = compression of seal from its free shape

t = thickness of seal leg

A = hydraulic pressure load applied to the chevron

B = hydraulic lifting load due to leakage pressure

C = load produced by the spring-loaded split-block loading ring

D = load produced by a single-block loading ring

E = hydraulic load on the loading ring that is transferred to the chevron

The stress analyses performed indicated the degree of severity of the stresses expected in the chevron seal designed for SST applications and having similar geometry to the reference 2, B-1 seal. Figure 55 shows stresses in a two-chevron second-stage seal configuration on a 0.0254 m (1.0 in.) diameter rod with an interstage pressure of 1.379×10^6 N/m^2 (200 psig). The seal was considered to rest in its free shape as it occupied a Military specification (ref. 16) standard depth gland and was able to move in the gland without resistance in the direction indicated by the rollers at the fixity points. The dashed line near the upstream element represents the deformed shape of the element under the loads stated. Maximum pressure stresses produced are shown for the inner fiber (pressure side) and outer fiber (atmospheric side) of each chevron.

Figure 56 shows stresses in the same seal configuration with a total interference deflection of 2.032×10^{-4} m (0.008 in.) compression from free state. The compression was equally distributed with 1.016×10^{-4} m (0.004 in.) on both ID and OD of the seal. Maximum stresses produced are shown on the diagram for the inner fiber (pressure side) and outer fiber (atmospheric side) of each chevron. The seal had no hydraulic pressure applied to the interstage cavity and was allowed to move freely in the gland, as shown by the rollers at the points of fixity. The maximum stress levels obtained in the plates due to pressure loading, figure 55, are additive to the static deflection stresses shown in figure 56, this sum providing the majority of the stress load for the static seal condition. The total stress showed the outer fiber of the inner seal was critical for the plates nearest the apex (plates 2037 and 2046). Total bending stress at these plates was approximately 5.447×10^7 N/m^2 (7.900 ksi). Considerations of the properties of Vespel SP-21 used in the chevron seal configuration indicated that a reasonable ultimate allowable stress would be 4.137×10^7 N/m^2 (6.000 ksi). The computer idealization indicated 32% greater stress, this being too large a discrepancy to remain within the band of uncertainty for the idealization.

Figure 57 shows a plot of reversal load conditions resulting from 356 N (80 lbf) of friction between the seal ID and the actuator rod with 1.379×10^6 N/m^2 (200 psig) hydraulic pressure applied to the interstage cavity (refer to fig. 55). The plot is for the outer (atmospheric side) chevron seal only and shows stress vs the plate identification indicated at the top of the figure. Maximum alternating stress is shown as the difference between stresses, at the critical plate, for the two directions of actuator rod motion. Alternating stress was linear with friction.

The friction case described was typical but not optimized for the seal design application. The result of $\pm 3.082 \times 10^7$ N/m^2 ($\pm$4.470 ksi) was compared to an endurance limit of $\pm 6.895 \times 10^6$ to $\pm 1.034 \times 10^7$ N/m^2 ($\pm$1.000 to $\pm$1.500 ksi) allowable for the Vespel SP-21 material in a chevron seal configuration.

The conclusion reached was that geometry modifications to the seal cross section were required to reduce stresses to within the material allowables.

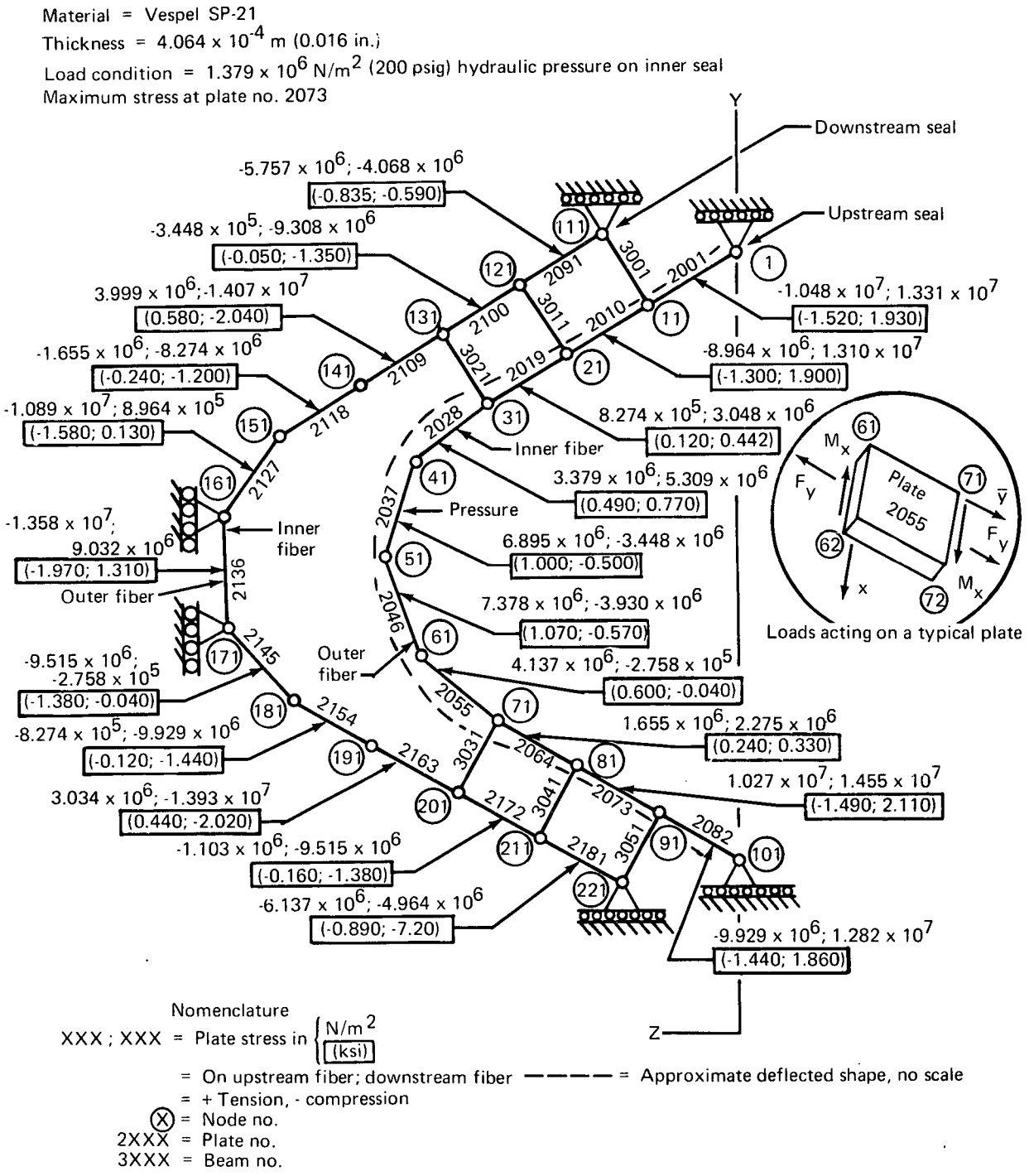

Figure 55.—Pressure stress loads: 0.524 rad (30°) Two-chevron V-seal SAMECS model

Material = Vespel SP-21
Thickness = 4.064×10^{-4}m (0.016 in.)
Load condition = 2.032×10^{-4}m (0.008 in.) interference fit
Maximum stress at plate no. 2037

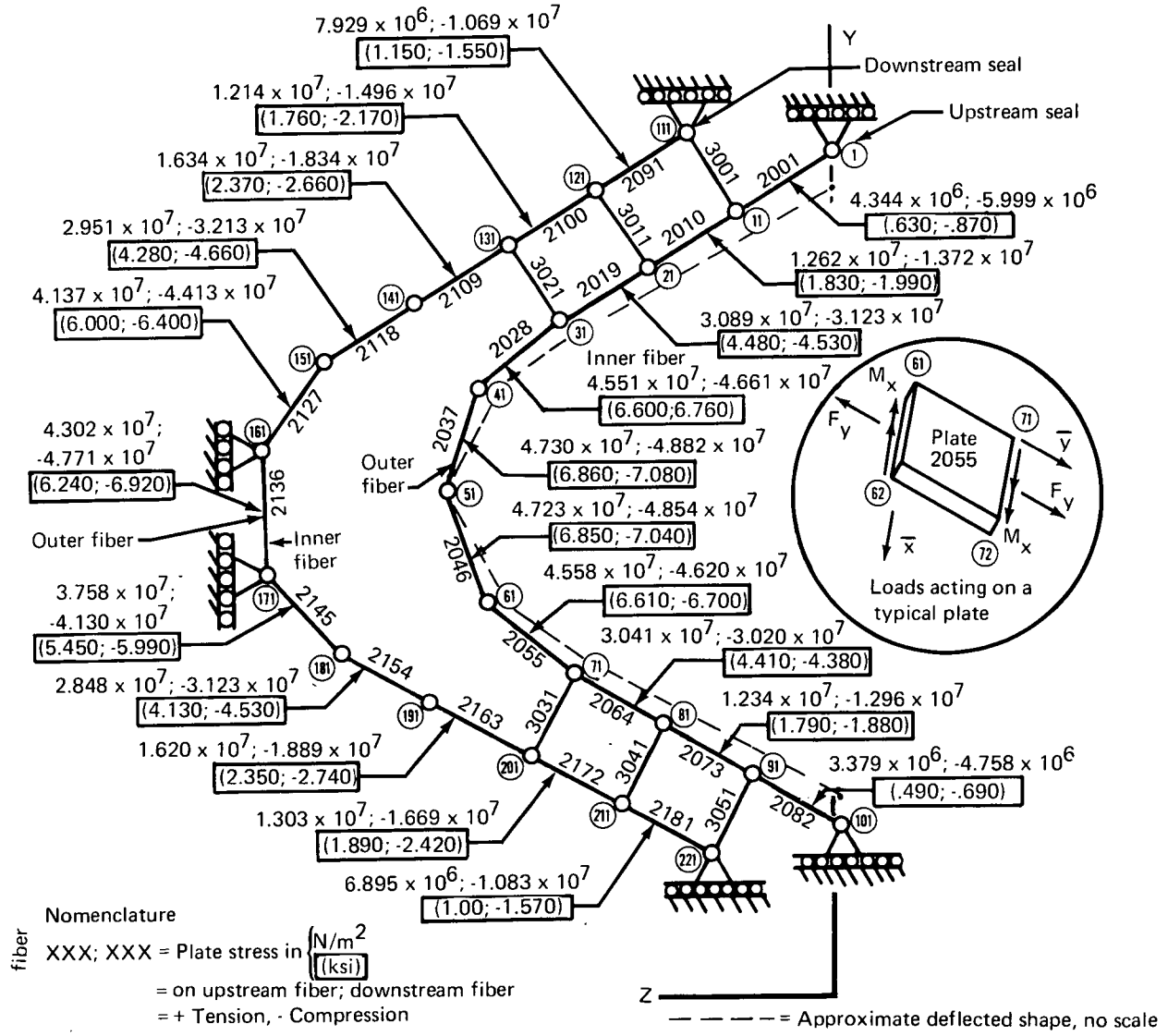

Figure 56.—Interference fit: 0.524 rad (30°) two-chevron V-seal SAMECS model

C.3

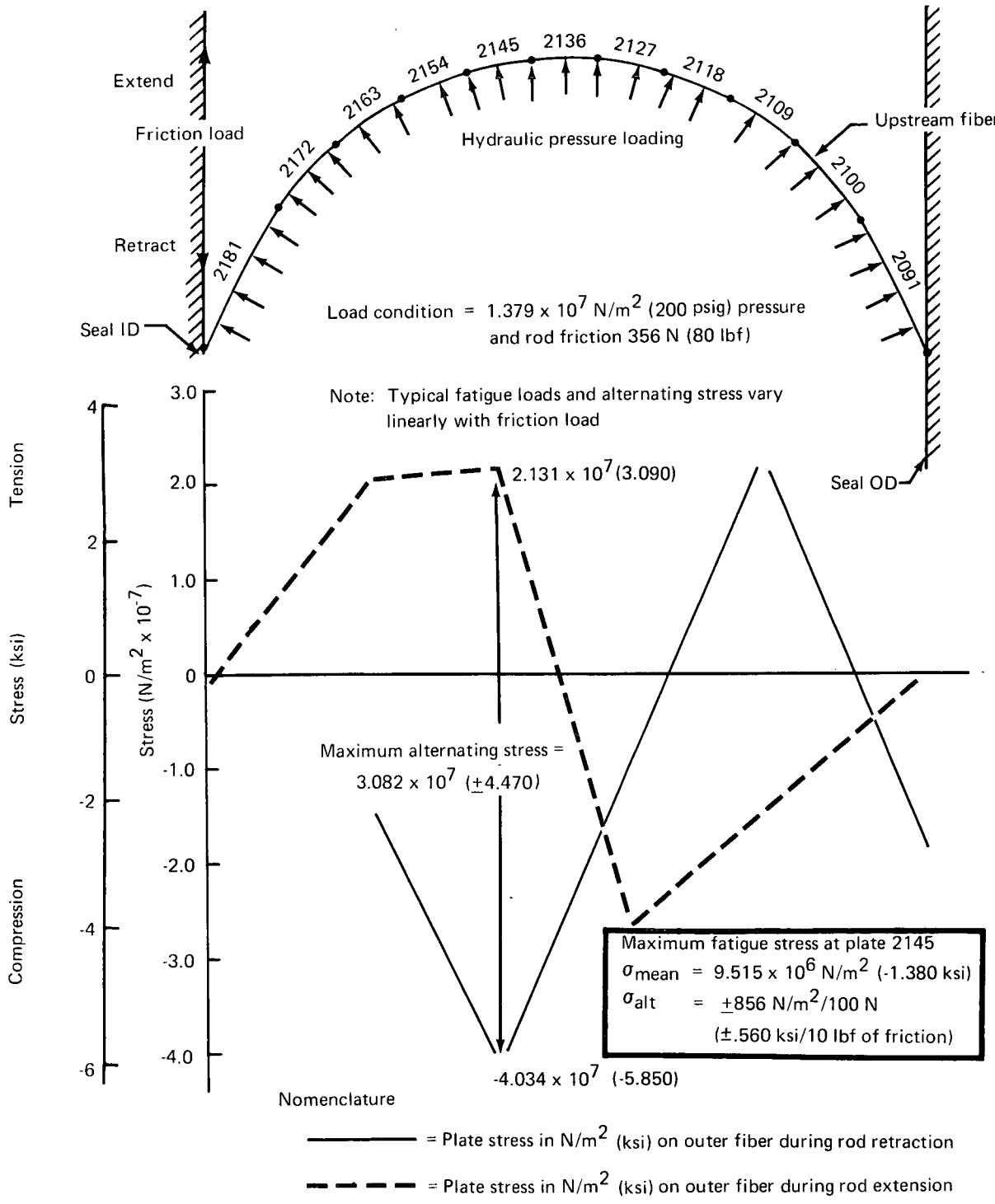

Figure 57.—Friction load: 0.524 rad (30°) downstream V-seal SAMECS model

ANALYSIS WITH HIGH COMPRESSION INTERFERENCE

Gland Depth Analysis

Figure 58 shows results of computer stress analyses for corresponding plate elements of both the upstream and downstream seals in the mathematical model. These plates are defined as numbers 2017 on the upstream seal and 2051 on the downstream seal, as described in figure 15. The data showed that gland depth did not affect material stress values nearly as much as did hydraulic pressure loading. The initial 2.286×10^{-4} m (0.009 in.) compression interference fit of the chevron seal in the gland, needed to ensure sealing at both high-and low-temperature extremes of 450° K and 228° K (+350° F and -50° F), respectively, imposed the stress values located on the abscissa of each curve. All stresses on plate 2017 of the upstream seal were in tension, and this condition produced the worst stress case for either chevron. The stresses on plate 2051 of the downstream seal were initially tension stresses which reduced and then crossed over to compressive stresses as hydraulic pressure loading was increased. Because this crossover existed, the critical stress of 4.137×10^7 N/m^2 (6.000 ksi) in the downstream seal was obtained at a much higher pressure loading than could be applied to the upstream seal to create the same stress. The critical maximum allowable pressure for the upstream chevron was 2.096×10^6 N/m^2 (304 psig) at plate 2017 for the maximum gland depth in the available test actuator. The maximum test actuator gland depth of 3.581×10^{-3} m (0.141 in.) was less than that stated as allowable in figure 10 for the large actuator rod, 0.0635 m (2.5 in.). This reduction was necessary to allow sufficient material thickness for the seal module installation.

Leg Thickness Analysis

Figure 59 shows the results of computer analysis to determine whether variations in chevron leg thickness would benefit designing for higher fluid pressures than the 2.096×10^6 N/m^2 (304 psig) limitation determined above. It was initially thought that increased thicknesses would provide the desired benefit. The data showed that, due to the nature of the slope of the curves and their intersection with the 4.137×10^7 N/m^2 (6.000 ksi) limiting stress level, the lesser thicknesses allowed higher pressure utilization. The curve for optimum thickness at plate 2017 was developed because this was the critical plate for seal stress design. The optimum leg thickness, i.e., the thickness allowing usage of the highest hydraulic pressure at a stress level of 4.137×10^7 N/m^2 (6.000 ksi), was 4.394×10^{-4} m (0.0173 in.) allowing use of 2.137×10^6 N/m^2 (310 psig) hydraulic pressure. It was easily concluded from this result that leg thickness variation from the reference 2 seal dimensional proportions provided only slight benefit toward use of greater hydraulic pressures.

Leg Angle Analysis

Figure 60 shows the results of stress analysis of a seal with optimum chevron leg thickness, installed in the maximum size test actuator gland with three variations of chevron leg angle: 0.698 rad (40°), 0.524 rad (30°), and 0.344 rad (20°). The data showed

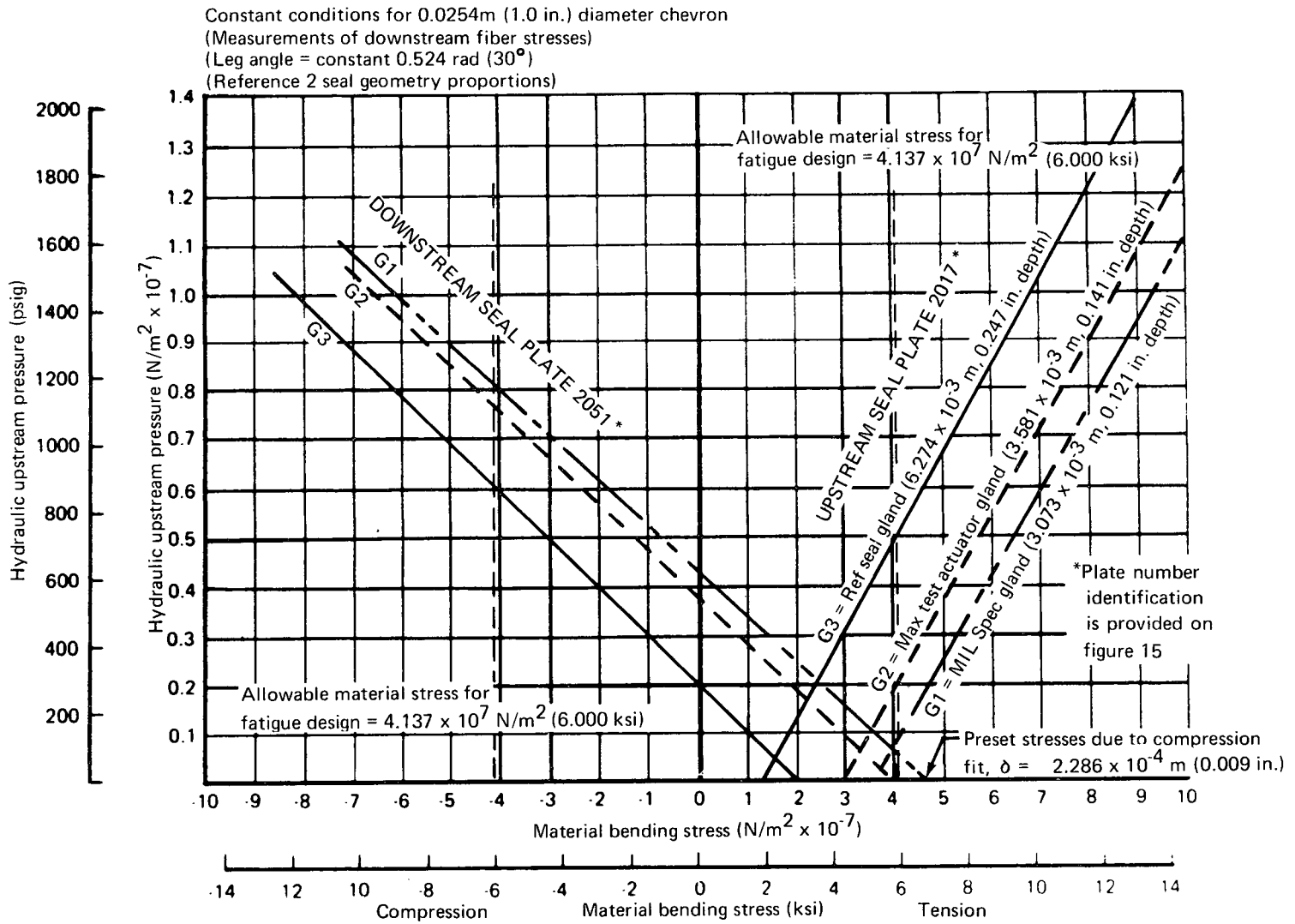

Figure 58.—Effects of gland depth variation—high preset seal

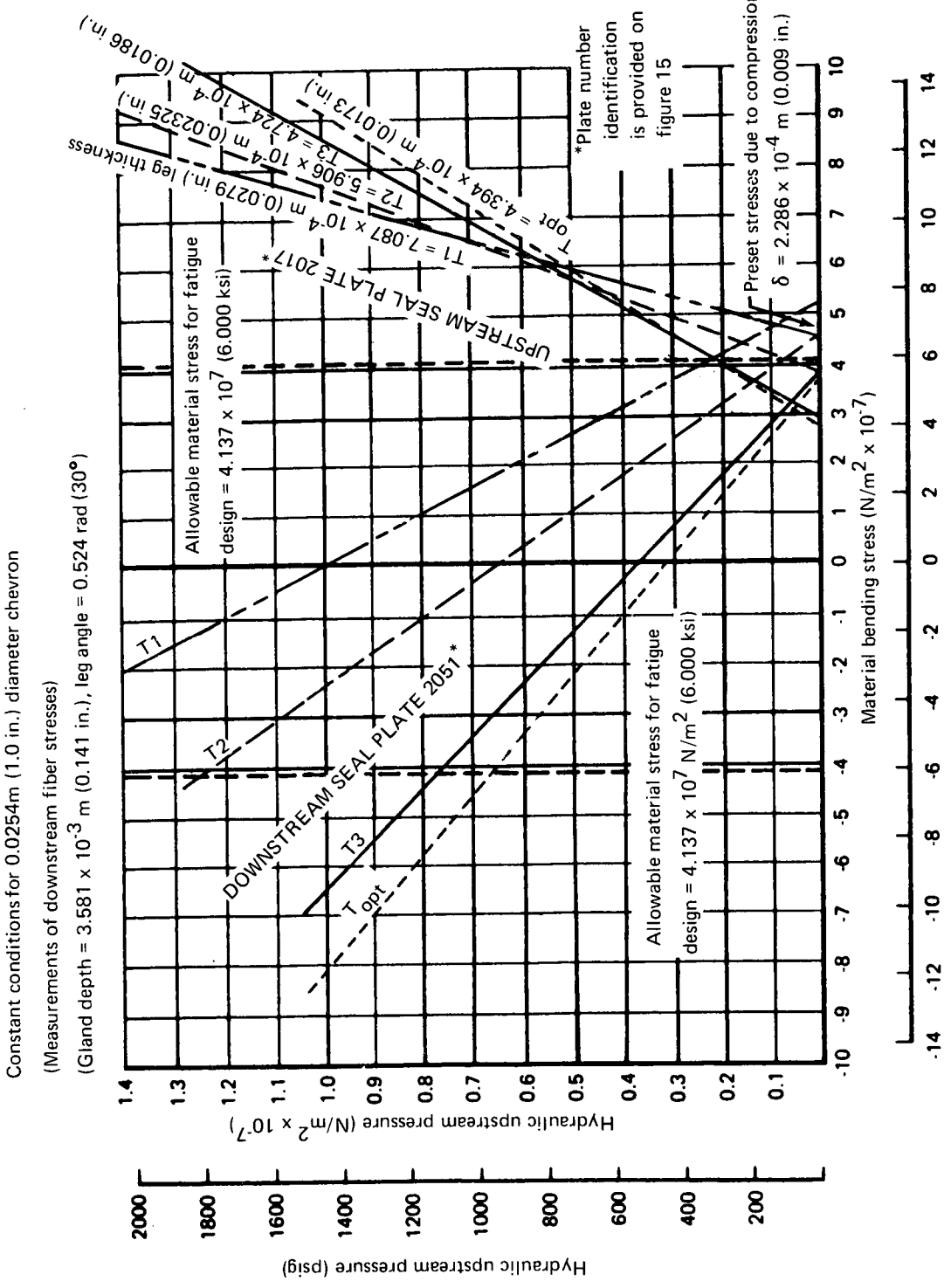

Figure 59.–Effects of leg thickness variation–high preset seal

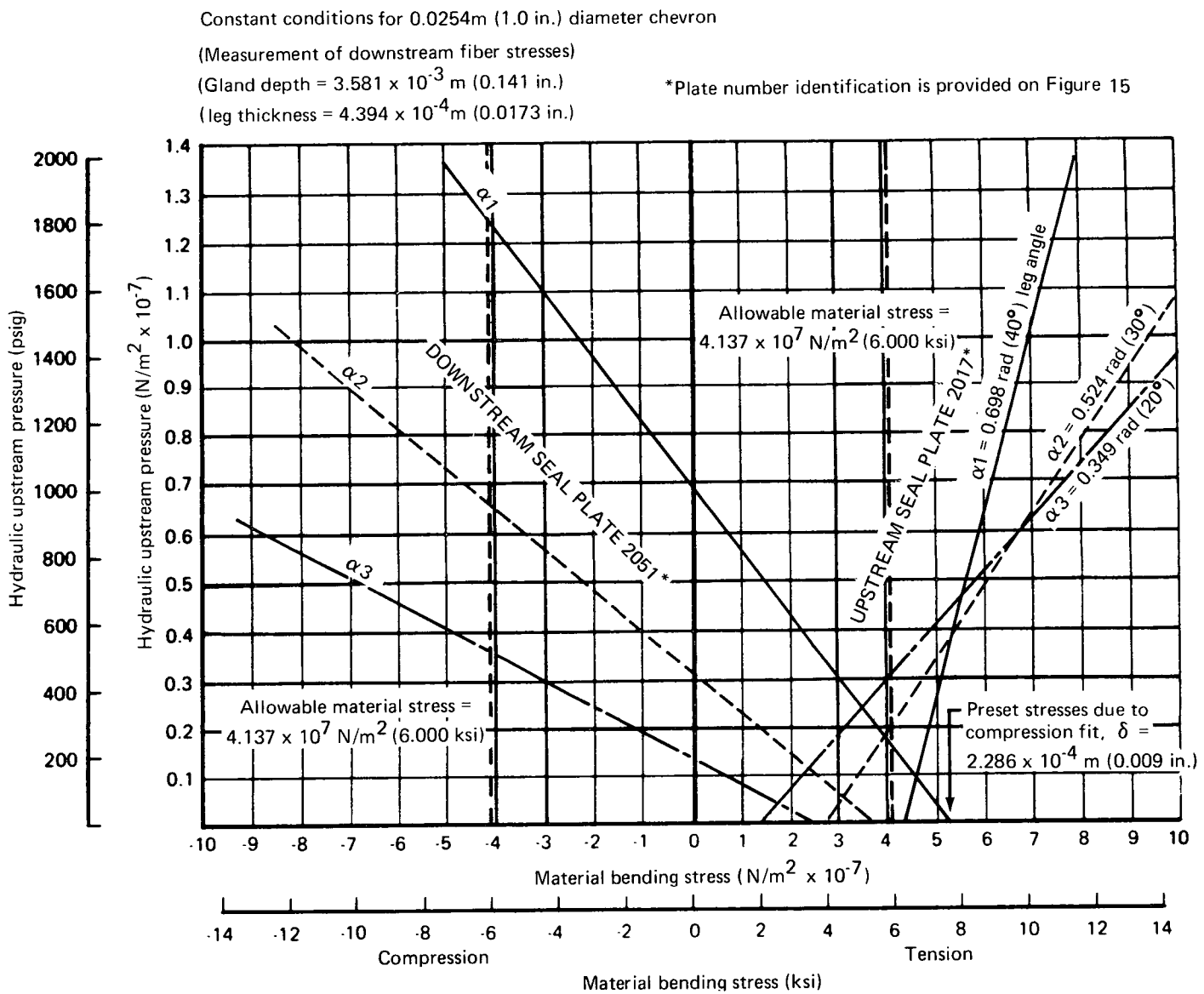

Figure 60.--Effects of leg angle variation--high preset seal

that reduced leg angle provided the largest benefit toward increasing the tolerable pressure level at the critical stress level because greater leg flexibility produced less stress with the large compression preset. Care was exercised in applying this result as a broad statement since at higher stress levels, i.e., 5.516×10^7 N/m^2 (8.000 ksi), the pressure-stress slopes created higher stress levels with lesser leg angles for a given hydraulic pressure. The reduction of leg angle resulted in a longer seal, which was a result opposite to the intent of design for minimum size.

The length of the chevron seal using a 0.349 rad (20°) leg angle was found to be acceptable within available volumes for the contract test actuators. This configuration was tentatively accepted as a beneficial design choice, increasing the allowable hydraulic pressure at the seal to 3.906×10^6 N/m^2 (449 psig). There was hesitancy that using a 0.349 rad (20°) leg angle might cause seal chatter problems during testing due to flexibility and the shallow angle with the rod. No conclusive statement as to the severity of this effect could be made based on the result of the stress analysis.

It was interesting to note that the change from a 0.698 rad (40°) angle to a 0.524 rad (30°) angle at 1.379×10^6 N/m^2 (200 psig) pressure loading caused a change from a non-acceptable seal, i.e., greater than 4.137×10^7 N/m^2 (6.000 ksi) stress, to one that was acceptable, less than 4.137×10^7 N/m^2 (6.000 ksi) stress. These data correlated well with the reference 2 design development, where leg angle was changed from 0.785 rad (45°) to 0.524 rad (30°).

Trends of Comparison

The data in figure 61 show some trends of stress values along the upstream and downstream faces of the seal's two chevrons. These data show stress variations with changes in gland depth and leg thickness. The data illustrate trends only, and were not intended to determine critical design stresses.

The original establishment of 2.286×10^{-4} m (0.009 in.) of seal preset interference fit was to prevent leakage resulting from differential expansion between the polyimide seal and steel actuator parts over the required temperature range. This interference condition is illustrated for the application temperature limits in figure 62 for the reference 2 B-1 seal configuration. The results show that stresses directly attributable to interference are $\geqslant$60% of the SP-21 material allowable for fatigue loading. Methods of reducing interference were therefore investigated which would allow a greater percentage of the material allowable to react against application reversal stresses.

ANALYSIS WITH OPTIMUM PRESET INTERFERENCE

The majority of the high stresses observed in the stress model results were due to the large compression preset required to retain sealing characteristics at minimum and maximum temperatures for the application. Reductions in this preset benefit raising the allowable

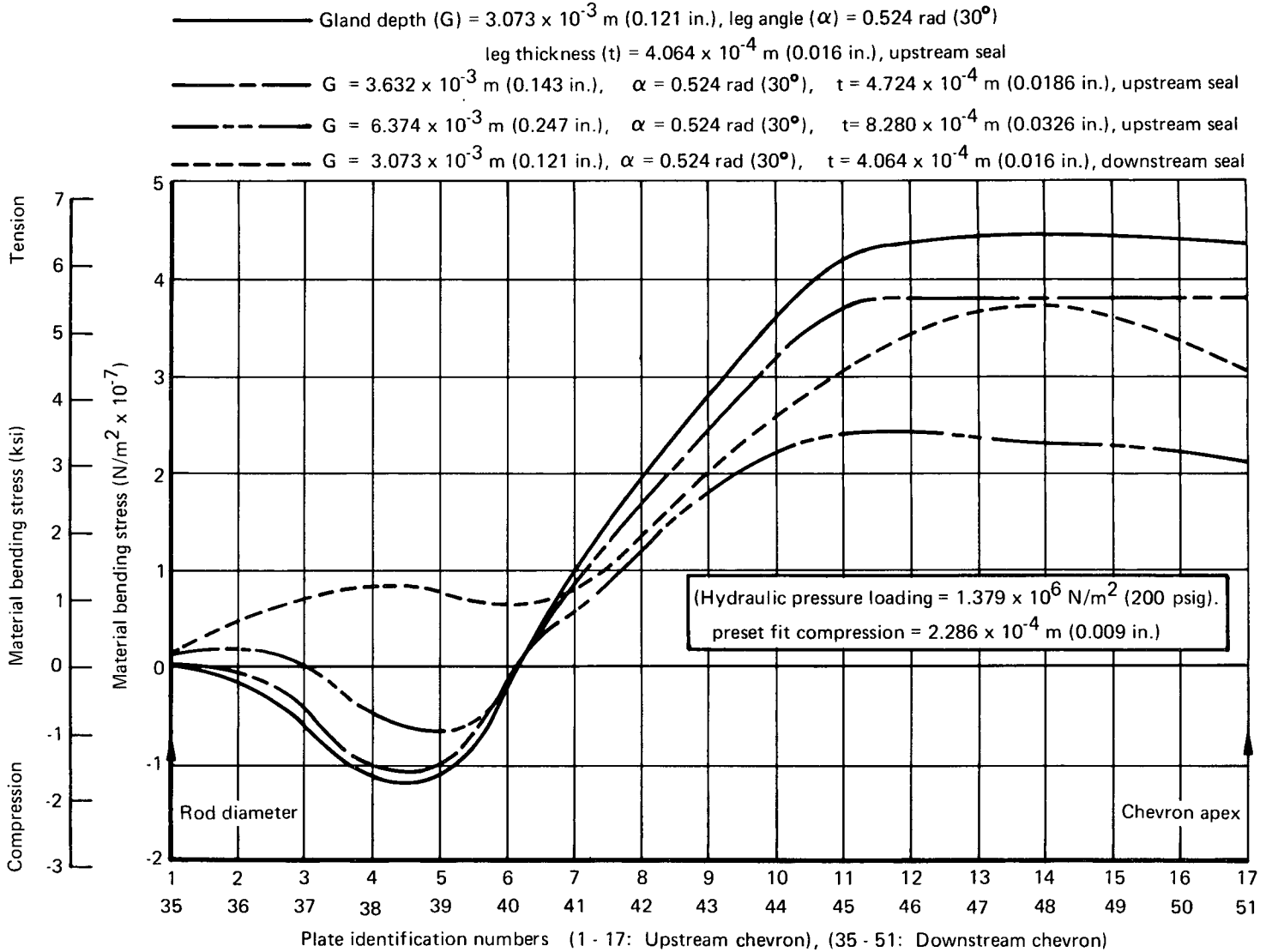

Figure 61.—Stress trends across chevrons with high preset

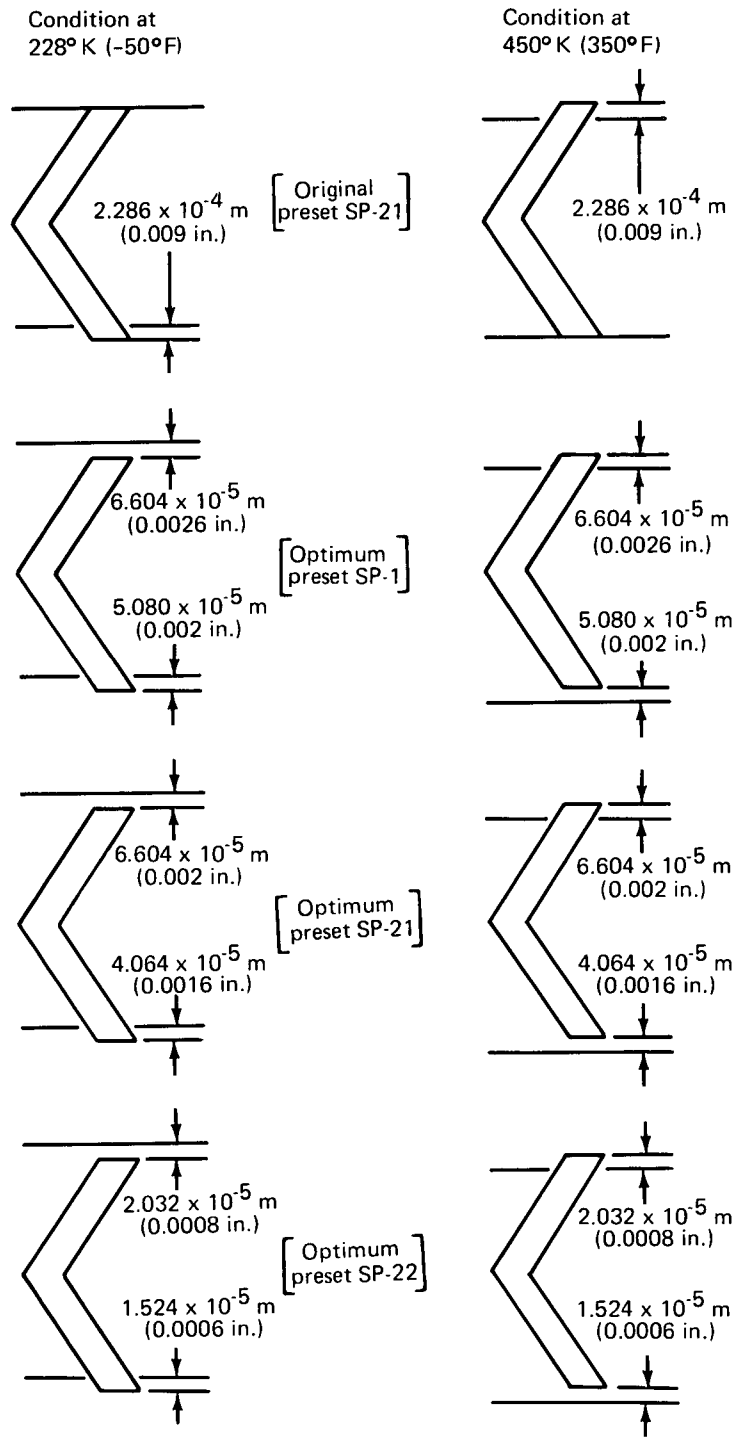

Figure 62.—Preset evaluation results

hydraulic pressure loading. A substantial reduction in preset stress could be achieved by considering nominal seal dimensions at a temperature midway between the minimum and maximum for the application. This resulted in minimum interference fit requirements at the temperature extremes. Further stress reduction was feasible by considering the properties of DuPont SP-22 polyimide, reference 13, in place of SP-21 as a baseline for the stress analysis. The preset stresses would be reduced because SP-22 had a 30% reduction in coefficient of thermal expansion compared to SP-21. Part of the stress reduction would be negated because there was also a 16% reduction in ultimate tensile strength of SP-22, which contained 40% graphite filler.

Seal design stress requirements for fatigue were determined for the SP-22 polyimide material in the same manner as performed with SP-21 and described under Stress Analysis Modeling.

- For SP-22 Allowable fatigue stress
  (using verbal property information obtained from DuPont)

$= 2.896 \times 10^7$ N/m^2 (4.200 ksi) @ 2×10^5 cycles, room temperature (for 1.043×10^7 N/m^2 (1500 psig) impulse during ground servicing) $= 1.724 \times 10^7$ N/m^2 (2.500 ksi) @ 2×10^5 cycles, 450° K (350° F) (for 6.895×10^6 N/m^2 (1000 psig) impulse during flight service)	Impulse Life
$= 2.413 \times 10^7$ N/m^2 (3.500 ksi) @ 8×10^6 cycles, room temperature (for 1.379×10^6 N/m^2 (200 psig) steady state ground service) $= 1.379 \times 10^7$ N/m^2 (2.000 ksi) @ 8×10^6 cycles, 450° K (350° F) (for 2.758×10^6 N/m^2 (400 psig) steady state flight service)	Fatigue Life

The envelope formed by the interconnection of the above points on a pressure vs stress graph was the locus of requirements that had to be satisfied by the seal to withstand the reversal stresses imposed by the application. This envelope was used to illustrate the degree of configuration acceptance in each iteration of the stress analysis described in the report sections.

The amount of preset required to keep the chevron seal in contact with the actuator rod and gland was directly proportional to the linear coefficient of thermal expansion for the material. These coefficients for SP-1, SP-21, and SP-22 materials were 50.4, 40.4, and 28.8×10^{-6} m/m°K (28, 23, and 16 microin./in.°F), respectively, with the material grain pattern aligned for minimum expansion. Data for SP-1 are presented to provide comparison to reference 2. Steel has an average coefficient of 12.6×10^{-6} m/m°K (7 microin./in.°F). By balancing the interference fit at one temperature limit with the clearance fit at the other limit for both the ID and OD of the seal, and using an upstream loading block to force closure of clearance fits, it was possible to significantly reduce the preset required for sealing. These optimum presets for each of the three materials stated above are also shown in figure 62.

The optimum presets for SP-21 and SP-22 materials were incorporated in the mathematical model for the chevron seal stress analysis to obtain pressure/stress relationships.

Stresses With Optimum Preset Using SP-21

Figure 63 illustrates the relationship of stress with applied hydraulic pressure for three seal gland depths. The results show that optimum preset allows a 147% increase in allowable hydraulic pressure for the same stress in the G2 groove when compared to the 2.286 x 10^{-4} m (0.009 in.) preset interference. Figure 64 illustrates the effects of seal leg thickness variations with optimum preset and the test actuator gland (G2). Optimum thickness lines for critical stress conditions show that room temperature requirements could be met without further optimization, but additional steps were necessary to meet 450° K (350° F) temperature requirements. Figure 65 illustrates the effects of variation of seal leg angle using optimum thickness and the G2 gland. Results show that temperature requirements were nearly met for tension loading using a 0.349 rad (20°) leg angle, but stresses were too severe to satisfy compression loading requirements. Figure 66 illustrates the effects of variation of the angle of contact between the downstream chevron and the support block downstream to this chevron. The stress effects were only evident on plates in the downstream chevron. The data illustrated are for the critical plate, which in all cases was the plate at the position where contact between the chevron and the support block terminates. Two sets of curves are shown. The high-stress curves illustrate backup angle variations corresponding to the analysis with a 2.286 x 10^{4} m (0.009 in.) preset. The lower stress curves show that, by optimizing preset, considerable increase in hydraulic compression loading can be allowed. This increase, however, was not sufficient to fully meet the maximum fatigue requirements for the application.

Stresses With Optimum Preset Using SP-22

Figures 67, 68, 69, and 70 illustrate the same information as shown in the figures for previous evaluations but with the material being SP-22. This material has a more desirable coefficient of thermal expansion but a lower allowable stress envelope. It was significant to note that optimum leg thickness was again sufficient to provide a configuration that would satisfy room temperature impulse and endurance requirements. The exercise of evaluating leg angle variation showed that all tension requirements and room temperature compression requirements could be satisfied. Further optimization by increasing downstream support block contact angle provided the increased capability needed to satisfy the high-temperature compression loading requirements.

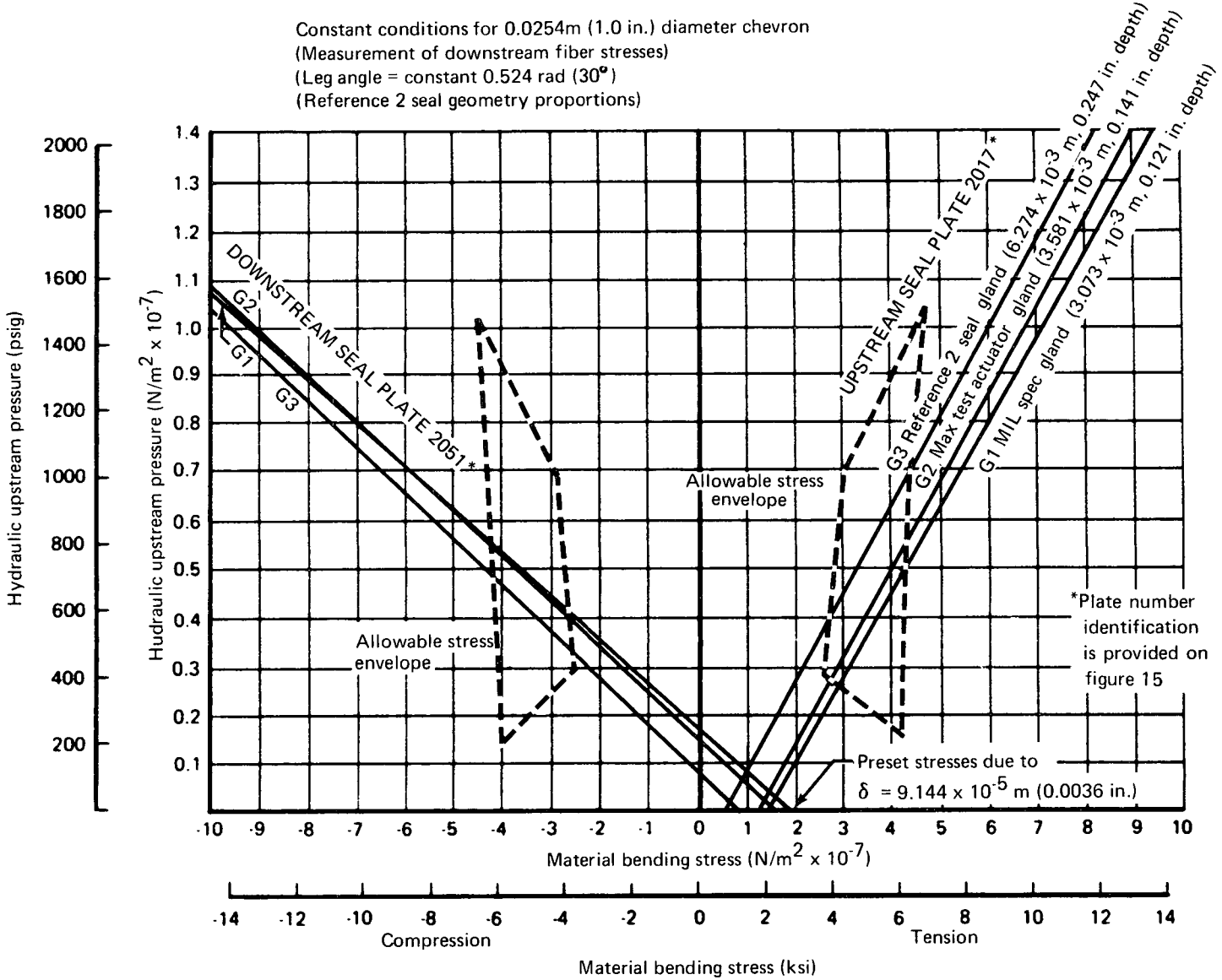

Figure 63.—Effects of gland depth variation—SP-21 material

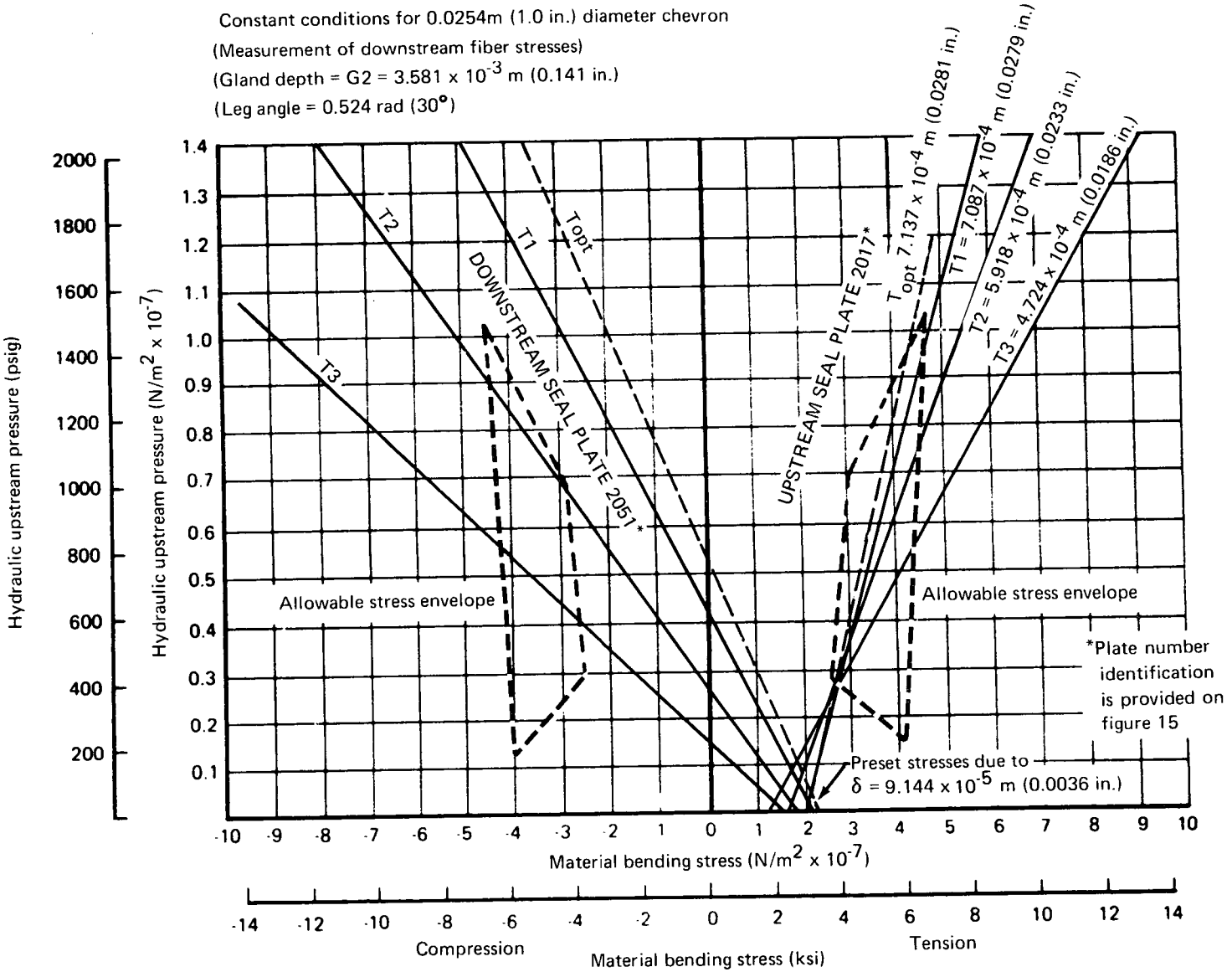

Figure 64.—Effects of leg thickness variation—SP-21 material

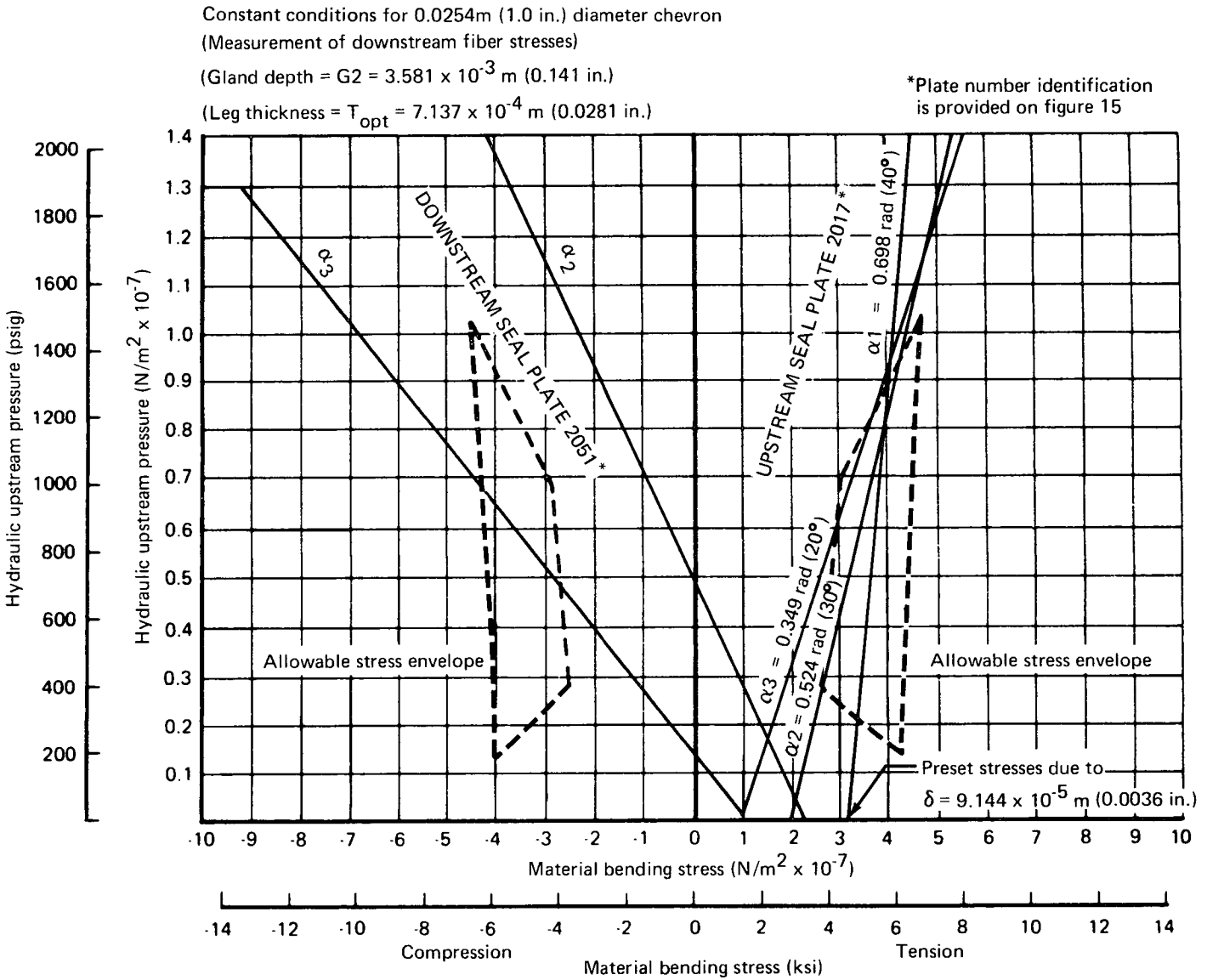

Figure 65.--Effects of leg angle variation—SP-21 material

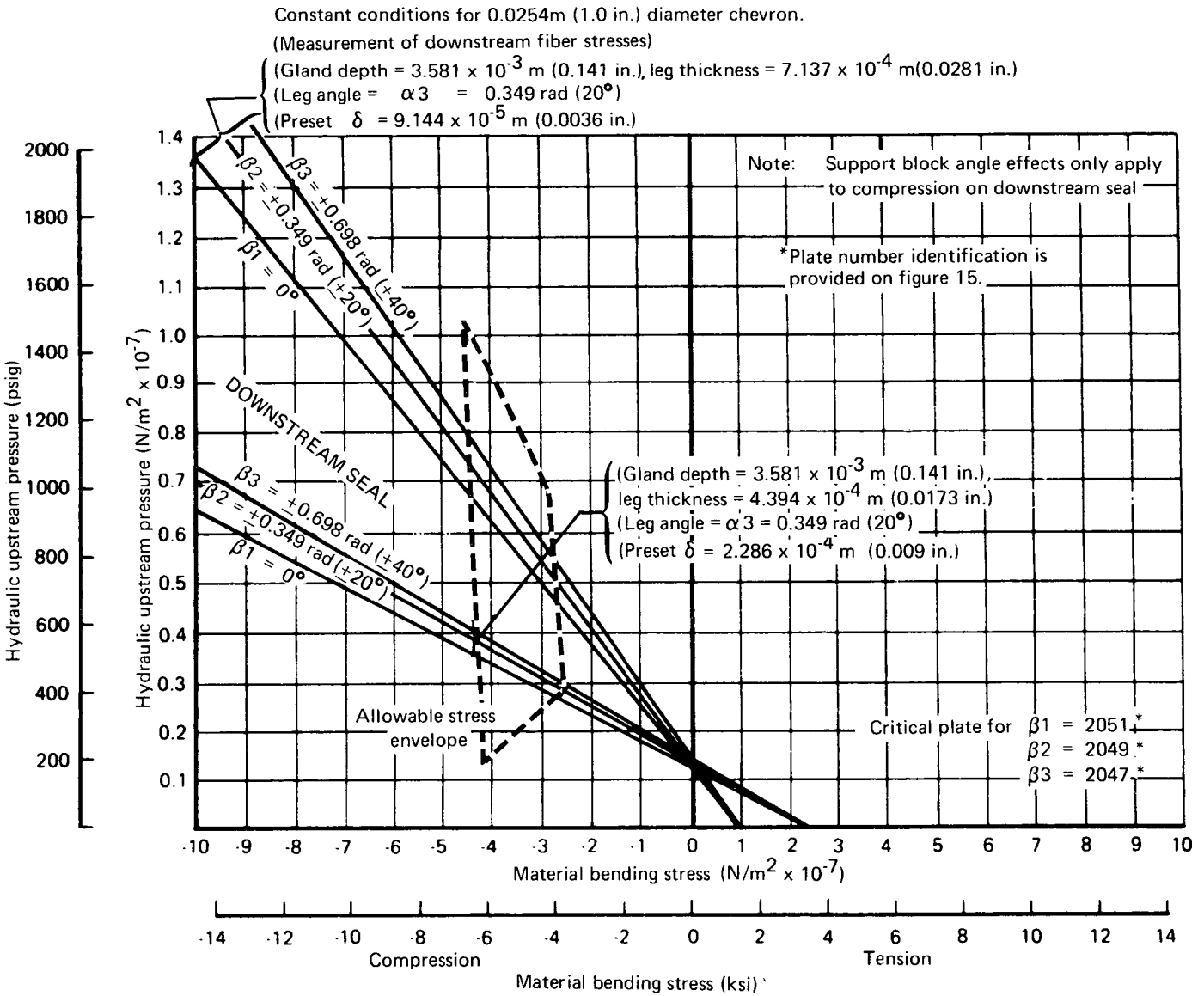

Figure 66.—Effects of support block angle variation—SP-21 material

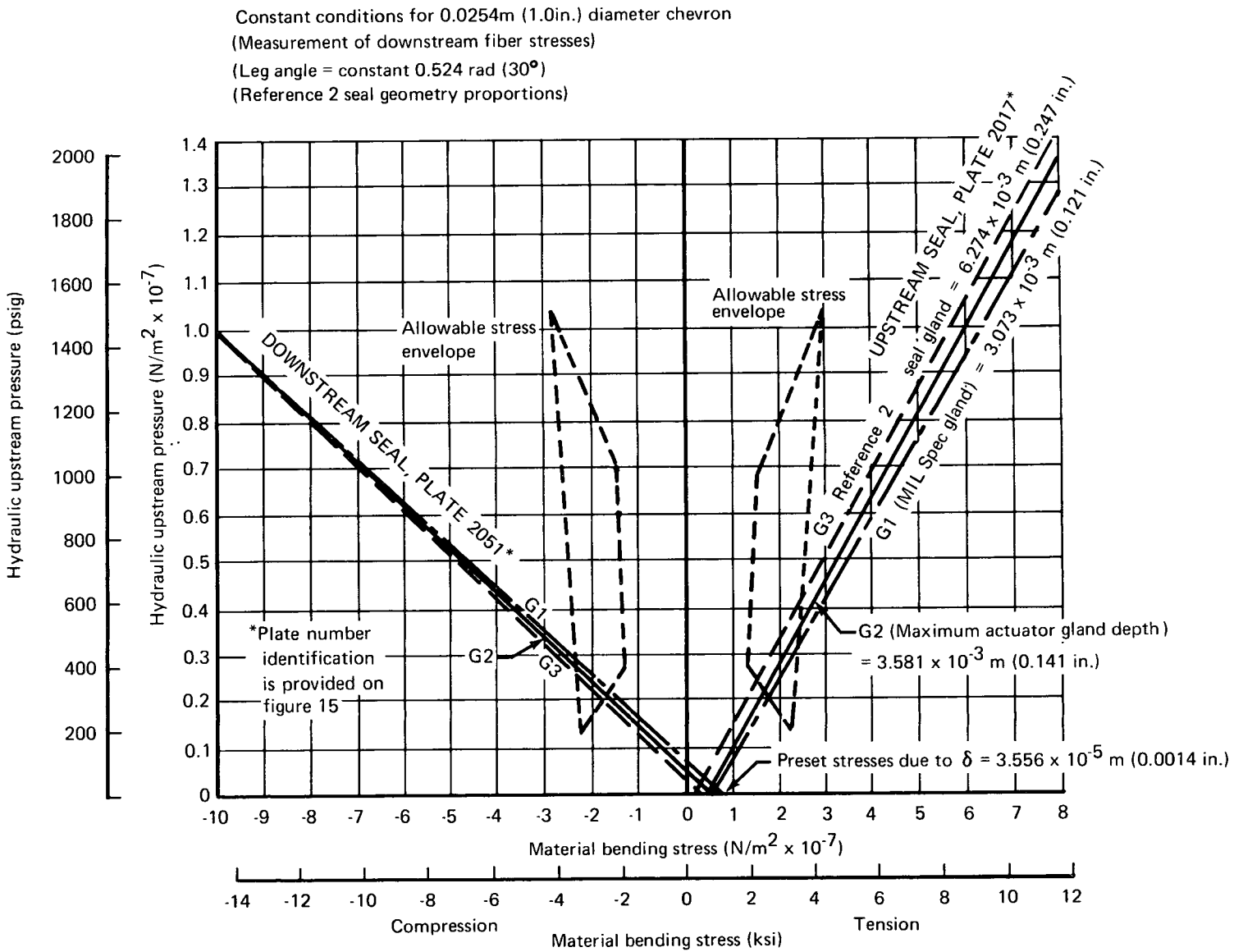

Figure 67.—Effects of gland depth variation—SP-22 material

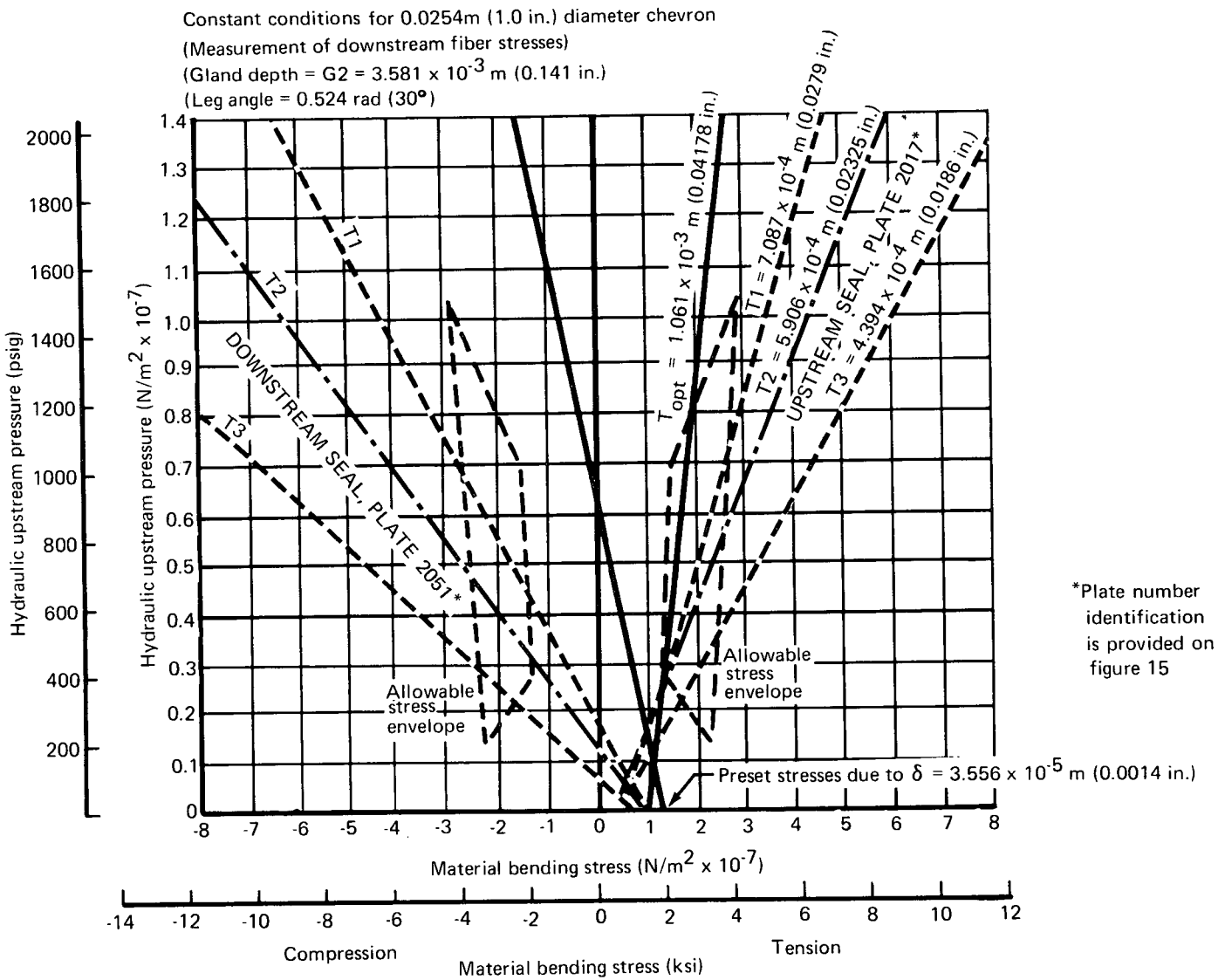

Figure 68.—Effects of leg thickness variation—SP-22 material

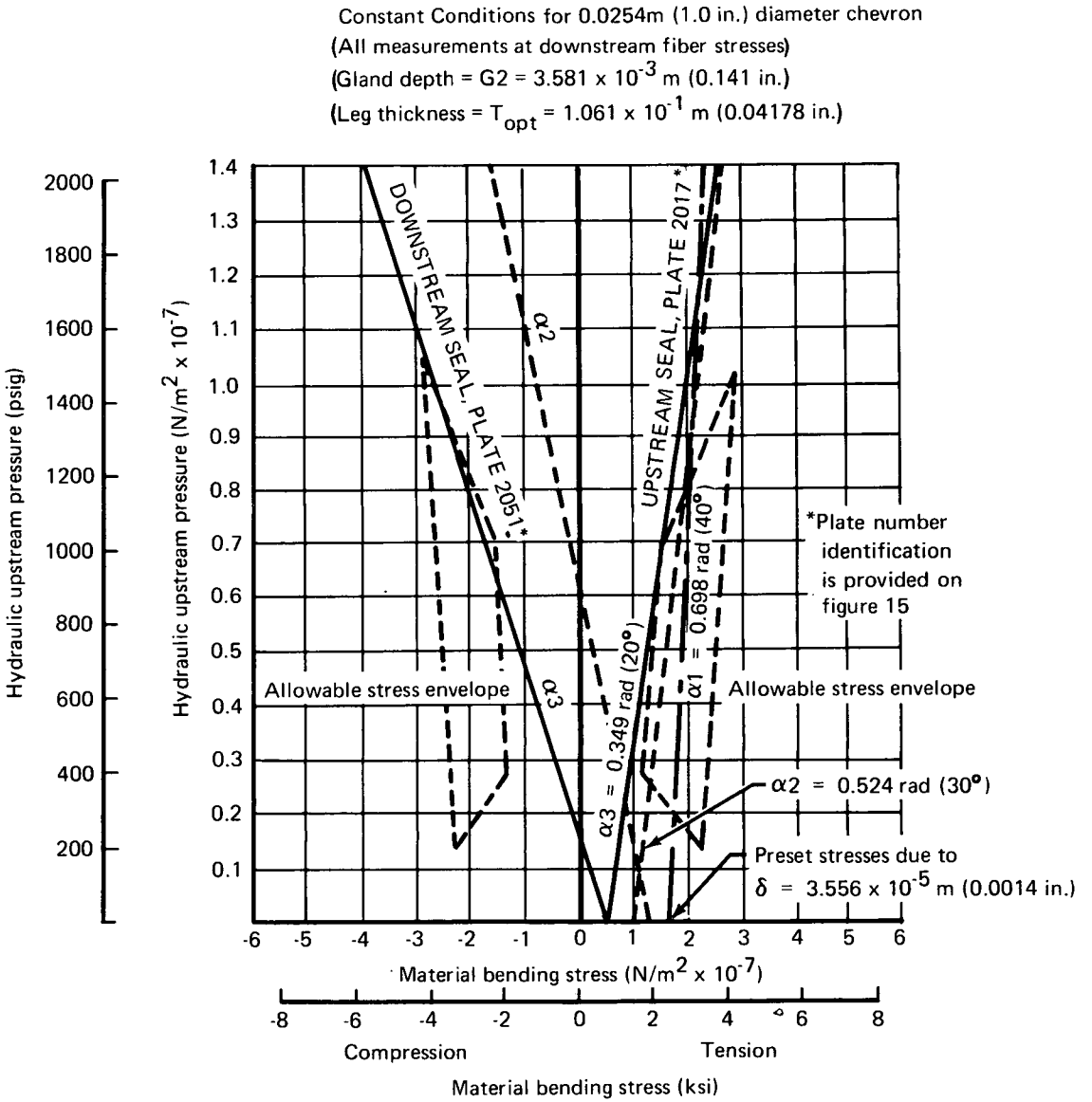

Figure 69.—Effects of leg angle variation on allowable stress—SP-22 material

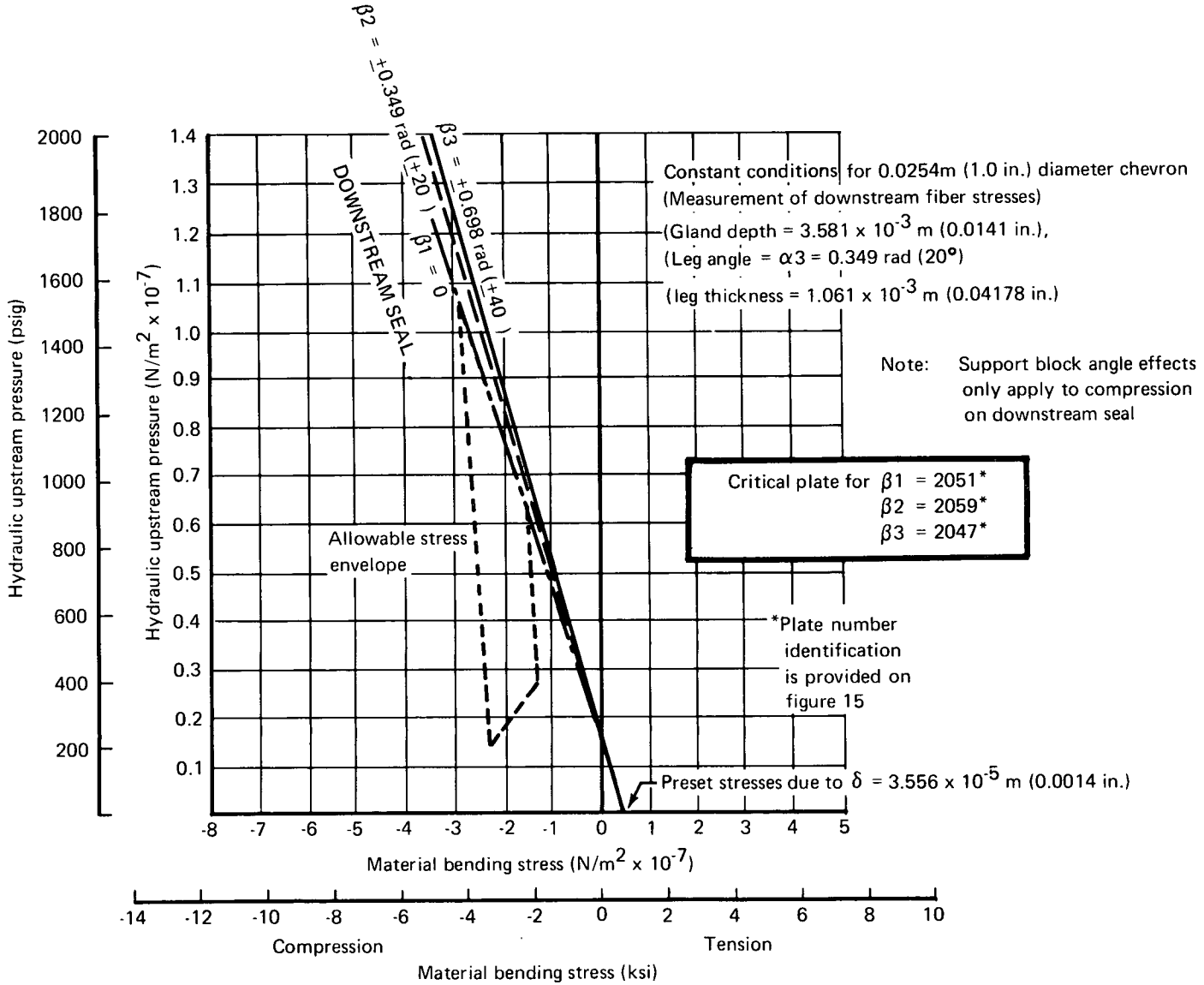

Figure 70.—Effects of support block angle variation—SP-22 material

APPENDIX 3

KOPPERS SPECIFICATIONS, BALANCED CONTRACTING TWO-PIECE ASSEMBLIES

Specifications for the first-stage seals, fabricated by Koppers Company, Inc., are shown in the following figures:

Figure 71 0.0254 m (1.0 in.), 30% balanced

Figure 72 0.0254 m (1.0 in.), 50% balanced

Figure 73 0.0254 m (1.0 in.), 70% balanced

Figure 74 0.0635 m (2.5 in.), 30% balanced

Figure 75 0.0635 m (2.5 in.), 50% balanced

Figure 76 0.0635 m (2.5 in.), 70% balanced

Figure 77 is a photograph of the six seals defined in the above specification drawings.

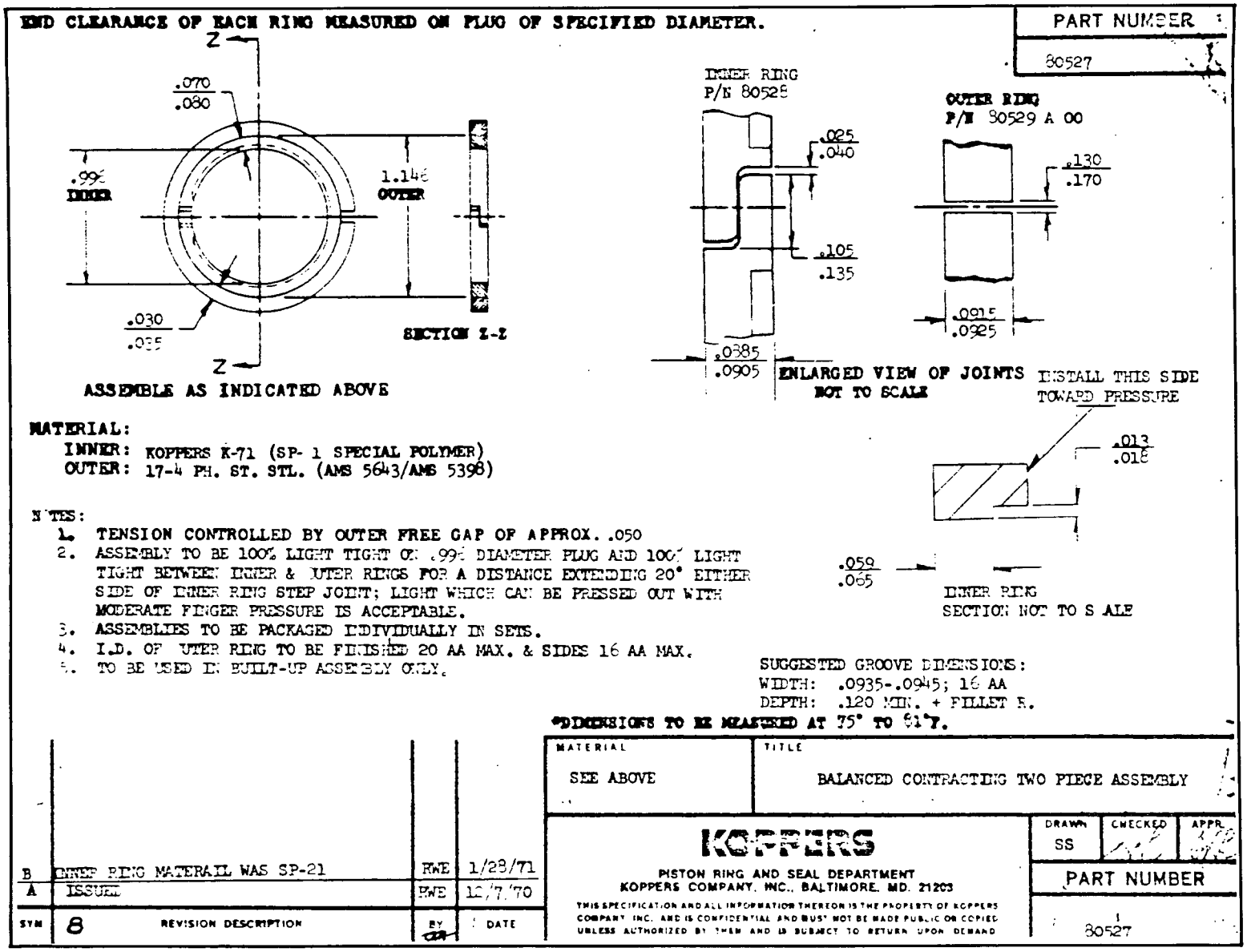

Figure 71.—Balanced contracting two-piece assembly (80527)

END CLEARANCE OF EACH RING MEASURED ON PLUG OF SPECIFIED DIAMETER.

PART NUMBER
80518

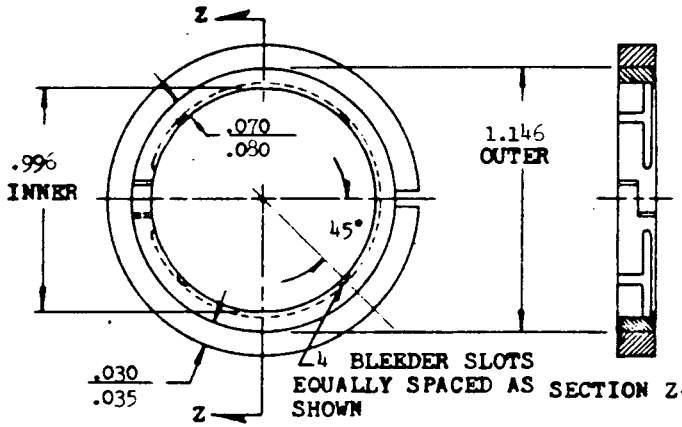

ASSEMBLE AS INDICATED ABOVE

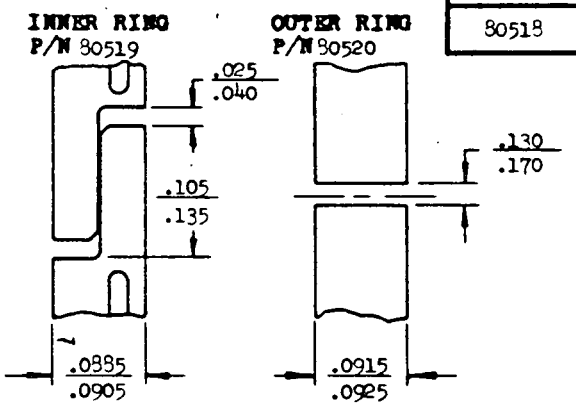

ENLARGED VIEW OF JOINTS

MATERIAL:
INNER: KOPPERS K-71 (SP-1 SPECIAL POLYMER)
OUTER: 17-4 PH. ST. STL. (AMS 5643/AMS 5398)

NOTES:
1. ASSEMBLY TO BE 100% LIGHT TIGHT ON .996 DIAMETER PLUG AND 100% LIGHT TIGHT BETWEEN INNER & OUTER RINGS FOR A DISTANCE EXTENDING 20° EITHER SIDE OF INNER RING STEP JOINT; LIGHT WHICH CAN BE PRESSED OUT WITH MODERATE FINGER PRESSURE IS ACCEPTABLE.
2. ASSEMBLIES TO BE PACKAGED INDIVIDUALLY IN SETS.
3. I.D. OF OUTER RING TO BE FINISHED 20 AA MAX. & SIDES 16 AA MAX.
4. TO BE USED IN BUILT-UP ASSEMBLY ONLY.

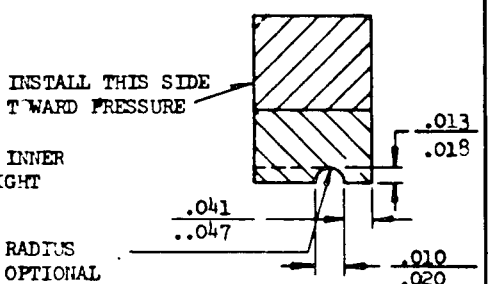

TYPICAL SECTION

TENSION CONTROLLED BY OUTER RING FREE GAP OF APPROX. .050

SUGGESTED GROOVE DIMENSIONS:
WIDTH: .0935-.0945; 16 AA
DEPTH: .120 MIN. + FILLET R.

SYM	REVISION DESCRIPTION	BY	DATE
B (1)	RADIUS OPTIONAL WAS 1/32 R.	RWE	4/23/71
B	INNER RING MATERIAL WAS SP-21	RWE	1/28/71
A	ISSUED	RWE	12/7/70

MATERIAL	TITLE
SEE ABOVE	BALANCED CONTRACTING TWO-PIECE ASSEMBLY

KOPPERS COMPANY, INC.
METAL PRODUCTS DIVISION
PISTON RING AND SEAL DEPARTMENT
BALTIMORE 3, MARYLAND

DRAWN	CHECKED	APPR.
SS		

PART NUMBER
80518

Figure 72.— Balanced contracting two-piece assembly (80518)

END CLEARANCE OF EACH RING MEASURED ON PLUG OF SPECIFIED DIAMETER.

PART NUMBER
80524

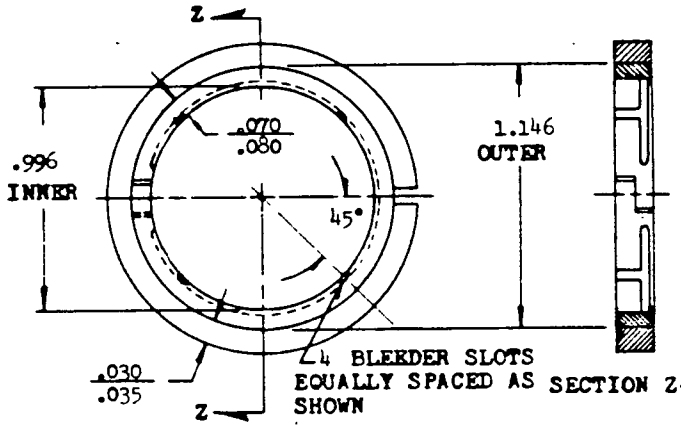

ASSEMBLE AS INDICATED ABOVE

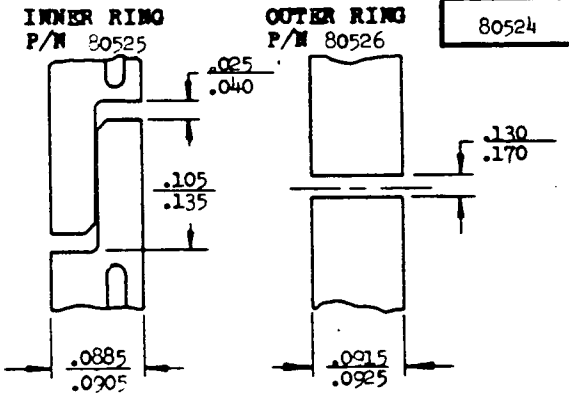

ENLARGED VIEW OF JOINTS

MATERIAL:
INNER: KOPPERS K-71 (SP-1 SPECIAL POLYMER)
OUTER: 17-4 PH. ST. STL. (AMS 5643/AMS 5398)

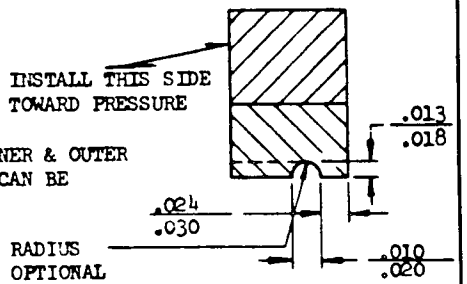

TYPICAL SECTION

NOTES:
1. ASSEMBLY TO BE 100% LIGHT TIGHT IN .996 DIAMETER PLUG AND 100% LIGHT TIGHT BETWEEN INNER & OUTER RINGS FOR A DISTANCE EXTENDING 20° EITHER SIDE OF INNER RING STEP JOINT; LIGHT WHICH CAN BE PRESSED OUT WITH MODERATE FINGER PRESSURE IS ACCEPTABLE.
2. ASSEMBLIES TO BE PACKAGED INDIVIDUALLY IN SETS.
3. I.D. OF OUTER RING TO BE FINISHED 20 AA MAX. & SIDES 16 AA MAX.
4. TO BE USED IN BUILT-UP ASSEMBLY ONLY.

TENSION CONTROLLED BY OUTER RING FREE GAP OF APPROX. .050

SUGGESTED GROOVE DIMENSIONS:
WIDTH: .0935-.0945; 16 AA
DEPTH: .120 MIN. + FILLET R.

SYM	REVISION DESCRIPTION	BY	DATE
B (1)	RADIUS OPTIONAL WAS 1/32 R.	RWE	4/23/71
B	INNER RING MATERIAL WAS SP-21	RWE	1/28/71
A	ISSUED	RWE	12/7/70

MATERIAL	TITLE
SEE ABOVE	BALANCED CONTRACTING TWO-PIECE ASSEMBLY

KOPPERS COMPANY, INC.
METAL PRODUCTS DIVISION
PISTON RING AND SEAL DEPARTMENT
BALTIMORE 3, MARYLAND

DRAWN	CHECKED	APPR.
SS		

PART NUMBER
80524

Figure 73.— Balanced contracting two-piece assembly (80524)

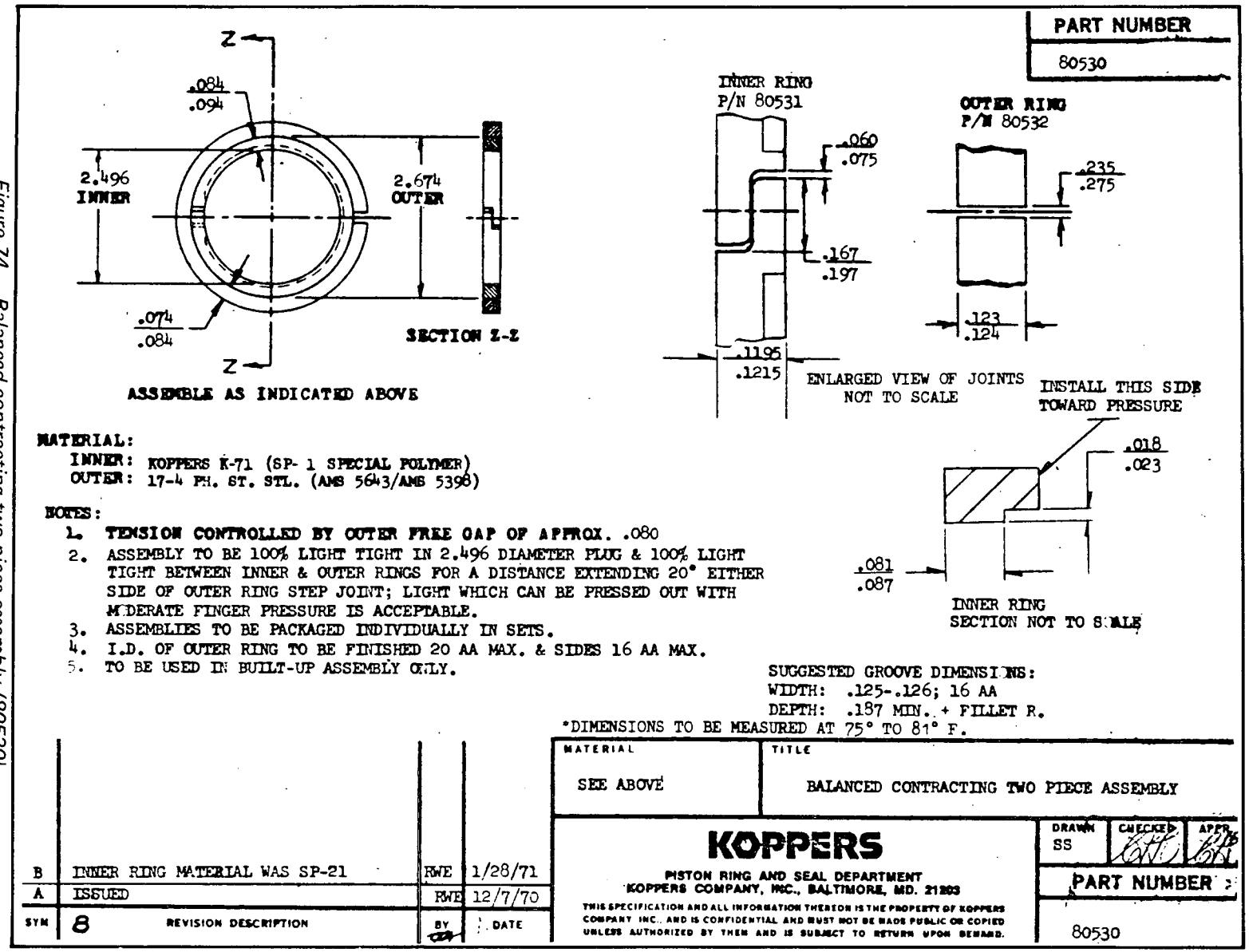

Figure 74.— Balanced contracting two-piece assembly (80530)

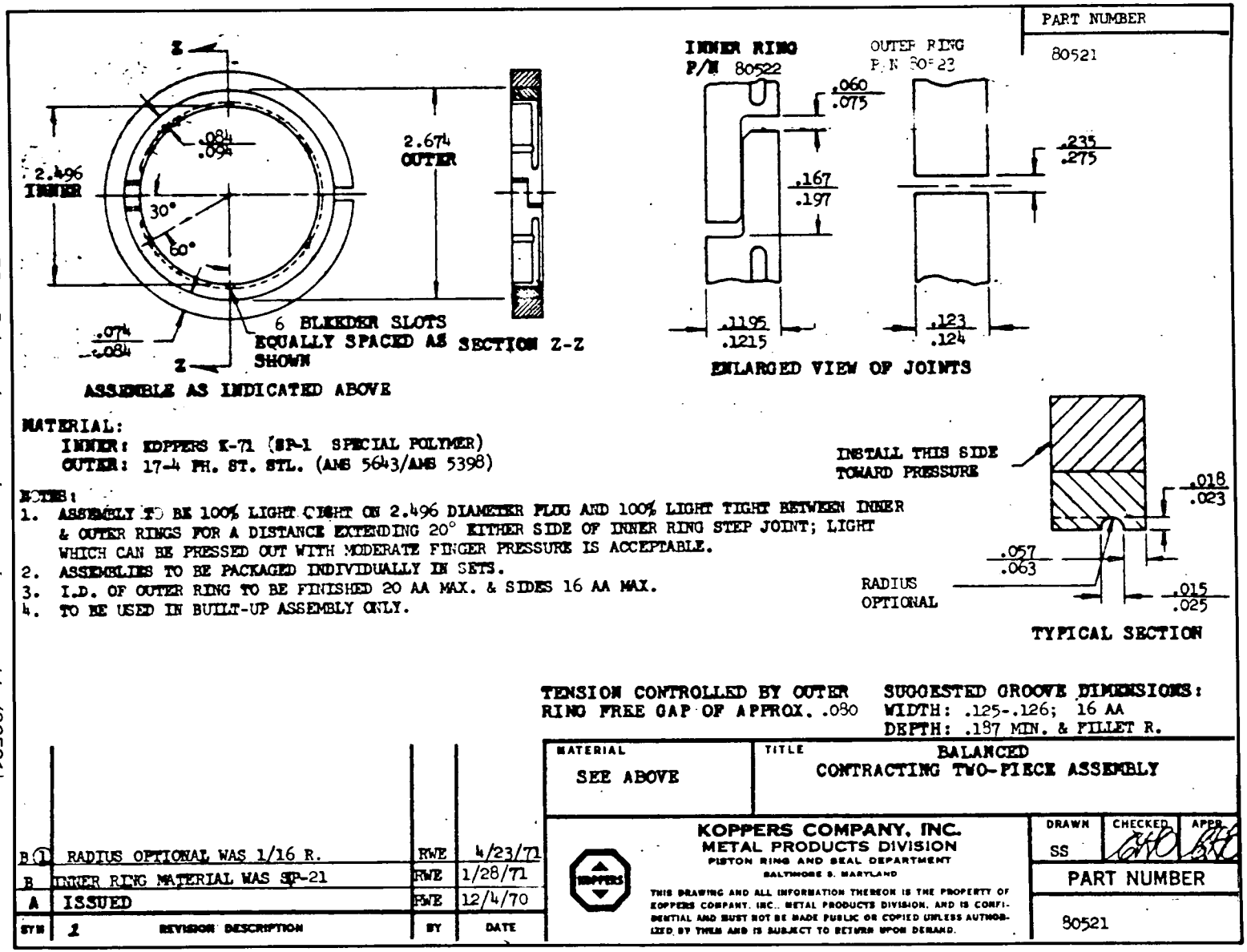

Figure 75.— Balanced contracting two-piece assembly (80521)

END CLEARANCE OF EACH RING MEASURED ON PLUG OF SPECIFIED DIAMETER.

PART NUMBER 80533

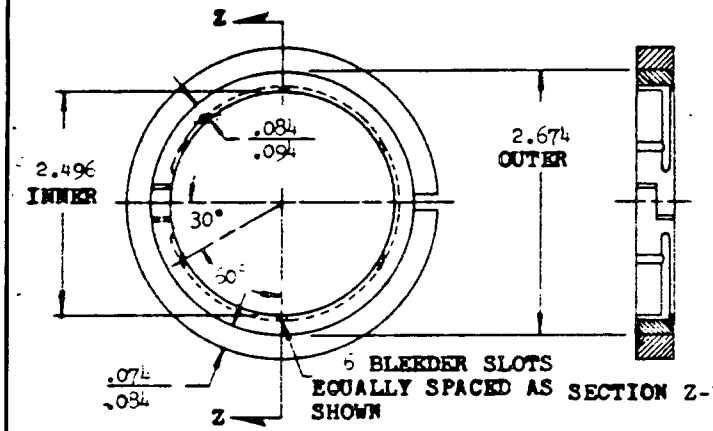

ASSEMBLE AS INDICATED ABOVE

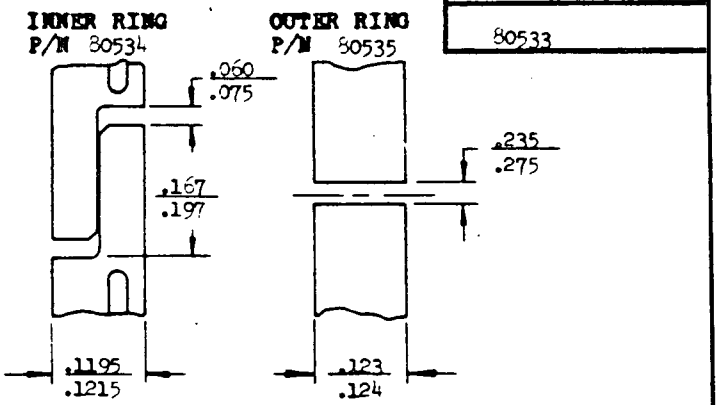

ENLARGED VIEW OF JOJNTS

MATERIAL:
INNER: KOPPERS K-71 (SP-21 SPECIAL POLYMER)
OUTER: 17-4 PH. ST. STL. (AMS 5643/AMS 5398)

NOTES:
1. ASSEMBLY TO BE 100% LIGHT TIGHT ON 2.496 DIAMETER PLUG AND 100% LIGHT TIGHT BETWEEN INNER & OUTER RINGS FOR A DISTANCE EXTENDING 20° EITHER SIDE OF INNER RING STEP JOINT; LIGHT WHICH CAN BE PRESSED OUT WITH MODERATE FINGER PRESSURE IS ACCEPTABLE.
2. ASSEMBLIES TO BE PACKAGED INDIVIDUALLY IN SETS.
3. I.D. OF OUTER RING TO BE FINISHED 20 AA MAX. & SIDES 16 AA MAX.
4. TO BE USED IN BUILT-UP ASSEMBLY ONLY.

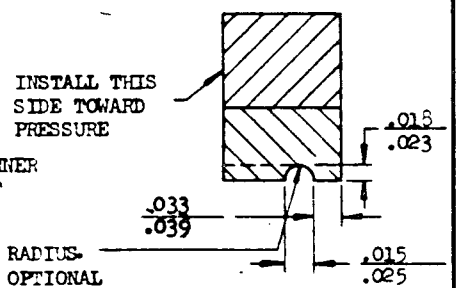

TYPICAL SECTION

TENSION CONTROLLED BY OUTER RING FREE GAP OF APPROX. .050

SUGGESTED GROOVE DIMENSIONS:
WIDTH: .125-.126; 16 AA
DEPTH: .197 MIN. + FILLET R.

SYM	REVISION DESCRIPTION	BY	DATE
C	RADIUS WAS 1/16 R.	RWE	4/23/71
B	INNER RING MATERIAL WAS SP-21	RWE	1/28/71
A	ISSUED	RWE	12/4/70

MATERIAL: SEE ABOVE

TITLE: BALANCED CONTRACTING TWO-PIECE ASSEMBLY
BOEING

KOPPERS COMPANY, INC.
METAL PRODUCTS DIVISION
PISTON RING AND SEAL DEPARTMENT
BALTIMORE 3, MARYLAND

DRAWN	CHECKED	APPR.
SS		

PART NUMBER 80533

Figure 76.— Balanced contracting two-piece assembly (80533)

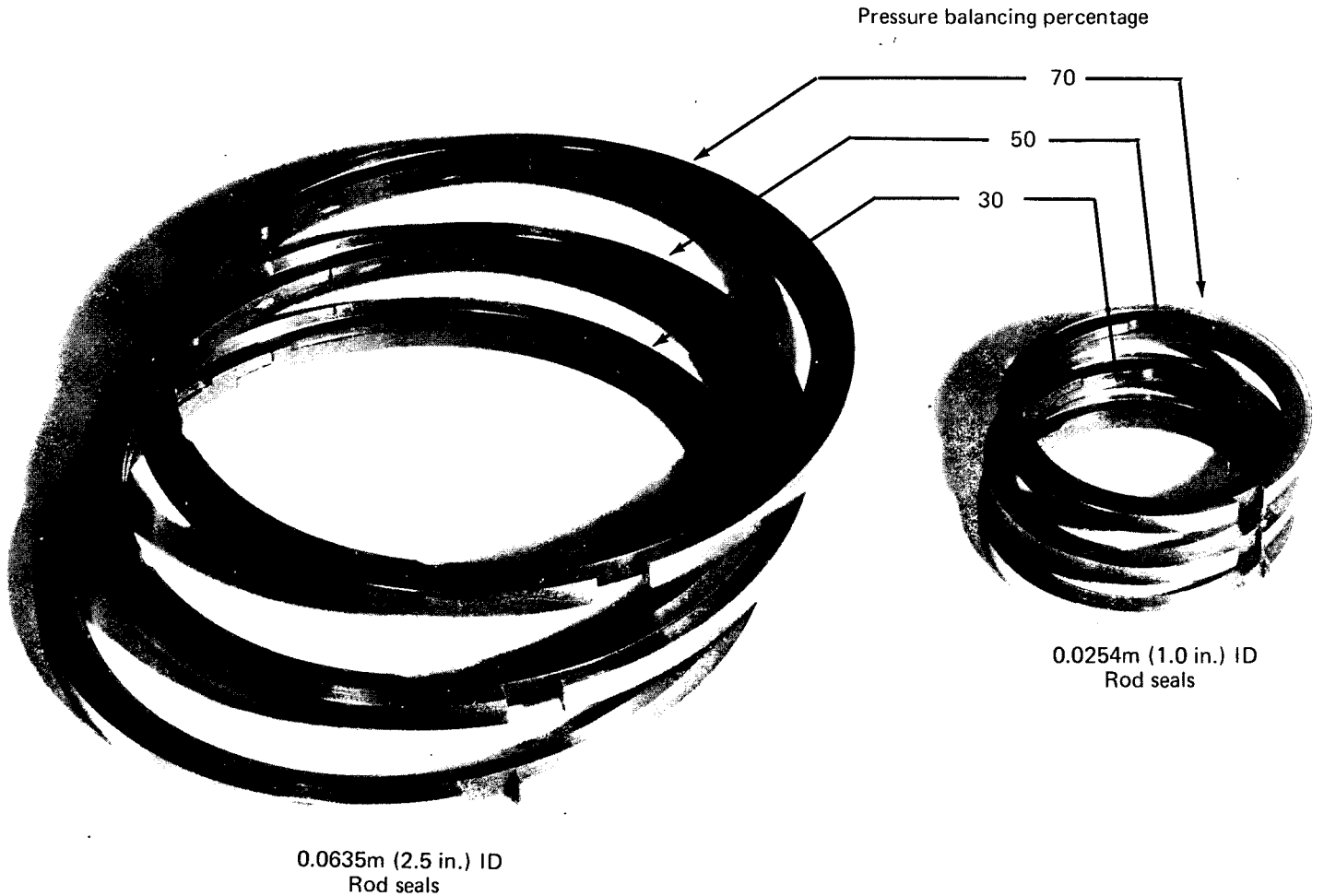

Figure 77.— First-stage test seal assemblies

APPENDIX 4

PRESSURE IMPULSE TEST–SYSTEM DESCRIPTION AND OPERATING SEQUENCE

TEST SYSTEM DESCRIPTION

Test Article

Each article to be tested by impulse cycling consisted of a single second-stage chevron or K-section assembly or a first-stage pressure balanced seal installed in a housing to retain the seal in a manner duplicating an aircraft installation. Existing hardware was used to the greatest extent possible to provide the necessary housings as illustrated in figure 78. Only one seal was tested in a single housing end. Thus, when a second-stage configuration was to be tested the first-stage gland was left empty. When the first-stage seal was tested, a Boeing seal was installed in the second-stage gland only to allow collection of leakage and was not considered to be under test.

Test Operation Components

The hydraulic system shown in figure 78 was the test rig used and is an existing rig developed primarily for impulse testing of tubing, fittings, and hoses. It consists of the following major components.

Hydraulic power supply	Denison 8-gpm pump unit
Hydraulic relief valve	Denison
Hydraulic filter	Purolator, T type (25 micron absolute)
Servovalve block	Boeing laboratory equipment (SK11-96025)
Intensifier (3-to-1 area ratio)	Boeing laboratory equipment
Heat exchanger	Harrison, water cooled
Accumulator	Hydrodyne, 3.785×10^{-3} m^3 (1 gal), 6.894×10^7 N/m^2 (10 000 psig)
Isolation Tube	0.013 m (1/2 in.) OD for first-stage test 0.0064 m (1/4 in.) OD for second-stage test

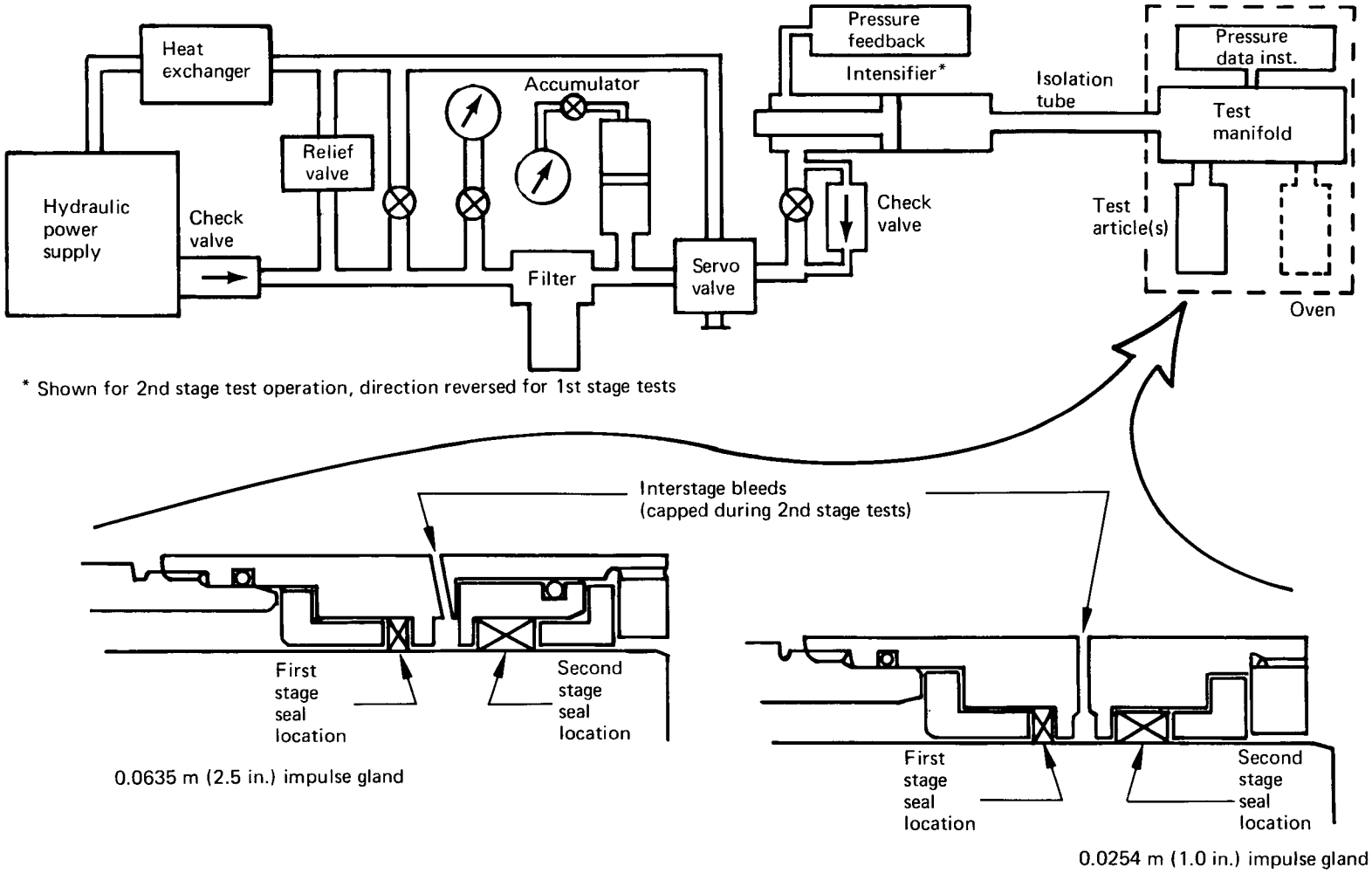

Figure 78.— Hydraulic installation, impulse test

The hydraulic power supply consists of a 5.047×10^{-4} m^3/sec (8 gpm) 3.442×10^7 N/m^2 (5000 psig) variable-displacement pump with reservoir. A high-pressure, piston-type accumulator is located in the supply line just upstream of the servovalve manifold to provide peak flow requirements beyond the maximum dynamic response of the pump. Ports within the servovalve block are oversized to reduce pressure drop. For tests requiring pressure rise rates below 1.033×10^9 N/m^2/sec (150 000 psig/sec), a 3-to-1 intensifier is placed between the servovalve and the test manifold. This allows the pump and servo to be operated well within their working pressure range while impulsing the test article at rather high pressure peaks.

For this series of tests reported, the fluid on the servo side of the intensifier was MIL-H-5606 and the fluid on the test article side of the intensifier was Humble WS 8228. (ref. 4). The test articles were attached to a distribution manifold which was located in an environmental chamber. The test article temperature was provided by controlling the ambient temperature within this chamber. Because the fluid in the test article was almost dead-ended, no preheating of the supply fluid was required. The test chamber was positioned approximately 1.524 m (60 in.) from the intensifier and connected by a suitable section of hydraulic tubing. This tube was used to isolate the test article temperature from the intensifier.

Control Circuit and Instrumentation

The control system for impulsing was based on an electrohydraulic closed-loop pressure control servo system. Components of this system were arranged as shown in figure 79. The control actuating device was the four-way, pressure control servovalve with one cylinder port blocked. The servo controller was a Boeing-built controller with an adjustable servo loop gain from unity to a multiplication of one hundred. The controller output stage was a voltage driver which also provided damping for the servovalve.

The servovalve was driven by two superimposed square waves of variable amplitude and period. The basic wave provided a signal corresponding to the desired working, or plateau, pressure level. The second wave with the same leading edge, a greater amplitude, and a shorter duration was superimposed to provide the overshoot pressure peak. The shape of the overshoot peak pressure wave was varied between a single damped wave to that of a nearly zero damped oscillatory wave by varying the controller loop gain. Additional fine adjustment of wave shape, rate of pressure rise, and pressure level was made by varying the servovalve input wave shape, hydraulic supply pressure, pressure loss in the supply line to the intensifier, and the test article volume. A Boeing-built fail-safe panel provided for system shutdown at loss of 10% of the peak pressure for one cycle or loss of 3% to 5% for several cycles.

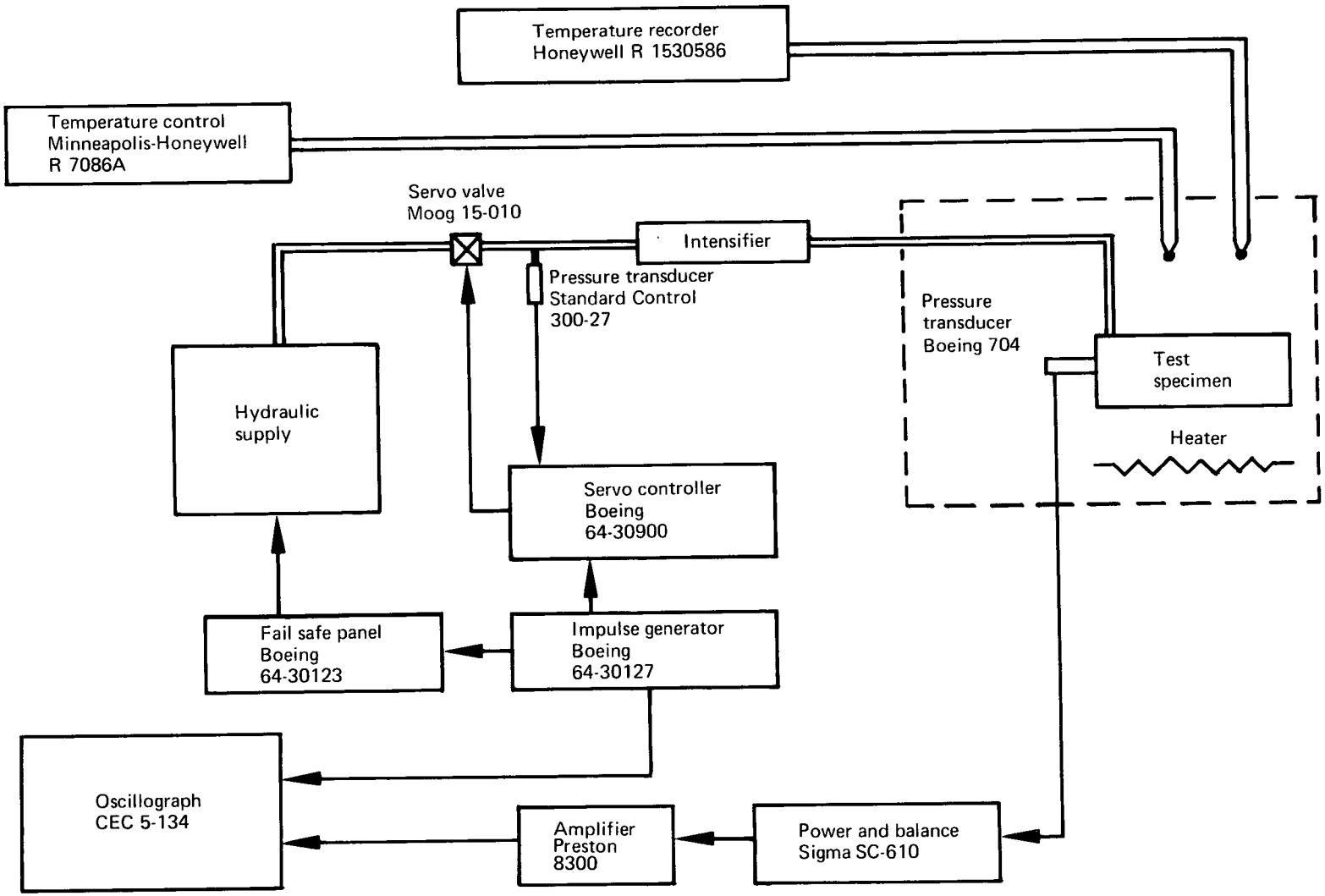

Figure 79.– Impulse test block diagram

Data

A data system was used to determine that proper adjustment had been made to the control system for the specific impulse profile. Cycle programmer output and servovalve current were used as reference control information. Output from a data system transducer, mounted on the test specimen manifold, provided a dynamic impulse pressure trace for visual monitoring. Oven temperatures were controlled automatically and monitored on a vertical temperature indicator. Instrumentation data accuracy is reported in appendix 8.

IMPULSE TEST PERFORMANCE SEQUENCE

Test Article Assembly

Test articles were assembled for four impulse test sequences. This was accomplished using double-ended housings with a central pressure supply port to test first-stage seals and two capped, single-ended housings ganged in parallel to test second-stage seals. The configurations tested together were:

- First-stage 0.0254 m (1.0 in.) 30% balanced and 50% balanced seals
- First-stage 0.0635 m (2.5 in.) 30% balanced and 70% balanced seals
- Second-stage 0.0254 m (1.0 in.) chevron and 0.0635 m (2.5 in.) K-section seals
- Second-stage 0.0254 m (1.0 in.) K-section and 0.0635 m (2.5 in.) chevron seals

Seals were installed by wetting the seal and gland surfaces with hydraulic fluid and using finger pressure to position the individual parts on the rod. The seal housing bushing was then used to push the seal assembly into its proper position in the gland. No sticking or binding was encountered during installation.

Test Operation

After the test article and data transducer were installed on the test manifold, a system pressure of 6.894×10^5 N/m^2 (100 psig) was applied to the intensifier and test article to allow air to be bled from the system. Full system pressure was thereafter applied and the servo controller used to manually vary pressure from zero to maximum to check for system leaks and control system stability.

The test data system was calibrated and the pressure impulse profile set to the requirements of figure 34 by:

- Adjusting the cycle programmer offset control to place the pressure plateau at the correct level
- Opening the programmer's leading edge width control just far enough to obtain desired peak pressure
- Adjusting the power supply pressure as necessary to obtain the correct peak pressure amplitude
- Adjusting the servo controller gain to shape the overshoot wave to the desired profile

Recordings were made to determine pressure rise, which was calculated as follows:

P = peak pressure in psig

$\Delta 1$ = time at 10% P (sec)

$\Delta 2$ = time at 90% P (sec)

Rate of rise in $N/m^2/sec$ (psig/sec) = $(0.9P - 0.1P)/(\Delta 2 - \Delta 1)$. This is the straight line slope of the pressure-time trace.

The 3-to-1 intensifier used to boost peak pressure during first-stage seal testing was reversed and used as a deboost cylinder for the low-pressure impulse test of the second-stage seals. In addition, the accumulator precharge was adjusted and the isolation tube size reduced to provide added correction to obtain the lower rate of rise for testing second-stage seals.

Heater controls were adjusted to maintain seal housing temperatures at the level prescribed for each segment of the impulse test as stated on table II. During testing, leakage was measured by collection in burettes or by visual monitoring where leakage was only an infrequent drop.

Posttest Inspection

The seals that completed impulse tests were examined for structural damage, cracking of the seal material, and contact surface polishing. The above were not considered as conditions of seal failure unless the leakage during the test was greater than the allowable. The inspection was performed by unaided visual observation to make a qualitative description of the seal, supplemented by observations using a microscope.

APPENDIX 5

SEAL FRICTION–TEST SYSTEM DESCRIPTION AND OPERATING SEQUENCE

TEST SYSTEM DESCRIPTION

Test Article

Each article to be tested to evaluate static and dynamic friction consisted of a pair of identical configuration seals installed in a double-ended housing. Existing hardware was used to the greatest extent possible to provide the necessary housings as illustrated in figure 80. First-stage seals were tested separately from second-stage configurations such that when first-stage seals were installed, second-stage glands were vacant, and vice versa. Friction test measurements provided data for the combined friction force of both seals in the double-ended housing.

Test Operation Components

The hydraulic system used in friction testing, shown in figure 80, is an existing test rig used for research evaluations of rod and piston seal friction. It consists of the following major components:

Hydraulic power supply	Rucker 20-gpm pumping unit
Solenoids	Adel three-way valves
Drive actuator	Miller 0.1016 m (4 in.) bore
Transfer cylinder	Miller 0.0508 m (2 in.) bore
Boost pump	Sprague, air-driven unit
Pressure reducing valve	Denison
Test actuator	Boeing laboratory equipment (SK11-11751)
Environmental enclosure	Boeing laboratory equipment

The MIL-H-5606 (red oil) hydraulic power supply was used to provide pressurized fluid flow in the drive actuator loop and provide pressurization of the reference 4 seal test fluid in the transfer cylinder. The drive actuator provided the mechanical power for motion of the rod through the seals under evaluation in the test actuator. The load transducer was rigidly attached to the test actuator rod and connected to the drive actuator with self-aligning bearings. The solenoids were used to control the oscillatory movement of the rod.

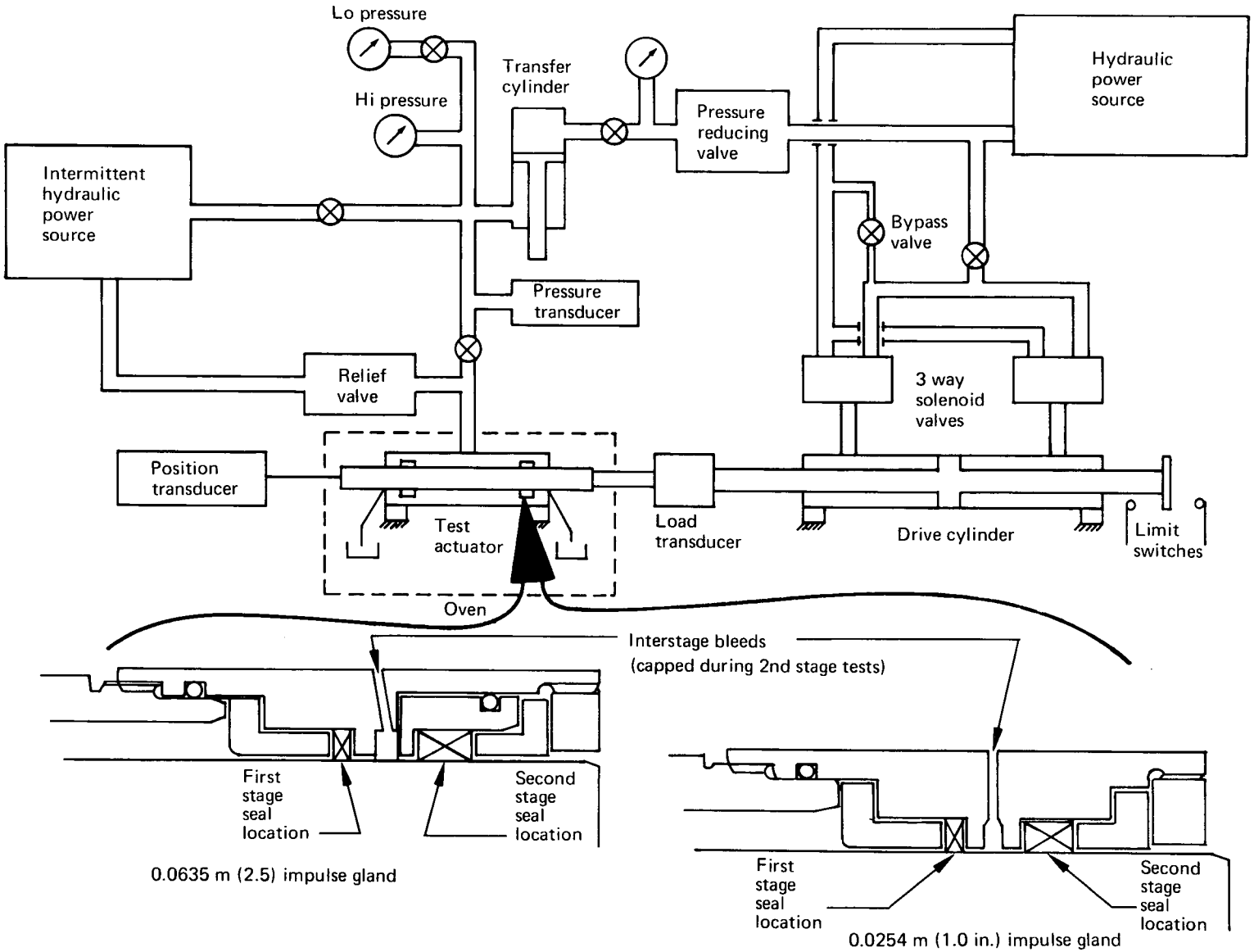

Figure 80.– Hydraulic installation, friction test

Fluid in the test actuator was kept under a static head controlled by the pressure-reducing valve setting. The reservoir allowed refilling of the transfer cylinder, using the air-driven pump, if volume became depleted due to seal leakage. The reservoir also acted as a receiver tank for fluid expanded in the test actuator by elevating temperature.

Control Circuit and Instrumentation

The control system for the existing friction test equipment was assembled prior to the reported contract for manual operation. A conversion to automatic control would have made testing more convenient for the operator but was not accomplished in the interest of economy. Components of the control system are shown in figure 81.

The solenoids, actuated through the stroke control limit switch circuit, controlled the reversals of motion. Speed of translation was manually adjusted using a hand-operated needle valve to achieve a given slope of the position-time trace on the direct-write oscillograph. Breakaway was also determined from observation of the position-time trace. Hydraulic pressure levels within the test actuator were set using the pressure-reducing valve and measured by the pressure transducer output recording on the oscillograph. Friction force was measured using the load transducer output reading on the oscillograph. The accuracy of the data system is described in appendix 8.

FRICTION TEST PERFORMANCE SEQUENCE

Test Article Assembly

Test articles were assembled for ten friction test sequences. Only one seal configuration was tested in each sequence; however, two seal assemblies of each configuration were used, one on either end of the test actuator housing. The configurations tested were:

- First-stage 0.0254 m (1.0 in.) 30% balanced, 50% balanced, and 70% balanced seals
- First-stage 0.0635 m (2.5 in.) 30% balanced, 50% balanced, and 70% balanced seals
- Second-stage 0.0254 m (1.0 in.) chevron and K-section seals
- Second-stage 0.0635 m (2.5 in.) chevron and K-section seals

Seals were installed by wetting the seals and gland surfaces with hydraulic fluid and using finger pressure to position the individual parts on the rod. The seal housing bushing was then used to push the seal assembly into their proper positions in the gland. No sticking or binding was encountered during installation.

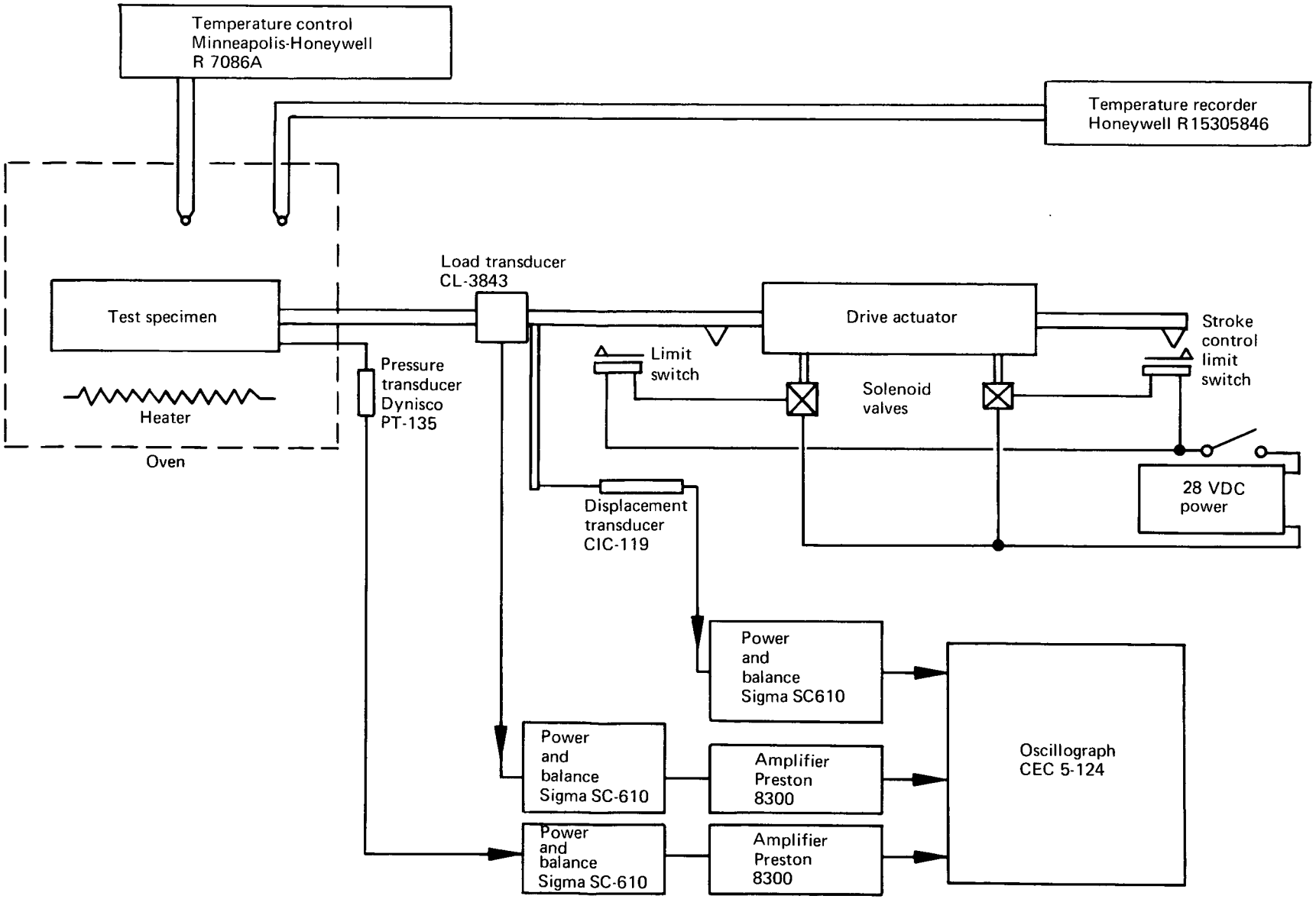

Figure 81.– Friction test block diagram

Testing Operation

The test actuator was installed in the system and aligned so that no side load would be introduced to the seals being tested. This was accomplished by positioning the rod in the test actuator at various rotational positions and checking for free movement of the attaching pin between the rod and the load cell. Any binding indicated the presence of side load.

The test actuator was pressurized to 2.068×10^7 N/m^2 (3000 psig) and the drive actuator operated at 0.0635 m/sec (2.5 in./sec) to accumulate 100 cycles on the test seals as a run-in prior to friction testing. The test sequence was then started by adjusting the test actuator temperature and pressure to the desired conditions. At each set condition static breakaway and running friction at 0.0635 m/sec (2.5 in./sec) were determined. Data were recorded for five repeated tests at each condition to obtain a base for statistical averaging.

Data Reduction

The static and dynamic friction values for a single seal were determined from the test data by averaging the data from the multiple runs to obtain a friction value for the pair of seals tested. One-half of this value was considered to be the friction for one seal based on the two seals of a single configuration being identical. The error introduced was that, within any given rod stroke, motion along the face of one seal was in the opposite direction of the motion (upstream to downstream) to that along the face of the other seal. This error was considered to be within instrument measurement accuracy.

Seal stick-slip friction, or chatter, produced data as a band of high-frequency friction oscillations within which a single clearly defined average was difficult to isolate. The best determination was selected as the center of the darkest portion of the high-frequency band, this being the statistical mean of the friction force within the chatter band. These average measurements were compared against the friction criteria established under Design Requirements in section III of this report.

Leakage was measured in a collecting tank and was not a major measurement in the friction tests because the test time at any single condition was very short. Leakage was qualitatively significant with the 70% balanced first-stage seal, where excessively high leakage was noticed at intermittent intervals.

Posttest Inspection

The seals that completed friction tests were examined for structural damage, cracking of the seal material, and contact surface polishing by unaided visual observation supplemented by observations using a microscope.

APPENDIX 6

THEORETICAL PRESSURE BALANCING ANALYSIS OF CONTRACTING FIRST-STAGE SEALS

INTRODUCTION

Pressure balancing of first-stage seals is desirable due to the otherwise large pressure differentials across the seal interface. Prime advantages are to reduce the net radial and axial forces acting on the seal. This feature tends to minimize the friction and wear between the seal and the contacting surface.

A high-speed digital computer program was written to evaluate the radial and axial sealing forces for various degrees of balancing. The model used for the analysis is shown below:

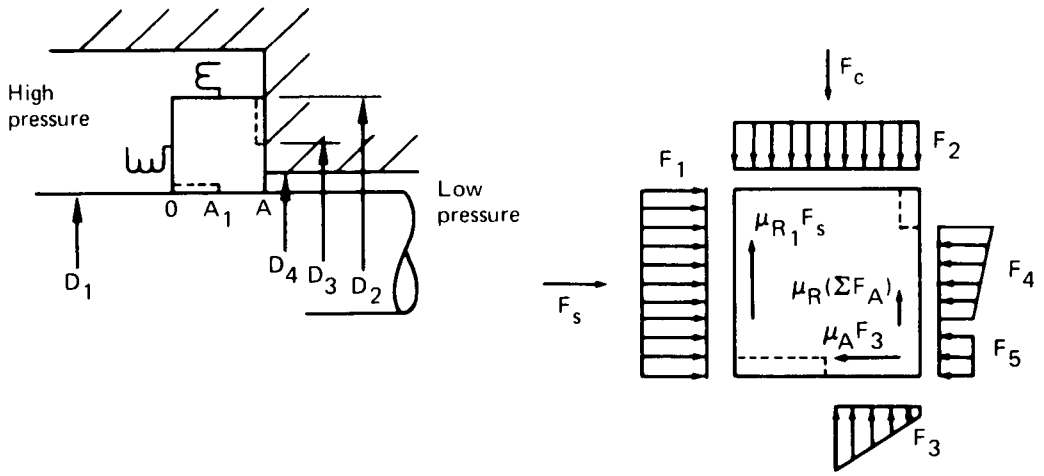

EQUATIONS

Forces in the Radial Direction

$F_2 = P_1 \pi D_2 A (A - A_1)$
F_C = initial preset compression
$F_3 = [(P_1 + P_2)/2] \pi D_1 (A - A_1)$

By balancing the forces in the radial direction the resultant force obtained is:

$$F_R = F_2 + F_C - F_3$$

Forces in the Axial Direction

$F_1 = P_1 (\pi/4) (D_2^2 - D_1^2)$
$F_4 = (P_1 + P_2) (\pi/4) (D_3^2 - D_4^2)/2$
F_S = spring force
$F_5 = P_2 (\pi/4) (D_4^2 - D_1^2)$

By balancing the forces in the axial direction the resultant force obtained is:

$$F_A = F_1 + F_S - F_4 - F_5$$

Net Sealing Forces

Net sealing forces in the radial direction (F_{RN}) and in the axial direction (F_{AN}) are dependent on the sealing forces F_R and F_A and on the values of coefficients of friction.

$F_{RN} = F_R - \mu_r F_A - \mu_{r_1} F_S$
$F_{AN} = F_A - \mu_A F_3$

where:

μ_r = downstream radial friction coefficient (along the axial sealing face)
μ_A = axial friction coefficient (along the radial sealing face between the seal and the rod)
μ_{r_1} = upstream radial friction coefficient (between the spring and the axial sealing force)

In developing these equations, it was assumed that there was a very thin hydrodynamic film layer of oil between the inside surface of the seal and the rod, and between the downstream surface of the seal and the gland.

Net Pressure Forces

Net pressures in the radial direction (P_{RN}) and in the axial direction (P_{AN}) are:

$$P_{RN} = F_{RN}/\pi D_1 (A - A_1) = [P_1(D_2/D_1) - (P_1+P_2)/2] - \mu_r F_A/\pi D_1 A(1 - A_1/A) - \mu_{r1} F_S$$

$$P_{AN} = F_{AN}/(\pi/4) (D_3^2 - D_4^2)$$

These pressures are indicative of the unit pressures on the sealing surfaces and may affect the values of friction coefficients.

Leakage Flow

Seal leakage flowing through the annular gap between the seal and the rod can be computed with the program. A gap width of $b = 5.08 \times 10^{-6}$ m (50 000 angstroms) was assumed. This is equivalent to a finish grind on the rod surface. Assuming a fully developed laminar flow in the fluid film between the rod and the seal, the ideal leakage flow Q is given by

$$Q = \frac{\pi D_1 (P_1 - P_2) b^3}{12\mu (A - A_1)}$$

The effect of unit contact pressure is to reduce the leakage flow. Thus the effective flow Q_1 may be written as

$$Q_1 = Q \frac{(P_1 - P_2) - P_{RN}}{P_1 - P_2}$$

APPLICATION

Inputs needed to the program are the seal dimensions, friction value, and the radial gap clearance. The computer program calculates all the forces in the axial and radial direction, leakage flows, and contact pressures.

The first-stage seals used in the reported contract were evaluated on the computer. Input data was as follows:

Smaller Seal

ID = 0.0253 m (0.996 in.)

OD = 0.0291 m (1.146 in.)

Width = 0.0023 m (0.0895 in.)

μ axial = 0.05 (assumed value—actual value is variable with contact pressure by an as yet undetermined relationship)

μ radial = 0.10 (assumed value)

Larger Seal

ID = 0.0570 m (2.496 in.)

OD = 0.0679 m (2.674 in.)

Width = 0.0031 m (0.1205 in.)

μ axial = 0.05 (assumed value)

μ radial = 0.10 (assumed value)

The computer program was run for various axial and radial balancing percentages and different system pressures. However, since the test seal was fabricated with zero axial balancing only those results pertaining to that configuration are reported.

RESULTS

Figure 82 shows net radial sealing forces for different system pressures and different degrees of balancing for the small and large seals, respectively.

The data show that the net radial sealing forces decrease with increasing balancing percentages at any given system pressure. The net sealing forces are larger for the 0.0635 m (2.5 in.) diameter seal than for the 0.0254 m (1.0 in.) diameter seal.

Figure 82 also shows the variation of average radial contact pressure on the sealing surface. The radial contact pressure decreased with increasing balancing percentage for all system pressures. As expected, the unit pressure was directly proportional to system pressure for both seal sizes.

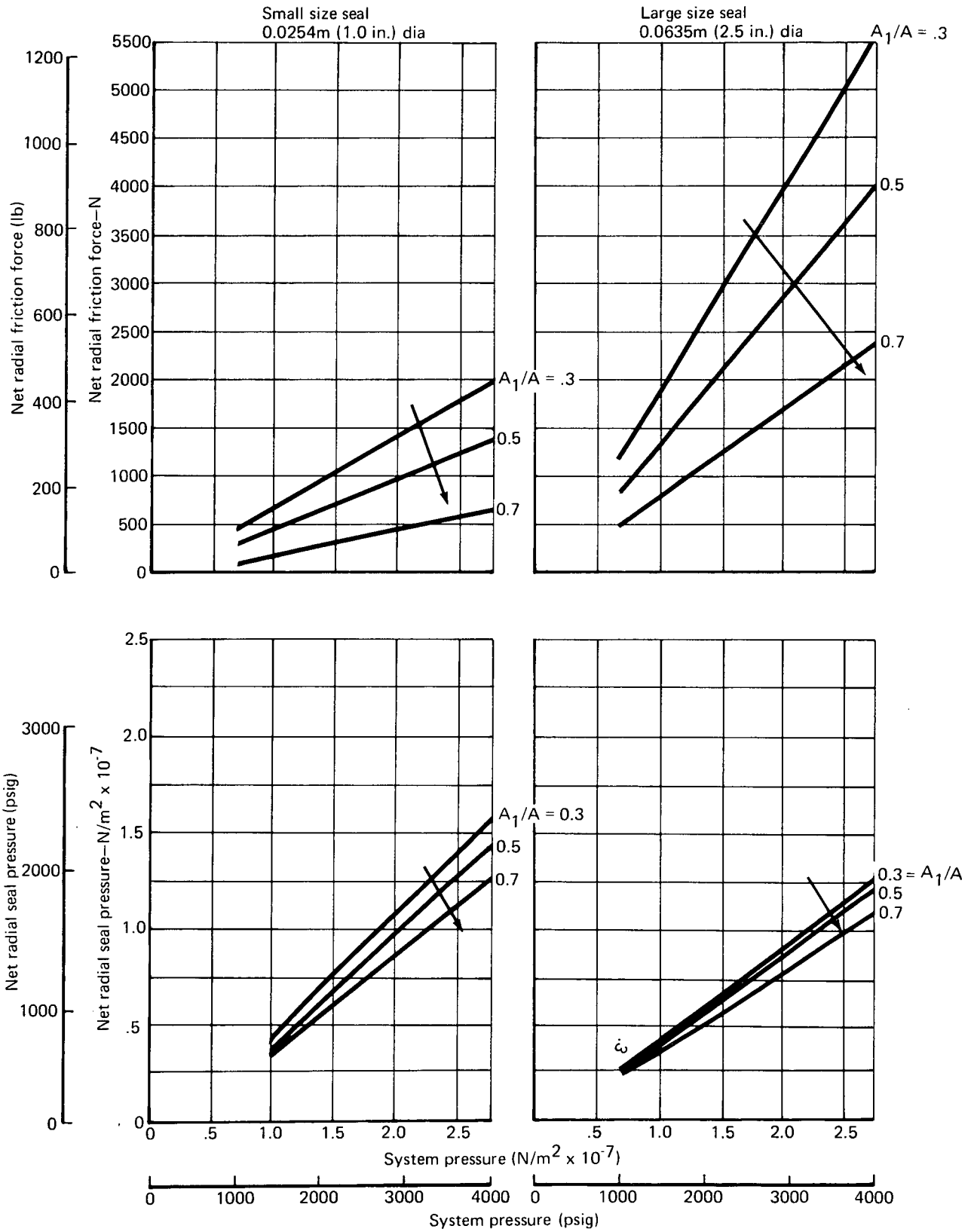

Figure 82.– Pressure balancing forces and pressures

Figure 83 shows the variation of the average contact pressure (P_{RN}) of both seals for various pressure balancing percentages. The data trend for both seals was a decrease in contact pressure for increased balancing percentages. The smaller seal had a larger contact pressure than the larger seal. This was due to the effect of D_2/D_1 diameter ratio in the P_{RN} equation. Figure 83 shows that, beyond 60% balancing, contact pressure drops rapidly. This occurs due to the decrease in contact area with higher balancing percentage. The sealing force with increased balancing eventually becomes equal to the friction force along the radial face of the seal. At this condition ($A_1/A \approx 0.8$) the net radial sealing force becomes zero.

CONCLUSIONS

The following conclusions may be derived from the analysis:

(1) Pressure balancing is desirable on all seals as it reduces the net sealing loads on the seal and increases the life of the seal.

(2) The optimum degree of balancing is dependent on the seal size. It is desirable to use as large a balancing percentage as permissible to reduce radial sealing forces. There is approximately a 30% change in sealing force for a 20% change in pressure balancing at 2.758×10^7 N/m^2 (4000 psig).

(3) A realistic upper limit for only axial balancing is near 60% to maintain an acceptable contact pressure for fluid containment and to avoid conditions of rapid variation of contact pressure as a function of balancing.

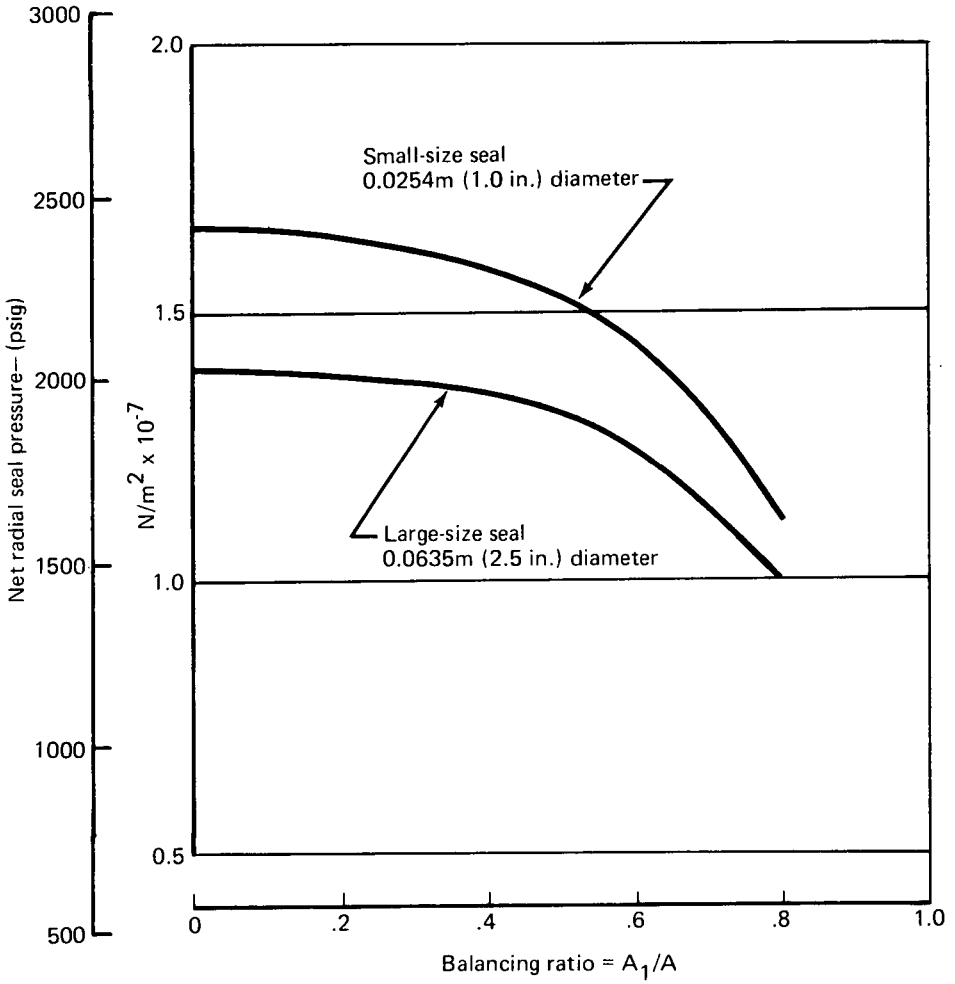

Figure 83.—Net pressure variation with balancing ratio

APPENDIX 7

ENDURANCE TEST–SYSTEM DESCRIPTION AND OPERATING SEQUENCE

TEST SYSTEM DESCRIPTION

Test Article

Each test article consisted of a two-stage rod seal configuration with the inner-stage cavity vented to return pressure. Actuators with 0.0254 m (1.0 in.) and 0.0635 m (2.5 in.) nominal rod diameters were evaluated. The larger rod seal configuration consisted of a 50% pressure balanced, step cut, contracting ring first stage and a K-section assembly second stage. These seals were assembled in the module configuration shown on figure 84, which was in turn installed in the actuator as shown on figure 85. The smaller rod seal configuration used the same first-stage design with a chevron assembly second-stage seal. The seals in the smaller actuator were installed independently in the actuator end cap, as shown in figure 86.

Existing test actuator components were used to the greatest extent possible. The 0.0635 m (2.5 in.) actuator minimum modifications needed to utilize the modular seal concept are defined in reference 21. The 0.0254 m (1.0 in.) actuator assembly was modified as shown in reference 22.

Test Operation Components

The test installation used in endurance testing is shown in figure 87 and is an existing rig developed primarily for testing actuator seals. The test installation consists of a load system, the hydraulic power supply with its associated plumbing, and the control electronics. The major power and loading components are as follows:

Oven–Dispatch model 203

High-Temperature Power Supply–Auto Controls Lab, Inc. model 4586

Load Fixture–Boeing laboratory equipment

Filter–Micro Porous (25 micron absolute)

Relief Valve–Republic 604B-12-8-2

Servo Valve Block–Boeing laboratory equipment (SK11-9605-1)

Accumulator–Hydrodyne 6.895×10^7 N/m^2 (10 000 psig)

The load system required for this series of tests consisted of a dual torsion bar rig capable of providing resisting torque for two independent actuators. The individual torque bar lengths were adjusted to provide a torsional load such as to require full system pressure at full stroke for each actuator. The linear actuator output was reacted to the torsion bar

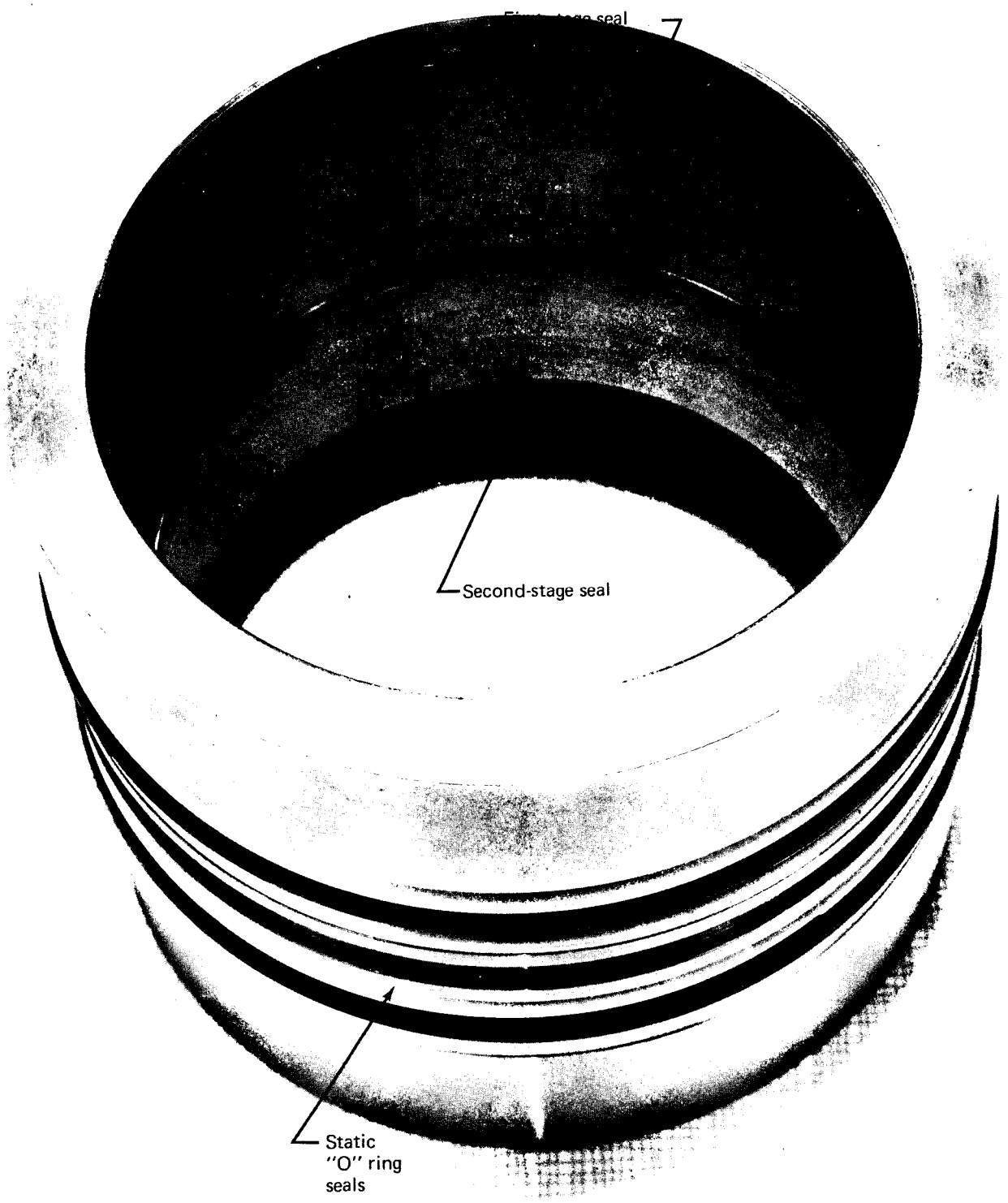

Figure 84.—0.0635m (2.5 in.) two stage seal module

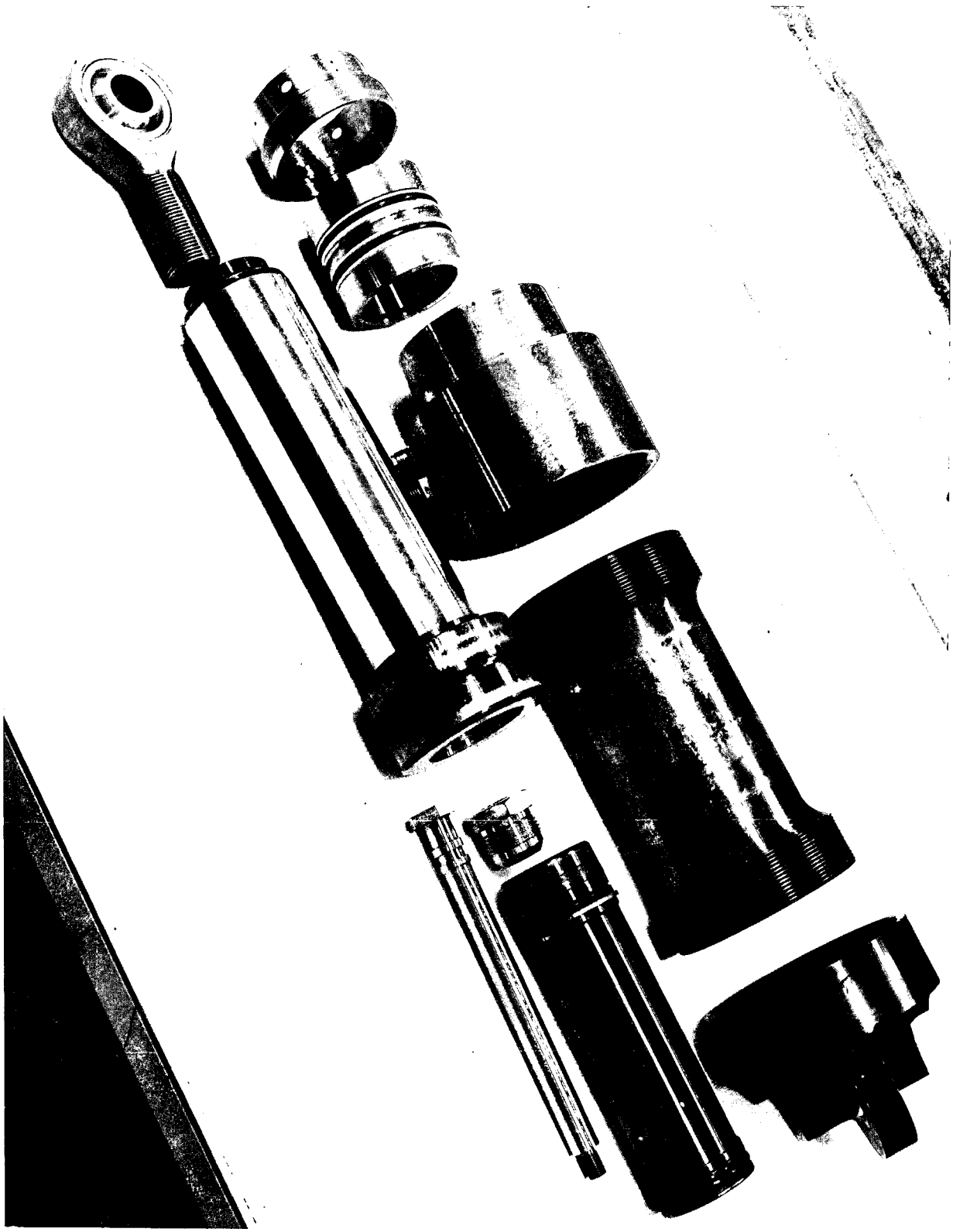

Figure 85.— 0.0635m (2.5 in.) endurance test actuator

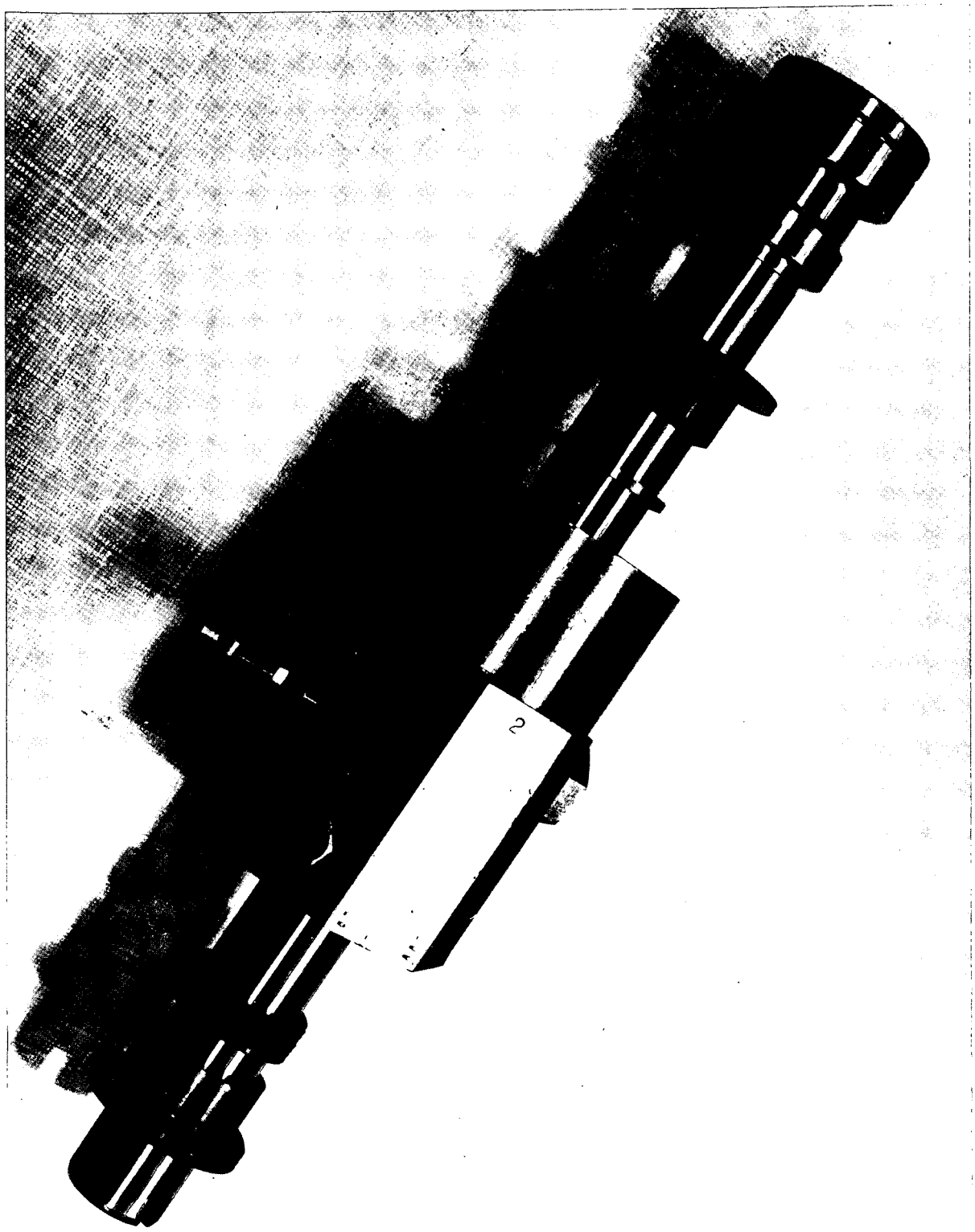

Figure 86.— 0.0254m (1.0 in.) endurance test actuator

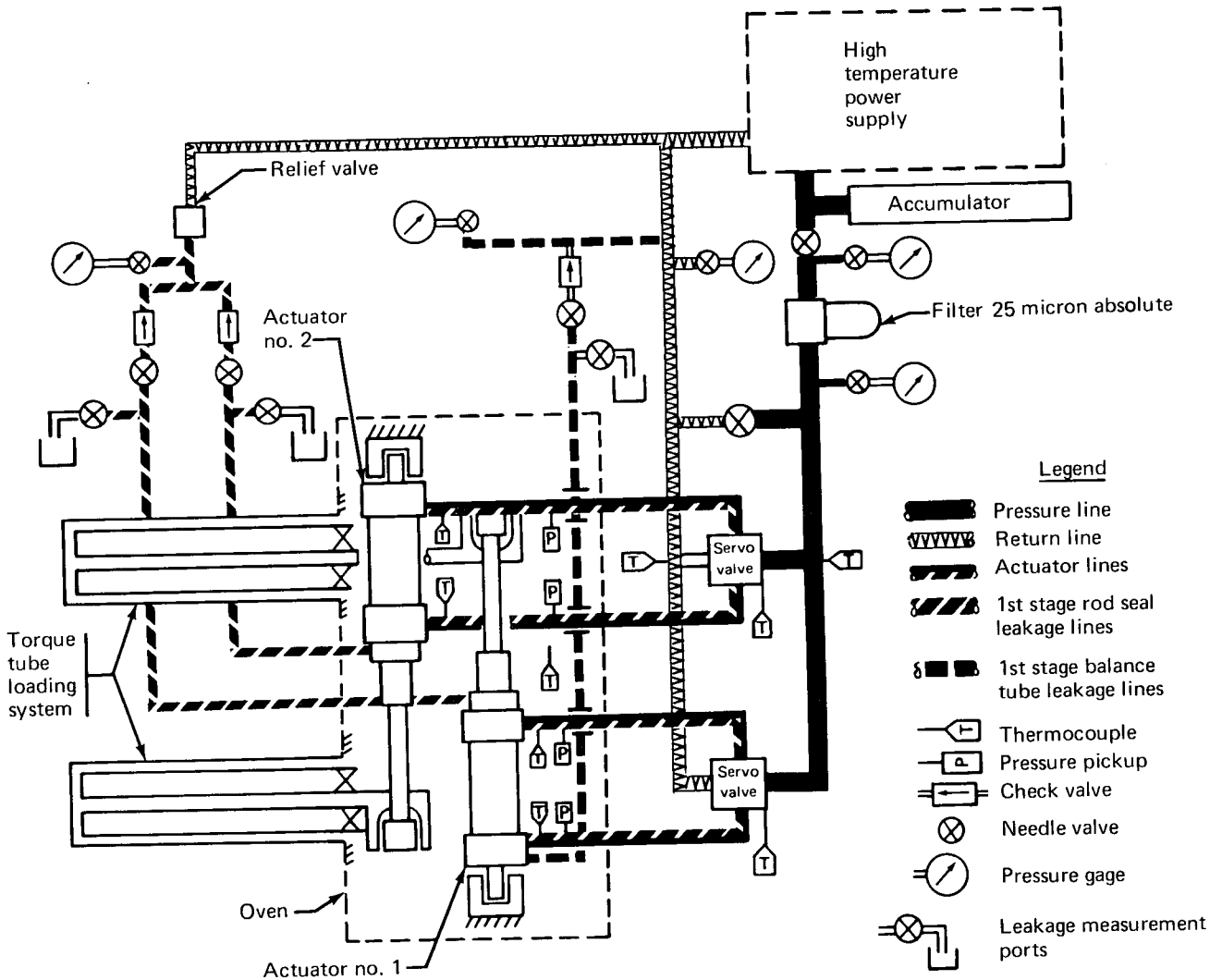

Figure 87.—Hydraulic installation, endurance test

through a lever arm and bearing assembly to simulate an airplane control surface hinge point. Self-aligning bearings were used for both actuator head and rod end connection points. No additional side load, other than bearing friction, was applied. The mounting base of the load system and the actuators were installed in the test oven. The torsion bars, due to their size, extended through the back of the oven and were supported externally at their extreme ends by pedestals. Hydraulic power was supplied by the 1.262×10^{-3} m^3/sec (20 gpm)Autocontrols Laboratory high-temperature power supply complete with all pressure and temperature controls. This unit supplied WS8228 (ref. 4) hydraulic fluid at 2.758×10^7 N/m^2 (4000 psig) and 450°K (350°F) to the test article. The 9.464×10^{-3} m^3 (2.5 gal) accumulator was located in the supply line between the power supply and the test rig. In addition to filtration within the power supply, a 25-micron-absolute filter was located in the supply line downstream of the accumulator. The cavities between the first- and second-stage seals in the test actuators were vented to return through relief valves to maintain second-stage seal pressure at 1.379×10^6 N/m^2 (200 psig). Additional check and isolation valves allowed measurement of first-stage leakage without interrupting cycling.

Control Electronics

The control of test operation cycling was provided by a closed-loop electrohydraulic flow control loop incorporating position feedback.

Components were arranged as shown in figure 88. The electrical loop consisted of the feedback transducer (LVDT), carrier amplifier, Boeing standard controller, and servo valve with the total loop completed mechanically through the fluid-powered actuator rod. The servo controllers were driven with a common function generator with a sinusoidal cycle at the required period. The actuator stroke amplitude and position were set at the servo controller command for the flow control servo valve. A failure detection system was provided which would sound an audible and visual alarm with loss of system pressure or an overtemperature condition.

Actuator head and rod end cylinder pressures were measured for both actuators and recorded on a direct-write oscillograph. The individual actuators' positions were also recorded on the oscillograph and monitored during test to ensure that proper position and stroke amplitudes were maintained.

Oven ambient, oil, and component temperatures were recorded on a stamping-type temperature recorder.

Instrumentation and recorded data accuracies are reported in appendix 8.

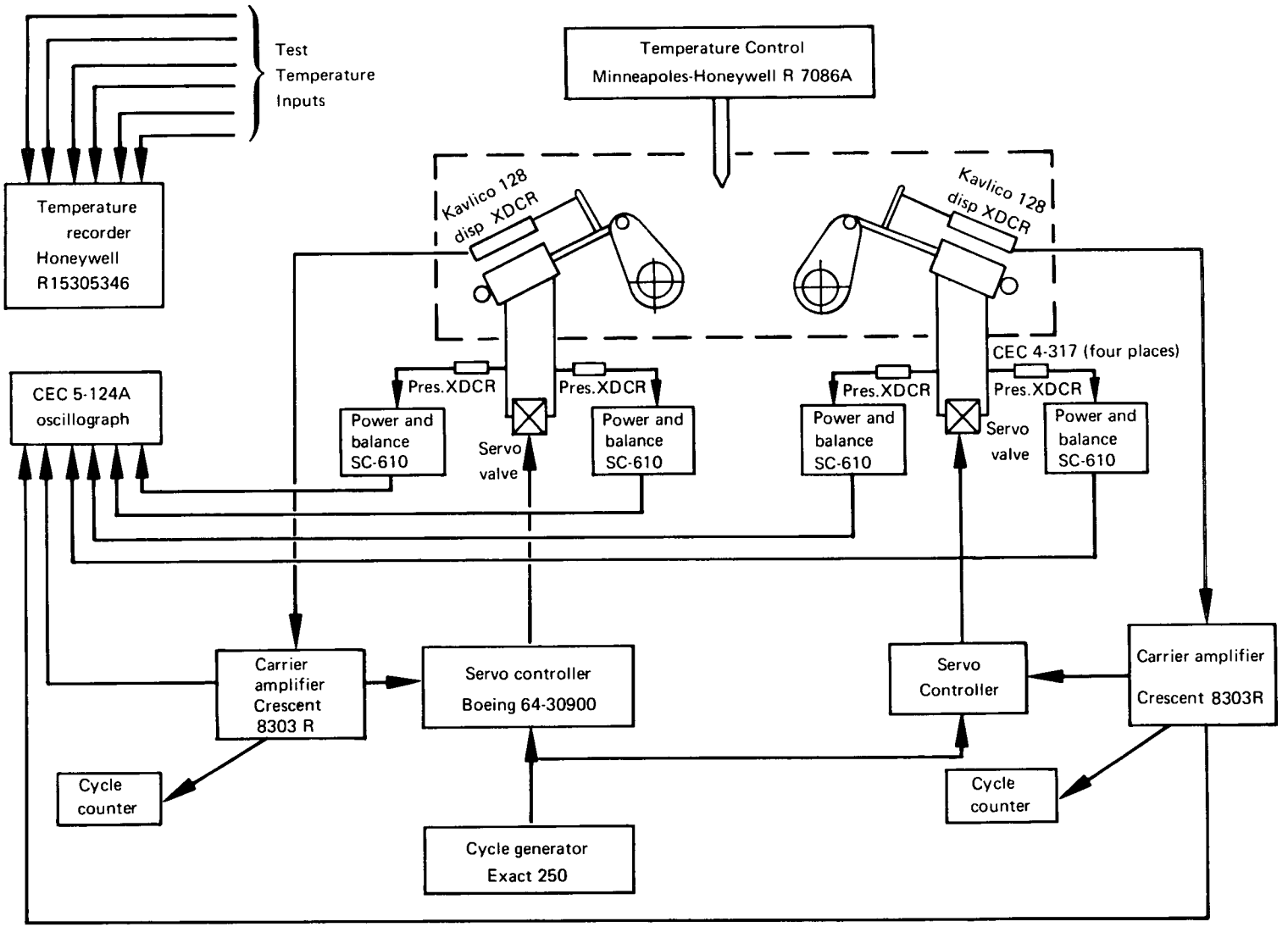

Figure 88.— Endurance test block diagram

ENDURANCE TEST PERFORMANCE SEQUENCE

The unpressurized assembled test actuators were manually inspected for binding. A proof pressure was then applied and pretest leakage rates established for the first-stage seals at room temperature.

Test Operation

After the test actuators and data transducers were installed in the loading fixture, a reservoir pressure of 3.442×10^5 N/m^2 (50 psig) was applied and air bled from the hydraulic system. A room temperature checkout was conducted, starting with a system pressure of 6.894×10^6 N/m^2 (1000 psig) and increased in incremental steps to working pressure while cycling. The test sequence defined in table I was established by adjusting:

- The hydraulic power supply to 450° K (350° F) temperature and 2.758×10^7 N/m^2 (4000 psig) nominal working pressure.
- The oven controls to maintain the test temperature for the mass of the actuators and fixture.
- The function generator to the cycle rate required by the test schedule.
- The servo controller to provide the desired actuator neutral cycling point and rod stroke.
- The interstage relief valve to maintain 1.379×10^6 N/m^2 (200 psig).

During testing, first-stage leakage was measured by its collection in burettes. The second-stage leakage was measured by visual observation.

Test cycles, supply and second-stage fluid pressures, seal leakage, and system temperatures were recorded each hour. Cylinder pressures were recorded at the start of each day, and actuator position and stroke length monitored continuously during test.

POSTTEST INSPECTION

The seals that completed endurance tests were examined for structural damage, cracking of the seal material, contact surface polishing, and unusual wear. This was conducted by unaided visual observation supplemented by observations using a microscope.

APPENDIX 8

INSTRUMENTATION CALIBRATION AND DATA ACCURACY

Test instrumentation equipment calibrations are traceable through the Boeing flight test calibration laboratory to the National Bureau of Standards. Strain gage bridge-type transducers were calibrated to determine nonlinearity, hysteresis, and R-shunt calibration transfer values. Position transducers were end to end calibrated in place by a calibrated scale/visual technique.

PRESSURE

Transducer accuracy within	±0.75% full scale
Power and balance/conditioning within	±0.1% full scale
Oscillograph accuracy within	±2.0% full scale
Pressure measuring system accuracy (RSS) within	±2.1% full scale

DISPLACEMENT

Transducer accuracy within	±0.1% full scale
Signal conditioning within	±0.1% full scale
Oscillograph accuracy within	±2.0% full scale
Displacement measuring system accuracy (RSS) within	±2.0% full scale

TEMPERATURE

Thermocouple accuracy within	±1.11° K (±2° F)
Temperature recorder within	±2.5° K (±4.5° F)
Temperature measuring system accuracy (RSS) within	±2.2° K (±4.0° F)

LOAD

Transducer accuracy within	±0.1% full scale
Signal conditioning within	±0.1% full scale
Oscillograph accuracy within	±2.0% full scale
Load measuring system accuracy (RSS) within	±2.0% full scale

APPENDIX 9

LIST OF SYMBOLS

Symbols identifying a measured quantity:

A	area
A, B, C, D, E	sequence of load types
B	balancing ratio
b	average clearance between rod and seal
c	one-half cross-section thickness
D	diameter
E	modulus of elasticity
F	force
[F]	force matrix
f_a	alternating stress
f_m	mean stress
G	gland depth
ID	inside diameter
[K]	stiffness matrix
K_I	curved beam inside fiber stress correction factor
K_O	curved beam outside fiber stress correction factor
K_T	stress concentration factor due to notch sensitivity
L	length of seal face
OD	outside diameter
P	pressure
Q	flow
R	radius
RSS	root sum square value of the independent errors
T	cross-section thickness
t	cross-section thickness
x, y, z	coordinate planes of direction
$\bar{x}, \bar{y}, \bar{z}$	opposite coordinates to x, y, z
α	leg angle
β	backup block contract angle
Δ	time
δ	preset compression of seal from its free shape
ϵ	eccentricity between rod and seal
μ	friction coefficient
υ	fluid viscosity
$[\rho]$	displacement matrix

σ	fatigue stress
%	percent
$\geqslant$	greater than or equal to
$<$	less than
$\approx$	approximately equal to

Subscripts:

A	axial
a	axial
alt	alternating
c	compression
d	downstream
N	net
opt	optimum
R	radial
r	upstream radial
r_1	downstream radial
S	spring
U	upstream
y	plane of stress direction
1, 2, 3, 4, 5, 6, 7	various alternate configurations, sizes, or locations

Symbols indicating units of measure:

SI units	English units	Measurement of:	Definition
N/m^2	psig ksi	pressure, stress	Newton per square meter = (pound per square inch) (6894.76) kip per square inch = (pound per square inch) (0.001)
m	in. ft	length	meter = (inch) (0.0254) meter = (foot) (0.3048)
m^2	$in.^2$	area	square meter = (square inch) (6.944×10^{-3})
m^3	$in.^3$	volume	cubic meter = (cubic inch) (1.639×10^{-5})
N	lbf	force	Newton = (pound force) (4.4482)
sec	sec min hr	time	second = (minute) (60) minute = (hours) (60)
m^3/sec	$in.^3/min$ gpm	flow	cubic meter per second = (cubic inch per minute) (2.73118×10^{-7}) gallon per minute = (cubic inch per minute) (4.329×10^{-2})
Hz	Hz cps	frequency	Hertz = cycle per second
π	π		$\pi = 3.141592$
rad	°(deg)	angle	radian = (degree) (0.01745)

All original calculations were performed in English units and converted to SI units for documentation. Dimensioned parts are not expressed in SI units because such dimensioning would reduce the usefulness of such drawings and sketches.

REFERENCES

1. J. Lee, *High-Temperature Hydraulic System Actuator Seals for Use in Advanced Supersonic Aircraft*, NASA CR-72354 (AIR-005301), Fairchild Hiller–Republic Aviation Division (contract NAS3-7264), September 1967.

2. J. Lee, *Development of High Temperature Polyimide Rod Seals*, NASA CR-72563 (AIR-23917), Fairchild Hiller–Republic Aviation Division (contract NAS3-11170), August 1969.

3. *Hydraulic Power Subsystem Specification–Model B-2707*, D6A10120-2, The Boeing Company, April 1970.

4. *Hydraulic Fluid Synthetic Base, Serviceable Over the Range -50°F to 450°F*, BMS 3-10, The Boeing Company, April 1970.

5. *General Requirements for Servoactuator Assemblies–Model B-2707*, D6A11144-1, The Boeing Company, April 1970.

6. *Specification Control Drawing–Master servo Unit, Model B-2707*, 60A10086, The Boeing Company, May 1970.

7. *Specification Control Drawing–Power Control Unit, Outboard Flaperon, Model B-2707*, 60A10207, The Boeing Company, May 1970.

8. *Specification Control Drawing–Power Control Unit, Upper Rudder, Model B-2707*, 60A10202, The Boeing Company, May 1970.

9. *Specification Control Drawing–Power Control Unit, Middle Rudder, Model B-2707*, 60A10203, The Boeing Company, May 1970.

10. *Specification Control Drawing–Power Control Unit, Lower Rudder, Model B-2707*, 60A10204, The Boeing Company, May 1970.

11. *Digital Computer Techniques for the Analysis of Hydraulic System Dymanics*, D6-58399, The Boeing Company, April 1969.

12. F. E. Ehlers, *Stress Distribution and Displacements in a Lubricated Elastic Seal*, D180-14141-1, The Boeing Company, September 1971.

13. *Vespel Precision Parts Design Handbook*, duPont de Nemours & Co., 1970.

14. *Application of Polyimide Actuator Rod Seals,* D6-54309, The Boeing Company, April 1970.

15. *Structural Analysis System—Theory Document*, D6-23757-2TN, The Boeing Company.

16. *Military Specification, Gland Design; Packings, Hydraulic, General Requirements for*, MIL-G-5514F, January 1969.

17. *Chevron Rod Seal, 1.0 Inch Inside Diameter*, 64-14047, The Boeing Company (contract NAS3-14317), July 1971.

18. *Chevron Rod Seal, 2.5 Inch Inside Diameter*, 64-14048, The Boeing Company (contract NAS3-14317), July 1971.

19. *K-Section Rod Seal, 2.5 Inch Inside Diameter*, 64-14050, The Boeing Company (contract NAS3-14317), July 1971.

20. *K-Section Rod Seal, 1.0 Inch Inside Diameter*, 64-14049, The Boeing Company (contract NAS3-14317), July 1971.

21. *Actuator Assembly—2.5 Inch Diameter (Test Only)*, 64-14051, The Boeing Company, August 1971.

22. *Hydraulic Actuator—1.0 Inch Diameter (Test Only)*, 64-14052, The Boeing Company, August 1971.

DISTRIBUTION LIST

Addressee	Copies
NASA Headquarters Washington, D.C. 20546	
Attn: N. F. Rekos	1
A. J. Evans	1
J. Maltz	1
FAA Headquarters 800 Independence Ave. SW Washington, D.C. 20553	
Attn: F. B. Howard	1
NASA Lewis Research Center 2100 Brookpark Road Cleveland, Ohio 44135	
Attn: A. Ginsburg	1
E. E. Bisson	1
R. L. Johnson	1
L. P. Ludwig	1
M. A. Swikert	1
C. H. Voit	1
L. W. Schopen	1
W. R. Loomis	1
B. Lubarsky	1
W. F. Hady	15
Report Control Office	1
Library	1
Technology Utilization Office	1
NASA Scientific and Technical Information Facility P.O. Box 33 College Park, Md. 20740	
Attn: NASA Representative	2
NASA Langley Research Center Langley Station Hampton, Va. 23365	
Attn: Mark R. Nichols	1

Addressee	Copies
United States Air Force Wright-Patterson Air Force Base Dayton, Ohio 45433	
Attn: J. L. Morris	1
S. Prete	1
R. L. Adamczak	1
L. M. Peterson	1
R. E. Headrick	1
Commanding Officer U.S. Navy Underwater Weapons Research and Engineering Section Newport, R.I. 02890	
Attn: Technical Library	1
U.S. Navy Marine Engineering Laboratory Friction and Wear Division Naval Academy Annapolis, Md. 21490	
Attn: R. B. Snapp	1
Department of the Army U.S. Army Aviation Materials Labs. Ft. Eustis, Va. 23604	
Attn: John W. White, Chief Propulsion Division	1
U. S. Naval Air Development Center Aeronautical Materials Department Warminster, Pa. 18974	
Attn: A. L. Lockwood	1
U. S. Naval Research Laboratory Washington, D.C. 20390	
Attn: Dr. William Zisman	1

DISTRIBUTION LIST (continued)

Addressee	Copies
Department of the Navy Washington D.C. 20013 Attn: Bureau of Naval Weapons	
A. B. Nehman	1
C. C. Singleterry	1
Bureau of Ships, Harry King	1
U.S. Army Ordnance Rock Island Arsenal Laboratory Rock Island, Ill. 61201 Attn: R. LeMar	1
AVCOM AMSA VEGTT Mart Building 405 S. 12th St. St. Louis, Mo. 63166 Attn: E. England	1
National Technical Information Service Springfield, Va. 22151	35
Aerospace Corporation Building A-2 P.O. Box 95085 Los Angeles, Calif. 90045 Attn: James Todd	1
Aerojet-General Corporation 5100 W. 164th St. Cleveland, Ohio 44142 Attn: W. L. Snapp	1
American Brake Shoe Co. Abex-Aerospace Division 3151 W. Fifth St. Oxnard, Calif. 93032 Attn: J. A. Mileti	1
Avco Corp. Lycoming Division 550 S. Main St. Stratford, Conn.	
Attn: R. Cuny	1
Mr. Saboe	1
Battelle Memorial Institute Columbus Laboratory 505 King Ave. Columbus, Ohio 43201 Attn: C. M. Allen	1
B. F. Goodrich Co. Aerospace & Defense-Products Div. Troy, Ohio 45373 Attn: L. S. Blalkowski	1
Borg-Warner Corp. Weston Hydraulics Ltd. Van Nuys, Calif. Attn: K. H. Knox	1
Cartiseal Corp. 634 Glann Ave. Wheeling, Ill. 60090 Attn: R. Voltik	1

DISTRIBUTION LIST (continued)

Addressee	Copies
Chevron Chemical Co. Oronite Division 200 Bush St. San Francisco, Calif. 94120 Attn: T. S. McClure	1
Chicago Rawhide Mfg. Co. 1311 Eston Ave. Chicago, Ill. 60622 Attn: R. Blair	1
Clevite Corp. Aerospace Research 540 E. 105th St. Cleveland, Ohio 44108 Attn: G. F. Davies	1
Continental Aviation and Engineering 12700 Kercheval Detroit, Mich. 48215 Attn: A. J. Follman	1
Crane Packing Company 6400 W. Oakton St. Morton Grove, Ill. 60053 Attn: Harry Tankus	1
Curtiss-Wright Corp. Wright Aeronautical Div. 333 W. First St. Dayton, Ohio 45402 Attn: F. F. Koogler D. Lombardo	1 1
Dow Chemical Company Abbot Road Buildings Midland, Mich. 48640 Attn: Dr. R. Gunderson	1
Dow Corning Company Midland, Mich. 48640 Attn: H. Schieffer	1
Durametallic Corp. Kalamazoo, Mich. 49001 Attn: H. Hummer	1
E.I. DuPont deNemours & Co., Inc. Plastic Department Wilmington, Del. 19898 Attn: R. B. Lewis E. B. Grover Dr. D. George	1 1 1
Fairchild-Hiller Corp. Republic Aviation Division Farmingdale, L.I., N.Y. 11735 Attn: C. Collis	1
Franklin Institute Research Labs. 20th & Parkway Philadelphia, Pa. 19103 Attn: W. Shapiro	1
Garlock, Inc. Palmyra, N.Y. 14522 Attn: E. W. Fisher	1

DISTRIBUTION LIST (continued)

Addressee	Copies
Garrett Corp. AiResearch Mfg. Division 9851-9951 Sepulveda Blvd. Los Angeles, Calif. 90009 Attn: A. Silver	1
General Dynamics Corp. 1025 Connecticut Ave. NW Washington, D.C. 20036 Attn: G. J. Vila	1
General Dynamics Corp. Ft. Worth, Texas 76101 Attn: L. H. Moffatt	1
General Electric Company Advanced Engine & Technology Dept. Cincinnati, Ohio 45415 Attn: L. B. Venable	1
General Motors Corp. Allison Division No. 3, Dept. 7339 Indianapolis, Ind. 46206 Attn: E. M. Deckman	1
Great Lakes Carbon Corp. 299 Park Ave. New York, N.Y. 10017 Attn: J. P. Sachs	1
Gulf General Atomics, Inc. P.O. Box 608 San Diego, Calif. 92112 Attn: J. C. Bokros	1
Grumman Aircraft Engineering Corp. Bethpage, N.Y. 11714 Attn: F. Wakefield	1
Hughes Aircraft Co. International Airport Station P.O. Box 98515 Los Angeles, Calif. 90052	1
Huyck Metals Co. P.O. Box 30 45 Woodmont Road Milford, Conn. 06460 Attn: J. I. Fisher	1
IIT Research Foundation 10 West 35 Street Chicago, Ill. 60616 Attn: Dr. Strohmeier	1
Kendall Refining Co. Bradford, Pa. 16701 Attn: F. I. I. Lawrence	1
Koppers Co., Inc. Metal Products Division Piston Ring and Seal Dept. P.O. Box 626 Baltimore, Md. 21203 Attn: E. Taschenburg C. Onken, Jr.	1 1
Lockheed Aircraft Co. 118 West First Street Dayton, Ohio 45402 Attn: R. R. Witte	1

DISTRIBUTION LIST (continued)

Addressee	Copies
Lockheed Aircraft Corp. Lockheed Missile and Space Co. Material Science Lab. 3251 Hanover St. Palo Alto, Calif. 94301 Attn: Francis J. Clauss	1
Los Alamos Scientific Lab University of California Los Alamos, N.Mex. 87544 Attn: M. C. Smith	1
Martin Marietta Corp. P.O. Box 14153 Dayton, Ohio 45414 Attn: Z. G. Horvath	1
McDonnell Douglas Aircraft Co., Inc. Missile and Space Systems Div. 3000 Ocean Park Blvd. Santa Monica, Calif. 90406 Attn: R. McCord	1
Mechanical Technology Inc. 968 Albany-Shaker Road Latham, N.Y. 12110 Attn: Donald F. Wilcock	1
Midwest Research Institute 425 Volker Blvd. Kansas City, Mo. 64110 Attn: Vern Hopkins	1
Mobil Oil Co. Research Dept. Paulsboro, N.J. 08066 Attn: Dr. E. Oberright	1
Moog Servocontrols, Inc. Proner Airport East Aurora, N.Y. 14052	1
Monsanto Company Organic Chemical Division 800 N. Lindbergh Blvd. St. Louis, Mo. 63166 Attn: Dr. R. Hatton	1
New York Airbrake Co. Stratopower Section Starbuck Ave. Watertown, N.Y. 13601	1
North American Aviation, Inc. Los Angeles International Airport Los Angeles, Calif. 90052 Attn: D. L. Posner	1
North American Rockwell Corp. 5100 W. 164th St. Cleveland, Ohio 44142 Attn: George Bremer	1
Northrop Corp. 1730 K Street NW Suite 903-5 Washington, D.C. 20006 Attn: S. W. Fowler, Jr.	1
Olin Mathieson Chemical Corp. Organics Division 275 Winchester Ave. New Haven, Conn. 06510 Attn: Dr. C. W. McMullon	1

DISTRIBUTION LIST (concluded)

Addressee	Copies
Parker Aircraft Co. 5827 W. Century Blvd. Los Angeles, Calif. 90052 Attn: K. L. Thompson	1
Pressure Technology Corp. of America 453 Amboy Ave. Woodbridge, N.J. 07095 Attn: A. Bobrowsky	1
Pure Carbon Co., Inc. MAIC Division St. Marys, Pa. 15857 Attn: John J. Sherlock	1
Rocketdyne 6633 Canoga Ave. Canoga Park, Calif. 91304 Attn: M. Butner	1
Royal Industries Tetrafluor Division 2051 E. Maple Ave. El Segundo, Calif. 90245 Attn: John Lee	1
Sealol Inc. P.O. Box 2158 Providence, R.I. 02905 Attn: Justus Stevens	1
Southwest Research Institute P.O. Drawer 28510 San Antonio, Texas 78284 Attn: P. M. Ku	1
Sperry Rand Corp. Vickers Inc. Div. Research and Development Dept. Troy, Mich. 48084 Attn: Dr. W. W. Chao	1
Stein Seal Co. 20th and Indiana Ave. Philadelphia, Pa. 19132 Attn: Dr. Stein	1
United Aircraft Corp. Pratt & Whitney Aircraft Div. Engineering Building EB1M-2 East Hartford, Conn. 06108 Attn: R. Shevchenko	1
The University of Tennessee Department of Mechanical and Aerospace Eng. Knoxville, Tenn. 37916 Attn: Prof. W. K. Stair	1
Westinghouse Electric Corp. 5100 W. 164th St. Cleveland, Ohio 44142 Attn: Lynn Powers	1